1972

Analyses of inelastic beam-columns, Ph. D. dissertation, 1972

Toshio Atsuta

ANALYSES OF INELASTIC BEAM-COLUMNS

by

Toshio Atsuta

A Dissertation

Presented to the Graduate Faculty

of Lehigh University

in Candidacy for the Degree of

Doctor of Philosophy

in Civil Engineering

Lehigh University

1972

CERTIFICATE OF APPROVAL

Approved and recommended for acceptance as a dissertation in partial fulfillment of the requirements for the degree of Doctor of Philosophy.

April 25, 1972
(Date)

W. F. Chen
W. F. Chen
Professor in Charge

Accepted May 3, 1972
(Date)

Special Committee directing the doctoral work of Mr. Toshio Atsuta

Professor J. H. Daniels
Chairman

Professor G. C. Driscoll

Professor D. P. Updike

Professor D. A. VanHorn

ACKNOWLEDGMENTS

The author wishes to express his sincere appreciation for the advice, comments and criticisms he received from Professor W. F. Chen, supervisor of this dissertation. The guidance received from the members of the special committee directing the author's doctoral work is gratefully acknowledged. The members of this committee are: Professor J. H. Daniels (Chairman), Professor W. F. Chen, Professor G. C. Driscoll, Professor D. P. Upkike and Professor D. A. VanHorn.

The author also extends his appreciation to Professor D. A. VanHorn, Chairman of the Department of Civil Engineering, Professor L. S. Beedle, Director of Fritz Engineering Laboratory, Professor T. Okumura in the University of Tokyo and Mr. N. Nakae, Managing Director of Kawasaki Heavy Industries, Ltd. for making possible all the necessary arrangements for him to devote himself to his doctoral work at Lehigh University. Special acknowledgments are due to Messrs. S. Parsanejad, R. T. Reese, P. W. Reed, N. Tebedge and S. Desai for their unceasing encouragement and suggestions to the author.

Acknowledgments are also due to Ms. S. Matlock and Ms. P. Raudenbush who typed the manuscript, and to Mr. J. M. Gera for the preparation of the drawings in this dissertation.

TABLE OF CONTENTS

LIST OF FIGURES

LIST OF TABLES

ABSTRACT

This dissertation presents

1. Analyses of in-plane beam-columns (Chapter 2, 3 and 4),
2. Analyses of biaxially loaded sections (Chapter 5, 6 and 8) and
3. Analyses of biaxially loaded columns (Chapter 7 and 9).

In Chapter 2, Column Curvature Curves (CCC) are used to solve general inelastic beam-column problems in a manner similar to the use of Column Deflection Curves (CDC). Curvature curves are obtained analytically from differential equations while rotations and deflections are computed by numerical integration of curvature. Three cases of Column Curvature Curves cover all possible cases of elastic-plastic beam-columns. Complete elastic-plastic responses of beam-columns are investigated. Interaction relationships between thrust and end moment for ultimate strength of a beam-column are given. Numerical results are presented for beam-columns with a rectangular section and a wide-flange section.

In Chapter 3, the strength of an eccentrically compressed wall is investigated by treating the wall as a beam-column. The solution adopted is the column-curvature-curve method and the strength is subject to the criteria of stability and strain limits. The material is assumed to be elastic-perfectly plastic. The yield stress levels in tension and compression may be different. Strain limits for cracking and crushing are considered. Thus, the analysis is applicable to materials such as steel, concrete and masonry. In selected cases, comparison is made with available results reported elsewhere and good

agreement is observed.

Computations to obtain the ultimate strength of an inelastic beam-column are fairly involved and, at present, only numerical methods are available to get the best possible solutions in most cases. For practical purposes, however, these numerical approaches are often laborious. Chapter 4 of this dissertation presents simple approximate forms of solutions by assuming an idealized relationship among moment, curvature and thrust in the full-plastic state of cross sections.

In Chapter 5, a simple method to obtain the exact interaction relationships of doubly symmetric sections under combined axial force and biaxial bending moments is presented. The uniqueness of the solution is proved by the coincidence of the upper and lower bound solutions provided by the limit analysis. For illustration, interaction curves for a wide-flange section, a box section and a circular section are developed using the method. Simple analytical expressions to approximate the interaction relations of wide-flange sections are proposed, and the associated plastic deformations are calculated.

Extension of above method to unsymmetric sections is made in Chapter 6 and the exact interaction curves of various structural shapes are presented.

In Chapter 7, the ultimate strength of biaxially loaded columns is solved by assuming deflection functions and an idealized relationship among biaxial moments and thrust in a manner similar to the method discussed in Chapter 4 for in-plane beam-columns. The

idealized relationship is assumed to be an equation bounded by initial yielding equation and the fully plastic interaction equation of a biaxially loaded section which is obtained in Chapter 5. Numerical examples are presented first for symmetrically loaded columns and then for unsymmetrically loaded columns.

In Chapter 8, the generalized stress-strain relationship of a biaxially loaded cross section is investigated. The generalized stresses are an axial thrust, two biaxial bending moments and a bi-moment and the corresponding generalized strains are an axial strain, two biaxial bending curvatures and a warping curvature. Elastic unloading is taken into consideration. Response to cyclic loadings and subsequent yield surfaces of a cross section are studied.

Finally, a method to solve the elastic plastic response of a biaxially loaded column is presented in Chapter 9. The column is assumed to be cut into finite segments and analyzed as a space structure by using the direct stiffness method. Warping deformation is taken into consideration. Non-linearities due to material plasticity and geometric change are overcome by the tangent stiffness approach.

1. INTRODUCTION

1.1 Introduction

The behavior of a space framed structure is characterized by the behavior of its individual members. The development of the basic knowledge on the response of each individual member to forces acting at its ends and/or to loads acting laterally on the member is of fundamental importance in the analysis and design of such a three-dimensional structure.

The stability problem of an axially loaded compression member is usually analysed as an eigenvalue problem for an ideal column. In most cases, however, in addition to axial thrust, columns are subjected to bending moments at the ends due either to eccentricity of applied thrust or to rotations of adjacent members (Fig. 1.1). Further, existence of lateral load and/or initial imperfections requires the column to be solved as a load-deflection problem rather than as an eigenvalue problem. The behavior of each individual compression member in a space structure should, therefore, be investigated as a beam-column problem or a biaxially loaded column problem.

Elastic analysis of two-dimensional in-plane beam-columns has been accomplished and the solutions can be found in several text books[1,2]. Inelastic analysis of beam-columns, and in particular, biaxially loaded columns, is a subject of wide interest in current column research. The difficulties encountered in the inelastic analysis of beam-columns are due partly to non-linearity caused by geometric changes and material plasticity and partly to a number of other factors

such as loading history dependence and initial imperfections which will influence the behavior of a compression member.

At present, the method most readily available for the design and analysis of inelastic in-plane beam-column is the CDC (Column Deflection Curve) method[3]. However, the labor involved in the numerical calculations based on the CDC method makes its practical use difficult.

What is needed for the practical design or inelastic analysis of beam-columns are simple methods or formulae the validity of which can be established by comparison with exact theory. In this dissertation, simple approximate methods will be presented as well as exact methods for the inelastic analysis of biaxially loaded columns and in-plane beam-columns.

Although special emphasis has been given to three dimensional biaxially loaded column analysis, three chapters in this dissertation are devoted to two-dimensional in-plane beam-column analysis.

1.2 Purpose and Scope

The purpose of this dissertation is to present the following eight different analyses for inelastic beam-columns and biaxially loaded columns.

1. An analysis of inelastic beam-columns by use of the Column Curvature Curve (CCC) method.
2. An extension of the CCC-method to beam-column made of a general material (concrete, masonry, etc.).

3. Derivation of simple interaction equations for in-plane beam-columns.
4. A simple method to obtain the exact interaction relationships of doubly symmetric shapes of section.
5. Exact interaction curves for various unsymmetric structural shapes of cross section.
6. Study of the hysteresis response and shakedown behavior of a wide-flange section.
7. An approximate solution for the ultimate strength of a biaxially loaded column under symmetric as well as unsummetric loads.
8. Inelastic analysis of a biaxially loaded column.

There are many factors which will affect the behavior and the maximum strength of biaxially loaded columns. Some have already been studied, but many remain to be investigated. Factors considered in this study are:

1. Elastic, plastic, strain hardening, elastic unloading, and Bauschinger effect of material.
2. Proportional or nonproportional loading.
3. Symmetric or unsymmetric loading.
4. Static or cyclic loading.
5. Residual stress.
6. Warping and bi-moment.

The basic assumptions which are made for all analyses are

1. Columns and beam-columns are prismatic,
2. Shear stress has no effect on yielding,
3. Local buckling is prevented and

4. Dynamic loading is not considered.

The other assumptions will be mentioned in each Chapter of the dissertation.

1.3 Previous Work

Previous work on the study of column behavior under biaxial loading was reviewed by Chen and Santathadaporn in 1968[4]. Since then, a number of studies have been reported in this field.

For the case of in-plane beam-columns, the analytic moment-curvature-thrust relationships for commonly used structural sections have been derived by Chen[5,6]. Using these results, beam-columns with equal end moments were solved exactly by Chen and Santathadaporn[7]. Chen also presented the general solution for beam-columns with a concentrated lateral load at the midspan[6]. An approximate solution of beam-columns with lateral loads and end moments was also presented by Chen[8] for symmetric loading cases. Lu and Kamalvand[9] presented solutions for the ultimate strength of laterally loaded columns using the CDC (Column Deflection Curve) method.

Stability and load carrying capacity of a concrete beam-column was reported by Yokel[10]. Chen and Chen studied reinforced concrete beam-columns[11] and concrete-filled steel tubular beam-columns[12] using the Column-Curvature Curve (CCC) method.

Interaction curves for wide-flange sections under combined biaxial bending and axial force were reported by Santathadaporn and Chen[13]. Morris and Fenves presented yield surface equations for

several shapes of cross section[14]. In the analyses, approximate interactions were given in several different cases based on the location of the neutral axis.

Several studies on the behavior of a biaxially loaded column have been reported. Following the study by Birnstiel and Michalos[15,16], Syal and Sharma[17] made an analysis of biaxially loaded columns using a collocation method. Experimental studies on I shape and box shape columns were reported by Vogel and Zimmermann[18,19]. Santathadaporn and Chen[20] presented an analysis of biaxially loaded columns for the case of a symmetric loading where the tangent stiffness method is utilized. On the application of the tangent stiffness method to biaxial bending problems, discussions were made by Tezcan and Mahapatra[21], Gurfinkel[22] and Santathadaporn and Chen[23].

Recent research on the behavior of beam-columns under biaxial bending was reviewed by Pillai for the Column Research Council[24,25]. An inelastic analysis of space frames using the results of biaxially loaded columns[20] was recently reported by Morino and Lu[26]. In this analysis the plastic hinge concept was utilized and the rates of plastic deformations were determined making use of the normality condition of the theory of plasticity.

1.4 Organization of Presentation

In Chapter 2, the Column Curvature Curve (CCC) method is developed combining the analytic solution of the column curvature due to Chen[5] with the equivalent column concept introduced by Von Kármán[27].

The CCC-method is essentially a simplification of the CDC-method. The main difference is that the CCC-method makes the best use of the equivalent column characteristics because of its analytical approach, while the CDC-method does not because of its numerical integration. Since three cases of the Column-Curvature Curves cover all possible cases of elastic-plastic beam-columns, the general response of elastic-plastic beam-columns can be obtained without laborious computations.

In Chapter 3, the CCC-method is extended to beam-column problems of a general material and applied to eccentrically loaded concrete or masonry walls. An extremely simple moment-thrust-curvature equation is derived to cover all possible cases of tension and/or compression yielding as well as tension cracking and/or compression cursching of concrete or masonry walls.

In most reference works on the approximate theory of beam-column problems[28,29], the deflected shape is often assumed to be a certain curve, such as a sine curve or a parabolic curve. As a consequence of this, the analysis of beam columns is considerably simplified. Simple interaction equations which define the load carrying capacity of a beam-column can then be obtained[30]. It has been found that this simplification gives satisfactory results for simply supported beam-columns under symmetric loading conditions. Most of the theories in the previous work, however, are not suitable for convenient determination of solutions of beam-columns with unsymmetric load or fixed end supports. An effort to help fill part of this gap is made in Chapter 4 where an alternate but extremely simple approximate method is developed and applied to various beam-column problems.

Interaction curves for wide flange sections under biaxial bending and thrust have been reported by Santathadaporn and Chen[13] where their accuracy was examined by the upper and lower bound techniques of limit analysis. In that work, all possible positions of the neutral axis of a cross section were considered and interaction equations were derived for each case. In Chapter 5, a simple method to obtain the exact interaction relationships for sections doubly symmetric is presented. Simple analytical expressions to approximate the interaction relations of wide-flange sections are proposed, and the associated plastic deformations are calculated.

The method presented in Chapter 5 for interaction relations is then extended in Chapter 6 for general sections, symmetric or unsymmetric. The exactness of the solution is proved by using the upper and lower bound techniques of limit analysis. Interaction curves for several unsymmetric structural shapes are presented for practical purposes.

In Chapter 7, the ultimate strength of biaxially loaded columns is solved approximately by assuming a deflection shape and an idealized relationship among biaxial moments and thrust. This is a direct extension of the method developed in Chapter 4 for two dimensional in-plane beam-columns to three dimensional biaxially loaded columns. Numerical examples are presented first for symmetrically loaded columns and then for unsymmetrically loaded columns.

Santathadaporn and Chen derived a generalized stress-strain relationship for wide flange shapes[20]. Two bending moments about

the principal axes and an axial thrust were taken as the generalized stresses. The corresponding generalized strains were two curvatures about the principal axes and an axial strain at its centroid. In Chapter 8, a similar but more general method is developed to obtain the generalized stress-strain relationships of a cross section. Bi-moment and warping deformation are considered as one of the generalized stresses and one of the generalized strains, respectively. Since strain hardening and elastic unloading are taken into account, the subsequent yield surfaces and the hysteresis response of the cross section subjected to various cyclic loadings are obtained.

Knowing the elastic-plastic response of the cross section (Chapter 8), the analysis of a biaxially loaded column is now possible. This is done in Chapter 9 by treating the column as a space structure composed of several finite segments. The direct stiffness method is applied by assuming that elastic-plastic sectional properties of the segment are uniform within the segment. Non-linearity due to material plasticity and geometric change are overcome by the tangent stiffness approach. Space structures can be solved by extending the method developed herein.

2. COLUMN CURVATURE CURVE METHOD FOR IN-PLANE BEAM-COLUMNS

2.1 Introduction

"A beam-column with different end moments can be considered to be a part of a buckled column." This is the equivalent column concept which was introduced by von Kármán[27] for elastic beam-column problems. The Column Deflection Curve method[3] in inelastic beam-column problem is an application of this concept, because of its numerical treatment, however, it does not make the best use of characteristics of the equivalent column. The Column Curvature Curve (CCC) method is developed using analytical curvature solutions due to Chen and Santathadaporn[7]. As a consequence, the equivalent column concept is clear and becomes a powerful means to solve moment gradient problems.

Only three cases of equivalent columns cover all possible elastic-plastic beam-columns. Determination of the equivalent column length is the major problem in the CCC-method, for it an iterative procedure is applied. Once the equivalent column length is determined, the curvature distribution is uniquely given in an analytical expression, thus calculation of slope or deflection is straightforward by numerical methods.

2.2 Moment-Curvature-Thrust Relationship

A symmetric cross section is considered herein. The initial yield quantities of the section are defined as

$$M_y = \sigma_y S \quad \text{for moment M}$$

$$P_y = \sigma_y A \quad \text{for thrust P} \tag{2.1}$$

$$\Phi_y = \frac{2\epsilon_y}{h} \quad \text{for curvature } \Phi$$

where σ_y, ϵ_y are yield stress and yield strain of the material, h, A are depth and area of the cross section and S is the elastic section modulus.

Non-dimensional parameters are defined as

$$m = \frac{M}{M_y}, \quad p = \frac{P}{P_y}, \quad \varphi = \frac{\Phi}{\Phi_y} \tag{2.2}$$

Following the work of Chen[5,6], the state of the generalized stress m in a cross section of a beam-column belongs to one of the following three regimes: Elastic regime, primary plastic regime, and secondary plastic regime as shown in Fig. 2.1. Referring to Fig. 2.2 the boundaries between the regimes are defined by initial yield curvature φ_1 and secondary yield curvature φ_2, respectively. A general m-φ-p curve is assumed to be closely represented by the following expressions (Ref. 5):

In the elastic regime $(0 \leq \varphi \leq \varphi_1)$

$$m = a\,\varphi \tag{2.3}$$

In the primary plastic regime $(\varphi_1 \leq \varphi \leq \varphi_2)$

$$m = b - \frac{c}{\sqrt{\varphi}} \tag{2.4}$$

In the secondary plastic regime $(\varphi_2 \leq \varphi)$

$$m = m_{pc} - \frac{f}{\varphi^2} \tag{2.5}$$

where a, b, c, f, m_{pc}, φ_1, and φ_2 are functions of the thrust parameter p and the shape of the cross section. These functions have been obtained in Ref. 6 for several commonly used structural sections. As a simple example, for the case of a rectangular cross section

$$a = 1 \quad , \quad b = 3\ (1-p) \quad , \quad c = 2\ (1-p)^{3/2}$$
$$f = \frac{1}{2} \ , \ m_{pc} = \frac{3}{2}\ (1-p^2) \ , \ \varphi_1 = 1-p \ , \ \varphi_2 = \frac{1}{1-p} \tag{2.6}$$

2.3 Concept of Equivalent Column

Fig. 2.3(a) shows a beam-column AB of length L subjected to axial compression P and bending moments M_A and M_B at its ends A and B, respectively. The vertical reactions V at the ends are, from moment equilibrium,

$$V = (M_B - M_A)/L \tag{2.7}$$

If the resultant force of P and V is taken as

$$P^* = \sqrt{P^2 + V^2} \tag{2.8}$$

another equilibrium state is obtained as shown in Fig. 2.3(b). The two resultant forces have the same magnitude and are parallel to the slope of the beam-column at C where curvature is a maximum (Appendix 11.1). As shown in Fig. 11.1, the section where the maximum curvature occurs does not coincide with the section corresponding to the maximum deflection.

From this state of equilibrium it is possible to conclude that a simply supported column DE of length L* can be chosen which is subjected to axial compression P* only so that a portion A*C*B* may be in the same condition as the original beam-column ACB, Fig. 2.3(c). This is the "equivalent column" of the original beam-column. The length of the equivalent column L* is unknown at this stage. The use of the equivalent column concept reduces the ten cases of a beam-column problem to only three cases of the equivalent column problem as shown in Fig. 2.4.

2.4 Governing Equation and Solutions

The equation of equilibrium for a beam-column is

$$\frac{d^2m}{dx^2} + k^2 \varphi = 0 \tag{2.9}$$

where

$$k = \sqrt{P^*/EI} \tag{2.10}$$

and

EI = bending rigidity of the elastic beam

Using the moment-curvature-thrust relations (Eqs. 2.3, 2.4 and 2.5) the basic differential equations of the beam-column in terms of φ are obtained as follows:

In the elastic regime ($\varphi \leq \varphi_1$)

$$\frac{d^2\varphi}{dx^2} + \frac{k^2}{a} \varphi = 0 \tag{2.11}$$

In the primary plastic regime ($\varphi_1 \leq \varphi \leq \varphi_2$)

$$\varphi \frac{d^2\varphi}{dx^2} - \frac{3}{2}\left(\frac{d\varphi}{dx}\right)^2 + \frac{2k^2}{c}\varphi^{7/2} = 0 \tag{2.12}$$

In the secondary plastic regime ($\varphi_2 \leq \varphi$)

$$\varphi \frac{d^2\varphi}{dx^2} - 3\left(\frac{d\varphi}{dx}\right)^2 + \frac{k^2}{2f}\varphi^5 = 0 \tag{2.13}$$

The general solutions are:

In the elastic regime ($\varphi \leq \varphi_1$)

$$\varphi = A_1 \cos\frac{kx}{\sqrt{a}} + B \sin\frac{kx}{\sqrt{a}} \tag{2.14}$$

In the primary plastic regime ($\varphi_1 \leq \varphi \leq \varphi_2$)

$$\frac{d\varphi}{dx} = \frac{2\sqrt{2}k}{\sqrt{c}}\left(D^{1/2} - \varphi^{1/2}\right)^{1/2}\varphi^{3/2} \tag{2.15}$$

$$x - x_p = -\frac{\sqrt{c}}{\sqrt{2}k} D^{-3/4}\left\{\left(\frac{D}{\varphi}\right)^{1/2}\left[1 - \left(\frac{\varphi}{D}\right)^{1/2}\right]^{1/2} + \tanh^{-1}\left[1 - \left(\frac{\varphi}{D}\right)^{1/2}\right]^{1/2}\right\} \tag{2.16}$$

In the secondary plastic regime ($\varphi_2 \leq \varphi$)

$$\frac{d\varphi}{dx} = \frac{k}{\sqrt{f}}(1 + G\varphi)^{1/2}\varphi^{5/2} \tag{2.17}$$

$$x - x_s = \frac{2}{3}\frac{\sqrt{f}}{k}\left(G + \frac{1}{\varphi}\right)^{1/2}\left(2G - \frac{1}{\varphi}\right) \tag{2.18}$$

where A_1, B, D, G, x_p, and x_s are constants of integration.

2.5 Boundary Conditions and Discontinuity Conditions

Consider the equivalent columns shown in Fig. 2.5 Curvatures corresponding to primary yielding φ_1 and secondary yielding φ_2 occur at sections $x = \rho_1$ and $x = \rho_2$, respectively. The maximum curvature occurs at midspan, $x = L^*/2$. The boundary conditions for curvature are, hence,

$$\begin{aligned} &\text{at} \quad x = 0, && \varphi = 0 \\ &\text{at} \quad x = \rho_1, && \varphi = \varphi_1 \\ &\text{at} \quad x = \rho_2, && \varphi = \varphi_2 \\ &\text{at} \quad x = L^*/2, && \varphi = \varphi_m \end{aligned} \tag{2.19}$$

Discontinuity conditions of $d\varphi/dx$ are obtained from continuity conditions of bending moment at the boundaries[5];

$$\begin{aligned} &\text{at} \quad x = \rho_1, && \frac{2a}{c}\,\varphi_1^{3/2}\,\left(\frac{d\varphi}{dx}\right)_E = \left(\frac{d\varphi}{dx}\right)_P \\ &\text{at} \quad x = \rho_2, && \frac{c}{4f}\,\varphi_2^{3/2}\,\left(\frac{d\varphi}{dx}\right)_P = \left(\frac{d\varphi}{dx}\right)_S \\ &\text{at} \quad x = L^*/2, && \frac{d\varphi}{dx} = 0 \end{aligned} \tag{2.20}$$

where subscripts, E, P, and S denote elastic, primary plastic and secondary plastic regimes, respectively.

2.6 Column Curvature Curves

From the general solutions and boundary conditions, Column Curvature Curves (CCC-s) for the three different cases (Fig. 2.5) are obtained as follows:

Elastic Column ($0 \leq \varphi_m \leq \varphi_1$)

$$kx = \sqrt{a}\ \sin^{-1}\left(\frac{\varphi}{\varphi_m}\ \sin\frac{kL^*}{2\sqrt{a}}\right) \tag{2.21}$$

where

$$kL^* = \pi\sqrt{a} \tag{2.22}$$

One-Side Plastic Column ($\varphi_1 \leq \varphi_m \leq \varphi_2$)

In elastic regime ($0 \leq x \leq \rho_1$)

$$kx = \sqrt{a}\ \sin^{-1}\left(\frac{\varphi}{\varphi_1}\ \sin\frac{k\rho_1}{\sqrt{a}}\right) \tag{2.23}$$

In primary plastic regime ($\rho_1 \leq x \leq L^*/2$)

$$kx = \frac{kL^*}{2} - \frac{\sqrt{c}}{\sqrt{2}}\varphi_m^{-3/4}\left\{\left[\frac{\varphi_m}{\varphi} - \left(\frac{\varphi_m}{\varphi}\right)^{1/2}\right]^{1/2} + \tanh^{-1}\left[1 - \left(\frac{\varphi}{\varphi_m}\right)^{1/2}\right]^{1/2}\right\} \tag{2.24}$$

where

$$k\rho_1 = \sqrt{a}\ \cot^{-1}\left\{\sqrt{\frac{2c}{a}}\ \varphi_1^{-3/4}\left[\left(\frac{\varphi_m}{\varphi_1}\right)^{1/2} - 1\right]^{1/2}\right\} \tag{2.25}$$

$$\frac{kL^*}{2} = k\rho_1 + \frac{\sqrt{c}}{\sqrt{2}}\varphi_m^{-3/4}\left\{\left[\frac{\varphi_m}{\varphi_1} - \left(\frac{\varphi_m}{\varphi_1}\right)^{1/2}\right]^{1/2} + \tanh^{-1}\left[1 - \left(\frac{\varphi_1}{\varphi_m}\right)^{1/2}\right]^{1/2}\right\} \tag{2.26}$$

Two-Sides Plastic Column ($\varphi_2 \leq \varphi_m$)

In elastic regime ($0 \leq x \leq \rho_1$)

$$kx = \sqrt{a}\ \sin^{-1}\left(\frac{\varphi}{\varphi_1}\sin\frac{k\rho_1}{\sqrt{a}}\right) \tag{2.27}$$

In primary plastic regime ($\rho_1 \leq x \leq \rho_2$)

$$kx = kx_p - \frac{\sqrt{c}}{\sqrt{2}}D^{-3/4}\left\{\left(\frac{D}{\varphi}\right)^{1/2}\left[1 - \left(\frac{\varphi}{D}\right)^{1/2}\right]^{1/2} + \tanh^{-1}\left[1 - \left(\frac{\varphi}{D}\right)^{1/2}\right]^{1/2}\right\} \tag{2.28}$$

In secondary plastic regime ($\rho_1 \leq x \leq L^*/2$)

$$kx = \frac{kL^*}{2} - \frac{2}{3}\sqrt{f}\ \varphi_m^{-3/2}\left(2 + \frac{\varphi_m}{\varphi}\right)\left(\frac{\varphi_m}{\varphi} - 1\right)^{1/2} \tag{2.29}$$

where

$$D = \left[\sqrt{\varphi_2} + \frac{2f}{c}\left(\frac{1}{\varphi_2} - \frac{1}{\varphi_m}\right)\right]^2 \tag{2.30}$$

$$k\rho_1 = \sqrt{a}\ \tan^{-1}\left[\sqrt{\frac{a}{2c}}\,\varphi_1 \Big/ \left(D^{1/2} - \varphi_1^{1/2}\right)^{1/2}\right] \tag{2.31}$$

$$kx_p = k\rho_1 + \sqrt{\frac{c}{2}}D^{-3/4}\left\{\left(\frac{D}{\varphi_1}\right)^{1/2}\left[1 - \left(\frac{\varphi_1}{D}\right)^{1/2}\right]^{1/2} + \tanh^{-1}\left[1 - \left(\frac{\varphi_1}{D}\right)^{1/2}\right]^{1/2}\right\} \tag{2.32}$$

$$k\rho_2 = kx_p - \sqrt{\frac{c}{2}}D^{-3/4}\left\{\left(\frac{D}{\varphi_2}\right)^{1/2}\left[1 - \left(\frac{\varphi_2}{D}\right)^{1/2}\right]^{1/2} + \tanh^{-1}\left[1 - \left(\frac{\varphi_2}{D}\right)^{1/2}\right]^{1/2}\right\} \tag{2.33}$$

$$kL^* = 2k\rho_2 + \frac{4}{3}\sqrt{f}\left(\frac{1}{\varphi_2} - \frac{1}{\varphi_m}\right)^{1/2}\left(\frac{1}{\varphi_2} + \frac{2}{\varphi_m}\right) \tag{2.34}$$

The length x is expressed explicitly here as a function of curvature φ. The length of the equivalent column kL* is obtained as a function of φ_m and p* from these equations and is shown in Table 2.1.

Figure 2.6 is an example of CCC-s for a rectangular cross section when the axial thrust is constant (p* = 0.5). In the secondary plastic regime ($\varphi \geq 2$) φ changes rapidly. The lowest curve (φ_m* = 0.5) represents curvatures in the elastic regime. The half width of the abscissa for the elastic curve is equal to $\pi/2$ which corresponds to Euler's buckling.

2.7 Method of Solution

Column Curvature Curves (CCC-s) are used to solve various beam-column problems. Consider a beam-column as shown in Fig. 2.7(a). First, p*, φ_A, φ_B, and kL are computed from M_A, M_B, P, L, and EI using Eqs. 2.3 to 2.10. For a fixed p*-value CCC-s are drawn from Eqs. 2.21 to 2.34 as shown in Fig. 2.7(c). The curve, in which φ_A, φ_B, and kL match, gives the maximum curvature φ_m*, the equivalent column length kL*, and the curvature distribution φ corresponding to the original beam-column.

It should be noted here that there can be two sets of matchings as shown in Fig. 2.8(a). This means, for a fixed thrust p*, there can be two states of equilibrium which are represented by two maximum curvatures φ_{m1}* and φ_{m2}*. These two different states correspond to the two points on the loading and unloading portions of a load-curvature curve, respectively, as shown in Fig. 2.8(b).

As shown here, the maximum curvature φ_m of a beam-column does not necessarily equal φ_m^*, the maximum curvature of the equivalent column. Figure 2.9 shows a comparison between the maximum curvature φ_m of a beam-column and φ_m^* of the equivalent column for a rectangular section in the loading case of $m_A = 0.4$ (constant) and $m_B = 0.2$ (constant). When p is small, φ_m and φ_m^* are much different from each other, which means the maximum curvature φ_m^* occurs outside the beam-column, while φ_m occurs at one end of the beam-column. In the figure φ_m stays constant ($\varphi_m = 0.4$) while φ_m^* decreases as the thrust p increases. At some stage both φ_m and φ_m^* start to increase and become equal after a while. After this, the maximum curvatures φ_m and φ_m^* remain the same and occur inside the beam-column.

Using Column Curvature Curves for single curvature beam-columns, beam-column problems with double curvature can be solved in exactly the same way as is done using the Column Deflection Curve method. This implies drawing another set of CCC-s continuous with the original CCC-s at one end, the continuation being mirror images of the original CCC-s as shown in Fig. 2.10. Using this modified set of CCC-s, beam-columns with many types of end loading can be solved.

2.8 Numerical Examples

Generally, the behavior of an elastic-plastic beam-column is determined by two independent non-dimensional variables,

$$\gamma = \frac{S}{AL} \quad \text{and} \quad \lambda = \frac{L}{r}\sqrt{\frac{\sigma_y}{E}} \tag{2.35}$$

where L/r is the slenderness ratio. Loading conditions for the left end A and the right end B are given by the following relations:

$$m_A = \alpha \cdot p + \bar{m}_A \ , \ m_B = \beta \cdot p + \bar{m}_B \tag{2.36}$$

where α and β represent non-dimensionally the eccentricities of the thrust at ends A and B, respectively. These are computed by the expressions,

$$\alpha = e_A \cdot \frac{A}{S} \quad \text{and} \quad \beta = e_B \frac{A}{S} \tag{2.37}$$

where e_A and e_B represent the actual eccentricities as shown in Fig. 2.11. Moments $\bar{m}_A$ and $\bar{m}_B$ are produced by rotation of adjacent members. In case of proportional loading Eq. 2.36 reduces to

$$m_A = \alpha \cdot p \ , \ m_B = \kappa m_A \tag{2.38}$$

As an example, numerical results for a beam-column (L = 600 in.) with a rectangular cross section (6" x 20") are considered. The moment-curvature-thrust relationship is determined by the parameters given in Eq. 2.6. Assuming A36 steel, and

$$E = 29{,}000 \text{ ksi} \ , \ \sigma_y = 36 \text{ ksi} \tag{2.39}$$

the non-dimensional variables of this beam-column are

$$\gamma = 5.56 \times 10^{-3} \ , \ \lambda = 3.51 \tag{2.40}$$

Figure 2.12 is a plot of the numerical results for maximum curvature φ_m vs. thrust p for the case with $\kappa = 0.5$ in Eq. 2.38. In the figure the (p, φ_m)-curves are divided into elastic regime, primary

plastic regime, and secondary plastic regime by two dotted straight lines. Rotational angles at the ends, θ_A and θ_B, can also be computed and plotted as shown by curves in Fig. 2.13. Picking up the maximum points of these curves, interaction curves for the ultimate strength of this beam-column corresponding to loads m_A, m_B, and p can be obtained as shown in Fig. 2.14 (see Appendix 11.2).

In Figs. 2.15, 2.16, and 2.17 numerical results for a 14WF246 cross section neglecting the influence of residual stresses are shown, other parameters used being identical with those of the rectangular section.

2.9 Further Applications

As the end rotations of a beam-column can be obtained, the stiffness of a beam-column which is the ratio of end moment to end rotation can be computed. From the member stiffnesses, the stiffness matrix for a whole frame, such as the one shown in Fig. 2.18, can be constructed and, thus, the elastic-plastic behavior of the frame can be obtained.

2.10 Summary

An approach using Column Curvature Curves (CCC-s) has been introduced to solve elastic-plastic beam-columns subjected to various end loadings. The basic idea is the same as in the method using Column Deflection Curves where deflections are obtained by numerical integration. The application of the CCC method is simple and three types of CCC-s cover all cases of elastic-plastic beam-columns. Complete elastic-plastic

response of beam-columns is presented and ultimate strength and interaction relations are obtained. End rotation which gives member stiffness is also computed.

3. ANALYSIS OF ECCENTRICALLY LOADED CONCRETE OR MASONRY WALLS BY CCC-METHOD

3.1 Introduction

Walls are generally treated as compression members in building design. The compressive forces may be applied eccentrically on the walls. Further, bending moments are often induced by rotation of the floor girders. The strength of a wall must hence be investigated using beam-column analysis. The ultimate strength is controlled by the stability limit or the strain limit. The Column-Curvature-Curve (CCC) method developed in Chapter 2 is used herein to perform the beam-column analysis.

3.2 Material Properties

The material considered in this report is elastic-perfectly plastic as shown in Fig. 3.1.

E = modulus of elasticity

σ_{ty} = tensile yield stress (positive)

σ_{cy} = compressive yield stress (negative)

ϵ_{to} = cracking strain (positive)

ϵ_{co} = crushing strain (negative)

$$\epsilon_{ty} = \frac{\sigma_{ty}}{E} \qquad \epsilon_{cy} = \frac{\sigma_{cy}}{E} \tag{3.1}$$

The yield stresses and strain are defined using the ratio μ and the absolute value σ_y of the yield stress in compression.

$$\sigma_{ty} = \mu\,\sigma_y \qquad \sigma_{cy} = -\sigma_y \qquad \varepsilon_y = \frac{\sigma_y}{E} \tag{3.2}$$

Thus, the analysis is applicable, in general, to materials which have different strengths in tension and in compression.

$$\begin{aligned} &\text{For idealized steel} && \mu = 1 \\ &\text{For idealized masonry} && \mu = 0 \\ &\text{For idealized concrete} && 0 < \mu < 1 \end{aligned} \tag{3.3}$$

3.3 Moment-Curvature-Thrust Relationship

The wall has the thickness t and the height h as shown in Fig. 3.2. The loads are the axial force P on the midthickness and the two end moments M_A and M_B.

The material properties, the geometry and the loads are considered invariant along the width. Hence, a wall with a unit width is considered in this report. Therefore, it is the same as a rectangular beam-column of depth t, width 1.0 and length h.

It is assumed that plane sections remain plane after deformation. Thus the strain distribution is linear through the wall thickness. In terms of the mean strain ε_m and the curvature Φ (Fig. 3.3), the strain ε at location y from center line is

$$\varepsilon = \Phi y + \varepsilon_m \tag{3.4}$$

The boundaries of compression yield y_{cy} and tension yield y_{ty} are given by

$$y_{ty} = \frac{1}{\Phi}(\epsilon_{ty}-\epsilon_m) \qquad y_{cy} = \frac{1}{\Phi}(\epsilon_{cy}-\epsilon_m) \tag{3.5}$$

Eq. 3.5 has meaning only for

$$-\frac{t}{2} \le y_{ty} \le \frac{t}{2} \qquad -\frac{t}{2} \le y_{cy} \le \frac{t}{2} \tag{3.6}$$

The stress is given by

$$\sigma = \begin{cases} \sigma_{cy} & (y \le y_{cy}) \\ E(\Phi y+\epsilon_m) & (y_{cy} \le y \le y_{ty}) \\ \sigma_{ty} & (y_{ty} \le y) \end{cases} \tag{3.7}$$

In order to derive simple expressions for axial force P and bending moment M, the following specially defined parentheses are convenient for use.

$$< S > = \begin{cases} S & (0 \le S) \\ 0 & (S \le 0) \end{cases} \tag{3.8}$$

Axial force and bending moment per unit width are

$$P = \int_{-\frac{t}{2}}^{\frac{t}{2}} \sigma dy \qquad M = \int_{-\frac{t}{2}}^{\frac{t}{2}} \sigma y dy \tag{3.9}$$

Using Eqs. 3.7, 3.8 and 3.9

$$P = \int_{-\frac{t}{2}}^{\frac{t}{2}} (E\Phi y+E\epsilon_m)\,dy - \int_{-\frac{t}{2}}^{\frac{t}{2}} <-E\Phi y-E\epsilon_m+\sigma_{cy}>\,dy - \int_{-\frac{t}{2}}^{\frac{t}{2}} <E\Phi y+E\epsilon_m-\sigma_{ty}>\,dy \tag{3.10}$$

$$M = \int_{-\frac{t}{2}}^{\frac{t}{2}} (E\Phi y^2+E\epsilon_m y)\,dy - \int_{-\frac{t}{2}}^{\frac{t}{2}} <E\Phi y^2+E\epsilon_m y-\sigma_{cy} y>\,dy - \int_{-\frac{t}{2}}^{\frac{t}{2}} <E\Phi y^2+E\epsilon_m y-\sigma_{ty} y>\,dy \tag{3.11}$$

These may now be reduced to two simple equations using Eqs. 3.2, 3.5 and 3.8 (Fig. 3.3),

$$P = E\epsilon_m t + \frac{E}{2\Phi}\left\langle\frac{\Phi t}{2} - \epsilon_y - \epsilon_m\right\rangle^2 - \frac{E}{2\Phi}\left\langle\frac{\Phi t}{2} - \mu\epsilon_y + \epsilon_m\right\rangle^2 \qquad (3.12)$$

$$M = \frac{E\Phi t^3}{12} - \frac{E}{6\Phi^2}\left\langle\frac{\Phi t}{2} - \epsilon_y - \epsilon_m\right\rangle^2 \left(\Phi t + \epsilon_y + \epsilon_m\right)$$

$$- \frac{E}{6\Phi^2}\left\langle\frac{\Phi t}{2} - \mu\epsilon_y + \epsilon_m\right\rangle^2 \left(\Phi t + \mu\epsilon_y - \epsilon_m\right) \qquad (3.13)$$

The equations are next simplified using non-dimensionalized quantities

$$\bar{\sigma} = \frac{\sigma}{\sigma_y} \qquad \bar{\epsilon} = \frac{\epsilon}{\epsilon_y} \qquad (3.14)$$

$$p = -\frac{P}{P_y} \qquad m = \frac{M}{M_y} \qquad \varphi = \frac{\Phi}{\Phi_y} \qquad (3.15)$$

where

$$P_y = \sigma_y t \qquad M_y = \sigma_y \frac{t^2}{6} \qquad \Phi_y = \epsilon_y \frac{2}{t} \qquad (3.16)$$

Also, henceforth, a positive value for p indicates compressive force. Thus Eq. 3.12 and Eq. 3.13 become

$$p = -\bar{\epsilon}_m - \frac{1}{4\varphi}\left[\left\langle\varphi - 1 - \bar{\epsilon}_m\right\rangle^2 - \left\langle\varphi - \mu + \bar{\epsilon}_m\right\rangle^2\right] \qquad (3.17)$$

$$m = \varphi - \frac{1}{4\varphi^2}\left[\left\langle\varphi - 1 - \bar{\epsilon}_m\right\rangle^2 \left(2\varphi + 1 + \bar{\epsilon}_m\right) + \left\langle\varphi - \mu + \bar{\epsilon}_m\right\rangle^2 \left(2\varphi + \mu - \bar{\epsilon}_m\right)\right] \qquad (3.18)$$

Elimination of $\bar{\epsilon}_m$ from Eqs. 3.17 and 3.18 yields a relationship among the bending moment m, the curvature φ and the thrust p in the elastic as well as elastic-plastic regimes.

Since direct elimination is not possible, the m-φ-p equations are derived in four different regimes separately (Fig. 3.4).

(a) Elastic Regime ($\varphi \leq \varphi_{et}$ and $\varphi \leq \varphi_{ec}$)

$$\bar{\epsilon}_m = -p \tag{3.19}$$

$$m = \varphi \tag{3.20}$$

(b) Tension Yield Regime ($\varphi_{et} \leq \varphi_{ec}$ and $\varphi_{et} < \varphi \leq \varphi_{tc}$)

$$\bar{\epsilon}_m = \varphi + \mu - 2\sqrt{\varphi\ (\mu+p)} \tag{3.21}$$

$$m = 3\ (\mu+p) - 2\sqrt{\frac{(\mu+p)^3}{\varphi}} \tag{3.22}$$

(c) Compression Yield Regime ($\varphi_{ec} < \varphi_{et}$ and $\varphi_{ec} < \varphi \leq \varphi_{ct}$)

$$\bar{\epsilon}_m = -\ (1+\varphi) + 2\sqrt{\varphi(1-p)} \tag{3.23}$$

$$m = 3\ (1-p) - 2\sqrt{\frac{(1-p)^3}{\varphi}} \tag{3.24}$$

(d) Combined Yield Regime ($\varphi_{tc} < \varphi$ or $\varphi_{ct} < \varphi$)

$$\bar{\epsilon}_m = \frac{\varphi}{1+\mu}\ (1-\mu-2p) - \frac{1-\mu}{2} \tag{3.25}$$

$$m = 3\ \frac{(1-p)(\mu+p)}{1+\mu} - \frac{(1+\mu)^3}{16\varphi^2} \tag{3.26}$$

In the present analysis, only positive curvature may be taken into account without violating the generality. The boundary curvatures used in Eqs. 3.19 to 3.26 are given by

$$\begin{aligned}
\varphi_{et} &= \mu + p && \text{(Elastic-tension Yield)} \\
\varphi_{ec} &= 1 - p && \text{(Elastic-compression Yield)} \\
\varphi_{tc} &= \frac{(1+\mu)^2}{4(\mu+p)} && \text{(Tension-compression Yield)} \\
\varphi_{ct} &= \frac{(1+\mu)^2}{4(1-p)} && \text{(Compression-tension Yield)}
\end{aligned} \tag{3.27}$$

The order in which the different distributions of stress as shown in Fig. 3.4(a), 3.4(b), 3.4(c) and 3.4(d) may occur with increasing φ is of importance in the analysis. If the section is elastic throughout under thrust p alone, its behavior under the bending moment m is initially governed by Fig. 3.4(a). The addition of the moment m will increase φ and for some value of m, the section will start to yield. Assuming the tension fibers begin to yield first, the behavior is now governed by Fig. 3.4(b), and the boundary curvature between Fig. 3.4(a) and Fig. 3.4(b) is φ_{et}. If the curvature φ can further be increased to φ_{tc}, the compression fibers also begin to yield and for any value of $\varphi > \varphi_{tc}$ the behavior of the section is governed by Fig. 3.4(d). By similar reasoning, the other sequence of yielding is Fig. 3.4(a), 3.4(c) and finally 3.4(d) and the corresponding boundary curvature between Fig. 3.4(a) and 3.4(c) and between Fig. 3.4(c) and 3.4(d) are φ_{ec} and φ_{ct} respectively.

Comparing the two initial yield curvatures φ_{et} and φ_{ec}, it is known that

$$\begin{aligned} &\text{if } p < \frac{1-\mu}{2}, \text{ tension yielding occurs first} \\ &\text{if } p > \frac{1-\mu}{2}, \text{ compression yielding occurs first} \end{aligned} \tag{3.28}$$

Using this relationship, Eq. 3.27 can be simplified to

$$\begin{aligned} \varphi_{et},\ \varphi_{ec} &= \frac{1+\mu}{2} - \left| \frac{1-\mu}{2} - p \right| = \varphi_1 \\ \varphi_{tc},\ \varphi_{ct} &= \frac{(1+\mu)^2}{4\varphi_1} = \varphi_2 \end{aligned} \tag{3.29}$$

Now there are only three regimes:

(a) Elastic Regime $(\varphi \leq \varphi_1)$

$$m = a\,\varphi \tag{3.30}$$

(b) Tension or Compression Yield Regime $(\varphi_1 < \varphi \leq \varphi_2)$

$$m = b - \frac{c}{\sqrt{\varphi}} \tag{3.31}$$

(c) Combined Yield Regime $(\varphi_2 < \varphi)$

$$m = m_{pc} - \frac{f}{\varphi^2} \tag{3.32}$$

where

$$a = 1 \qquad b = 3\varphi_1 \qquad c = 2\varphi_1^{3/2}$$
$$f = \frac{(1+\mu)^3}{16} \qquad m_{pc} = 3\,\frac{(1-p)(\mu+p)}{1+\mu} \tag{3.33}$$

The m-φ-p relationships derived in Chapter 2 and Ref. 7 for steel beam-columns and in Refs. 12 and 10 for plain concrete and masonry walls are special cases of Eqs. 3.30 to 3.33 with $\mu = 1.0$ and $\mu = 0$ respectively.

3.4 Strain Limits

As one of the strength criteria, the wall is assumed to reach its ultimate state when the strain at the extreme fiber reaches the strain limit of the material. The strain limits are

$$\begin{aligned} \varepsilon_{co} &= \text{crushing strain (negative)} \\ \varepsilon_{to} &= \text{cracking strain (positive)} \end{aligned} \tag{3.34}$$

Since the strain distribution is given by Eq. 3.4, these conditions are reached when

$$\begin{aligned} \varepsilon_{co} &= -\frac{\phi t}{2} + \varepsilon_m \\ \varepsilon_{to} &= \frac{\phi t}{2} + \varepsilon_m \end{aligned} \tag{3.35}$$

or non-dimensionally

$$\bar{\varepsilon}_m = \begin{cases} \varphi + \bar{\varepsilon}_{co} \\ -\varphi + \bar{\varepsilon}_{to} \end{cases} \tag{3.36}$$

Substituting this $\bar{\varepsilon}_m$ into Eqs. 3.19 to 3.26, the cracking curvature φ_{to} and crushing curvature φ_{co} are obtained as follows:

(a) Elastic Regime $(\varphi_{to} \le \varphi_1,\ \varphi_{co} \le \varphi_1)$

$$\begin{aligned} \varphi_{to} &= \bar{\varepsilon}_{to} + p \\ \varphi_{co} &= -(\bar{\varepsilon}_{co} + p) \end{aligned} \tag{3.37}$$

(b) Tension or Compression Yield Regime $(\varphi_1 < \varphi_{to} \le \varphi_2, \varphi_1 < \varphi_{co} \le \varphi_2)$

$$\begin{aligned} \varphi_{to} &= \frac{\bar{\varepsilon}_{to}+p}{2} + \frac{1}{2}\sqrt{(\bar{\varepsilon}_{to}+p)^2 - (\mu-\bar{\varepsilon}_{to})^2} \\ \varphi_{co} &= -\frac{(\bar{\varepsilon}_{co}+p)}{2} + \frac{1}{2}\sqrt{(\bar{\varepsilon}_{co}+p)^2 - (1+\bar{\varepsilon}_{co})^2} \end{aligned} \tag{3.38}$$

(c) Combined Yield Regime $(\varphi_2 < \varphi_{to},\ \varphi_2 < \varphi_{co})$

$$\begin{aligned} \varphi_{to} &= \frac{1}{1-p}\left(\frac{1+\mu}{2}\bar{\varepsilon}_{to} + \frac{1-\mu^2}{4}\right) \\ \varphi_{co} &= \frac{-1}{\mu+p}\left(\frac{1+\mu}{2}\bar{\varepsilon}_{co} + \frac{1-\mu^2}{4}\right) \end{aligned} \tag{3.39}$$

3.5 Column Curvature Curves

For a beam-column AB of length L which is subjected to an axial force P and bending moments M_A and M_B at the ends, there is an equivalent column of length L* which is subjected only to the axial

$$P^* = \sqrt{P^2 + \left(\frac{M_A - M_B}{L}\right)^2} \tag{3.40}$$

The beam-column AB is a part of its equivalent column A*B* as shown in Fig. 3.5. The proof is presented in Appendix 11.1.

Since the end curvatures Φ_A and Φ_B are known from end moments M_A and M_B, using the previously obtained moment-curvature-thrust relationship, the curvature distribution along the beam-column AB is determined if the curvature distribution of the equivalent column A*B* (the column curvature curves) is known (Fig. 3.6).

The column curvature curves were obtained in Chapter 2, and the procedure is briefly given here. There are five different types of equivalent columns as shown in Fig. 3.7. The governing equation of a beam-column is

$$\frac{d^2M}{ax^2} + k^2\Phi = 0 \tag{3.41}$$

in which

$$k = \sqrt{\frac{P^*}{EI}} \tag{3.42}$$

$$EI = \frac{Et^3}{12} \qquad \text{(bending rigidity)} \tag{3.43}$$

Using the previously derived moment-curvature-thrust relationships, (Eqs. 3.30, 3.31, and 3.32), Eq. 3.41 may be reduced to a set of differential equations in Φ and P only.

For each type of column shown in Fig. 3.7, the curvature φ is not solved explicitly. Instead kx is obtained as a function of φ. In the solution, the maximum curvature at the center φ_m^* is included as an integral constant. Details of the solution for each case have been reported in Chapter 2.

(a) Elastic Column $(\varphi_m^* \leq \varphi_1)$

$$kL^* = \pi\sqrt{a} \tag{3.44}$$

$$kx = \frac{kL^*}{2} - f_1\left(\sqrt{a},\ \varphi,\ \varphi_m^*,\ \frac{kL^*}{2}\right) \tag{3.45}$$

(b) One Side Plastic Column $(\varphi_1 < \varphi_m^* \leq \varphi_2)$

$$k\rho_1 = g\ (\sqrt{a},\ c,\ \varphi_1,\ \varphi_m^*)$$

$$kL^* = 2k\rho_1 + 2f_2\ (c,\ \varphi_m^*,\ \varphi_1) \tag{3.46}$$

$$kx = \begin{cases} \dfrac{kL^*}{2} - f_1\ (\sqrt{a},\ \varphi,\ \varphi_1,\ k\rho_1) & (\varphi \leq \varphi_1) \\ f_2\ (c,\ \varphi_m^*,\ \varphi) & (\varphi_1 < \varphi) \end{cases} \tag{3.47}$$

(c) Combined Plastic Column $(\varphi_2 < \varphi_m^*)$

$$\varphi_o = \left[\sqrt{\varphi_2} + \frac{2f}{c}\left(\frac{1}{\varphi_2} - \frac{1}{\varphi_m^*}\right)\right]^2$$

$$k\rho_1 = g\ (\sqrt{a},\ c,\ \varphi_1,\ \varphi_o)$$

$$kx_p = k\rho_1 + f_2\ (c,\ \varphi_o,\ \varphi_1) \tag{3.48}$$

$$k\rho_2 = kx_p - f_2\ (c,\ \varphi_o,\ \varphi_2)$$

$$kL^* = 2k\rho_2 + 2f_3\ (f,\ \varphi_2,\ \varphi_m^*)$$

$$kx = \begin{cases} \dfrac{kL^*}{2} - f_1\ (\sqrt{a},\ \varphi,\ \varphi_1,\ k\rho_1) & (\varphi \leq \varphi_1) \\ \dfrac{kL^*}{2} - kx_p + f_2\ (c,\ \varphi_o,\ \varphi) & (\varphi_1 < \varphi \leq \varphi_2) \\ f_3\ (f,\ \varphi,\ \varphi_m^*) & (\varphi_2 < \varphi) \end{cases} \tag{3.49}$$

where the functions are given by

$$f_1\ (\sqrt{a},\ \varphi,\ \varphi_1,\ k\rho) = \sqrt{a}\ \sin^{-1}\left(\frac{\varphi}{\varphi_1}\ \sin\frac{k\rho}{\sqrt{a}}\right)$$

$$f_2\ (c,\ \varphi_o,\ \varphi) = \sqrt{\frac{c}{2}}\ \varphi_o^{-3/4}\left[\sqrt{\frac{\varphi_o}{\varphi}\left(1-\sqrt{\frac{\varphi}{\varphi_o}}\right)} + \tanh^{-1}\sqrt{1-\sqrt{\frac{\varphi}{\varphi_o}}}\right]$$

$$f_3\ (f,\ \varphi,\ \varphi_m) = \frac{2}{3}\sqrt{\frac{f}{\varphi} - \frac{f}{\varphi_m}}\left(\frac{2}{\varphi_m} + \frac{1}{\varphi}\right) \tag{3.50}$$

$$g\ (\sqrt{a},\ c,\ \varphi_1,\ \varphi_m) = \sqrt{a}\ \tan^{-1}\frac{\sqrt{a}\ \varphi_1}{\sqrt{2c\ (\sqrt{\varphi_m}-\sqrt{\varphi_1})}}$$

Figure 3.8 shows a set of such column curvature curves obtained from Eqs. 3.44 to 3.50 for a wall of $\mu = 0$ and $p = 0.2$.

3.6 Method of Solution

If the maximum column curvature φ_m^* is known, the location x_A and x_B corresponding to the end curvatures φ_A and φ_B are obtained exactly from Eqs. 3.45, 3.47 and 3.50. The actual value of φ_m^* must be searched by iteration until the computed length L_{AB} between x_A and x_B becomes close to the length L of the beam-column.

$$L_{AB} \approx L \tag{3.51}$$

The length L_{AB} is computed in four different cases as shown in Fig. 3.9. In each case, the maximum curvature of the beam-column φ_m and its location x_m are given by the following equations.

(a) Single Curvature $(\varphi_A \varphi_B \geq 0)$

Type 1 $L_{AB} = x_B - x_A$

$$\varphi_m = \varphi_A, \; x_m = 0 \tag{3.52}$$

Type 2 $L_{AB} = x_B + x_A$

$$\varphi_m = \varphi_m^*, \; x_m = x_A \tag{3.53}$$

(b) Double Curvature $(\varphi_A \varphi_B < 0)$

Type 1 $L_{AB} = L^* - x_A - x_B$

$$\varphi_m = \varphi_A, \; x_m = 0 \tag{3.54}$$

Type 2 $L_{AB} = L^* + x_A - x_B$

$$\varphi_m = \varphi_m^*, \; x_m = x_A \tag{3.55}$$

In the above derivation, it is assumed (without loss of generality) that

$$\left| \varphi_B \right| \leq \varphi_A \tag{3.56}$$

3.7 Numerical Examples

Results of some numerical calculations are presented in Figs. 3.10 and 3.11. The ordinate is the axial force p and the abscissa is the maximum curvature of the wall φ_m. The p-φ_m planes are divided by the two dotted lines φ_1 and φ_2 into four regimes: the elastic regime, tension yield regime, compression yield regime and the combined yield regime. The thick solid lines represent load curvature curves for various slenderness ratios of h/t. Each curve consists of a loading portion and an unloading portion. The peak points indicate the stability limit of the walls. Strain limits are plotted by thin solid lines.

The stability limits (peak points)occur just after tension yield. Unloading takes place mostly in the combined yield regime except for tall walls with no tensile strength ($\mu = 0$, $h/t > 30$).

Figure 3.12 shows stability limits of walls with varying tensile strength ($\mu = 0$ to 1.0). It should be noted here that a small amount of tensile strength ($\mu = 0.1$) improves the strength of walls considerably. Thus the tensile yield stress should not be neglected in analysis of plain concrete or masonry walls.

Tensile yield stress greater than half of compressive yield stress ($\mu > 0.5$) has no effect except for very short walls ($h/t < 10$).

Figures 3.13 and 3.14 show the ultimate strength of a wall due to strain limits of $\mu = 0$ and $\mu = 0.1$ respectively. The thick solid line shows the stability limit. The dotted lines and thin solid lines represent crushing failure and cracking failure, respectively.

Crushing occurs only in shorter walls but cracking occurs in most walls. A small amount of ductility improves the strength of the wall considerably. This effect is noticeable especially during cracking in masonry wall (Fig. 3.13). Large ductility ($\epsilon_{to} > 0.5\ \epsilon_y$, $|\epsilon_{co}| > 2\epsilon_y$) has little effect on strength of walls.

Figure 3.15 shows the stability limit of a wall ($\mu = 0$ and 0.1) against different types of loading. The parameter α is ratio of end moments ($\alpha = m_B/m_A$). Three loading cases are investigated: symmetric loading ($\alpha = 1$), one moment loading ($\alpha = 0$) and antisymmetric loading ($\alpha = -1$).

The strength of the wall under unsymmetric loading ($\alpha = 0, -1$) is considerably greater than that in the symmetric case. This is because of the difference in the critical length. Also, in these cases, the plastic hinge occurs at an end and the strength becomes constant when the wall is short (Fig. 3.15).

3.8 Comparison with Reported Results

In Ref. 10 ultimate strengths of walls are reported. The material has no tensile strength ($\mu = 0$). The compressive strain limit

is the same as the initial yield strain ($\varepsilon_{co} = -\varepsilon_y$) and the tensile strain limit is not defined ($\varepsilon_{to} = \infty$). The loading is symmetric ($\alpha = 1$) but eccentricity of the axial force is variable (e = t/6 and e = t/3 are taken in the example). The yield strain is $\varepsilon_y = 0.001215$ in pure compression. Strength in flexure is 1.6 times the strength in pure compression ($\varepsilon_y = 0.001944$). Results of Ref. 10 are plotted by circles in Fig. 3.16.

To recompute these results using the approach here, the ultimate strength of the walls is investigated in four cases (Examples--AO, DO, AO', DO' in Table 3.1). In Fig. 3.16, the solid curves (a) and (b) represent stability limits of the walls with $\varepsilon_y = 0.001215$ and $\varepsilon_y = 0.001944$, respectively. Since there are strain limits ($\varepsilon_{co} = -\varepsilon_y$), the strengths are reduced to the dotted lines (a') and (b'). Applying the factor 1.6 to the p-value of curve (b'), the crushing strength curve (c) is obtained. The ultimate strength is represented by the stability part of curve (a) and crushing part of curve (c). Figure 3.16 shows good agreement between the two results in both cases of eccentricity.

3.9 Summary

A method to analyze strength of walls of general materials is presented. An elastic-perfectly plastic material is considered. The yield stresses and limit strains in tension and compression may be different. In the analysis, the column-curvature-curve method is used.

The loadings are axial compression and bending moments at the ends, which may be unsymmetric. Further, the end moments are not

necessarily due to eccentricity of the axial force, they may be applied independently.

The small tensile strength and ductility of plain concrete or masonry are found to have a significant effect on the strength of walls and should not be neglected in analysis. For plain concrete or masonry walls, compressive ductility greater than twice the initial yield strain ϵ_y and tensile ductility greater than half the initial yield strain ϵ_y are desirable features.

A good agreement was observed in some special cases with other reported results.

4. SIMPLE INTERACTION EQUATIONS FOR IN-PLANE BEAM-COLUMNS

4.1 Introduction

In most reference works [28,29] on the approximate theory of beam-column problems the axis of the deflected beam-column is often assumed to be a certain shape of curve, such as a sine curve or a parabolic curve. As a consequence of this, the analysis of beam-column problems is considerably simplified. Simple interaction equations which define the load carrying capacity of the beam-column can then be obtained. It has been found [1, 8] that this simplification gives satisfactory results for simply supported beam-columns under symmetric loading conditions. It is clear, however, that this type of simplification is not very suitable for the fast determination of beam-column strength for unsymmetric cases or for the case of beam-column with fixed end supports.

The work reported in this paper is an effort to help fill part of this gap. Toward this purpose, an alternate but extremely simple approximate analysis is developed and applied to various beam-column problems.

In the analysis, the moment-curvature-thrust relationship is idealized as elastic-perfectly plastic. The moment-curvature relationship for a constant thrust is assumed to be linear up to a certain moment level M_{mc}. From here on the section is assumed to flow plastically at the constant moment M_{mc} (Fig. 4.1). The adoption of this idealized relationship must not be thought of as neglecting curvature work-hardening, but rather as averaging its effect over the entire beam-column. The

appropriate average flow moment M_{mc} must lie between the initial yield moment M_{yc} and the plastic limit moment M_{pc} of the cross section (Fig. 4.1). The choice of the level M_{mc} is dependent on the section used as well as on the geometry and loading of the entire beam-column. Once the proper value of M_{mc} is selected, the maximum load carrying capacity of beam-columns can be computed in a rather simple manner by an elastic analysis. The subsequent discussion in this chapter shows how this average flow moment M_{mc} may be determined.

4.2 Estimation of Average Flow Moment

All beam-columns to be considered are assumed to be made of an ideally plastic material which is elastic up to the yield point and then flows under constant stress. The corresponding moment-curvature-thrust relationship of a common structural section with or without the influence of residual stress is shown by the curve O-E-F in Fig. 4.1. The curve may be divided into two parts: Linear elastic part (O-E) with an initial yield moment M_{yc} and curvature work-hardening part (E-F), with the moment asymptotically approaching the limit value M_{pc} as curvature φ tends to infinity. If M_{yc} is used for the idealized flow moment, the ultimate strength of a beam-column will be lower than the actual one, on the other hand, if M_{pc} is used, the solution will be an upper bound. The exact solution is thus bounded by the two extreme solutions. A satisfactory selection of the average flow moment M_{mc} will therefore enable the estimation of the ultimate strength of the beam-column with high accuracy.

The yield moment M_{yc} and the plastic limit moment M_{pc} for a constant thrust P have been obtained in Refs. 5,6 for several commonly

used structural sections. As an example, the expression for strong axis bending of a wide flange section including the influence of residual stress is

$$\frac{M_{yc}}{M_y} = \begin{cases} 0.9 - \left(\frac{P}{P_y}\right) & \left(\frac{P}{P_y} \leq 0.8\right) \\ -1.1 + 3.1\left(\frac{P}{P_y}\right) - 2\left(\frac{P}{P_y}\right)^2 & \left(\frac{P}{P_y} \geq 0.8\right) \end{cases}$$

$$\frac{M_{pc}}{M_y} = \begin{cases} 1.11 - 2.64\left(\frac{P}{P_y}\right)^2 & \left(\frac{P}{P_y} \leq 0.225\right) \\ 1.238 - 1.143\left(\frac{P}{P_y}\right) - 0.095\left(\frac{P}{P_y}\right)^2 & \left(\frac{P}{P_y} \geq 0.225\right) \end{cases} \qquad (4.1)$$

where P is the applied thrust, P_y is the yield thrust, and M_y is the yield moment in the absence of the thrust P.

Since the average flow moment M_{mc} must lie between the values M_{yc} and M_{pc}, the value of M_{mc} may be represented by

$$M_{mc} = M_{pc} - f\,(M_{pc} - M_{yc}) \qquad (4.2)$$

where f is a parameter function

f = 0 corresponds to $M_{mc} = M_{pc}$ (the upper bound solution)

f = 1 corresponds to $M_{mc} = M_{yc}$ (the lower bound solution)

The parameter f will be a function of the thrust P, the lenght L and the boundary conditions of a beam-column. For simplicity, the parameter function f is assumed to have the form

$$f = f_1 \left(\frac{P}{P_y}\right) f_2 \left(\frac{L}{r}\right) f_3 \text{ (B.C.)} \qquad (4.3)$$

the functions f_1, f_2, and f_3 need to be determined for each type of beam-column.

Example 1 Beam-Column with an Uniformly Distributed Lateral Load (Fig. 4.2a)

If $P/P_y = 0$, it is a beam problem and the plastic limit moment M_{pc} will govern the ultimate state, i.e., $f = 0$. If $P/P_y \approx 1$, it is an axially loaded short column problem and the yield moment M_{yc} will be the governing one, i.e., $f = 1$. The elastic solution [see Ref. 2] using $f = 0$ and $f = 1$ then gives the upper- and lower-bound interaction plot shown in Fig. 4.3. The solution $f = f_1 = P/P_y$ (assuming $f_2 = 1.0$, $f_3 = 1.0$) is found to be in good agreement with the exact solution reported in Ref. 9 . The approximate solution can be improved by taking $f = f_1 = (P/P_y)^{0.6}$. The improved result is plotted as small circles in Fig. 4.3 and gives a very good approximation to the exact solution. Therefore, it seems reasonable to assume that the function f_1 has the general form

$$f_1 \left(\frac{P}{P_y}\right) = \left(\frac{P}{P_y}\right)^N \qquad (4.4)$$

Consider, next, the second parameter f_2 (L/r), where L/r is the slenderness ratio of the beam-column. If the member is very short, it will lose the nature of a column, and the value of f should be close to 0. By comparison with the exact solution, the following formula is an appropriate one as a correction for short beam-columns.

$$f_2\left(\frac{L}{r}\right) = \begin{cases} 1 & \left(\frac{L}{r} \geq 60\right) \\ \frac{1}{40}\left(\frac{L}{r}\right) - \frac{1}{2} & \left(20 \leq \frac{L}{r} < 60\right) \\ 0 & \left(\frac{L}{r} < 20\right) \end{cases} \tag{4.5}$$

Usually, the slenderness ratio of a column is greater than 60, so that $f_2(L/r)$ may be chosen as unity.

The third parameter $f_3(B.C.)$ is determined based on boundary conditions. If a beam-column is fixed, plastic hinges will form at the ends first as shown in Fig. 4.4a. Until the third (and the last) plastic hinge forms at center C, large rotations will have been experienced at the previously formed plastic hinges at both ends. At the ultimate state, the moments at both ends will be close to M_{pc} and the moment at center C will be close to M_{yc}. Therefore, the mean value of M_{yc} and M_{pc} will be one of the approximate values of M_{mc}; or $f_3(\text{fixed}) = 0.5$. On the other hand, if the beam-column is simply supported, M_{yc} will be the governing flow moment; $f_3(\text{simple}) = 1.0$.

In summary, for a beam-column of usual length ($L/r \geq 60$), M_{mc} has the form

$$M_{mc} = \begin{cases} M_{pc} - \frac{P}{P_y}\left(M_{pc} - M_{yc}\right) & \text{(simply supported)} \\ M_{pc} - 0.5\,\frac{P}{P_y}\left(M_{pc} - M_{yc}\right) & \text{(fixed end)} \end{cases} \tag{4.6}$$

Using the average flow moment M_{mc} in Eq. 4.6, the ultimate load w of the beam-column shown in Fig. 4.2a can be computed by the formula [2]:

$$Q = wL = k\, M_{mc}\, kL\, \frac{\lambda + \cos\frac{kL}{2}}{1 - \cos\frac{kL}{2}} \tag{4.7}$$

where

$$k^2 = \frac{P}{EI}$$

and $\lambda = 0$ for simple supports and $\lambda = 1$ for fixed ends.

Using the proposed values, a comparison is made with the exact solution of a beam-column of a wide flange section (8 W 31) with residual stresses and shown in Fig. 4.5 (simply supported) and Fig. 4.6 (fixed ends). The solid lines are exact solutions reported in Ref. 9, and the dotted lines are results obtained by the present method. They show a sufficiently good agreement with each other. In case of simply supported beam-columns, however, an approximation by N = 0.6 gives a better result as plotted by small circles in Fig. 4.5.

Example 2 Beam-Column with a Concentrated Lateral Load (Fig. 4.2b)

The parameter f for the average flow moment M_{mc} will be the same as in the case of a uniform load. For a fixed end beam-column, since plastic hinges will be formed at both ends and under the load at the same time (Fig. 4.4b), the governing flow moment will still be the mean value of M_{yc} and M_{pc}, i.e., f_3(fixed) = 0.5

Using the average flow moment M_{mc} in Eq. 4.6, the ultimate load Q of the beam-column shown in Fig. 4.2b can be computed by the formula:

$$Q = 2k\, M_{mc}\, \frac{\lambda + \cos\frac{kL}{2}}{\sin\frac{kL}{2}} \tag{4.8}$$

Comparison with the exact solution [9] is shown in Fig. 4.7 (simply supported) and Fig. 4.8 (fixed ends). A good agreement is observed in both cases. Eq. 4.8 can be rewritten in the form:

$$Q_s = 2k\, M_{mc}\, \cot\frac{kL}{2} \qquad \text{(simply supported)} \tag{4.9}$$

$$Q_f = 2k\, M_{mc}\, \cot\frac{kL}{4} \qquad \text{(fixed end)} \tag{4.10}$$

It is seen that in these two cases equations are analogous to each other (note: the values of M_{mc} are different, see Eq. 4.6), and the ultimate strength for a beam-column with both ends fixed (Eq. 4.10) may be computed from the beam-column with hinged ends having a reduced length equal to half the actual length. (It is evident from symmetry that this conclusion is true for the actual situation).

Referring now to the partially distributed load cases represented in Fig. 4.2(c) and proceeding as for an elastic solution with plastic hinges, one finds the following expressions for the ultimate lateral load:

$$Q = wC = 2k\, M_{mc}\, \frac{\frac{kC}{4}}{\sin\frac{kC}{4}}\, \frac{\lambda + \cos\frac{kL}{2}}{\sin\left(\frac{kL}{2} - \frac{kC}{4}\right)} \tag{4.11}$$

where M_{mc} is given by Eq. 4.6. As can be seen here, the ultimate load for the fully distributed load case (Eq. 4.7) and the concentrated load case (Eq. 4.8) are particular cases of Eq. 4.11.

Example 3 Beam-Column with End-Moments (Fig. 4.2d)

Consider, next, a beam-column subjected to end moments M_o and κM_o as shown in Fig. 4.2d. The average plastic moment M_{mc} is assumed in a similar form as before:

$$M_{mc} = M_{pc} - \left(\frac{P}{P_y}\right)^N (M_{pc} - M_{yc}) \tag{4.12}$$

Here, N = 1/2 gives a good approximation for M_{mc}. A plastic hinge occurs either within the span or at one of the end supports depending upon the ratio of applied moments κ. The ultimate moment M_o is given by the following formulae [2];

$$\text{if} \quad \kappa \leq \cos kL$$

$$M_o = M_{mc} \tag{4.13}$$

$$\text{if} \quad \kappa \geq \cos kL$$

$$M_o = M_{mc} \frac{\sin kL}{\sqrt{\sin^2 kL + (\kappa - \cos kL)^2}}$$

Comparison with exact solutions obtained in Chapter 2 is shown in Fig. 4.9 (κ = 1). Results by the present method (dotted lines) are computed using N = 1/2. A sufficiently good agreement is observed.

4.3 Unsymmetrically Loaded Beam-Columns

The average flow moment M_{mc} for a symmetrically loaded beam-column has been obtained in the previous section. This result (Eq. 4.6) is considered to be applicable to unsymmetric problems as well, if the unsymmetry is not very large.

The ultimate concentrated load applied unsymmetrically to a beam-column (Fig. 4.2e) is computed by assuming that the last plastic hinge is formed under the load. It has the form

$$Q = 2k\, M_{mc} \sin \frac{kL}{2} \frac{\lambda \cos \frac{kL_A - kL_B}{2} + \cos \frac{kL}{2}}{\sin kL_A \sin kL_B} \tag{4.14}$$

In case of partially distributed load (Fig. 4.2f), the expression for ultimate strength becomes lengthy (see Appendix 11.3), but a simple form of analogous solution can be based on the results for the symmetrically distributed case (Eq. 4.11), and the unsymmetrically concentrated load case (Eq. 4.14) as

$$Q = 2k\, M_{mc} \frac{\frac{kC}{4}}{\sin \frac{kC}{4}} \sin \left(\frac{kL}{2} - \frac{kC}{4}\right) \frac{\lambda \cos \frac{kL_A - kL_B}{2} + \cos \frac{kL}{2}}{\sin\left(kL_A - \frac{kC}{4}\right) \sin\left(kL_B - \frac{kC}{4}\right)} \tag{4.15}$$

This is considered to be the most general form of solution for a laterally loaded beam-column, as it covers the ultimate value of a symmetrically distributed load ($L_A = L_B = L/2$), Eq. 4.11, or a concentrated load ($C = 0$), Eq. 4.14.

Accuracy of Eq. 4.15 is investigated by comparing with the elastic solution (Eqs. 4.25 to 4.29) presented in Appendis 11.3, where the location of plastic hinge is computed exactly. In Fig. 4.10 to 4.13, the comparison of interaction relationships between thrust P and lateral load Q is made. Diagrams drawn to the right represent the loaction of the last plastic hinge.

In the case of uniform load of width L/3 (Figs. 4.10 and 4.11) some difference is observed between the two solutions. If the eccentricity of the load is less than L/6, the error remains within 5% and for e = L/4, it is 13%. Location of the plastic hinge moves in as P increases, and when P reaches the critical value P_{cr} (Euler's buckling load) the hinge is formed at the center, in this state the allowable lateral load Q is zero as seems to be obvious.

In the case of concentrated load (Fig.s 4.12 and 4.13), results by Eq. 4.15 check very well even for large eccentricity of loading. The location of the plastic hinge does not move until P reaches certain values, then it moves in as P increases following a curve shown in the right diagram of Fig. 4.12. It is interesting to note that this curve is common for all values of eccentricity of loading.

4.4 Summary

The ultimate strengths of beam-columns are obtained in simple closed forms. Although they are approximate solutions, their validity has been shown by comparison with exact solutions in symmetrically loaded cases. This validity is considered to be true in unsymmetric cases also provided the unsymmetry is not very large. The formulas for the ultimate

strength of beam-columns may be considered as suitable bases for a method of design for symmetrically as well as unsymmetrically loaded compression members.

5. INTERACTION RELATIONS OF BIAXIALLY LOADED SYMMETRIC SECTIONS

5.1 Introduction

A biaxial interaction relationship of rectangular and wide-flange sections has been reported [13,14]. In Ref. 14, a procedure is presented for deriving approximate lower bound interaction equations in terms of axial force, torsional moment and biaxial bending moments. In Ref. 13, the accuracy of the solution was checked by limit analysis, and the interaction relation was presented for several different cases based on the location of the neutral axis. In that paper two Lagrange multipliers were used to solve the variational problem in the case of the lower bound solution. Since the two multipliers have no specific physical meaning, the solutions derived in the several different cases could be verified only numerically.

Herein, two independent parameters with physical meanings are chosen. As a consequence, only one equation is needed for all possible cases and its exactness will be shown in what follows. This approach gives exact interaction relations and is applicable to any cross section doubly symmetrical.

Using the exact interaction relation, the ultimate strength of biaxially loaded column could be found. In order to get an analytical solution, simple interaction equations are desired. This is done by curve fitting and it is found that interaction relations of wide-flange sections can be expressed by two simple equations with four constants which are dependent on the size of the section.

5.2 Exact Interaction Relations for a Rectangular Section

Consider a rectangular section of width 2b and depth 2d as shown in Fig. 5.1. If the section is fully plastified, the normal stress can be assumed to be $-\sigma_y$ above the neutral axis (N.A.) and $+\sigma_y$ below the N.A. without loss of generality. Only axial stress is considered and the effect of shear stress on the yielding is neglected.

The location of the N.A. can be determined by two independent parameters: the vertical distance e and the angle with the horizontal axis θ. The resultant forces of the section are obtained uniquely as functions of e and θ:

$$P = f_p(e,\theta): \text{ Axial force} \tag{5.1}$$

$$M_x = f_x(e,\theta): \text{ Moment about horizontal axis} \tag{5.2}$$

$$M_y = f_y(e,\theta): \text{ Moment about vertical axis} \tag{5.3}$$

These functions are to be determined by the two limit analyses: the lower bound analysis and the upper bound analysis. The resulting functions, derived in the succeeding sections, are the same and hence exact.

5.2.1 Lower Bound Analysis

Since the state of stress given in Fig. 5.1 satisfies the yield condition and the equilibrium conditions, integration of stress over the section gives a lower bound solution for the biaxial bending forces.

The rectangular section can be divided into three parts: P-1, P-2 and P-3 by the neutral axis (N.A.) and a straight line N.B.

as shown in Fig. 5.2. Lines N.B. and N.A. are symmetric with respect to the origin. From symmetry with respect to both the x-axis and y-axis, the part P-2 contributes only to the axial force P and the parts P-1 and P-3 contribute only to bending moments M_x and M_y. The axial force P and the bending moment M_x and M_y are considered positive when the axial force causes tension and the bending moments produce compressive stress in the first quadrant of the coordinate system shown. Then the three resultant forces can be expressed as

$$P = \sigma_y A_2 \tag{5.4}$$

$$M_x = \sigma_y A_1 e_{y1} + \sigma_y A_3 e_{y3} \tag{5.5}$$

$$M_y = \sigma_y A_1 e_{x1} + \sigma_y A_3 e_{x3} \tag{5.6}$$

where A_1, A_2 and A_3 are areas of parts P-1, P-2 and P-3, respectively, and e_{xj} and e_{yj} are the centroidal coordinates of portion P-j

$$(e_{x2} = e_{y2} = 0)$$

From symmetry again,

$$A_3 = A_1 \tag{5.7}$$

$$e_{x3} = e_{x1} \tag{5.8}$$

$$e_{y3} = e_{y1} \tag{5.9}$$

Thus

$$A_2 = A - 2A_1 \tag{5.10}$$

where A = 4bd is total area of the rectangular section.

Equations 5.4, 5.5 and 5.6 become

$$P = \sigma_y A_2 = \sigma_y A_p \tag{5.11}$$

$$M_x = 2\sigma_y A_1 e_{y1} = \sigma_y Q_x \tag{5.12}$$

$$M_y = 2\sigma_y A_1 e_{x1} = \sigma_y Q_y \tag{5.13}$$

where

$$A_p = A - 2A_1 \tag{5.14}$$

$$Q_x = 2A_1 e_{y1} \tag{5.15}$$

$$Q_y = 2A_1 e_{x1} \tag{5.16}$$

In order to express A_1, e_{x1} and e_{y1} in terms of the two parameters e and θ, let us define a pair of parentheses which have the meaning

$$\langle S \rangle = \begin{cases} 0 & (S \leq 0) \\ S & (S \geq 0) \end{cases} \tag{5.17}$$

or in a single expression

$$\langle S \rangle = \frac{S + |S|}{2} \tag{5.18}$$

Considering the part P-1, there are three different cases possible as shown in Fig. 5.3. For each case, the area and centroid can be obtained using the specially defined parentheses:

Part 4

$$A_4 = \frac{1}{2} \langle b \tan\theta + d - e \rangle^2 \cot\theta \tag{5.19}$$

$$e_{y4} = \frac{1}{3} (-b \tan\theta + 2d + e) \tag{5.20}$$

$$e_{x4} = \frac{1}{3} (2b \tan \theta - d + e) \cot \theta \tag{5.21}$$

Part 5

$$A_5 = \frac{1}{2} \langle b \tan \theta + d - e \rangle^2 \cot \theta \tag{5.22}$$

$$e_{y5} = \frac{1}{3} (b \tan \theta + 2d + e) \tag{5.23}$$

$$e_{x5} = \frac{1}{3} (2b \tan \theta + d - e) \cot \theta \tag{5.24}$$

Part 6

$$A_6 = \frac{1}{2} \langle b \tan \theta - d - e \rangle^2 \cot \theta \tag{5.25}$$

$$e_{y6} = \frac{1}{3} (b \tan \theta + 2d - e) \tag{5.26}$$

$$e_{x6} = \frac{1}{3} (2b \tan \theta + d + e) \cot \theta \tag{5.27}$$

and

$$A_1 = A_4 - A_5 - A_6 \tag{5.28}$$

$$A_1 e_{x1} = A_4 e_{x4} + A_5 e_{x5} - A_6 e_{x6} \tag{5.29}$$

$$A_1 e_{y1} = A_4 e_{y4} - A_5 e_{y5} + A_6 e_{y6} \tag{5.30}$$

Equations 5.14, 5.15 and 5.16 become

$$A_p = 4bd - \langle b \tan \theta + d - e \rangle^2 \cot \theta + \langle -b \tan \theta + d - e \rangle^2 \cot \theta + \langle b \tan \theta - d - e \rangle^2 \cot \theta \tag{5.31}$$

$$Q_x = \frac{1}{3}\langle b \tan\theta + d - e\rangle^2 \,(-b \tan\theta + 2d + e)\cot\theta$$

$$- \frac{1}{3}\langle -b \tan\theta + d - e\rangle^2 \,(b \tan\theta + 2d + e)\cot\theta \qquad (5.32)$$

$$+ \frac{1}{3}\langle b \tan\theta - d - e\rangle^2 \,(b \tan\theta + 2d - e)\cot\theta$$

$$Q_y = \frac{1}{3}\langle b \tan\theta + d - e\rangle^2 \,(2b \tan\theta - d + e)\cot^2\theta$$

$$+ \frac{1}{3}\langle -b \tan\theta + d - e\rangle^2 \,(2b \tan\theta + d - e)\cot^2\theta \qquad (5.33)$$

$$- \frac{1}{3}\langle b \tan\theta - d - e\rangle^2 \,(2b \tan\theta + d + e)\cot^2\theta$$

Define the non-dimensional forces as

$$p = \frac{P}{P_y} \quad , \quad m_x = \frac{M_x}{M_{px}} \quad , \quad m_y = \frac{M_y}{M_{py}} \qquad (5.34)$$

in which

$$P_y = \sigma_y A \quad , \quad M_{px} = \sigma_y Z_x \quad , \quad M_{py} = \sigma_y Z_y \qquad (5.35)$$

Therefore

$$p = \frac{A_p}{A} \quad , \quad m_x = \frac{Q_x}{Z_x} \quad , \quad m_y = \frac{Q_y}{Z_y} \qquad (5.36)$$

in which

$$A = 4bd \quad \text{total area of the section} \qquad (5.37)$$

$$Z_x = 2bd^2 \quad \text{plastic section modulus about x-axis} \qquad (5.38)$$

$$Z_y = 2b^2 d \quad \text{plastic section modulus about y-axis} \qquad (5.39)$$

The resultant forces p, m_x and m_y have now been expressed as functions of e and θ. The values of θ is valid in the region

$$0^\circ \leq \theta \leq 90^\circ \qquad (5.40)$$

5.2.2 Upper Bound Analysis

An upper bound solution can be obtained by equating the internal rate of energy dissipation $\dot{D}_I$ due to an assumed strain field $\dot{\epsilon}$ to the rate of external work $\dot{W}_E$ due to the increments of the resultant forces $\dot{P}$, $\dot{M}_x$ and $\dot{M}_y$.

Assume the rate of strain field as (Fig. 5.4)

$$\dot{\epsilon} = - \dot{\eta} \dot{\kappa} \tag{5.41}$$

in which η is the distance from fiber to the N.A.

The rate of internal dissipation is

$$\dot{D}_I = \int_A \sigma \dot{\epsilon} \, dA = \sigma_y \dot{\kappa} \left[\int_{A1} \eta \, dA - \int_{A2} \eta \, dA - \int_{A3} \eta \, dA \right] \tag{5.42}$$

$$= \sigma_y \dot{\kappa} \, (\eta_1 A_1 + \eta_2 A_2 + \eta_3 A_3)$$

in which η_i is the distance from the neutral axis N.A. to the centroids of the part P-i in η coordinate and

$$\eta_3 = 2\eta_2 + \eta_1 \, , \quad A_3 = A_1 \tag{5.43}$$

From Fig. 5.5, η_1 and η_2 are related to e, θ, e_{x1} and e_{y1} as

$$\begin{aligned} \eta_1 &= e_{x1} \sin \theta + e_{y1} \cos \theta - e \cos \theta \\ \eta_2 &= e \cos \theta \end{aligned} \tag{5.44}$$

and the dissipation becomes

$$\dot{D}_I = \sigma_y \dot{\kappa} [2\eta_1 A_1 + (2A_1 + A_2) \eta_2]$$

$$= \sigma_y \dot{\kappa} (2A_1 e_{x1} \sin\theta + 2A_1 e_{y1} \cos\theta + A_2 e \cos\theta) \quad (5.45)$$

The rate of external work is

$$\dot{W}_E = \dot{\epsilon}_o P + \dot{\kappa}_x \dot{M}_x + \dot{\kappa}_y M_y \quad (5.46)$$

where

$$\dot{\epsilon}_o = \text{strain rate at the centroid 0} \quad (5.47)$$

$$\dot{\kappa}_x = \text{curvature rate about x-axis} \quad (5.48)$$

$$\dot{\kappa}_y = \text{curvature rate about y-axis} \quad (5.49)$$

and

$$\dot{\epsilon}_o = \dot{\kappa} e \cos\theta \quad (5.50)$$

$$\dot{\kappa}_x = \dot{\kappa} \cos\theta \quad (5.51)$$

$$\dot{\kappa}_y = \dot{\kappa} \sin\theta \quad (5.52)$$

Then

$$\dot{W}_E = \dot{\kappa} (P e \cos\theta + M_x \cos\theta + M_y \sin\theta) \quad (5.53)$$

Equating the rate of internal energy dissipation to the rate of external work, $\dot{W}_E = \dot{D}_I$, one obtains

$$P\ e \cos\theta + M_x \cos\theta + M_y \sin\theta$$

$$= \sigma_y (A_2\ e \cos\theta + 2A_1\ e_{y1} \cos\theta + 2A_1\ e_{x1} \sin\theta) \tag{5.54}$$

Equation 5.54 must be valid for all values of e and θ. It follows that

$$P = \sigma_y A_2$$

$$M_x = 2\sigma_y\ e_{y1}\ A_1 \tag{5.55}$$

$$M_y = 2\sigma_y\ e_{x1}\ A_1$$

which is identical to Eqs. 5.11 to 5.13 from the lower bound analysis. Therefore, it can be concluded that the solution is exact.

5.3 Exact Interaction Relations for Double-Web Sections

A double web section as shown in Fig. 5.6 is a general case, and Eqs. 5.31 to 5.33 and 5.37 to 5.39 can be extended to the general case. The function A_p for the general case, for example, can be obtained by first finding the functions $A_p\ (b_o,d_o)$, $A_p\ (b_o, d_1)$, $A_p\ (b_1,d_1)$, and $A_p\ (b_2,d_1)$ corresponding to the rectangular sections $2b_o \times 2d_o$, $2b_o \times 2d_1$, $2b_1 \times 2d_1$, and $2b_2 \times 2d_1$, respectivley. The function A_p for the double web section is then obtained by the simple algebraic summation,

$$A_p = A_p(b_o,d_o) - A_p(b_o,d_1) + A_p(b_1,d_1) - A_p(b_2,d_1) \tag{5.56}$$

similarly,

$$Q_x = Q_x(b_o,d_o) - Q_x(b_o,d_1) + Q_x(b_1,d_1) - Q_x(b_2,d_1) \tag{5.57}$$

$$Q_y = Q_y(b_o,d_o) - Q_y(b_o,d_1) + Q_y(b_1,d_1) - Q_y(b_2,d_1) \tag{5.58}$$

$$A = 4\,(b_o\,d_o - b_o\,d_1 + b_1\,d_1 - b_2\,d_1) \tag{5.59}$$

$$Z_x = 2\,(b_o\,d_o^2 - b_o\,d_1^2 + b_1\,d_1^2 - b_2\,d_1^2) \tag{5.60}$$

$$Z_y = 2\,(b_o^2\,d_o - b_o^2\,d_1 + b_1^2\,d_1 - b_2^2\,d_1) \tag{5.61}$$

Particular cases may then be handled using these equations and the special properties in each case.

Rectangular Section (B x D)

$$b_o = \frac{1}{2}B \quad , \quad b_1 = \frac{1}{2}B \quad , \quad b_2 = 0$$
$$d_o = \frac{1}{2}D \quad , \quad d_1 = 0 \tag{5.62}$$

Box Section (B x D, t_f, t_w)

$$b_o = \frac{1}{2}B \quad , \quad b_1 = \frac{1}{2}B \quad , \quad b_2 = \frac{1}{2}B - t_w$$
$$d_o = \frac{1}{2}D \quad , \quad d_1 = \frac{1}{2}D - t_f \tag{5.63}$$

Wide-Flange Section (B x D, t_f, t_w)

$$b_o = \frac{1}{2}B \quad , \quad b_1 = \frac{1}{2}t_w \quad , \quad b_2 = 0$$
$$d_o = \frac{1}{2}D \quad , \quad d_1 = \frac{1}{2}D - t_f \tag{5.64}$$

5.4 Exact Interaction Relations for a Circular Section

Consider a solid circular section of radius r as shown in Fig. 5.7. The neutral axis (N.A.) is at a distance e from the center and makes an angle θ with x-axis. The part P-1 above the N.A. is assumed to be fully stressed by σ_y. The area and centroid of this portion are given by

$$A_1 = r^2 \left(\varphi - \frac{1}{2} \sin 2\varphi\right) \tag{5.65}$$

$$e_{x1} = \frac{1}{2} r \sin\theta \frac{\sin\varphi - \frac{1}{3}\sin 3\varphi}{\varphi - \frac{1}{2}\sin 2\varphi} \tag{5.66}$$

$$e_{y1} = \frac{1}{2} r \cos\theta \frac{\sin\varphi - \frac{1}{3}\sin 3\varphi}{\varphi - \frac{1}{2}\sin 2\varphi} \tag{5.67}$$

where

$$\varphi = \cos^{-1} \frac{\bar{e}}{r} \tag{5.68}$$

$$\frac{\bar{e}}{r} = \begin{cases} \frac{e}{r} & \left(\frac{e}{r} \leq 1\right) \\ 1 & \left(\frac{e}{r} \geq 1\right) \end{cases} \tag{5.69}$$

or

$$\frac{\bar{e}}{r} = 1 - \left\langle 1 - \frac{e}{r} \right\rangle \tag{5.70}$$

and the corresponding quantities are derived as

$$A_p(r) = A - 2A_1 = \pi r^2 - 2r^2 \left(\varphi - \frac{1}{2}\sin 2\varphi\right) \tag{5.71}$$

$$Q_x(r) = 2A_1 e_{y1} = r^3 \cos\theta \left(\sin\varphi - \frac{1}{3}\sin 3\varphi\right) \tag{5.72}$$

$$Q_y(r) = 2A_1 \, e_{x1} = r^3 \sin\theta \, (\sin\varphi - \frac{1}{3}\sin 3\varphi) \tag{5.73}$$

and

$$A = \pi r^2 \tag{5.74}$$

$$Z_x = \frac{4}{3} r^3 \tag{5.75}$$

$$Z_y = \frac{4}{3} r^3 \tag{5.76}$$

Using Eqs. 5.71 to 5.76, the corresponding expressions for a hollow circular section of external radius r_o and internal radius r_i can be obtained (Fig. 5.8)

$$A_p = A_p(r_o) - A_p(r_i) \tag{5.77}$$

$$Q_x = Q_x(r_o) - Q_x(r_i) \tag{5.78}$$

$$Q_y = Q_y(r_o) - Q_y(r_i) \tag{5.79}$$

and

$$A = \pi \, (r_o^2 - r_i^2) \tag{5.80}$$

$$Z_x = \frac{4}{3} \, (r_o^3 - r_i^3) \tag{5.81}$$

$$Z_y = \frac{4}{3} \, (r_o^3 - r_i^3) \tag{5.82}$$

5.5 Numerical Results

Figures 5.9, 5.10 and 5.11 show numerical results for a wide-flange section, a double web section, and a hollow circular section, respectively. Referring to curves for the wide-flange section, W14x426 (Fig. 5.9), the solid lines represent the present exact solutions and

the dotted lines are the results reported previously by Santathadaporn and Chen [13]. It is seen that they are practically identical to each other except in a small region. This small difference results from the fact that in Ref. 13 it is assumed that the N.A. cuts through the web horizontally as shown in Fig. 5.12a.

Furthermore, in Ref. 13 the case where the N.A. cuts through an edge of the flange plate was omitted (Fig. 5.12a). As a consequence, a sharp corner appears on each of the interaction curves. Such corners do not show up on the exact interaction curves as one can see in the figure.

It should be noted that the present solution is exact only for the idealized wide-flange shape (Fig. 5.12b). An actual wide-flange shape has, of course, rounded corners and edges (Fig. 5.12c), not accounted for in this paper. Hence, emphasis must not be put on its exactness, but rather, on its simplicity in calculations.

5.6 Simple Interaction Equations for Wide-Flange Sections

In order to handle the interaction relation analytically, simple interaction equations are required. As a general form of the interaction equation, assume

$$\frac{m_x^{\alpha}}{1 - p^{\beta}} + \frac{m_y^{\mu}}{1 - p^{\nu}} + p^{\gamma} = 1 \qquad (5.83)$$

where α, β, γ, μ and ν are constants to be determined from the exact interaction relation. For most wide-flange sections, it is found that good agreement results when $\mu = 1$ and $\nu = \infty$.

When the strong axis bending moment M_x is large, the weak axis bending moment M_y has little effect on the interaction as shown in Fig. 5.9. Hence, the following two equations are assumed as the interaction equations for wide-flange sections

$$f_1 (m_x, m_y, p) = \frac{m_x^{\alpha}}{1 - p^{\beta}} + m_y + p^{\gamma} - 1 = 0$$

$$f_2 (m_x, m_y, p) = m_x + d^{\delta} - 1 = 0 \qquad (5.84)$$

The actual interaction equation, $f(m_x, m_y, p) = 0$, is given by

$$f = f_1 (m_x, m_y, p) \qquad (\text{when } m_y \geq \bar{m}_y)$$

$$f = f_2 (m_x, m_y, p) \qquad (\text{when } m_y \leq \bar{m}_y) \qquad (5.85)$$

and

$$\bar{m}_y = 1 - p^{\gamma} - \frac{(1 - p^{\delta})^{\alpha}}{1 - p^{\beta}} \qquad (5.86)$$

The four constants, α, β, γ and δ, are determined using values of p, m_x and m_y corresponding to four representative points in the exact interaction relation.

As examples, the interaction curves for two wide-flange shape W8x31 and W14x426 were calculated and shown in Fig. 5.13 and

5.7 Force-Deformation Rate Relationships

The analytical description of the interaction relations given in the preceding section may be considered as a suitable basis for a three-dimensional space frame analysis. With this concept, the interaction surface (Eq. 5.84) is assumed to be the perfectly plastic yield surface, and the force-deformation rate relations can then be derived from the normality condition (flow rule).

Thus, if $f\ (m_x, m_y, p) = 0$ denotes the yield condition, with $f < 0$ corresponding to stress states below yield, then

$$\begin{aligned} \dot{\kappa}_x &= \lambda \frac{\partial f}{\partial m_x} / M_{px} \\ \dot{\kappa}_y &= \lambda \frac{\partial f}{\partial m_y} / M_{py} \\ \dot{\varepsilon}_o &= \lambda \frac{\partial f}{\partial p} / P_y \end{aligned} \tag{5.89}$$

If either (i) $f < 0$ or (ii) $f = 0$ and $\dot{f} < 0$

$$\dot{\kappa}_x = \dot{\kappa}_y = \dot{\varepsilon}_o = 0 \tag{5.90}$$

where λ is a positive scalar.

According to the concept of perfect plasticity, the vector representing the deformation rate is normal to the yield surface at a regular point. At a singular point of the yield surface, the deformation rate vector lies within the directions of the normals to the surface at adjacent points. For example, the normals drawn to the curve AB and line BC in Fig. 5.15 are the projections on the plane p = constant of Fig. 5.15 of possible deformation rates for stress points lying on

curve AB and line BC. When the stress point lies at the corner B in Fig. 5.15, the deformation rate vector lies in the fan bounded by the normals to the sides which meet at the corner.

For the face AB of the yield surface, $m_y > \bar{m}_y$

$$\dot{\kappa}_x = \frac{\lambda}{M_{px}} \frac{\alpha}{1 - p^{\beta}} m_x^{\alpha-1}$$

$$\dot{\kappa}_y = \frac{\lambda}{M_{py}} \tag{5.91}$$

$$\dot{\epsilon}_o = \frac{\lambda}{P_y} \left[\frac{\beta\, p^{\beta-1}}{(1 - p^{\beta})^2} m_x^{\alpha} + \gamma\, p^{\gamma-1} \right]$$

where $\bar{m}_y$ is the value at the edge of the yield surface as given by Eq. 5.86.

For the face BC of the yield surface, $m_y < \bar{m}_y$

$$\dot{\kappa}_x = \frac{\lambda}{M_{px}}$$

$$\dot{\kappa}_y = 0 \tag{5.92}$$

$$\dot{\epsilon}_o = \frac{\lambda}{P_y} \delta\, p^{\delta-1}$$

At the edge B of the yield surface, $m = \bar{m}_y$, it is convenient to introduce a scalar parameter ρ ($0 \leq \rho \leq 1$ at most) of position and time whose increase corresponds to a transition between the regular faces reckoned in a counter-clockwise sense round the yield curve CBA.

$$\dot{\kappa}_x = \frac{\lambda}{M_{px}} \left[1 - \rho + \frac{\alpha}{1 - p^{\beta}} m_x^{\alpha-1} \rho \right]$$

$$\dot{\kappa}_y = \frac{\lambda}{M_{py}} \rho \qquad (5.93)$$

$$\dot{\epsilon}_o = \frac{\lambda}{P_y} \left[\frac{\beta p^{\beta-1}}{(1 - p^{\beta})^2} m_x^{\alpha} \rho + \gamma p^{\gamma-1} \rho + \delta p^{\delta-1} (1 - \rho) \right]$$

5.8 Summary

A simple method has been presented to arrive at the exact interaction relation of doubly symmetric sections under combined axial force and biaxial bending moments. The exactness of the solution is checked by the upper and lower bound limit analyses. Simple interaction equations of wide-flange sections are proposed and their associated plastic deformation rates are derived.

6. INTERACTION RELATIONS OF BIAXIALLY LOADED GENERAL SECTIONS

6.1 Introduction

Biaxial interaction relationships of rectangular and wide-flange sections under combined axial force and biaxial bending have been reported in Refs. 13 and 14, where some approximations are made and interaction equations are obtained for several different cases based on the location of the neutral axis.

In Chapter 5, a simple method to obtain exact interaction relationships for a doubly symmetric section is developed. Herein, the method presented in Chapter 5 is extended to the case of an unsymmetric section composed of rectangular elements which meet each other at a right angle. This restriction is met by most structural steel sections (Fig. 6.1). The present analysis includes most existing solutions as a special case, so that it may be considered as a generalization of all previous solutions. Since information in terms of interaction curves for the unsymmetric cases has been scarcely reported, herein, several commonly used unsymmetrical structural steel sections are presented. The results for the symmetric cases have been reported elsewhere and in Chapter 5.

6.2 Limit Analyses

The i-th element of a section composed of n-rectangular elements is shown in Fig. 6.2. The origin of x- and y-axes is assumed at the centroid of the entire section. The x- and y-axes are parallel to the sides of the section but are not necessarily the principal axes

of the section.

The straight line shown in Fig. 6.2 is the neutral axis (N.A.) defined by the two parameters α and β:

$$y_N = \alpha x + \beta \tag{6.1}$$

The resultant forces acting on the entire section are

$$\begin{aligned} P &= \text{axial force} \\ M_x &= \text{bending moment about x-axis} \\ M_y &= \text{bending moment about y-axis} \end{aligned} \tag{6.2}$$

First, only the portion above the N.A. (the shaded portion in Fig. 6.2) is considered and its contribution to the resultant forces is investigated by the lower bound and upper bound techniques of limit analysis. These two limit analysis solutions will be shown to lead to the same equations, and thus proved to be exact.

Since all equations are linear to the forces and deformations, superposition is applicable and the exactness established for the i-th element will hold for the resulting equations for the entire section.

6.2.1 Lower Bound Analysis

A lower bound solution is obtained from an assumed stress field and equilibrium conditions.

Assuming the stress in the shaded portion of Fig. 6.2 to be equal to tensile yield stress ($+\sigma_y$), then its contributions to the sectional forces are obtained from the equilibrium conditions as

$$P'_i = \sigma_y A'_i$$
$$M'_{xi} = \sigma_y Q'_{xi} \qquad (6.3)$$
$$M'_{yi} = -\sigma_y Q'_{yi}$$

where

A'_i = area of the shaded area

Q'_{xi} = static moment of inertia of the shaded area about x axis (6.4)

Q'_{yi} = static moment of inertia of the shaded area about y axis

6.2.2 Upper Bound Analysis

An upper bound solution is obtained from an assumed strain rate field and the virtual work principle. Assuming the strain rate field is shown in Fig. 6.2:

$$\dot{\epsilon} = \dot{\chi}\,\eta \qquad (6.5)$$

where

$\dot{\epsilon}$ = strain rate

$\dot{\chi}$ = curvature rate about the N.A. (6.6)

η = distance from the N.A.

The rate of internal energy dissipation associated with this strain field is

$$\dot{D}_I = \int_{A_i} \sigma\,\dot{\epsilon}\,dA = \sigma_y \dot{\chi}\,\eta_i A_i \qquad (6.7)$$

in which η_i is the distance from C_i to the N.A.

$$\eta_i = \int_{A_i} \eta \, dA \tag{6.8}$$

The rate of external work done is

$$\dot{W}_E = \dot{\varepsilon}_o \, P + \dot{\kappa}_x \, M_{xi} + \dot{\kappa}_y \, M_{yi} \tag{6.9}$$

where

$$\begin{aligned} \dot{\varepsilon}_o &= \text{strain rate at centroid 0 of the section} \\ \dot{\kappa}_x &= \text{curvature rate about x-axis} \\ \dot{\kappa}_y &= \text{curvature rate about y-axis} \end{aligned} \tag{6.10}$$

Using these notations, the strain rate at any point (x, y) is expressed by

$$\dot{\varepsilon} = \dot{\varepsilon}_o + \dot{\kappa}_x \, y - \dot{\kappa}_y \, x \tag{6.11}$$

Evaluate Eq. 6.11 at the centroid $C_i(e_{xi}, e_{yi})$ and get

$$\dot{\kappa} \, \eta_i = \dot{\varepsilon}_o + \dot{\kappa}_x \, e_{yi} - \dot{\kappa}_y \, e_{xi} \tag{6.12}$$

On the neutral axis N.A., there is no strain, thus from Eq. 6.1 and Eq. 6.11

$$\dot{\varepsilon}_o + \dot{\kappa}_x \, (\alpha x + \beta) - \dot{\kappa}_y \, x = 0 \tag{6.13}$$

Since this must be true for all values of x

$$\alpha \, \dot{\kappa}_x - \dot{\kappa}_y = 0 \tag{6.14}$$

$$\beta \, \dot{\kappa}_x + \dot{\varepsilon}_o = 0 \tag{6.15}$$

From Eqs. 6.12, 6.14 and 6.15, one solves

$$\begin{aligned} \dot{\varepsilon}_o &= - \frac{\beta \, \eta_i}{e_{yi} - \alpha \, e_{xi} - \beta} \, \dot{\kappa} \\ \dot{\kappa}_x &= \frac{\eta_i}{e_{yi} - \alpha \, e_{xi} - \beta} \, \dot{\kappa} \\ \dot{\kappa}_y &= \frac{\alpha \, \eta_i}{e_{yi} - \alpha \, e_{xi} - \beta} \, \dot{\kappa} \end{aligned} \tag{6.16}$$

Substitution of Eq. 6.16 into Eq. 6.9 gives

$$\dot{W}_E = \frac{-\beta P_i + M_{xi} + \alpha M_{yi}}{e_{yi} - \alpha e_{xi} - \beta} \dot{\chi} \eta_i \tag{6.17}$$

Equating the internal rate of energy dissipation, Eq. 6.7, to the external rate of work done, Eq. 6.17

$$-\beta P_i + M_{xi} + \alpha M_{yi} = (-\beta + e_{yi} - \alpha e_{xi}) \sigma_y A_i \tag{6.18}$$

Since Eq. 6.18 must hold for all values of α and β,

$$\begin{aligned} P_i &= \sigma_y A_i \\ M_{xi} &= \sigma_y A_i e_{yi} = \sigma_y Q_{xi} \\ M_{yi} &= -\sigma_y A_i e_{xi} = -\sigma_y Q_{yi} \end{aligned} \tag{6.19}$$

Equations 6.19 are identical to Eq. 6.3 which was obtained as a lower bound solution. Thus these equations are proved to be exact for the i-th element of the section. Since the equations for the entire section can be obtained by the method of superposition, the resulting equations must be also exact.

6.3 Derivation of Interaction Equations

The equations for A_i, Q_{xi} and Q_{yi} for the i-th element of the general section will be first derived in what follows and the resulting equations for the entire section will then be obtained by the method of superposition.

Consider a horizontal line element AB as shown in Fig. 6.3, which is defined by the two points

$$A(x_a, y_o), B(x_b, y_o) \tag{6.20}$$

Assuming the neutral axis N.A., as given by Eq. 6.1, intersects the horizontal line AB at the point C with a x-ccordinate of

$$x_c = \frac{y_o - \beta}{\alpha} \tag{6.21}$$

The shaded area below the line AB and above the N.A. is of primary concern in the computations (Fig. 6.3). There are six different cases possible according to the relative locations of the N.A. and the line AB as shown in Fig. 6.4. It will be convenient herein to introduce the following specially defined integral and parentheses

$$\oint_A^B S\,dx = \begin{cases} \int_A^B S\,dx & (A \leq B) \\ 0 & (B \leq A) \end{cases} \tag{6.22}$$

and

$$< S > = \begin{cases} S & (0 \leq S) \\ 0 & (S \leq 0) \end{cases} \tag{6.23}$$

This integral and parentheses are useful in the derivation of the general interaction equations.

Referring to Fig. 6.4, the contributions of the shaded area can be expressed by

$$\bar{A} = \int_A^B < y_o - y_N > dx \tag{6.24}$$

$$\bar{Q}_x = \frac{1}{2}\int_A^B < y_o - y_N > (y_o + y_N)\,dx \tag{6.25}$$

$$\bar{Q}_y = \int_A^B < y_o - y_N > x\,dx \tag{6.26}$$

Taking the point C into consideration, one obtains

$$\bar{A} = \begin{cases} \oint_A^C (y_o - y_N)\, dx - \oint_B^C (y_o - y_N)\, dx & (\alpha > 0) \\ \oint_C^B (y_o - y_N)\, dx - \oint_C^A (y_o - y_N)\, dx & (\alpha < 0) \end{cases} \tag{6.27}$$

$$\bar{Q}_x = \begin{cases} \frac{1}{2}\oint_A^C (y_o^2 - y_N^2)\, dx - \frac{1}{2}\oint_B^C (y_o^2 - y_N^2)\, dx & (\alpha > 0) \\ \frac{1}{2}\oint_C^B (y_o^2 - y_N^2)\, dx - \frac{1}{2}\oint_C^A (y_o^2 - y_N^2)\, dx & (\alpha < 0) \end{cases} \tag{6.28}$$

$$\bar{Q}_y = \begin{cases} \oint_A^C (y_o - y_N)\, x\, dx - \oint_B^C (y_o - y_N)\, x\, dx & (\alpha > 0) \\ \oint_C^B (y_o - y_N)\, x\, dx - \oint_C^A (y_o - y_N)\, x\, dx & (\alpha < 0) \end{cases} \tag{6.29}$$

Substituting Eq. 6.1 into Eqs. 6.27, 6.28 and 6.29 and making use of Eq. 6.21, one obtains

$$\begin{aligned} \bar{A} &= \bar{A}\,(x_a, x_b, x_c, \alpha) \\ &= \frac{1}{2\alpha} < \alpha\,(x_c - x_a) >^2 - \frac{1}{2\alpha} < \alpha\,(x_c - x_b) >^2 \end{aligned} \tag{6.30}$$

$$\begin{aligned} \bar{Q}_x &= \bar{Q}_x\,(x_a, x_b, x_c, \alpha, y_o) \\ &= \frac{1}{6\alpha} < \alpha\,(x_c - x_a) >^2 [3\, y_o - \alpha\,(x_c - x_a)] - \frac{1}{6\alpha} < \alpha\,(x_c - x_b) >^2 \\ &\quad [3\, y_o - \alpha\,(x_c - x_b)] \end{aligned} \tag{6.31}$$

$$\begin{aligned} \bar{Q}_y &= \bar{Q}_y\,(x_a, x_b, x_c, \alpha) \\ &= \frac{1}{6\alpha} < \alpha\,(x_c - x_a) >^2 (x_c + 2\, x_a) - \frac{1}{6\alpha} < \alpha\,(x_c - x_b) >^2 (x_c + 2\, x_b) \end{aligned} \tag{6.32}$$

For the i-th rectangular element (ABB'A') as shown in Fig. 6.2, Eqs. 6.30, 6.31 and 6.32 can be extended to obtain the solutions.

The function A_i for the i-th element, for example, can be obtained by first finding the functions $\bar{A}\ (x_a, x_b, x_c, \alpha)$ and $\bar{A}\ (x_a, x_b, x'_c, \alpha)$ corresponding to the areas ABED and A'C'D respectively. The function A_i for the area ABEC'A' (shaded area in Fig. 6.2) is then obtained by the simple albegraic summation

$$A_i = \bar{A}\ (x_a, x_b, x_c, \alpha) - \bar{A}\ (x_a, x_b, x'_c, \alpha) \tag{6.33}$$

Similarly

$$Q_{xi} = \bar{Q}_x\ (x_a, x_b, x_c, \alpha, y_o) - \bar{A}\ (x_a, x_b, x'_c, \alpha, y'_o) \tag{6.34}$$

$$Q_{yi} = \bar{Q}_y\ (x_a, x_b, x_c, \alpha) - \bar{Q}_y\ (x_a, x_b, x'_c, \alpha) \tag{6.35}$$

where the four points are located as

$$A(x_a, y_o),\ B(x_b, y_o),\ A'(x_a, y'_o),\ B'(x_b, y'_o) \tag{6.36}$$

and

$$x'_c = \frac{y'_o - \beta}{\alpha} \tag{6.37}$$

Summing up these values for all n-rectangular elements, the sectional force and moments are obtained. Assuming the area above the N.A. to be yielded by tension ($+\sigma_y$) and the portion below the N.A. by compression ($-\sigma_y$), the axial force P and the bending moments M_y and M_y are obtained by

$$P = \sigma_y\ (A_o - 2\ \Sigma\ A_i) \tag{6.38}$$

$$M_x = 2\ \sigma_y\ \Sigma\ Q_{xi} \tag{6.39}$$

$$M_y = -\ 2\ \sigma_y\ \Sigma\ Q_{yi} \tag{6.40}$$

where the summations are executed for all elements of the section.

Using the following fully plastic quantities of the section

$$P_y = \sigma_y A_o \tag{6.41}$$

$$M_{px} = \sigma_y Z_x \tag{6.42}$$

$$M_{py} = \sigma_y Z_y \tag{6.43}$$

To define the non-dimensional variables

$$p = \frac{P}{P_y} = 1 - 2 \Sigma A_i / A_o \tag{6.44}$$

$$m_x = \frac{M_x}{M_{px}} = 2 \Sigma Q_{xi} / Z_x \tag{6.45}$$

$$m_y = \frac{M_y}{M_{py}} = - 2 \Sigma Q_{yi} / Z_y \tag{6.46}$$

in which

$$\begin{aligned} A_o &= \text{total area of the section} \\ Z_x &= \text{plastic section modulus about x-axis} \\ Z_y &= \text{plastic section modulus about y-axis} \end{aligned} \tag{6.47}$$

The sectional constants, A_o, Z_x and Z_y can be computed by

$$A_o = \Sigma (y_o - y_o') (x_b - x_a) \tag{6.48}$$

$$Z_x = \frac{1}{2} \Sigma (x_b - x_a) (y_o |y_o| - y_o' |y_o'|) \tag{6.49}$$

$$Z_y = \frac{1}{2} \Sigma (y_o - y_o') (x_b |x_b| - x_a |x_a|) \tag{6.50}$$

Equations 6.44, 6.45 and 6.46 give the exact interaction relationships of the section. If the two parameters α and β can be eliminated among these three equations, an exact interaction equation relating p_y, m_x and m_y will result. Since this is not possible for a general cross section, numerical computations are carried out. The

formulation and the method is found to be extremely powerful and efficient for a computer solution.

6.4 Interaction Curves of Structural Shapes

Using the present method, the interaction curves of various shapes of cross section are presented in Figs. 6.5 to 6.9.

Figure 6.5 shows the interaction curves of a wide-flange section (W8 x 31). Since the wide flange section is doubly symmetric, its interaction curves are also symmetric. These curves were compared with those obtained previously for doubly symmetric sections, and an excellent agreement was found in all cases.

Figure 6.6 shows the interaction curves of the angle section with unequal legs (L4 x 3 x 3/8). The largest oval loop represents the interaction curve without thrust (p = 0). When p increases, the loop becomes smaller and its shape becomes closer to a triangle. However, the convexity condition of yield surface or interaction surface is not violated. Since the section has no axes of symmetry, all interaction curves are not symmetric with respect to any axis. It should be noted, however, that in a three dimensional plot (m_x, m_y, p space), the interaction surface is symmetric with respect to its origin. This follows directly from the condition that tension and compression yield stress levels are equal.

Figures 6.7, 6.8 and 6.9 show interaction curves of a channel section (C10 x 20) a structural tee section (WT 15 x 66) and a double-angle section (2L 6 x 6 x ½) respectively. Since these sections are

symmetric either with respect to the x-axis or y-axis, their interaction curves are also seen to be symmetric with respect to the m_y axis or m_x axis.

In order to investigate the effect of cross section sizes on the interaction curves, two extreme sizes of each shape were selected for the following four structural shapes a) channels (MC 10 x 6.5 and MC 3 x 9); b) angles (L 9 x 4 x 1 and L 6 x 6 x 1); c) tees (MT 6 x 5.9 and MT 2 x 8.15); d) double-angle (2 L 9 x 4 x ½ and 2 L 9 x 4 x 1). Comparisons between these two extreme sizes are given in Figs. 6.10 to 6.13. For each shape of cross section, two values of P/P_y (0.2 and 0.8) are shown. The dotted curves in the figures represent a somewhat averaged curve for a particular shape of cross section. These averaged interaction curves have been previously selected and presented in detail in Figs. 6.6 to 6.9. Variation of the interaction curves due to various weights of the same shape were also investigated for the above four structural shapes. It was found that the effect of section weights on the interaction curves is much less than that of section sizes. Two extreme cases of weight were found to give interaction curves almost identical to the average curves (dotted) shown in Figs. 6.10 to 6.13. It can therefore be concluded that the interaction curves presented in Figs. 6.6 to Fig. 6.9 may be considered as representative curves for those shapes of section. It is of interest to note that interaction curves of structural tee shapes (Fig. 6.8) are found to be almost identical to those of double-angle shapes (Fig. 6.9).

6.5 Summary

A simple method has been presented to arrive at the exact interaction relationships of general structural sections under combined axial force and biaxial bending moments. The exactness of the solution was checked by the upper and lower bound techniques of limit analysis. Interaction curves of several structural steel sections were obtained and illustrated.

7. ULTIMATE STRENGTH OF BIAXIALLY LOADED COLUMNS

7.1 Introduction

The maximum strengths of biaxially loaded columns simply supported at their ends are frequently used in engineering structures but design data to assess their maximum values are very scant. This lack of information is largely due to the very difficult procedures in analysis encountered and the labor involved in computations when conventional methods are used. In particular, the biaxially loaded column under unsymmetric loading condition poses special problems, and even with drastically simplified analysis such as assuming elastic-perfectly plastic moment curvature relationships for the cross section, sinusoidal or parabolic forms for the deflections and equilibrium conditions satisfied only at selected sections, etc., an analytical formula is still not possible.

In Chapter 4, an alternate but extremely simple approximate analysis was developed and simple interaction equations of in-plane beam-columns were presented for various loading conditions. In that work, the moment-curvature-thrust relationship for a uniaxially loaded cross section was idealized to be elastic-perfectly plastic. The approximate average flow moment M_{mc} was assumed to lie between the initial yield moment M_{yc} and the plastic limit moment M_{pc}.

Extension of this two-dimensional approximate approach for in-plane beam-columns to three-dimensional analysis for biaxially loaded columns is attempted herein. The biaxial moment-curvature-thrust relation-

ship is assumed to be elastic-perfectly plastic. The approximate averaged flow surface is assumed to lie between the initial yield surface and the fully plastic limit surface. Once the proper values for the averaged flow surface are selected, the maximum load carrying capacity of the biaxially loaded column can be computed in a rather simple manner by an elastic analysis.

7.2 Governing Equations

Consider a column of length L in a space (X, Y, Z) as shown in Fig. 7.1. The location of a cross section is defined by the Z-coordinate, on which the local coordinates (ξ, η, ζ) are placed.

The centroidal displacements of the column are chosen to be

$$\begin{aligned} U &= \text{displacement in X direction} \\ V &= \text{displacement in Y direction} \\ \Theta &= \text{rotation about Z axis} \end{aligned} \tag{7.1}$$

Neglecting the second order terms, the internal moments are approximately related to the displacements by [20]

$$\begin{aligned} M_\xi &= E\, I_\xi\, (V'' - \Theta\, U'') \approx E\, I_\xi\, V'' \\ M_\eta &= -\, E\, I_\eta\, (U'' + \Theta\, V'') \approx -\, E\, I_\eta\, U'' \\ M_\zeta &= E\, I_\omega\, \Theta''' - (GK_T + \bar{K})\, \Theta' \end{aligned} \tag{7.2}$$

where

$$\begin{aligned} E,\ G &= \text{moduli of elasticity} \\ I_\xi,\ I_\eta &= \text{moment of inertia} \\ I_\omega &= \text{warping moment of inertia} \\ K_T &= \text{St. Venant torsion constant} \\ \bar{K} &= \int_A \sigma\, (\xi^2 + \eta^2)\, d\xi\, d\eta \end{aligned} \tag{7.3}$$

The external forces and moments acting at each end of the column (Z = 0 and Z = L) are

$$\begin{aligned} P &= \text{axial force} \\ M_{XO},\ M_{XL} &= \text{bending moments about X axis} \\ M_{YO},\ M_{YL} &= \text{bending moments about Y axis} \\ M_{ZO},\ M_{ZL} &= \text{twisting moments about Z axis} \end{aligned} \tag{7.4}$$

in which the axial force P and the bending moments M_x and M_y are the applied forces and the twisting moments M_z are considered to be the reactions associated with the rotation constraints at the ends.

The equilibrium equations to be satisfied by the external forces and the internal forces are

$$\begin{aligned} M_\xi &= M_X - P\,V + M_Y\,\Theta \\ M_\eta &= M_Y + P\,U - M_X\,\Theta \\ M_\zeta &= M_Z + M_X\,U' + M_Y\,V' \\ &\quad - \frac{V}{L}(M_{YL} - M_{YO}) - \frac{U}{L}(M_{XL} - M_{XO}) \end{aligned} \tag{7.5}$$

where

$$\begin{aligned} M_X &= M_{XO} + \frac{Z}{L}(M_{XL} - M_{XO}) \\ M_Y &= M_{YO} + \frac{Z}{L}(M_{YL} - M_{YO}) \\ M_Z &= M_{ZO} = M_{ZL} \end{aligned} \tag{7.6}$$

The governing differential equations of the biaxially loaded column are obtained from Eq.7.2 and Eq.7.5,

$$\begin{aligned} &E\,I_\xi\,V'' + P\,V - M_Y\,\Theta = M_X \\ &E\,I_\eta\,U'' + P\,U - M_X\,\Theta = -M_Y \\ &E\,I_\omega\,\Theta''' - (G\,K_T + \bar{K})\,\Theta' - M_X\,U' - M_Y\,V' \\ &+ \frac{V}{L}(M_{YL} - M_{YO}) + \frac{U}{L}(M_{XL} - M_{XO}) = M_Z \end{aligned} \tag{7.7}$$

7.3 Non-Dimensionalization

The coordinates and displacements are non-dimensionalized by

$$x = \frac{X}{L}, \quad y = \frac{Y}{L}, \quad z = \frac{Z}{L}$$
$$u = \frac{U}{L}, \quad v = \frac{V}{L}, \quad \theta = \Theta \tag{7.8}$$

and the axial force, bending moments and twisting moment are non-dimensionalized by

$$p = \frac{P}{P_Y}, \quad m_x = \frac{M_X}{M_{p\xi}}, \quad m_y = \frac{M_y}{M_{p\eta}}, \quad m_z = \frac{M_Z}{M_{p\omega}} \tag{7.9}$$

in which the full plastic states of the cross section are given by the initial yield normal stress σ_y and the initial yield shear stress τ_y and the plastic section moduli Z_ξ, Z_η and Z_ω

$$P_y = \sigma_y A, \quad M_{p\xi} = \sigma_y Z_\xi, \quad M_{p\eta} = \sigma_y Z_\eta, \quad M_{p\omega} = \tau_y Z_\omega \tag{7.10}$$

The plastic section moduli are defined by

$$A = \int_A dA, \quad Z_\xi = \int_A \eta \, dA, \quad Z_\eta = \int_A \xi \, dA, \quad Z_\omega = \int_A \sqrt{\xi^2 + \eta^2} \, dA \tag{7.11}$$

The modulus Z_ω is the fully plastic section modulus due to warping torsion only for sections doubly symmetric. In the case of symmetric section, the value $\bar{K}$ in Eq. 7.3, can be expressed in the simple form

$$\bar{K} = -\frac{P}{A}(I_\xi + I_\eta) \tag{7.12}$$

Equation 7.7 can now be rewritten in the non-dimensional form

$$\begin{aligned} &v'' + p_\xi v - m_{y\xi}\theta = m_{x\xi} \\ &u'' + p_\eta u - m_{x\eta}\theta = -m_{y\eta} \\ &\theta''' - p_\omega \theta' - m_{x_\omega} u' - m_{y_\omega} v' \\ &+ v(m_{y_\omega L} - m_{y_\omega o}) + u(m_{x_\omega L} - m_{x_\omega o}) = m_{z_\omega} \end{aligned} \tag{7.13}$$

in which

$$p_\xi = \frac{\sigma_y}{E}\frac{AL^2}{I_\xi}\,p, \qquad p_\eta = \frac{\sigma_y}{E}\frac{AL^2}{I_\eta}\,p$$

$$p_\omega = \frac{G}{E}\frac{K_T L^2}{I_\omega} + \frac{\sigma_y}{E}\frac{L^2}{I_\omega}\,p\,(I_\xi + I_\eta) \tag{7.14}$$

and

$$m_{x\xi} = \frac{\sigma_y}{E}\frac{Z_\xi L}{I_\xi}\,m_x, \qquad m_{y\xi} = \frac{\sigma_y}{E}\frac{Z_\eta L}{I_\xi}\,m_y$$

$$m_{x\eta} = \frac{\sigma_y}{E}\frac{Z_\xi L}{I_\eta}\,m_x, \qquad m_{y\eta} = \frac{\sigma_y}{E}\frac{Z_\eta L}{I_\eta}\,m_y \tag{7.15}$$

$$m_{x\omega} = \frac{\sigma_y}{E}\frac{Z_\xi L^3}{I_\omega}\,m_x, \qquad m_{y\omega} = \frac{\sigma_y}{E}\frac{Z_\eta L^3}{I_\omega}\,m_y$$

and $$m_{z\omega} = \frac{\tau_y}{E}\frac{Z_\omega L^3}{I_\omega}\,m_z$$

7.4 Deflection Functions

Assuming the deflected shapes of the column as

$$\begin{aligned} u &= A_o \sin \pi z + z(1-z)\,(A_1 + A_2 z) \\ v &= B_o \sin \pi z + z(1-z)\,(B_1 + B_2 z) \\ \theta &= C_o \sin \pi z + z(1-z)\,(C_1 + C_2 z) \end{aligned} \tag{7.16}$$

where A_o, A_1, A_2, B_o, B_1, B_2, C_o, C_1 and C_2 are the constants to be determined from the governing equations and the boundary conditions.

These deflection functions satisfy the simply supported boundary conditions except for the warping deformations:

$$u = 0, \quad v = 0, \quad \theta = 0 \quad \text{at} \quad z = 0 \quad \text{and} \quad 1 \tag{7.17}$$

7.5 Warping Restraint

The warping restraint factors $\gamma_{\omega o}$ and $\gamma_{\omega L}$ at the ends of the column are introduced by

$$C_1 = - \gamma_{\omega o} \pi C_o + (1-\gamma_{\omega o}) C_2$$
$$C_1 = - \gamma_{\omega L} \pi C_o - (2-\gamma_{\omega L}) C_2 \qquad (7.18)$$

So that the warping boundary conditions may be satisfied at both ends

$$\gamma_\omega = 0 \text{ implies } \theta'' = 0 \quad \text{warping permitted}$$
$$\gamma_\omega = 1 \text{ implies } \theta' = 0 \quad \text{warping restrained} \qquad (7.19)$$

From Eq. 7.18 the constants C_1 and C_2 are solved in terms of C_o

$$C_1 = - \pi \gamma_1 C_o$$
$$C_2 = \pi \gamma_2 C_o \qquad (7.20)$$

where

$$\gamma_1 = \frac{2 \gamma_{\omega o} + \gamma_{\omega L} - 2 \gamma_{\omega o} \gamma_{\omega L}}{3 - \gamma_{\omega o} - \gamma_{\omega L}}$$
$$\gamma_2 = \frac{\gamma_{\omega o} - \gamma_{\omega L}}{3 - \gamma_{\omega o} - \gamma_{\omega L}} \qquad (7.21)$$

7.6 Method of Solution

Substituting the deflection functions, Eq. 7.16, into the governing differential equations, Eq. 7.13, one finds

$$\pi^2 B_o \sin \pi z - 2(B_2 - B_1) + 6 B_2 z$$
$$- p_\xi [B_o \sin \pi z + z (1 - z) (B_1 + B_2 z)]$$
$$+ m_{y\xi} [C_o \sin \pi z + z (1 - z) (C_1 + C_2 z)] = - m_{x\xi} \qquad (7.22)$$

$$\pi^2 A_o \sin \pi z - 2(A_2 - A_1) + 6 A_2 z$$

$$- p_\eta [A_o \sin \pi z + z (1 - z) (A_1 + A_2 z)]$$

$$+ m_{x\eta} [C_o \sin \pi z + z (1 - z) (C_1 + C_2 z)] = m_{y\eta} \qquad (7.23)$$

$$\pi^3 C_o \cos \pi z + 6 C_2$$

$$+ p_\omega [\pi C_o \cos \pi z + C_1 + 2(C_2 - C_1) z - 3 C_2 z^2]$$

$$+ m_{x\omega} [\pi A_o \cos \pi z + A_1 + 2(A_2 - A_1) z - 3 A_2 z^2] \qquad (7.24)$$

$$+ m_{y\omega} [\pi B_o \cos \pi z + B_1 + 2(B_2 - B_1) z - 3 B_2 z^2]$$

$$- (m_{y\omega L} - m_{y\omega o}) [B_o \sin \pi z + z(1 - z) (B_1 + B_2 z)]$$

$$- (m_{x\omega L} - m_{x\omega o}) [A_o \sin \pi z + z(1 - z) (A_1 + A_2 z)] = m_{z\omega}$$

Evaluating Eqs. 7.22, 7.23 and 7.24 at the end $z = 0$ and $z = 1$ one obtains

$$2(B_2 - B_1) = m_{x\xi o}$$

$$2(A_2 - A_1) = - m_{y\eta o}$$

$$\pi^3 C_o + 6 C_2 + p_\omega (\pi C_o + C_1) \qquad (7.25)$$

$$+ m_{x\omega o} (\pi A_o + A_1) + m_{y\omega o} (\pi B_o + B_1) = m_{z\omega o}$$

and

$$2(B_1 + 2 B_2) = - m_{x\xi L}$$

$$2(A_1 + 2 A_2) = m_{y\eta L}$$

$$\pi^3 C_o - 6 C_2 + p_\omega (\pi C_o + C_1 + C_2) \qquad (7.26)$$

$$+ m_{x\omega L} (\pi A_o + A_1 + A_2) + m_{y\omega L} (\pi B_o + B_1 + B_2) = - m_{z\omega L}$$

here the moments with subscript 0 or L are the moments (Eqs. 7.15) evaluated at the ends $Z = 0$ or $Z = L$, respectively.

From the first two equations in Eqs. 7.25 and Eqs. 7.26, the four constants A_1, A_2, B_1 and B_2 are obtained

$$\begin{aligned} A_1 &= \frac{1}{6}\,(m_{y\eta L} + 2\,m_{y\eta o}) \\ A_2 &= \frac{1}{6}\,(m_{y\eta L} - m_{y\eta o}) \\ B_1 &= -\frac{1}{6}\,(m_{x\xi L} + 2\,m_{x\xi o}) \\ B_2 &= -\frac{1}{6}\,(m_{x\xi L} - m_{x\xi o}) \end{aligned} \tag{7.27}$$

From the last equation in Eqs. 7.25 and 7.26, one obtains

$$\begin{aligned} &2\pi\,(\pi^2 + p_\omega)\,C_o + 2\,p_\omega\,C_1 + p_\omega\,C_2 \\ &= -\,m_{x\omega o}\,(\pi\,A_o + A_1) - m_{x\omega L}\,(\pi\,A_o + A_1 + A_2) \\ &- m_{y\omega o}\,(\pi\,B_o + B_1) - m_{y\omega L}\,(\pi\,B_o + B_1 + B_2) \end{aligned} \tag{7.28}$$

The constants A_o, B_o, C_o and $m_{z\omega}$ in Eqs. 7.22, 7.23 and 7.24 can be determined from the condition at the mid-span of the column ($z = 1/2$) and Eq. 7.28

$$\begin{aligned} &(\pi^2\,B_o + 2\,B_1 + B_2) - \frac{1}{8}\,p_\xi\,(8\,B_o + 2\,B_1 + B_2) \\ &\quad + \frac{1}{16}\,(m_{y\xi o} + m_{y\xi L})\,(8\,C_o + 2\,C_1 + C_2) \\ &\quad = -\frac{1}{2}\,(m_{x\xi o} + m_{x\xi L}) \end{aligned} \tag{7.29}$$

$$\begin{aligned} &(\pi^2\,A_o + 2\,A_1 + A_2) - \frac{1}{8}\,p_\eta\,(8\,A_o + 2\,A_1 + A_2) \\ &\quad + \frac{1}{16}\,(m_{x\eta o} + m_{x\eta L})\,(8\,C_o + 2\,C_1 + C_2) \\ &\quad = \frac{1}{2}\,(m_{y\eta o} + m_{y\eta L}) \end{aligned} \tag{7.30}$$

$$\begin{aligned} &\frac{1}{8}\,(m_{x\omega o} + m_{x\omega L})\,A_2 + \frac{1}{8}\,(m_{y\omega o} + m_{y\omega L})\,B_2 \\ &\quad - \frac{1}{8}\,(m_{y\omega L} - m_{y\omega o})\,(8\,B_o + 2\,B_1 + B_2) \\ &\quad - \frac{1}{8}\,(m_{x\omega L} - m_{x\omega o})\,(8\,A_o + 2\,A_1 + A_2) \\ &\quad + 6\,C_2 + \frac{1}{4}\,p_\omega\,C_2 = m_{z\omega} \end{aligned} \tag{7.31}$$

Solving A_o, B_o, C_o and m_{z_ω} from Eqs. 7.28, 7.29, 7.30 and 7.31, using Eq. 7.20 and Eq. 7.27, the following four equations are obtained

$$\frac{1}{2}\,(m_{x_{\omega o}} + m_{x_{\omega L}})\,A_o + \frac{1}{2}\,(m_{y_{\omega o}} + m_{y_{\omega L}})\,B_o + [\pi^2 + p_\omega\,(1 - \gamma_1 + \tfrac{1}{2}\gamma_2)]\,C_o = \frac{1}{12\,\pi}\,[-m_{x_{\omega o}}\,(m_{y\eta L} + 2\,m_{y\eta o}) + m_{y_{\omega o}}\,(m_{x\xi L} + 2\,m_{x\xi o}) - m_{x_{\omega L}}\,(2\,m_{y\eta L} + m_{y\eta o}) + m_{y_{\omega L}}\,(2\,m_{x\xi L} + m_{x\xi o})] \tag{7.32}$$

$$(\pi^2 - p_\xi)\,B_o + \frac{1}{16}\,(m_{y\xi o} + m_{y\xi L})\,(8 - 2\,\pi\,\gamma_1 + \pi\,\gamma_2)\,C_o = \frac{-1}{16}\,p_\xi\,(m_{x\xi o} + m_{x\xi L}) \tag{7.33}$$

$$(\pi^2 - p_\eta)\,A_o + \frac{1}{16}\,(m_{x\eta o} + m_{x\eta L})\,(8 - 2\,\pi\,\gamma_1 + \pi\,\gamma_2)\,C_o = \frac{1}{16}\,p_\eta\,(m_{y\eta o} + m_{y\eta L}) \tag{7.34}$$

and

$$m_{z_\omega} = -(m_{x_{\omega L}} - m_{x_{\omega o}})\,A_o - (m_{y_{\omega L}} - m_{y_{\omega o}})\,B_o + (6 + \tfrac{1}{4}\,p_\omega)\,\gamma_z\,C_o - \frac{1}{24}\,m_{x_{\omega o}}\,(m_{y\eta L} + 2\,m_{y\eta o}) + \frac{1}{24}\,m_{y_{\omega o}}\,(m_{x\xi L} + 2\,m_{x\xi o}) + \frac{1}{24}\,m_{x_{\omega L}}\,(2\,m_{y\eta L} + m_{y\eta o}) - \frac{1}{24}\,m_{y_{\omega L}}\,(2\,m_{x\xi L} + m_{x\xi o}) \tag{7.35}$$

7.7 Stability Considerations

Equations 7.32, 7.33 and 7.34 are the three simultaneous equations in terms of the three unknowns A_o, B_o and C_o or in the matrix form

$$[K]\,[D] = [F] \tag{7.36}$$

in which

$$[K] = \begin{bmatrix} [\pi^2 - p_\eta] & 0 & [\frac{1}{16}\ (m_{x\eta o} + m_{x\eta L})\ (8 - 2\pi\ \gamma_1 + \pi\ \gamma_2)] \\ 0 & [\pi^2 - p_\xi] & [\frac{1}{16}\ (m_{y\xi o} + m_{y\xi L})\ (8 - 2\pi\ \gamma_1 + \pi\ \gamma_2)] \\ [\frac{1}{2}\ (m_{x\omega o} + m_{x\omega L})] & [\frac{1}{2}\ (m_{y\omega o} + m_{y\omega L})] & [\pi^2 + p_\omega\ (1 - \gamma_1 + \frac{1}{2}\ \gamma_2)] \end{bmatrix} \tag{7.37}$$

$$[D] = \begin{bmatrix} A_o \\ B_o \\ C_o \end{bmatrix} \tag{7.38}$$

and

$$[F] = \begin{bmatrix} [\frac{1}{16}\ p_\eta\ (m_{y\eta o} + m_{y\eta})] \\ [-\frac{1}{16}\ p_\xi\ (m_{x\xi o} + m_{x\xi L})] \\ \frac{1}{12\pi}\ [-m_{x\omega o}\ (m_{y\eta L} + 2\ m_{y\eta o}) + m_{y\omega o}\ (m_{x\xi L} + 2\ m_{x\xi o}) \\ \qquad - m_{x\omega L}\ (2\ m_{y\eta L} + m_{y\eta o}) + m_{y\omega L}\ (2\ m_{x\xi L} + m_{x\xi o})] \end{bmatrix} \tag{7.39}$$

In order to investigate the physical meaning of Eq. 7.36, let us express it in terms of dimensional parameters. Use of Eqs. 7.14 and 7.15 and some operations of constant multiplication converts Eq. 7.37, Eq. 7.38 and Eq. 7.39 into

$$[K] = \begin{bmatrix} [\frac{\pi^2\ EI_\eta}{L^2} - P] & 0 & [\frac{M_{XO} + M_{XL}}{2L}] \\ 0 & [\frac{\pi^2\ EI_\xi}{L^2} - P] & [\frac{M_{YO} + M_{XL}}{2L}] \\ [\frac{M_{XO} + M_{XL}}{2L}][\frac{M_{YO} + M_{YL}}{2L}] & [\frac{\pi^2\ EI_\omega}{L^4} - \left(P\ \frac{I_\xi + I_\eta}{AL^2} - \frac{GK_T}{L^2}\right) \frac{1 - \gamma_1 + \frac{1}{2}\ \gamma_2}{1 - \frac{\pi}{4}\ \gamma_1 + \frac{\pi}{8}\ \gamma_2}] \end{bmatrix} \tag{7.40}$$

$$[D] = \begin{bmatrix} A_o \\ B_o \\ C_o \left(1 - \frac{\pi}{4}\gamma_1 + \frac{\pi}{8}\gamma_2\right) \end{bmatrix} \tag{7.41}$$

$$[F] = \begin{bmatrix} \left[\frac{PL\ (M_{YO} + M_{YL})}{8\ EI_\eta}\right] \\ \left[-\frac{PL\ (M_{XO} + M_{XL})}{8\ EI_\xi}\right] \\ \frac{L}{12\pi}\left[\frac{M_{YO}\ (2M_{XO} + M_{XL}) + M_{YL}\ (M_{XO} + 2M_{XL})}{EI_\xi}\right. \\ \left. -\frac{M_{XO}\ (2M_{YO} + M_{YL}) + M_{XL}\ (M_{YO} + 2M_{YL})}{EI_\eta}\right] \end{bmatrix} \tag{7.42}$$

In the special case when the loads are symmetric ($M_{XO} = M_{XL}$ and $M_{YO} = M_{YL}$) and when end warpings are free ($\gamma_1 = \gamma_2 = 0$), the matrix [K] is identical to the coefficient matrix derived by Culver in Ref. 31. From Eqs. 7.40 to 7.42, all information about elastic stability of a column is obtained. First, when the column is centrally loaded, [F] = 0, the simultaneous equations Eq. 7.36 become homogeneous,

$$\begin{bmatrix} \frac{\pi^2\ EI_\eta}{L^2} - P & 0 & 0 \\ 0 & \frac{\pi^2\ EI_\xi}{L^2} - P & 0 \\ 0 & 0 & \frac{\pi^2\ EI_\omega}{L^4} - \left(p\ \frac{I_\xi + I_\eta}{AL^2} - \frac{GK_T}{L^2}\right)\frac{1 - \gamma_1 + \frac{1}{2}\gamma_2}{1 - \frac{\pi}{4}\gamma_1 + \frac{\pi}{8}\gamma_2} \end{bmatrix} \times \begin{bmatrix} A_o \\ B_o \\ C_o\left(1 - \frac{\pi}{4}\gamma_1 + \frac{\pi}{8}\gamma_2\right) \end{bmatrix} = \begin{bmatrix} 0 \\ 0 \\ 0 \end{bmatrix} \tag{7.43}$$

In order that a non-trivial solution for A_o, B_o and C_o exists,

$$\det [K] = 0$$

from which three stability limit loads are solved:

$$P = \frac{\pi^2 EI_\eta}{L^2}$$

$$P = \frac{\pi^2 EI_\xi}{L^2} \tag{7.44}$$

$$P = \frac{A}{I_\xi + I_\eta}\left(\frac{\pi^2 EI_\omega}{L^2}\frac{1 - \frac{\pi}{4}\gamma_1 + \frac{\pi}{8}\gamma_2}{1 - \gamma_1 + \frac{1}{2}\gamma_2} + GK_T\right)$$

The first two equations in Eqs. 7.44 are flexure buckling loads about the weak axis and the strong axis of the cross section, respectively. The last equation in Eqs. 7.44 is torsion buckling load. If end warpings are not restrained ($\gamma_1 = \gamma_2 = 0$), then this torsion buckling load coincides with the well-known torsion-buckling expression such as Timoshenko's solution [2].

Lateral torsional buckling can also be examined. Assuming in-plane bending moment about strong axis only (M_{XO}, M_{XL}), Eq. 7.36 yields

$$\begin{bmatrix} \frac{\pi^2 EI_\eta}{L^2} - P & 0 & \frac{M_{xo} + M_{xL}}{2L} \\ 0 & \frac{\pi^2 EI_\xi}{L^2} - P & 0 \\ \frac{M_{xo} + M_{xL}}{2L} & 0 & \frac{\pi^2 EI_\omega}{L^4} - \left(P\frac{I_\xi + I_\eta}{AL^2} - \frac{GK_T}{L^2}\right)\frac{1 - \gamma_1 + \frac{1}{2}\gamma_2}{1 - \frac{\pi}{4}\gamma_1 + \frac{\pi}{8}\gamma_2} \end{bmatrix}$$

$$\times \begin{bmatrix} A_o \\ B_o \\ C_o\,(1 - \frac{\pi}{4}\gamma_1 + \frac{\pi}{8}\gamma_2) \end{bmatrix} = \begin{bmatrix} 0 \\ -\frac{PL\,(M_{XO} + M_{XL})}{8\,EI_\xi} \\ 0 \end{bmatrix} \tag{7.45}$$

or

$$B_o = - \frac{PL\ (M_{XO} + M_{XL})}{8\ EI_\xi} \Big/ \left(\frac{\pi^2\ EI_\xi}{L^2} - P\right) \tag{7.46}$$

and

$$\begin{bmatrix} \left[\frac{\pi^2 EI_\eta}{L^2} - P\right] & \left[\frac{M_{XO}+M_{XL}}{2L}\right] \\ \left[\frac{M_{XO}+M_{XL}}{2L}\right] & \left[\frac{\pi^2 EI_\omega}{L^4} - \left(P\frac{I_\xi + I_\eta}{AL^2} - \frac{GK_T}{L^2}\right)\frac{1-\gamma_1+\frac{1}{2}\gamma_2}{1-\frac{\pi}{4}\gamma_1+\frac{\pi}{8}\gamma_2}\right] \end{bmatrix} \begin{bmatrix} A_o \\ C_o\left(1-\frac{\pi}{4}\gamma_1+\frac{\pi}{8}\gamma_2\right) \end{bmatrix} = \begin{bmatrix} 0 \\ 0 \end{bmatrix} \tag{7.47}$$

Equating determinant of the coefficient matrix (Eq. 7.47) to zero, the lateral torsional buckling condition is obtained as

$$\left(\frac{\pi^2\ EI_\eta}{L^2} - P\right)\left[\frac{\pi^2\ EI_\omega}{L^4} - \left(P\ \frac{I_\xi + I_\eta}{AL^2} - \frac{GK_T}{L^2}\right)\frac{1 - \gamma_1 + \frac{1}{2}\gamma_2}{1 - \frac{\pi}{4}\gamma_1 + \frac{\pi}{8}\gamma_2}\right] = \left(\frac{M_{XO} + M_{XL}}{2L}\right)^2 \tag{7.48}$$

When the column is subjected to biaxial bending as well as axial thrust, Eqs. 7.36 are not homogeneous the column must be treated as a load deflection problem. The solutions for this problem exist only when

$$\det\ [K] \geq 0 \tag{7.49}$$

This criterion can be checked conveniently by the stability function

$$F_{st} = \frac{1}{32}\left[\frac{8 - 2\pi\ \gamma_1 + \pi\ \gamma_2}{\pi^2 + p_\omega\ (1 - \gamma_1 + \frac{1}{2}\ \gamma_2)}\right]\left[\frac{(m_{x\omega o} + m_{x\omega L})(m_{x\eta o} + m_{x\eta L})}{\pi^2 - p_\eta}\right.$$

$$\left. + \frac{(m_{y\omega o} + m_{y\omega L})(m_{y\xi o} + m_{y\xi L})}{\pi^2 - p_\xi}\right] \tag{7.50}$$

Namely,

$F_{st} < 1$ implies $\det [K] > 0$ stable

$F_{st} = 1$ implies $\det [K] = 0$ stability limit

$F_{st} > 1$ implies $\det [K] < 0$ unstable

7.8 Solution to Deflection Coefficients

When the column is stable ($F_{st} < 1$), Eq. 7.36 can be solved for A_o, B_o and C_o as

$$\begin{aligned} C_o = \Big\{ & \frac{8}{3\pi} \left[m_{y\omega o} \left(m_{x\xi L} + 2\, m_{x\xi o} \right) + m_{y\omega L} \left(2\, m_{x\xi L} + m_{x\xi o} \right) \right. \\ & \left. - m_{x\omega o} \left(m_{y\eta L} + 2\, m_{y\eta o} \right) - m_{x\omega L} \left(2\, m_{y\eta L} + m_{y\eta o} \right) \right] \\ & - \frac{p_\eta}{\pi^2 - p_\eta} \left(m_{x\omega o} + m_{x\omega L} \right) \left(m_{y\eta o} + m_{y\eta L} \right) \\ & + \frac{p_\xi}{\pi^2 - p_\xi} \left(m_{y\omega o} + m_{y\omega L} \right) \left(m_{x\xi o} + m_{x\xi L} \right) \Big\} \\ & / \, 32 \left[\pi^2 + p_\omega \left(1 - \gamma_1 + \frac{1}{2} \gamma_2 \right) \right] (1 - F_{st}) \end{aligned} \tag{7.51}$$

and

$$\begin{aligned} A_o &= -\left[\frac{8 - 2\pi\gamma_1 + \pi\gamma_2}{16} \right] \left[\frac{m_{x\eta o} + m_{x\eta L}}{\pi^2 - p_\eta} \right] C_o + \frac{p_\eta}{16} \left[\frac{m_{y\eta o} + m_{y\eta L}}{\pi^2 - p_\eta} \right] \\ B_o &= -\left[\frac{8 - 2\pi\gamma_1 + \pi\gamma_2}{16} \right] \left[\frac{m_{y\xi o} + m_{y\xi L}}{\pi^2 - p_\xi} \right] C_o - \frac{p_\xi}{16} \left[\frac{m_{x\xi o} + m_{x\xi L}}{\pi^2 - p_\xi} \right] \end{aligned} \tag{7.52}$$

Since all the deflection functions have been determined, the elastic column has been solved under biaxial loading. The moments at an arbitrary section can now be computed from Eqs. 7.2 and 7.16,

$$m_\xi = -\frac{E}{\sigma_y}\frac{I_\xi}{Z_\xi L}\left[\pi^2 B_o \sin \pi z + 2(B_1 - B_2) + 6 B_2 z\right]$$

$$m_\eta = \frac{E}{\sigma_y}\frac{I_\eta}{Z_\eta L}\left[\pi^2 A_o \sin \pi z + 2(A_1 - A_2) + 6 A_2 z\right] \qquad (7.53)$$

$$m_\zeta = -\frac{E}{\sigma_y}\frac{I_\omega}{Z_\omega L^3}\left[\pi(\pi + p_\omega) C_o \cos \pi z + (1 - 2z)p_\omega C_1 + (6 + 2 p_\omega z - p_\omega z^2) C_2\right]$$

7.9 Critical Section

The critical section is the section where the yield condition

$$F_y (p, m_\xi, m_\eta, m_\zeta) - 1 = 0 \qquad (7.54)$$

is reached first. Since in the elastic regime, $F_y < 1$, the location of the critical section ($z = z^*$) is determined by

$$\left.\frac{\partial F_y}{\partial z}\right|_{z = z^*} = 0 \qquad (7.55)$$

As it will be seen leter, the expression for the yield function F_y is not simple enough such that Eq. 7.55 can be solved analytically. Herein, the simple approximate function

$$F_y = |p| + |m_\xi| + |m_\eta| \qquad (7.56)$$

is used for the determination of the critical section. Substituting Eq. 7.53 into Eq. 7.56,

$$F_y = \left\{\pi^2\left(\frac{I_\eta}{Z_\eta L} A_o - \frac{I_\xi}{Z_\xi L} B_o\right) \sin \pi z + 6\left(\frac{I_\eta}{Z_\eta L} A_2 - \frac{I_\xi}{Z_\xi L} B_2\right) z + 2\left[\frac{I_\eta}{Z_\eta L}(A_1 - A_2) - \frac{I_\xi}{Z_\xi L}(B_1 - B_2)\right]\right\}\frac{E}{\sigma_y} + p \qquad (7.57)$$

From the condition $\partial F_y/\partial z = 0$ at $z = z^*$, the location of the critical section is obtained

$$z^* = \frac{1}{\pi} \cos^{-1} \left(- \frac{6}{\pi^3} \frac{\frac{I_\xi}{Z_\xi L} B_2 - \frac{I_\eta}{Z_\eta L} A_2}{\frac{I_\xi}{Z_\xi L} B_o - \frac{I_\eta}{Z_\eta L} A_o} \right) \tag{7.58}$$

Thus the moments at the critical section are obtained from Eq. 7.53,

$$\begin{aligned}
m_\xi^* &= - \frac{E}{\sigma_y} \frac{I_\xi}{Z_\xi L} [\pi^2 B_o \sin \pi z^* - 2(B_2 - B_1) + 6 B_2 z^*] \\
m_\eta^* &= \frac{E}{\sigma_y} \frac{I_\eta}{Z_\eta L} [\pi^2 A_o \sin \pi z^* - 2(A_2 - A_1) + 6 A_2 z^*] \\
m_\zeta^* &= - \frac{E}{\tau_y} \frac{I_\omega}{Z_\omega L^3} [\pi(\pi^2 + p_\omega) C_o \cos \pi z^* + (1 - 2 z^*) p_\omega C_1 \\
&\qquad + (6 + 2 p_\omega z^* - 3 p_\omega z^{*2}) C_2]
\end{aligned} \tag{7.59}$$

The biaxially loaded column reaches its ultimate strength when these moments on the critical section satisfy an interaction relationship for the cross section as given by Eq. 7.54. This interaction relationship will be discussed further in the following section.

For the special case of a symmetric loading ($\gamma_{\omega o} = \gamma_{\omega L}$, $m_{xo} = m_{xL}$, $m_{yo} = m_{yL}$), the critical section is at the midheight ($z^* = \frac{1}{2}$), and Eq. 7.59 reduces to

$$m_\xi^* = \frac{E}{\sigma_y} \frac{I_\xi}{Z_\xi L} \left[\frac{\pi}{2} \frac{m_{y\xi}}{\pi^2 - p_\xi} \frac{(1 - \frac{\pi}{4} \frac{p_\xi}{\pi^2 - p_\xi}) m_{y\omega} m_{x\xi} - (1 - \frac{\pi}{4} \frac{p_\eta}{\pi^2 - p_\eta}) m_{x\omega} m_{y\eta}}{\frac{\pi^2 - p_\omega (1 - \gamma_\omega)}{1 - \frac{\pi}{4} \gamma_\omega} - \frac{1}{32} (\frac{m_{x\omega} m_{y\eta}}{\pi^2 - p_\eta} + \frac{m_{y\omega} m_{y\xi}}{\pi^2 - p_\xi})} \right.$$

$$\left. + (1 + \frac{\pi^2}{8} \frac{p_\xi}{\pi^2 - p_\xi}) m_{x\xi} \right]$$

$$m_\eta^* = \frac{E}{\sigma_y}\frac{I_\eta}{Z_\eta L}\left[-\frac{\pi}{2}\frac{m_{x\eta}}{\pi^2 - p_\eta}\frac{(1-\frac{\pi}{4}\frac{p_\xi}{\pi^2-p_\xi})\,m_{y\omega}\,m_{x\xi} - (1-\frac{\pi}{4}\frac{p_\eta}{\pi^2-p_\eta})\,m_{x\omega}\,m_{y\eta}}{\frac{\pi^2 - p_\omega\,(1-\gamma_\omega)}{1-\frac{\pi}{4}\gamma_\omega} - \frac{1}{32}\left(\frac{m_{x\omega}\,m_{y\eta}}{\pi^2-p_\eta} + \frac{m_{y\omega}\,m_{y\xi}}{\pi^2-p_\xi}\right)}\right.$$

$$\left. + (1 + \frac{\pi^2}{8}\frac{p_\eta}{\pi^2-p_\eta})\,m_{y\eta}\right] \qquad (7.60)$$

$$m_\zeta^* = 0$$

Further, for an uniaxial loading case (either $m_x = 0$ or $m_y = 0$), only the last term will be non-zero.

7.10 Interaction Equations of Section

Following the previous work on in-plane beams columns (Chapter 4), a certain averaged interaction relationship ($F_A = 0$) for a biaxially loaded cross section between initial yielding and the fully plastic state of the cross section can be found among the axial force (p) and the biaxial bending moments (m_ξ, m_η) at the critical section when the ultimate state of the column is reached. The contribution of the twisting moment (m_ζ) to the yield condition is neglected herein.

This averaged interaction relationship ($F_A = 0$) is bounded by the initial yield condition ($F_y = 0$) and the fully plastic limiting yield condition ($F_p = 0$) as seen in Fig. 7.2.

$$F_y \le F_A \le F_p \qquad (7.61)$$

In the following discussion, the wide flange shape of cross section is selected as an example for illustration. The initial yield function for a wide flange shape of cross section is

$$F_y = f_{s\xi}\,m_\xi + f_{s\eta}\,m_\eta + p - 1 = 0 \qquad (7.62)$$

where $f_{s\xi}$, $f_{s\eta}$ = shape factors of cross section.

The fully plastic yield function of a wide flange cross section has been derived approximately in Chapter 5 as

$$F_p = \begin{cases} \dfrac{m_\xi^a}{1 - p^b} + m_\eta + p^c - 1 & (m_\eta \geq \bar{m}_\eta) \\ m_\xi + p^d - 1 & (m_\eta \leq \bar{m}_\eta) \end{cases} \tag{7.63}$$

in which

$$\bar{m}_\eta = 1 - p^c - \frac{(1 - p^d)^a}{1 - p^b} \tag{7.64}$$

The four constants, a, b, c and d are determined according to the size of a particular wide flange cross section. For the cross section W8x31, for example, these constants are found to be

$$a = 2.453, \quad b = 1.209, \quad c = 2.714, \quad d = 1.987 \tag{7.65}$$

The approximate fully plastic interaction curves ($F_p = 0$) calculated from Eq. 7.63 using the above constants are compared in Fig. 7.3 with the exact curves shown in Chapter 5. Good agreement is observed.

In order to obtain the averaged interaction relationship, the averaging factors α and β are introduced as shown in Fig. 7.2.

$$\begin{aligned} m_{\xi a} &= m_{\xi u} - \alpha(m_{\xi u} - m_{\xi \ell}) \\ m_{\eta a} &= m_{\eta u} - \beta(m_{\eta u} - m_{\eta \ell}) \end{aligned} \tag{7.66}$$

where

$m_{\xi\ell}$, $m_{\eta\ell}$ = initial yield moments in uniaxial bending

$m_{\xi u}$, $m_{\eta u}$ = fully plastic moments in uniaxial bending

From Eqs. 7.62 and 7.63,

$$m_{\xi\ell} = (1 - p)/f_{s\xi} \qquad m_{\eta\ell} = (1 - p)/f_{s\eta}$$
$$m_{\xi u} = 1 - p^{d} \qquad m_{\eta u} = 1 - p^{c} \tag{7.67}$$

For simplicity, the averaged yield curve F_A is assumed to have the same form as that of the fully plastic yield curve, Eq. 7.63, but the biaxial bending moments m_ξ and m_η are proportionally reduced by the factors $m_{\xi a}/m_{\xi u}$ and $m_{\eta a}/m_{\eta u}$ respectively. Using Eq. 7.66, one obtains

$$F_A = \begin{cases} \dfrac{1}{1 - p^{b}}\left[\dfrac{m_\xi}{1 - \alpha + \alpha\, m_{\xi\ell}/m_{\xi u}}\right]^{a} + \dfrac{m_\eta}{1 - \beta + \beta\, m_{\eta\ell}/m_{\eta u}} & \\ \qquad + p^{c} - 1 & (m_\eta \geq \bar{\bar{m}}_\eta) \\ \dfrac{m_\xi}{1 - \alpha + \alpha\, m_{\xi\ell}/m_{\xi u}} + p^{d} - 1 & (m_\eta \leq \bar{\bar{m}}_\eta) \end{cases} \tag{7.68}$$

in which

$$\bar{\bar{m}}_\eta = (1 - \beta + \beta\, m_{\eta\ell}/m_{\eta u})\left[1 - p^{c} - \frac{(1 - p^{d})^{a}}{1 - p^{b}}\right] \tag{7.69}$$

When $\alpha = \beta = 0$, the averaged yield curve $F_A = 0$ becomes identical to the fully plastic yield curve $F_p = 0$ (upper bound) and when $\alpha = \beta = 1$, the curve passes through the two points which represent the initial yield condition $F_y = 0$ in the uniaxial bending cases ($m_\xi = 0$ or $m_\eta = 0$), but the two curves are not identical. For practical purposes, the values of α and β are assumed to be bounded by

$$0 \leq \alpha \leq 1, \qquad 0 \leq \beta \leq 1 \tag{7.70}$$

The choice of a proper value for α and β for a biaxially loaded column at its ultimate state will be discussed in what follows.

7.11 Ultimate Strength of Column

Using the averaged yield condition, Eq. 7.68, and the bending moments at the critical section of the column, Eq. 7.59, the ultimate strength of the column can be calculated as the combination of the applied end forces (p, m_{xo}, m_{yo}, m_{xL}, m_{yL}). This is the maximum strength of the biaxially loaded column

$$F_c\ (p,\ m_{xo},\ m_{yo},\ m_{xL},\ m_{yL}) = 0 \tag{7.71}$$

where

$$F_c = \begin{cases} \dfrac{1}{1 - p^b}\left[\dfrac{m_\xi^*}{1 - \alpha + \alpha/f_{s\xi}}\right]^a + \dfrac{m_\eta^*}{1 - \beta + \beta/f_{s\eta}} + p^c - 1 & (m_\eta^* \geq \bar{m}_\eta) \\ \dfrac{m_\xi^*}{1 - \alpha + \alpha/f_{s\xi}} + p^d - 1 & (m_\eta^* \leq \bar{m}_\eta) \end{cases} \tag{7.72}$$

Figure 7.4 shows the interaction curves for a column (W8x31) under the symmetric loading condition. The open circles are the results reported in Ref.20. These results are bounded by the two limiting curves (solid lines) and the averaging factors of $\alpha = \beta = 0.6$ is seen to give a good approximation to the more accurate results [20] as shown by the dotted line.

After a number of trial calculations, it is found that the following formula gives a good estimation of the averaging flow factors

$$\alpha = \beta = \begin{cases} \dfrac{P_y}{P_E} \\ 1.0 \ (\text{if } P_E \leq P_y) \end{cases} \tag{7.73}$$

in which P_E is the Euler's buckling load given by

$$P_E = \frac{\pi^2\ E\ I_\eta}{L^2} \tag{7.74}$$

This is a reasonable estimation because when $P_E \ll P_y$, elastic buckling will occur first, thus the initial yield condition will govern ($\alpha = \beta = 1$). If $P_E \gg P_y$, yielding of section will take place first and the ultimate state will be much closer to the fully plastic yield condition ($\alpha = \beta = 0$).

Using the formula (Eq. 7.73), the interaction curves for the biaxially loaded column (W8x31) with different slenderness ratios were caluclated where the axial force was kept constant ($p = 0.3$) as shown in Fig. 7.5. A good agreement is observed with the results reported in Ref. 20.

7.12 Numerical Examples

Figures 7.6 to 7.9 show the numerical results for a symmetrically loaded column of W8x31 cross section. The averaging factors α and β are determined according to Eq. 7.73. Since the loading is symmetric, the critical section is at the mid-span ($z^* = 1/2$). In such a case, a good agreement with more accurate results was usually observed (Fig. 7.5).

Figures 7.10 to 7.13 show results for an unsymmetrically loaded column with W8x31 section. The bending moments are applied only at the top end of the column ($z = 1$) and the critical section is located between the mid-span and the top end ($0.5 < z^* < 1.0$).

Harstead and Birnstiel reported experimental and theoretical analyses of biaxially loaded H-Columns [15], [37]. Using the same specimens,

Syal and Sharma calculated their ultimate strength [17]. Details of the H-sections are listed in Table 7.1. The results of the ultimate strength are also compared in Table 7.1 with the present approximate solutions. In Table 7.1 example No. H1 is the only unsymmetric loading case. The present solution is seen to give good approximation comparing with the results reported by Syal and Sharma [17].

7.13 Summary

A simple method to obtain the maximum strength of a biaxially loaded column is presented using an averaged yield condition of a cross section. Although it is an approximate solution, its validity has been shown by comparison with other reported results in symmetric as well as in an unsymmetric loading case. The interaction curves presented for the ultimate strength of a biaxially loaded column will be useful in the design of such columns for the various loading conditions specified.

8. ELASTIC-PLASTIC BEHAVIOR OF BIAXIALLY LOADED SECTIONS

8.1 Introduction

In analyses of biaxially loaded columns, investigation of cross sectional characteristics is essential. In elastic cases, cross sectional properties remain constant during the history of loadings and the method of solution is straightforward although non-linearity does exist due to the geometry change of the column. In inelastic cases, however, cross sectional properties will be a function of the loading history and the current state and past experience of stress and strain of a column section are important. Thus an exact analytical solution is difficult to obtain and numerical procedures appear inevitable.

Several investigations were reported on the elastic-plastic behavior of column cross sections. Most of these however are concerned with two dimensional in-plane loading. Further, proportional loading is often assumed so that the state of stress may be independent of loading history.

Santathadaporn and Chen [20,23] reported a generalized stress-strain relationship of biaxially loaded sections under monotonically increased loadings, where effects of shear stresses due to St. Venant torsion and warping torsion as well as normal stresses due to axial force and bending moments are taken into account in the yield condition. Baron and Venkatesan [32] presented hysteresis curves of an uniaxially loaded section. These curves will be used herein for comparison with

the present method of solution.

Herein, inelastic response of biaxially loaded sections is studied. Elastic unloading is taken into account so that nonproportional loading or repeated loading may be applied. Hysteresis curves are obtained which are important in low cycle fatigue and shakedown analysis.

Residual stresses existing in the section and strain hardening of the material are also included in the analysis. Only normal stress is assumed to contribute to the yield condition and the effects of shear stress on the yielding of the material are neglected.

The generalized stress-strain relationship presented herein will enable analysis of the response of columns or framed structures. The generalized stresses considered are an axial force, two bending moments about the principal axes and a bi-moment (or a warping force) and the corresponding generalized strains are an axial strain at the centroid of the section, two bending curvatures about the principal axes, and a warping curvature.

8.2 Stress-Strain Relationship Including Hysteresis

The stress-strain relationship is assumed to be tri-linear as shown in Fig. 8.1a. The initial stress-strain curve is composed of three regimes, elastic regime (OA or O A'), plastic regime (AB or A'B') and strain hardening regime (BC or B'C'). The points with a prime indicate the state of stress in a compression regime.

For the monotonically increased loading case, the stress-strain points follow the solid lines OABC or O A'B'C'. In this case

the state of stress (σ) is determined uniquely by the state of strain (ε).

The elastic unloading behavior is idealized as following. If the material is compressed after plastic extension up to the point G, it follows the path GG'B'C'. If unloaded from the point B, the corresponding unloading path is BD'B'C'. The material exhibits no "Bauschinger effect". However, if the material is unloaded and then compressed after some strain hardening up to the point H, the reversed path is HH'D"B"C', and some "Bauschinger effects" are exhibited.

This strain hardening, elastic unloading rule and "Bauschinger effect" are interpreted clearly by using a kinematic model of the parallelogram BD'B'D and the straight line AA' as shown in Fig. 8.2. Elastic loading or unloading within the line AA' does not change the condition at all (Fig. 8.2a). Plastic loading along lines DB or D'B' changes the position of line AA' only (Fig. 8.2b). Strain hardening along lines BC or B'C' translates the position of the parallelogram BD'B'D in parallel to the lines BC and B'C' (Fig. 8.2c). In this case, the elastic line AA' coincides with the line BD'. Positions of the lines BC and B'C' do not change for any loading history.

The state of stress A as shown in Fig. 8.1b is a general case and can be used to establish the limits of each regime. Regimes of state of stress are determined by the current strain ε:

$$\begin{aligned} &\varepsilon_1' \le \varepsilon \le \varepsilon_1 && \text{elastic regime} \\ &\varepsilon_2' \le \varepsilon < \varepsilon_1' \text{ or } \varepsilon_1 < \varepsilon \le \varepsilon_2 && \text{plastic regime} \\ &\varepsilon < \varepsilon_2' \text{ or } \varepsilon_2 < \varepsilon && \text{strain hardening regime} \end{aligned} \tag{8.1}$$

in which ϵ_1, ϵ_1', ϵ_2 and ϵ_2' are strain limits for each regime. These strain limits will also depend on the current strain ϵ as seen in Fig. 8.2. These strain limits can be expressed mathematically as:

elastic regime

$$\epsilon_1' \le \epsilon \le \epsilon_1: \quad \text{no changes on all strain limits} \tag{8.2a}$$

plastic regime

$$\epsilon_1 < \epsilon \le \epsilon_2: \quad \epsilon_1 = \epsilon,\ \epsilon_1' = \epsilon - 2\,\epsilon_y$$
$$\epsilon_2,\ \epsilon_2' \text{ no change} \tag{8.2b}$$
$$\epsilon_2' \le \epsilon < \epsilon_1': \quad \epsilon_1' = \epsilon,\ \epsilon_1 = \epsilon + 2\,\epsilon_y$$
$$\epsilon_2,\ \epsilon_2' \text{ no change}$$

strain hardening regime

$$\epsilon_2 < \epsilon: \quad \epsilon_1 = \epsilon \quad \epsilon_1' = \epsilon - 2\,\epsilon_y$$
$$\epsilon_2 = \epsilon \quad \epsilon_2' = \epsilon - 2\,\epsilon_H \tag{8.2c}$$
$$\epsilon < \epsilon_2': \quad \epsilon_1' = \epsilon \quad \epsilon_1 = \epsilon + 2\,\epsilon_y$$
$$\epsilon_2' = \epsilon \quad \epsilon_2 = \epsilon + 2\,\epsilon_H$$

where ϵ_y = initial yield strain

ϵ_H = initial hardening strain

The moduli of the stress-strain curve are defined as

E : elastic loading and all unloadings

$E_p = 0$: plastic loading

E_H : strain hardening

The current state of stress is determined uniquely by these three moduli, the current state of strain and the strain limits:

elastic regime

$$\varepsilon_1' \le \varepsilon \le \varepsilon_1: \quad \sigma = E(\varepsilon - \frac{\varepsilon_1+\varepsilon_1'}{2}) + E_H \frac{\varepsilon_2+\varepsilon_2'}{2} \tag{8.3}$$

plastic regime

$$\begin{aligned} \varepsilon_1 < \varepsilon \le \varepsilon_2: \quad & \sigma = E \frac{\varepsilon_1-\varepsilon_1'}{2} + E_H \frac{\varepsilon_2+\varepsilon_2'}{2} \\ \varepsilon_2' \le \varepsilon < \varepsilon_1': \quad & \sigma = E \frac{\varepsilon_1'-\varepsilon_1}{2} + E_H \frac{\varepsilon_2'+\varepsilon_2}{2} \end{aligned} \tag{8.4}$$

strain hardening regime

$$\begin{aligned} \varepsilon_2 < \varepsilon: \quad & \sigma = E \frac{\varepsilon_1-\varepsilon_1'}{2} + E_H(\varepsilon - \frac{\varepsilon_2-\varepsilon_2'}{2}) \\ \varepsilon < \varepsilon_2': \quad & \sigma = E \frac{\varepsilon_1'-\varepsilon_1}{2} + E_H(\varepsilon - \frac{\varepsilon_2'-\varepsilon_2}{2}) \end{aligned} \tag{8.5}$$

The above stress strain relationships are summarized in Table 8.1.

8.3 Partitioning of Cross Section

The cross section is cut into finite elements in order to compute the sectional forces. As an example, consider a wide flange section (D x B). Let the principal axes be the X and Y coordinates and the centroid of the section be the origin of the coordinates, the non-dimensionalized coordinates are

$$x = \frac{X}{B/2}, \qquad y = \frac{Y}{D/2} \tag{8.6}$$

The sectional properties, area A, moment of inertia I_x and I_y and warping moment of inertia I_w are calculated by

$$A = \int_A dA = \frac{BD}{4} \iint dxdy = \frac{BD}{4} \bar{A}$$

$$I_x = \int_A Y^2\ dA = \frac{D^2}{4}\frac{BD}{4}\iint y^2\ dxdy = \frac{BD^3}{16}\bar{I}_x$$

$$I_y = \int_A X^2\ dA = \frac{B^2}{4}\frac{BD}{4}\iint x^2\ dxdy = \frac{B^3D}{16}\bar{I}_y \tag{8.7}$$

$$I_w = \int_A X^2\ Y^2\ dA = \left(\frac{BD}{4}\right)^3 \iint x^2\ y^2\ dxdy = \left(\frac{BD}{4}\right)^3 \bar{I}_w$$

in which the non-dimensional quantities are

$$\begin{aligned} \bar{A} &= \iint dxdy \\ \bar{I}_x &= \iint y^2\ dxdy \\ \bar{I}_y &= \iint x^2\ dxdy \\ \bar{I}_w &= \iint x^2\ y^2\ dxdy \end{aligned} \tag{8.8}$$

Consider a rectangular element of the section ABCD as shown in Fig. 8.3. The coordinates of the two diagonal points A and C are

$$A\ (x_A,\ y_A) \quad \text{and} \quad C\ (x_C,\ y_C) \tag{8.9}$$

Cut the section into m x n finite elements, then the sizes of each element are

$$\Delta x = \frac{x_C - x_A}{m}, \qquad \Delta y = \frac{y_C - y_A}{n} \tag{8.10}$$

and the coordinates of the center point of the element (i,j) are

$$\begin{aligned} x_{ij} &= x_A + (i - \tfrac{1}{2})\ \Delta x \\ y_{ij} &= y_A + (j - \tfrac{1}{2})\ \Delta y \end{aligned} \tag{8.11}$$

Sectional properties of the rectangular element are

$$\bar{A} = \iint dxdy = \sum_{i=1}^{m}\sum_{j=1}^{n} \Delta x\ \Delta y$$

$$\bar{I}_x = \iint y^2 \, dxdy = \sum_{i=1}^{m} \sum_{j=1}^{n} y_{ij}^2 \, \Delta x \, \Delta y$$

$$\bar{I}_y = \iint x^2 \, dxdy = \sum_{i=1}^{m} \sum_{j=1}^{n} x_{ij}^2 \, \Delta x \, \Delta y \qquad (8.12)$$

$$\bar{I}_w = \iint x^2 \, y^2 \, dxdy = \sum_{i=1}^{m} \sum_{j=1}^{n} x_{ij}^2 \, y_{ij}^2 \, \Delta x \, \Delta y$$

8.4 Residual Stress

The residual stress distribution for a wide flange section is assumed to be linear in each plate element. The maximum compressive residual stress σ_{rc} occurs at the tips of flange plates. Since the residual stress is in self-equilibrium, the maximum tensile residual stress σ_{rt} at the junction point of flange and web is

$$\sigma_{rt} = \frac{\sigma_{rc}}{1 + \frac{D}{B}\frac{t_w}{t_f} - 2\frac{t_w}{B}} \qquad (8.13)$$

where

D = depth of wide flange section

B = width of flange plates

t_f = thickness of flange plate (8.14)

t_w = thickness of web plate

Using σ_{rc} and σ_{rt} the distribution of residual stress σ_r in the flange can be expressed as

$$\sigma_r = \sigma_{rt} - \frac{\sigma_{rc}+\sigma_{rt}}{B/2} |X| \qquad (8.15)$$

or non-dimensionally

$$\bar{\sigma}_r = \bar{\sigma}_{rt} - (\bar{\sigma}_{rc} + \bar{\sigma}_{rt}) |x| \qquad (8.16)$$

For most shapes of wide flange cross section the maximum residual stress of

$$\bar{\sigma}_{rc} = \frac{\sigma_{rc}}{\sigma_y} = 0.3 \tag{8.17}$$

is normally assumed.

8.5 Generalized Stress-Strain Relationships

Since only normal stress and normal strain are considered, deformation quantities related to normal strain are taken as generalized strains of the section:

$$\begin{aligned}
\epsilon_o &= \frac{1}{A}\int \epsilon \, dA && \text{strain at centroid} \\
\varphi_x &= \frac{1}{A}\int \frac{\partial \epsilon}{\partial Y} \, dA && \text{curvature about X-axis} \\
\varphi_y &= \frac{1}{A}\int \frac{\partial \epsilon}{\partial X} \, dA && \text{curvature about Y-axis} \\
\omega &= \frac{1}{A}\int \frac{\partial^2 \epsilon}{\partial X \partial Y} \, dA && \text{warping curvature about the centroid}
\end{aligned} \tag{8.18}$$

Strain distribution is assumed to be linear in X and Y coordinate,

$$\epsilon = \alpha + \beta X + \gamma Y + \delta XY \tag{8.19}$$

Using the doubly symmetric property of the cross section,

$$\begin{aligned}
\epsilon_o &= \frac{1}{A}\left[\alpha \int dA + \beta \int X \, dA + \gamma \int Y \, dA + \delta \int X\,Y \, dA\right] = \alpha \\
\varphi_x &= \frac{1}{A}\left[\gamma \int dA + \delta \int X \, dA\right] = \gamma \\
\varphi_y &= \frac{1}{A}\left[\beta \int dA + \delta \int Y \, dA\right] = \beta \\
\omega &= \frac{1}{A}\left[\delta \int dA\right] = \delta
\end{aligned} \tag{8.20}$$

Equation 8.19 has the form

$$\epsilon = \epsilon_o + \varphi_y X + \varphi_x Y + \omega X Y \tag{8.21}$$

The corresponding generalized stresses are determined from the rate of internal energy dissipation

$$\dot{D}_I = \int \sigma \dot{\epsilon} \, dA$$

$$= \dot{\epsilon}_o \int \sigma \, dA + \varphi_y \int \sigma X \, dA + \varphi_x \int \sigma Y \, dA + \dot{\omega} \int \sigma X Y \, dA \quad (8.22)$$

Namely,

$$\begin{aligned} P &= \int \sigma \, dA && \text{axial thrust} \\ M_x &= \int \sigma Y \, dA && \text{bending moment about X-axis} \\ M_y &= \int \sigma X \, dA && \text{bending moment about Y-axis} \\ M_\omega &= \int \sigma X Y \, dA && \text{warping moment about the centroid} \end{aligned} \quad (8.23)$$

These are the resultant forces or generalized stresses producing normal stress over the entire cross section (Fig. 8,4).

Introducing the non-dimensional variables

$$\bar{\sigma} = \frac{\sigma}{\sigma_y}, \qquad \bar{\epsilon} = \frac{\epsilon}{\epsilon_y} \quad (8.24)$$

and initial yielding quantities

$$\begin{aligned} P_y &= A \sigma_y, \quad \epsilon_{oy} = \epsilon_y \\ M_{px} &= \frac{I_x \sigma_y}{D/2}, \quad \varphi_{px} = \frac{\epsilon_y}{D/2} \\ M_{py} &= \frac{I_y \sigma_y}{B/2}, \quad \varphi_{py} = \frac{\epsilon_y}{B/2} \\ M_{p\omega} &= \frac{I_\omega \sigma_y}{BD/4}, \quad \omega_p = \frac{\epsilon_y}{BD/4} \end{aligned} \quad (8.25)$$

Then the generalized stresses are

$$p = \frac{P}{P_y} = \frac{1}{A \sigma_y} \int \sigma \, dA = \frac{1}{A} \int \bar{\sigma} \, da$$

$$m_x = \frac{M_x}{M_{px}} = \frac{D/2}{I_x \sigma_y} \int \sigma \, Y \, dA = \frac{1}{\bar{I}_x} \int \bar{\sigma} \, y \, da$$

$$m_y = \frac{M_y}{M_{py}} = \frac{B/2}{I_y \sigma_y} \int \sigma \, X \, dA = \frac{1}{\bar{I}_y} \int \bar{\sigma} \, x \, da \qquad (8.26)$$

$$m_\omega = \frac{M_\omega}{M_{p\omega}} = \frac{BD/4}{I_\omega \sigma_y} \int \sigma \, X \, Y \, dA = \frac{1}{\bar{I}_\omega} \int \bar{\sigma} \, x \, y \, da$$

in which $da = dx \, dy$

and the generalized strains are

$$\bar{\epsilon}_o = \frac{\epsilon_o}{\epsilon_{oy}} = \frac{\epsilon_o}{\epsilon_y} = \frac{1}{\bar{A}} \int \bar{\epsilon} \, da$$

$$\bar{\varphi}_x = \frac{\varphi_x}{\varphi_{px}} = \frac{D/2}{\epsilon_y} \varphi_x = \frac{1}{\bar{A}} \int \frac{\partial \bar{\epsilon}}{\partial y} da$$

$$\bar{\varphi}_y = \frac{\varphi_y}{\varphi_{py}} = \frac{B/2}{\epsilon_y} \varphi_y = \frac{1}{\bar{A}} \int \frac{\partial \bar{\epsilon}}{\partial x} da \qquad (8.27)$$

$$\bar{\omega} = \frac{\omega}{\omega_p} = \frac{BD/4}{\epsilon_y} \omega = \frac{1}{\bar{A}} \int \frac{\partial^2 \bar{\epsilon}}{\partial x \, \partial y} da$$

8.6 Tangent Stiffness

For simplicity, introduce the notation E_t, the tangent modulus of the material

$$E_t = \begin{cases} E & \text{elastic loading or all unloadings} \\ 0 & \text{plastic loading} \\ E_H & \text{strain hardening loading} \end{cases} \qquad (8.28)$$

Denoting the non-dimensional form of the moduli as

$$\bar{E}_t = E_t/E \qquad \bar{E}_H = E_H/E \qquad (8.29)$$

the loading and unloading criteria for each regime are obtained

elastic regime

$$\epsilon_1' \le \epsilon \le \epsilon_1 \qquad \bar{E}_t = 1.0 \tag{8.30a}$$

plastic regime

$$\begin{aligned} &\epsilon_1 < \epsilon \le \epsilon_2 && \dot{\epsilon} > 0 && \bar{E}_t = 0.0 \\ &&& \dot{\epsilon} < 0 && \bar{E}_t = 1.0 \\ &\epsilon_2' \le \epsilon < \epsilon_1' && \dot{\epsilon} > 0 && \bar{E}_t = 1.0 \\ &&& \dot{\epsilon} < 0 && \bar{E}_t = 0.0 \end{aligned} \tag{8.30b}$$

strain hardening regime

$$\begin{aligned} &\epsilon_2 < \epsilon && \dot{\epsilon} > 0 : && \bar{E}_t = \bar{E}_H \\ &&& \dot{\epsilon} < 0 : && \bar{E}_t = 1.0 \\ &\epsilon < \epsilon_2' && \dot{\epsilon} > 0 : && \bar{E}_t = 1.0 \\ &&& \dot{\epsilon} < 0 : && \bar{E}_t = \bar{E}_H \end{aligned} \tag{8.30c}$$

The nondimensional strain distribution including the residual strains ϵ_r has the form (Eq. 8.20)

$$\begin{aligned} \bar{\epsilon} = \frac{\epsilon}{\epsilon_y} &= \frac{1}{\epsilon_y}\left(\epsilon_o + Y\,\varphi_x + X\,\varphi_y + X\,Y\,\omega + \epsilon_r\right) \\ &= \bar{\epsilon}_o + y\,\bar{\varphi}_x + x\,\varphi_y + x\,y\,\bar{\omega} + \bar{\epsilon}_r \end{aligned} \tag{8.31}$$

since the residual strain, ϵ_r, is independent of time, therefore $\dot{\epsilon}_r = 0$, the strain rate equation of Eq.8.31 is

$$\dot{\bar{\epsilon}} = \dot{\bar{\epsilon}}_o + y\,\dot{\bar{\varphi}}_x + x\,\dot{\bar{\varphi}}_y + x\,y\,\dot{\bar{\omega}} \tag{8.32}$$

Using the tangent modulus $\bar{E}_t$, the stress-strain rate relationship can be expressed as

$$\dot{\bar{\sigma}} = \frac{\dot{\sigma}}{\sigma_y} = \frac{E_t}{\sigma_y}\dot{\epsilon} = \frac{E_t\,\epsilon_y}{\sigma_y}\dot{\bar{\epsilon}} = \frac{E_t}{E}\dot{\bar{\epsilon}} = \bar{E}_t\,\dot{\bar{\epsilon}} \tag{8.33}$$

Generalized stress-strain rate relationships are obtained from Eqs. 8.26, 8.32 and 8.33.

$$\dot{p} = \frac{1}{A}\left[\dot{\bar{\epsilon}}_o \int \bar{E}_t\, da + \dot{\bar{\varphi}}_x \int \bar{E}_t\, y\, da + \dot{\bar{\varphi}}_y \int \bar{E}_t\, x\, da + \dot{\bar{\omega}} \int \bar{E}_t\, x\, y\, da\right]$$

$$\dot{m}_x = \frac{1}{\bar{I}_x}\left[\dot{\bar{\epsilon}}_o \int \bar{E}_t\, y\, da + \dot{\bar{\varphi}}_x \int \bar{E}_t\, y^2\, da + \dot{\bar{\varphi}}_y \int \bar{E}_t\, x\, y\, da + \dot{\bar{\omega}} \int \bar{E}_t\, x\, y^2\, da\right] \tag{8.34}$$

$$\dot{m}_y = \frac{1}{\bar{I}_y}\left[\dot{\bar{\epsilon}}_o \int \bar{E}_t\, x\, da + \dot{\bar{\varphi}}_x \int \bar{E}_t\, x\, y\, da + \dot{\bar{\varphi}}_y \int \bar{E}_t\, x^2\, da + \dot{\bar{\omega}} \int \bar{E}_t\, x^2\, y\, da\right]$$

$$\dot{m}_\omega = \frac{1}{\bar{I}_\omega}\left[\dot{\bar{\epsilon}}_o \int \bar{E}_t\, x\, y\, da + \dot{\bar{\varphi}}_x \int \bar{E}_t\, x\, y^2\, da + \dot{\bar{\varphi}}_y \int \bar{E}_t\, x^2\, y\, da + \dot{\bar{\omega}} \int \bar{E}_t\, x^2\, y^2\, da\right]$$

or in a matrix form

$$\dot{f} = K\,\dot{\delta} \tag{8.35}$$

where

$\dot{f}$ = non-dimensional generalized stress rate vector

$\dot{\delta}$ = non-dimensional generalized strain rate vector

K = stiffness matrix

namely,

$$\dot{f} = \begin{bmatrix} \dot{p} \\ \dot{m}_x \\ \dot{m}_y \\ \dot{m}_\omega \end{bmatrix} \qquad \dot{\delta} = \begin{bmatrix} \dot{\bar{\epsilon}}_o \\ \dot{\bar{\varphi}}_x \\ \dot{\bar{\varphi}}_y \\ \dot{\bar{\omega}} \end{bmatrix} \tag{8.36}$$

and

$$K = \begin{bmatrix} \int \bar{E}_t \, da/\bar{A} & \int \bar{E}_t \, y \, da/\bar{A} & \int \bar{E}_t \, x \, da/\bar{A} & \int \bar{E}_t \, x \, y \, da/\bar{A} \\ \int \bar{E}_t \, y \, da/\bar{I}_x & \int \bar{E}_t \, y^2 \, da/\bar{I}_x & \int \bar{E}_t \, x \, y \, da/\bar{I}_x & \int \bar{E}t \, x \, y^2 \, da/\bar{I}_x \\ \int \bar{E}_t \, x \, da/\bar{I}_y & \int \bar{E}_t \, x \, y \, da/\bar{I}_y & \int \bar{E}_t \, x^2 \, da/\bar{I}_y & \int \bar{E}_t \, x^2 \, y \, da/\bar{I}_y \\ \int \bar{E}_t \, x \, y \, da/\bar{I}_\omega & \int \bar{E}_t \, x \, y^2 \, da/\bar{I}_\omega & \int \bar{E}_t \, x^2 \, y \, da/\bar{I}_\omega & \int \bar{E}_t \, x^2 \, y^2 \, da/\bar{I}_\omega \end{bmatrix} \quad (8.37)$$

In the elastic regime, $\bar{E}_t = 1$, and the stiffness matrix K becomes the unit matrix K_o using the doubly symmetric property of the cross section,

$$K_o = \begin{bmatrix} 1 & 0 & 0 & 0 \\ 0 & 1 & 0 & 0 \\ 0 & 0 & 1 & 0 \\ 0 & 0 & 0 & 1 \end{bmatrix} \quad (8.38)$$

8.7 Method of Solution

Herein, a solution is sought for the relationship of generalized stresses f and generalized strains δ for a biaxially loaded cross section. Since the problem is not linear, an iterative procedure must be applied. The numerical solution of Eq. 8.35 can be obtained by the tangent stiffness method. Details of the method have been given in Ref. 23. A brief description of the tangent stiffness method will be given herein.

Consider a generalized stress or a force vector f, a generalized strain or a deformation vector δ and their relationship as shown in

Fig. 8.5. The cross section has experienced loading along the path OA. At point A, the current force vector f_A, deformation vector δ_A and the stiffness matrix K_A are assumed to be known, the problem is to find the corresponding deformation vector δ_B when the force vector is increased from f_A to f_B.

Since the deformation increment $d\delta$, or $\dot{\delta}_1$ can be calculated from the force increment df or

$$\dot{f} = f_B - f_A \tag{8.39}$$

using the tangent stiffness K_A at the current state A

$$\dot{\delta}_1 = K_A^{-1} \dot{f} \tag{8.40}$$

The first approximate value of total deformation is obtained by

$$\delta_1 = \delta_A + \dot{\delta}_1 \tag{8.41}$$

From this approximate deformation δ_1, the total strain distribution $\bar{\epsilon}$ can be determined from Eq. 8.31 and hence the corresponding state of new stress can be determined uniquely from Eqs. 8.3, 8.4, 8.5 or Table 8.1. The strain limits are now changed according to these new strains. These new strain limits can be determined directly from Eq. 8.2. Integration of the stress over the entire cross section gives the new internal force vector f_1 using Eq. 8.26. This new state is expressed by the point 1 in Fig. 8.5. The new tangent stiffness K_1 at point 1 corresponding to the state f_1 and δ_1 can now be computed. The new internal force vector f_1 is now not in equilibrium with the externally applied force vector f_B. The first unbalanced force vector df_1 or $\dot{f}_1$ is computed from

$$\dot{f}_1 = f_B - f_1 \tag{8.42}$$

The next step is to find a correction deformation vector $d\delta_2$ or $\dot{\delta}_2$ which will be added to δ_1 in order to eliminate the unbalance force f_1. Vector $\dot{\delta}_2$ is obtained from

$$\dot{\delta}_2 = K_1^{-1} \dot{f}_1 \tag{8.43}$$

Repeating the same procedure for point 2 again, the second internal force vector f_2 and the unbalanced force vector

$$\dot{f}_2 = f_B - f_2 \tag{8.44}$$

are obtained.

Repeating the same procedure as at point 2 until the unbalanced force df_n or $\dot{f}_n$ at point n becomes zero or is within a prescribed tolerance limit, the final deformation vector is then obtained by

$$\delta_B \approx \delta_n \tag{8.45}$$

During the procedure, the unbalance force vector df may be negative as shown in Fig. 8.6. This happens when there is some strain hardening in the material. In such a case, tangent stiffness rather than elastic unloading stiffness should be used in the comuptations because this negative force vector is an imaginary unloading.

In most cases, a few cycles of iteration are found to be sufficient to obtain an accurate solution. Even with a large incremental force or a rather accurate calculation of large deformation on a plastic plateau the solution will generally converge within just a few more cycles of iteration.

8.8 Numerical Examples

Figure 8.7 is a proportional loading case with the loads $(P/P_y, M_x/M^*_{px}, M_y/M^*_{py})$ being increased proportionally and monotonically between 99% (point A) and -99% (point B) of the full plastic limit state (0.3, 0.6, 0.6). Strain hardening and residual stress are considered but warping deformation is restrained. For the case of no residual stresses over the cross section, the deformations $(\bar{\epsilon}_o, \bar{\varphi}_x, \bar{\varphi}_y)$ are found to be exactly the same at point A before and after the cycle of loading. At point B, they have the opposite sign but the magnitudes are the same. Since the warping deformation is assumed to be completely restrained, the corresponding warping moment M_w required for such a restraint is considered as a reaction. Its magnitude is also found to be the same at points A and B. The presence of residual stress is seen to have some effects on the elastic-plastic behavior of the curves but the effect of material strain hardening on the curves is found to be not significant. The energy dissipation during the first cycle of the loading is also shown in Fig. 8.7.

The influence of loading path on the curves is shown in Fig. 8.8. Five different loading paths are chosen in the figure to reach the same loading point A ($P/P_y = 0.3$, $M_x/M^*_{px} = 0.6$, $M_y/M^*_{py} = 0.6$).

As can be seen the same values of deformations are reached for all different loading paths. Although all the loading paths are monotonically increased, a large yielded portion of the section is seen to be unloaded elastically from load point D to H as shown in Fig. 8.8. The energy dissipations corresponding to each loading path are also shown in Fig. 8.8.

8.9 Response to Cyclic Loading

Response of section under a cyclic loading is of major importance in the low-cycle fatigue and shakedown analysis. In these analyses, estimation of energy dissipation during the loading cycle plays an important role.

Figure 8.9a shows the load m_y fluctuating between some limits, the other two loads are kept constant ($p = 0.3$, $m_x = 0.4$). The half amplitude of the limits for the moment m_y is, 0.6, 0.8, 0.9, 1.0 and 1.1. Since the elastic region is bounded by $-0.3 \leq m_y \leq 0.3$, plastic deformations are produced in all cases.

Numerical results are illustrated in Fig. 8.9b. In all cases, curvature $\bar{\varphi}_y$ decreases with loading cycles and tends to converge to a certain limit value. The deformations $\bar{\epsilon}_o$ and $\bar{\varphi}_x$ and the energy dissipation are seen to increase monotonically with the loading cycles for large amplitudes but tend to converge for small amplitudes ($m_y < 1.0$).

8.10 Subsequent Yield Surfaces

Since the loading condition is kept constant during the repetition of loadings, shakedown is possible only when the subsequent yield surface is transformed so that the loading points will eventually move within the yield surface.

Figure 8.10 shows subsequent yield surfaces due to loadings $p = 0$, $m_x = 0.4$ and m_y between 0.8 and -0.8. The dotted lines are the initial yield surface and the limiting yield surface. A load point

inside and outside of the yield surface represent elastic and elastic-plastic states of stress, respectively. No load point can move outside the limiting surface.

After the first loading (point A), the yield surface translates so that the load point A is now on the subsequent yield surface. There are two interesting points: a). The opposite side of point A moves towards the origin (Bauschinger Effect); b). The subsequent yield surface has a corner at the loading point.

After the second loading (point B), the subsequent yield surface changes again and both points A and B are now inside the surface. Thus the repetition of loading between A and B proceeds all in elastic regime and further plastic deformation has ceased, or the section has shaken down.

Figure 8.11 shows changes of the subsequent yield surface due to repeated loading p = 0.3, m_x = 0.4 and m_y between 1.1 and -1.1. The repeated loading m_y is applied between the points A and B. When the amplitude of m_y is small (m_y = 0.8, Fig. 8.10) the subsequent yield surface tends to change so that the section shakes down. When the amplitude is large (m_y = 1.1, Fig. 11), the tendency of shakedown is not observed.

8.11 Comparison with Other Report

In order to check the accuracy of the present solution, two uniaxial loading cases were investigated for which the numerical results

were reported (Ref. 32). The properties of the section and the materials are given as

wide flange section	:	W 14 x 176
yield stress	:	σ_y = 36 ksi
elastic modulus	:	E = 29000 ksi
residual stress	:	none
strain hardening	:	none

Figure 8.12 shows the results of two loading paths: a). strong axis bending moment M_x is applied alone; b). strong axis bending moment M_x and axial force P are loaded then unloaded proportionally. The solid line indicates the present solution and the open circles are results of Ref. 32. A good agreement is observed for the first loading case. Since the maximum deformation is very sensitive to the maximum load applied, some disagreement is observed in the second loading case. If the maximum load is adjusted so that the maximum axial strain ε_o matches to that of Ref. 32 a good agreement is then obtained for both axial strain and curvature as shown by dotted lines in Fig. 8.12.

8.12 Function Fitting of the Generalized Stress-Strain Curves

A generalized stress-strain hysteresis curve of a common structural section usually has the shape shown diagrammatically in Fig. 8.13. The curve is composed of three portions: initial loading portion, unloading portion, and reloading portion. For each portion, a function similar to a Ramberg-Osgood type of equation may be assumed. A somewhat similar technique for a steel building connection under cyclic loads has been reported in Ref. 33.

Initial Loading Portion (0 → A)

$$\frac{\Delta}{\Delta_o} = \frac{P}{P_o} + \alpha\left(\frac{P}{P_o}\right)^N \tag{8.46}$$

Unloading Portion (A → B)

$$\frac{\Delta-\Delta_A}{2\,\Delta_o} = \frac{P-P_A}{2\,P_o} - \alpha\left(\frac{P-P_A}{2\,P_o}\right)^N \tag{8.47}$$

Reloading Portion (B → A)

$$\frac{\Delta-\Delta_B}{2\,\Delta_o} = \frac{P-P_B}{2\,P_o} + \alpha\left(\frac{P-P_B}{2\,P_o}\right)^N \tag{8.48}$$

The last two equations are directly obtained from the first one by doubling the scale and shifting the origin. The four constants α, N, Δ_o and P_o are to be determined so that a given P-Δ curve can be closely represented by the functions. The following four conditions may be used for the determination of these four constants.

(a) P_o is assumed to be equal to P_A

$$P_o = P_A \tag{8.49}$$

(b) the slope γ at the origin must be fitted

$$\Delta_o = \frac{P_o}{\gamma} \tag{8.50}$$

(c) the function satisfies the point A

$$\alpha = \frac{\Delta_A}{\Delta_o} - 1 \tag{8.51}$$

(d) the farthest point C from the line OA is selected to satisfy the function

$$N = \frac{\log \dfrac{\gamma\,\Delta_A - P_A}{\gamma\,\Delta_C - P_C}}{\log \dfrac{P_A}{P_C}} \tag{8.52}$$

As an example, Fig. 8.14 shows the curve-fitting for the moment-curvature curve (M_x-φ_x curve) discussed in Fig. 8.7. The solid line is the actual numerical result and the dotted curve represents curve-fitting. The agreement observed is good. In this case, the four constants used in Eqs. 8.46, 8.47 and 8.48 are found to be:

$$\alpha = 4.38,\ N = 21,\ \varphi_{xo} = 0.636\ \varphi_{px},\ M_{xo} = 0.594\ M_{px} \tag{8.53}$$

8.13 Summary

1. A method of analysis for biaxially loaded sections is presented. In the analysis, residual stresses, strain-hardening and elastic unloading are considered.

2. Loading history dependence of the plastic deformation of a wide flange section is shown numerically. The plastic deformations are found to be independent of loading path provided the loads are increased monotonically.

3. Response of a cross section under a cyclic loading is studied. Shakedown of the cross section is investigated from the viewpoint of transformation of the subsequent yield surfaces.

4. Accuracy of the analysis is examined by comparing the solution with other reported results in uniaxial bending cases and good agreement is observed.

9. ANALYSIS OF BIAXIALLY LOADED COLUMNS

9.1 Introduction

The general analysis of a biaxially loaded column is essentially the same as the analysis of a space structure. In this Chapter, the column is assumed to consist of a number of segments and is treated as a space structure as shown in Fig. 9.1. Three dimensional displacements, rotations and a warping are taken into account at each node.

In computation of the segment stiffness matrices, the direct stiffness method is utilized. The elastic-plastic section properties are calculated making use of the method discussed in Chapter 8. Geometric and material nonlinearities are handled by application of a modified tangent stiffness approach.

The following assumptions are assumed in this Chapter:

1. Cross-sectional shapes considered herein are wide-flange sections.
2. Material properties governing stress-strain behavior is elastic-perfectly plastic.
3. Yielding is considered to be a function of normal stress only.
4. Segmental stiffnesses are based on undeformed straight segment behavior.
5. Section properties for the tangent stiffness of a segment are invariants within the segment and are calculated using the elastic portion of the cross section.

6. In computation of the warping moment of inertia, yielding is considered to occur only in the flange plates.
7. The direction change of warpings and bi-moments between two adjacent segments are neglected because of the small angle changes between segments.

9.2 Elastic-Plastic Section Properties

Consider a wide-flange section which has its centroid and shear center initially at the origin 0. The initial principal axes are represented by ξ_o and η_o as shown in Fig. 9.2a. At a moment after application of some loading, the section may be partially plastified as shown by the shaded portions in Fig. 9.2b. The instantaneous centroid and shear center move to point C and S, respectively. The instantaneous principal axes ξ and η are also determined for the remaining elastic portion of the section.

As generalized strain rates on the cross section, the following four deformation rates are considered:

$\dot{\epsilon}_c$ = normal strain rate at the centroid C

$\dot{\phi}_\xi$ = bending curvature rate about the ξ-axis

$\dot{\phi}_\eta$ = bending curvature rate about the η-axis

$\dot{\phi}_\omega$ = warping curvature rate about the shear center S

from which the normal strain rate distribution on the entire section is given by

$$\dot{\varepsilon} = \dot{\varepsilon}_c + \eta\dot{\phi}_\xi - \xi\dot{\phi}_\eta + \delta_\eta\dot{\phi}_\omega \tag{9.1}$$

where ω_η is normalized warping on the section which will be calculated by Eq. 9.17 as explained later. The current total strain distribution is obtained by addition of the strain rate $\dot{\varepsilon}$ to the strain ε_o in the previous state,

$$\varepsilon = \varepsilon_o + \dot{\varepsilon} \tag{9.2}$$

Since the material is assumed to be elastic-perfectly plastic and only normal stress contributes to yielding, the tangent modulus E_t at a point on the section is uniquely determined from the total strain ε and the strain rate $\dot{\varepsilon}$ using the rule discussed in Chapter 8 (See Table 8.1).

$$E_t = \begin{cases} E & \text{for elastic or unloading portion} \\ 0 & \text{for plastic loading portion} \end{cases} \tag{9.3}$$

The shear modulus G is used only in elastic regime,

$$G = \frac{E}{2(1+\nu)} \tag{9.4}$$

where ν is Poisson's ratio.

Section properties of the elastic portion are calculated first about the initial principal axes ξ_o and η_o,

$$\begin{aligned} EA_o &= \int E_t dA \\ EQ_{\xi o} &= \int E_t \eta_o dA \\ EQ_{\eta o} &= \int E_t \xi_o dA \\ EI_{\xi o} &= \int E_t \eta_o^2 dA \\ EI_{\eta o} &= \int E_t \xi_o^2 dA \\ EI_{\xi\eta o} &= \int E_t \xi_o \eta_o dA \end{aligned} \tag{9.5}$$

The above integrations are carried out using finite elements cut from the section as was done in Chapter 8.

The location of the instantaneous centroid C $(C_{\xi o}, C_{\eta o})$ and rotation angle of the instantaneous principal axes are calculated by

$$C_{\xi o} = \frac{EQ_{\eta o}}{EA_o} , \quad C_{\eta o} = \frac{EQ_{\xi o}}{EA_o} \tag{9.6}$$

and

$$\beta = \tan^{-1}\left[\sqrt{1+\left(\frac{EI_{\xi o}-EI_{\eta o}}{2EI_{\xi\eta o}}\right)^2} - \frac{EI_{\xi o}-EI_{\eta o}}{2EI_{\xi\eta o}}\right] \tag{9.7}$$

Rigidities of the section against force rates with respect to the instantaneous principal axes ξ and η are now obtained as follows:

(a) Tensile Rigidity (EA)

$$EA = EA_o \tag{9.8}$$

(b) Bending Rigidities ($EI_\xi EI_\eta$)

$$\begin{aligned} EI_\xi &= \cos^2\beta EI_\xi' + \sin^2\beta EI_\eta' - 2\sin\beta\cos\beta EI_{\xi\eta}' \\ EI_\eta &= \cos^2\beta EI_\eta' + \sin^2\beta EI_\xi' + 2\sin\beta\cos\beta EI_{\xi\eta}' \end{aligned} \tag{9.9}$$

in which

$$\begin{aligned} EI_\xi' &= EI_{\xi o} - C_{\eta o}^2 EA_o \\ EI_\eta' &= EI_{\eta o} - C_{\xi o}^2 EA_o \\ EI_{\xi\eta}' &= EI_{\xi\eta o} - C_{\xi o} C_{\eta o} EA_o \end{aligned} \tag{9.10}$$

(c) St. Venant Torsion Rigidities (GK_T)

$$GK_T = \frac{1}{3} G \Sigma b t^3 \tag{9.11}$$

where b and t are width and thickness of the elastic plate elements of the section.

(d) Warping Torsion Rigidity (EI_ω)

Location of the instantaneous shear center S $(s_{\xi o}, s_{\eta o})$ is determined so that the warping moment of inertia I_ω of the elastic portion of the section about the point may be minimum. For this purpose, it is assumed herein that the web plate remains elastic and the elastic portion of the section is idealized as shown in Fig. 9.3. The elastic length of flange plate in each quadrant may be calculated approximately by

$$b_i = \frac{1}{Et_f} \int_{A_i} E_t dA \quad (i = 1, \cdots 4) \tag{9.12}$$

First, the location of the shear center S $(s_{\xi o}, s_{\eta o})$ is assumed using the distances ρ_1 and ρ_2 from the upper flange and the web plate as shown in Fig. 9.3a.

$$S_{\xi o} = \rho_2, \quad S_{\eta o} = \frac{d}{2} - \rho_1 \tag{9.13}$$

Warping about the assumed shear center S is expressed by

$$\omega_o = \begin{cases} S_1\rho_1 & \text{for upper flange} \\ S_2\rho_2 + b_1\rho_1 & \text{for web plate} \\ (S_3 - b_3)(d-\rho_1) + b_1\rho_1 + d\rho_2 & \text{for lower flange} \end{cases} \tag{9.14}$$

in which S_1, S_2, and S_3 are coordinates on each plate element along its length from an edge as shown in Fig. 9.3b. The warping is normalized as

$$\omega_n = \bar{\omega}_o - \omega_o \tag{9.15}$$

where

$$\bar{\omega}_o = \frac{1}{A}\int \omega_o dA \tag{9.16}$$

$$= e_1\rho_1 + e_2\rho_2 + e_3$$

and

$$\begin{aligned} e_1 &= \frac{1}{2A}[(b_1+b_2)^2 t_f + 2b_1(b_3+b_4)t_f - (b_4^2-b_3^2)t_f + 2b_1 dt_\omega] \\ e_2 &= \frac{1}{2A} d[dt_\omega + 2(b_3+b_4)t_f] \\ e_3 &= \frac{1}{2A} dt_f(b_4^2-b_3^2) \end{aligned} \tag{9.17}$$

The distribution of ω_n is shown in Fig. 9.3b. This normalized warping is used for computation of normal strain rate $\dot{\varepsilon}$ in Eq. 9.1.

The warping moment of inertia about the assumed shear center is now calculated by

$$I_\omega = C_1\rho_1^2 + C_2\rho_1\rho_2 + C_3\rho_2^2 + C_4\rho_1 + C_5\rho_2 + C_6 \tag{9.18}$$

in which

$$C_1 = e_1^2(b_1+b_2)t_f - e_1(b_1+b_2)^2 t_f + (e_1-b_1)^2 dt_w + \frac{1}{3}(b_1+b_2)^3 t_f$$
$$+(e_1-b_1-b_3)^2(b_3+b_4)t_f + (e_1-b_1-b_3)(b_3+b_4)^2 t_f + \frac{1}{3}(b_3+b_4)^3 t_f$$

$$C_2 = 2e_1e_2(b_1+b_2)t_f - e_2(b_1+b_2)^2 t_f + 2(e_1-b_1)bdt_w - (e_1-b_1)d^2 t_w$$
$$+2(e_1-b_1-b_3)(e_2-d)(b_3+b_4)t_f + (e_2-d)(b_3+b_4)^2 t_f$$

$$C_3 = e_2^2(b_1+b_2)t_f + e_2^2 dt_w - bd^2 t_w + (b-d)^2(b_3+b_4)t_f + \frac{1}{3}d^3 t_w \qquad (9.19)$$

$$C_4 = 2e_1e_3(b_1+b_2)t_f - e_3(b_1+b_2)^2 t_f + 2(e_1-b_1)e_3 dt_w$$
$$+2(e_1-b_1-b_3)(e_3+b_3 d)(b_3+b_4)t_f + (e_3+b_3 d)(b_3+b_4)^2 t_f$$
$$-(e_1-b_1-b_3)(b_3+b_4)^2 dt_f - \frac{2}{3}(b_3+b_4)^3 d$$

$$C_5 = 2e_2e_3(b_1+b_2)t_f + 2e_2e_3 dt_w - e_3 d^2 t_w$$
$$+2(e_2-d)(e_3+b_3 d)(b_3+b_4)t_f - (e_2-d)(b_3+b_4)^2 dt_f$$

$$C_6 = e_3^2(b_1+b_2)t_f + e_3^2 dt_w + (e_3+b_3 d)^2(b_3+b_4)t_f$$
$$-(e_3+b_3 d)(b_3+b_4)^2 dt_f + \frac{1}{3}d^2(b_3+b_4)^3 t_f$$

Minimize I_ω using the conditions,

$$\frac{\partial I_\omega}{\partial \rho_1} = 0 \quad \text{and} \quad \frac{\partial I_\omega}{\partial \rho_2} = 0 \qquad (9.20)$$

and get the location of shear center

$$\rho_1 = (C_2C_5-2C_3C_4)/(4C_1C_3-C_2^2)$$
$$\rho_2 = (C_2C_4-2C_1C_5)/(4C_1C_3-C_2^2) \qquad (9.21)$$

Substitution of Eq. 9.21 into Eq. 9.18 gives the warping moment of inertia I_ω of the elastic portion of the section.

(e) Contribution of Axial Force to Twisting Moment ($\overline{K}$)

When warping ω exists on a section, axial stress σ has some contribution to twisting moment m_ζ. As explained in Reference 34 this relation is expressed by

$$m_\zeta = \overline{K}\omega \qquad (9.22)$$

and

$$\overline{K} = \int \sigma a^2 dA \qquad (9.23)$$

where "a" is the distance from the point to the current center of torsion which does not necessarily coincide with the instantaneous shear center S. In the present analysis, the center of torsion is assumed at the origin 0 for simplicity and the average value of σ for the entire section is used, thus

$$\overline{K} = -\frac{P}{A}(I_{\xi o}+I_{\eta o}) \tag{9.24}$$

in which P is axial compressive force acting on the section.

9.3 Segment Stiffness Matrix

Consider an undeformed segment AB of length L as shown in Fig. 9.4. The local coordinates (ξ,η,ζ) are defined as principal axes of the elastic portion of the section according to the right hand rule,

ξ = strong axis of the elastic section

η = weak axis of the elastic section

ζ = longitudinal axis from A to B

Forces and displacements at ends A and B are related by the stiffness relationship. Since warping is considered only in the longitudinal direction of the segment, there are seven forces and seven displacements at each end, namely,

Three forces and three displacements

$$[f(3)] = \begin{Bmatrix} f_\xi \\ f_\eta \\ f_\zeta \end{Bmatrix} \qquad [u(3)] = \begin{Bmatrix} u_\xi \\ u_\eta \\ u_\zeta \end{Bmatrix} \tag{9.25}$$

Three moments and three rotations

$$[m(3)] = \begin{bmatrix} m_\xi \\ m_\eta \\ m_\zeta \end{bmatrix} \qquad [\theta(3)] = \begin{bmatrix} \theta_\xi \\ \theta_\eta \\ \theta_\zeta \end{bmatrix} \tag{9.26}$$

A bi-moment and a warping

$$[m_\omega(1)] = m_\omega \qquad [\omega(1)] = \omega \tag{9.27}$$

In this Chapter, the parentheses [ ] indicate an array of numbers such as vector and matrix and the integer in ( ) shows the size of the array.

The bi-moment (moment distance product due to warping) and the warping are defined here specially for wide-flange sections to be

$$m_\omega = EI_\omega \theta''_\zeta \qquad \omega = \theta'_\zeta \tag{9.28}$$

where the prime indicates derivative with respect to ζ.

The segment stiffness matrix [k(14x14)] relates the fourteen forces [f(14)] to the fourteen displacements [u(14)].

$$\begin{bmatrix} f_A(3) \\ m_A(3) \\ m_{\omega A}(1) \\ f_B(3) \\ m_B(3) \\ m_{\omega B}(1) \end{bmatrix} = \begin{bmatrix} \quad k(14x14) \quad \end{bmatrix} \begin{bmatrix} u_A(3) \\ \theta_A(3) \\ \omega_A(1) \\ u_B(3) \\ \theta_B(3) \\ \omega_B(1) \end{bmatrix} \tag{9.29}$$

The subscripts A and B indicate the quantities at the end points A and B, respectively.

The segment stiffness matrix [k(14x14)] is computed considering axial deformation, bending-shear deformation and torsion-warping deformation, separetely. Further, the section properties are assumed to be constant within the segment. Thus the elastic analysis is available.

(a) Axial Stiffness

The segment AB is subjected to the axial end forces f_A and f_B, and the end displacements are u_A and u_B as shown in Fig. 9.5(a). The governing equation is

$$EA\, u''_\zeta = 0 \tag{9.30}$$

The general solution is

$$u_\zeta(\zeta) = C_1 + C_2\zeta \tag{9.31}$$

where C_1 and C_2 are integration constants. At the boundaries A and B,

$$\begin{bmatrix} u_{\zeta A} \\ u_{\zeta B} \end{bmatrix} = \begin{bmatrix} u_\zeta(0) \\ u_\zeta(L) \end{bmatrix} = \begin{bmatrix} 1 & 0 \\ 1 & L \end{bmatrix} \begin{bmatrix} C_1 \\ C_2 \end{bmatrix} \tag{9.32}$$

and

$$\begin{bmatrix} f_{\zeta A} \\ f_{\zeta B} \end{bmatrix} = EA \begin{bmatrix} -u'_\zeta(0) \\ u'_\zeta(L) \end{bmatrix} = EA \begin{bmatrix} 0 & -1 \\ 0 & 1 \end{bmatrix} \begin{bmatrix} C_1 \\ C_2 \end{bmatrix} \tag{9.33}$$

Eliminate C_1 and C_2 and get the stiffness relationship,

$$\begin{bmatrix} f_{\zeta A} \\ f_{\zeta B} \end{bmatrix} = EA \begin{bmatrix} 1 & -1 \\ 1 & 1 \end{bmatrix} \begin{bmatrix} u_{\zeta A} \\ u_{\zeta B} \end{bmatrix} \tag{9.34}$$

(b) Bending and Shear Stiffness

The segment AB is subjected to end forces $f_{\eta A}$, $f_{\eta B}$, $m_{\xi A}$, and $m_{\xi B}$. The end displacements are $u_{\eta A}$, $u_{\eta B}$, $\theta_{\xi A}$, and $\theta_{\xi B}$ as shown in Fig. 9.5b.

The governing equation is

$$EI_\xi u''''_\eta + P u''_\eta = 0 \tag{9.35}$$

or

$$u''''_\eta + k_3^2 u''_\eta = 0 \tag{9.36}$$

where P is the axial compressive force,

$$P = f_{\zeta A} = -f_{\zeta B} \tag{9.37}$$

and

$$k_\xi = \sqrt{\frac{P}{EI_\xi}} \tag{9.38}$$

The general solution is

$$u_\eta(\xi) = C_1 \cos k_\xi \xi + C_2 \sin k_\xi \xi + C_3 \xi + C_4 \tag{9.39}$$

where $C_1 \ldots C_4$ are the integration constants.

At the boundaries A and B,

$$\begin{bmatrix} u_{\eta A} \\ \theta_{\xi A} \\ u_{\eta B} \\ \theta_{\xi B} \end{bmatrix} = \begin{bmatrix} u_\eta(0) \\ -u'_\eta(0) \\ u_\eta(L) \\ -u'_\eta(L) \end{bmatrix} = \begin{bmatrix} 1 & 0 & 0 & 1 \\ 0 & -k & -1 & 0 \\ C_\xi & S_\xi & L & 1 \\ k_\xi S_\xi & -k_\xi C_\xi & -1 & 0 \end{bmatrix} \begin{bmatrix} C_1 \\ C_2 \\ C_3 \\ C_4 \end{bmatrix} \tag{9.40}$$

and

$$\begin{bmatrix} f_{\eta A} \\ m_{\xi A} \\ f_{\eta B} \\ m_{\xi B} \end{bmatrix} = EI_\xi \begin{bmatrix} u'''_\eta(0) + k_\xi u'_\eta(0) \\ u''_\eta(0) \\ -u'''_\eta(L) - k_\xi u'_\eta(L) \\ -u''_\eta(L) \end{bmatrix}$$

$$= EI_\xi k_\xi^2 \begin{bmatrix} 0 & 0 & 1 & 0 \\ -1 & 0 & 0 & 0 \\ 0 & 0 & -1 & 0 \\ C_\xi & S_\xi & 0 & 0 \end{bmatrix} \begin{bmatrix} C_1 \\ C_2 \\ C_3 \\ C_4 \end{bmatrix} \tag{9.41}$$

where

$$C_\xi = \cos k_\xi L \quad \text{and} \quad S_\xi = \sin k_\xi L \tag{9.42}$$

Eliminate $C_1 \ldots C_4$ and get the stiffness relation,

$$\begin{Bmatrix} f_{\eta A} \\ m_{\xi A} k_\xi \\ f_{\eta B} \\ m_{\xi B} k_\xi \end{Bmatrix} = \frac{EI_\xi k_\xi^2}{2-2C_\xi - k_\xi L S_\xi} \begin{bmatrix} S_\xi & C_\xi - 1 & -S_\xi & C_\xi - 1 \\ C_\xi - 1 & S_\xi - k_\xi L C_\xi & 1 - C_\xi & k_\xi L - S_\xi \\ -S_\xi & 1 - C_\xi & S_\xi & 1 - C_\xi \\ C_\xi - 1 & k_\xi L - S_\xi & 1 - C_\xi & S_\xi - k_\xi L C_\xi \end{bmatrix} \begin{Bmatrix} U_{\eta A} k_\xi \\ \theta_{\xi A} \\ U_{\eta B} k_\xi \\ \theta_{\xi B} \end{Bmatrix} \tag{9.43}$$

In a similar way, the bending and shear stiffness relationship about the η-axis is given by,

$$\begin{Bmatrix} f_{\xi A} \\ m_{\eta A} k_\eta \\ f_{\xi B} \\ m_{\eta B} k_\eta \end{Bmatrix} = \frac{EI_\eta k_\eta^2}{2-2C_\eta - k_\eta L S_\eta} \begin{bmatrix} S_\eta & 1 - C_\eta & -S_\eta & 1 - C_\eta \\ 1 - C_\eta & S_n - k_\eta L C_\eta & C_\eta - 1 & k_\eta L - S_\eta \\ -S_\eta & C_\eta - 1 & S_\eta & C_\eta - 1 \\ 1 - C_\eta & k_\eta L - S_\eta & C_\eta - 1 & S_\eta - k_\eta L C_\eta \end{bmatrix} \begin{Bmatrix} U_{\xi A} k_\xi \\ \theta_{\eta A} \\ U_{\xi B} k_\eta \\ \theta_{\eta B} \end{Bmatrix} \tag{9.44}$$

where

$$k_\eta = \sqrt{\frac{P}{EI_\eta}} \tag{9.45}$$

and

$$C_\eta = \cos k_\eta L \quad \text{and} \quad S_\eta = \sin k_\eta L \tag{9.46}$$

(c) Torsion and Warping Stiffness

The segment AB is subjected to the end forces $m_{\zeta A}$, $m_{\zeta B}$, $m_{\omega A}$, and $m_{\omega B}$. The end displacements are $\theta_{\zeta A}$, $\theta_{\zeta B}$, ω_A, and ω_B as shown in Fig. 9.5c. The governing equation is

$$EI\ \theta_\zeta'''' - (GK_T+\bar{K})\theta_\zeta'' = 0 \tag{9.47}$$

or

$$\theta_\zeta'''' - k_\zeta^2\theta''_\zeta = 0 \tag{9.48}$$

where

$$k_\zeta = \sqrt{\frac{GK_T+\bar{K}}{EI_\omega}} \tag{9.49}$$

The general solution is

$$\theta_\zeta(\zeta) = C_1\cosh k_\zeta\zeta + C_2\sinh k_\zeta\zeta + C_3 k_\zeta\zeta + C_4 \tag{9.50}$$

where $C_1 \ldots C_4$ are integration constants. At the boundaries A and B,

$$\begin{bmatrix} \theta_{\zeta A} \\ \omega_A \\ \theta_{\zeta B} \\ \omega_B \end{bmatrix} = \begin{bmatrix} \theta_\zeta(0) \\ \theta'_\zeta(0) \\ \theta_\zeta(L) \\ \theta'_\zeta(L) \end{bmatrix} = \begin{bmatrix} 1 & 0 & 0 & 1 \\ 0 & k_\zeta & k_\zeta & 0 \\ C_\zeta & S_\zeta & k_\zeta L & 1 \\ k_\zeta S_\zeta & k_\zeta C_\zeta & k_\zeta & 0 \end{bmatrix} \begin{bmatrix} C_1 \\ C_2 \\ C_3 \\ C_4 \end{bmatrix} \tag{9.51}$$

and

$$\begin{bmatrix} m_{\zeta A} \\ m_{\omega A} \\ m_{\zeta B} \\ m_{\omega B} \end{bmatrix} = EI_\omega \begin{bmatrix} \theta'''_\zeta(0) - k_\zeta^2\theta'_\zeta(0) \\ -\theta''_\zeta(0) \\ -\theta'''_\zeta(L) + k_\zeta^2\theta'_\zeta(L) \\ \theta''_\zeta(L) \end{bmatrix}$$

$$= k_\zeta^3 EI_\omega \begin{bmatrix} -1/k_\zeta & 0 & 0 & 0 \\ 0 & 0 & -1 & 0 \\ C_\zeta/k_\zeta & S_\zeta/k_\zeta & 0 & 0 \\ 0 & 0 & 1 & 0 \end{bmatrix} \begin{Bmatrix} C_1 \\ C_2 \\ C_3 \\ C_4 \end{Bmatrix} \tag{9.52}$$

where $S_\zeta = \sinh k_\zeta L$ and $C_\zeta = \cosh k_\zeta L$ (9.53)

Eliminate $C_1 \ldots C_4$ and get the stiffness relationship,

$$\begin{Bmatrix} m_{\zeta A} \\ m_{\omega A} k_\zeta \\ m_{\zeta B} \\ m_{\omega B} k_\zeta \end{Bmatrix} = \frac{k_\zeta^3 EI_\omega}{2-2C_\zeta+k_\zeta L S_\zeta} \begin{bmatrix} S_\zeta & C_\zeta-1 & -S_\zeta & C_\zeta-1 \\ C_\zeta-1 & k_\zeta L C_\zeta - S_\zeta & 1-C_\zeta & S_\zeta - k_\zeta L \\ -S_\zeta & 1-C_\zeta & S_\zeta & 1-C_\zeta \\ C_\zeta-1 & S_\zeta - k_\zeta L & 1-C_\zeta & k_\zeta L C_\zeta - S_\zeta \end{bmatrix} \begin{Bmatrix} \theta_{\zeta A} \\ \omega_A/k_\zeta \\ \theta_{\zeta B} \\ \omega_B/k_\zeta \end{Bmatrix} \tag{9.54}$$

This stiffness matrix was dirived first by Krajcinovic in Reference 36.

Summing up the above stiffness relationships together, the segment stiffness matrix [k] is composed,

$$[k(14x14)] = \begin{bmatrix} k_{AA}(7x7) & k_{AB}(7x7) \\ k_{BA}(7x7) & k_{BB}(7x7) \end{bmatrix} \tag{9.55}$$

where $[k_{AA}]$ =

$$\begin{bmatrix}
\frac{EI_\eta k_\eta^3 S_\eta}{2-2C_\eta-k_\eta LS_\eta} & & & & & & \\
0 & \frac{EI_\xi k_\xi^3 S_\xi}{2-2C_\xi-k_\xi LS_\xi} & & & & & \\
0 & 0 & \frac{EA}{L} & & & & \\
0 & -\frac{EI_\xi k_\xi^2(1-C_\xi)}{2-2C_\xi-k_\xi LS_\xi} & 0 & \frac{EI_\xi k_\xi(S_\xi-k_\xi LC_\xi)}{2-2C_\xi-k_\xi LS_\xi} & & & \\
\frac{EI_\eta k_\eta^2(1-C_\eta)}{2-2C_\eta-k_\eta LS_\eta} & 0 & 0 & 0 & \frac{EI_\eta k_\eta(S_\eta-k_\eta LC_\eta)}{2-2C_\eta-k_\eta LS_\eta} & & \\
0 & 0 & 0 & 0 & 0 & \frac{EI_\omega k_\zeta^3 S_\zeta}{2-2C_\zeta+k_\zeta LS_\zeta} & \\
0 & 0 & 0 & 0 & 0 & \frac{EI_\omega k_\zeta^2(C_\zeta-1)}{2-2C_\zeta+k_\zeta LS_\zeta} & \frac{EI_\omega k_\zeta(k_\zeta LC_\zeta-S_\zeta)}{2-2C_\zeta+k_\zeta S_\zeta}
\end{bmatrix}$$

SYM.

(9.56)

$[k_{AB}]$ =

$$\begin{bmatrix}
\frac{-EI_\eta k_\eta^3 S_\eta}{2-2C_\eta-k_\eta LS_\eta} & & & & & & \\
0 & \frac{-EI_\xi k_\xi^3 S_\xi}{2-2C_\xi-k_\xi LS_\xi} & & & & & \\
0 & 0 & \frac{-EA}{L} & & & & \\
0 & \frac{EI_\xi k_\xi^2(1-C_\xi)}{2-2C_\xi-k_\xi LS_\xi} & 0 & \frac{EI_\xi k_\xi(k_\xi L-S_\xi)}{2-2C_\xi-k_\xi LS_\xi} & & & \\
\frac{-EI_\eta k_\eta^2(1-C_\eta)}{2-2C_\eta-k_\eta LS_\eta} & 0 & 0 & 0 & \frac{EI_\eta k_\eta(k_\eta L-S_\eta)}{2-2C_\eta-k_\eta LS_\eta} & & \\
0 & 0 & 0 & 0 & 0 & \frac{-EI_\omega k_\zeta^3 S_\zeta}{2-2C_\zeta+k_\zeta LS_\zeta} & \\
0 & 0 & 0 & 0 & 0 & \frac{-EI_\omega k_\zeta^2(C_\zeta-1)}{2-2C_\zeta+k_\zeta LS_\zeta} & \frac{-EI_\omega k_\zeta(k_\zeta LC-S_\zeta)}{2-2C_\zeta+k_\zeta LS_\zeta}
\end{bmatrix}$$

ANTI-SYM.

(9.57)

$$[k_{BB}] =$$

$$\begin{bmatrix}
\frac{EI_\eta k_\eta^3 S_\eta}{2-2C_\eta-k_\eta LS_\eta} & & & & & & \\
0 & \frac{EI_\xi k_\xi^3 S_\xi}{2-2C_\xi-k_\xi LS_\xi} & & & & \underline{\text{SYM.}} & \\
0 & 0 & \frac{EA}{L} & & & & \\
0 & \frac{EI_\xi k_\xi^2(1-C_\xi)}{2-2C_\xi-k_\xi LS_\xi} & 0 & \frac{EI_\xi k_\xi(S_\xi-k_\xi LC_\xi)}{2-2C_\xi-k_\xi LS_\xi} & & & \\
\frac{-EI_\eta k_\eta^2(1-C_\eta)}{2-2C_\eta-k_\eta LS_\eta} & 0 & 0 & 0 & \frac{EI_\eta k_\eta(S_\eta-k_\eta LC_\eta)}{2-2C_\eta-k_\eta LS_\eta} & & \\
0 & 0 & 0 & 0 & 0 & \frac{EI_\omega k_\zeta^3 S_\zeta}{2-2C_\zeta-k_\zeta LS_\zeta} & \\
0 & 0 & 0 & 0 & 0 & \frac{-EI_\omega k_\zeta^2(C_\zeta-1)}{2-2C_\zeta-k_\zeta LS_\zeta} & \frac{EI_\omega k_\zeta(k_\zeta LC_\zeta-S_\zeta)}{2-2C_\zeta-k_\zeta S_\zeta}
\end{bmatrix}$$

(9.58)

and

$$[k_{BA}] = [k_{AB}]^T \tag{9.59}$$

In computation of the segment stiffness, constant section properties are used throughout the segment as given by Eqs. 9.8 to 9.34. The sectional deformation rates which are necessary in computation of strain rate distribution in Eq. 9.1 are calculated as averages of the end displacement rates of the segment.

$$\begin{aligned}
\dot{\varepsilon}_c &= \dot{U}'_\zeta = \frac{\dot{U}_{\zeta B} - \dot{U}_{\zeta A}}{L} \\
\dot{\phi}_\xi &= \dot{\theta}'_\xi = \frac{\dot{\theta}_{\xi B} - \dot{\theta}_{\xi A}}{L} \\
\dot{\phi}_\eta &= -\dot{\theta}'_\eta = -\frac{\dot{\theta}_{\eta B} - \dot{\theta}_{\eta A}}{L} \\
\dot{\phi}_\omega &= \dot{\omega}' = \frac{\dot{\omega}_B - \dot{\omega}_A}{L}
\end{aligned} \tag{9.60}$$

The warping curvature ϕ_ω, the warping ω and the torsion angle θ_ζ are related by

$$\phi_\omega = \omega' = \theta''_\xi \tag{9.61}$$

9.4 Rotation Matrix and Master Stiffness Matrix

In order to make the master stiffness matrix for the whole structure by stacking up the segment stiffness matrices, a rotation matix [R(3x3)] is required which transforms a vector from the global system (X, Y, Z) to the local system (ξ,η,ζ)

$$[V_{local}] = [R(3x3)][V_{global}] \tag{9.62}$$

or

$$\begin{bmatrix} V_\xi \\ V_\eta \\ V_\zeta \end{bmatrix} = \begin{bmatrix} (\xi X) & (\xi Y) & (\xi Z) \\ (\eta X) & (\eta Y) & (\eta Z) \\ (\zeta X) & (\zeta Y) & (\zeta Z) \end{bmatrix} \begin{bmatrix} V_X \\ V_Y \\ V_Z \end{bmatrix} \tag{9.63}$$

where (ξX) is the direction cosine between the local ξ-axis and the global X-axis etc.

In computation of the rotation matrix, [R(3x3)], total displacements of segments rather than their rates must be taken into account. Let us consider a segment AB deformed from the original state A_0B_0 in the global system as shown in Fig. 9.6. The location of the original points A_0 and B_0 and the unit vectors in the local axes $\vec{v}_{\xi 0}$, $\vec{v}_{\eta 0}$, and $\vec{v}_{\zeta 0}$ are known,

$$\vec{v}_{\xi o}: \begin{bmatrix} (\xi_o X) \\ (\xi_o Y) \\ (\xi_o Z) \end{bmatrix} \quad \vec{v}_{\xi o}: \begin{bmatrix} (\eta_o X) \\ (\eta_o Y) \\ (\eta_o Z) \end{bmatrix} \quad \vec{v}_{\zeta o}: \begin{bmatrix} (\zeta_o X) \\ (\zeta_o Y) \\ (\zeta_o Z) \end{bmatrix} \tag{9.64}$$

After the deformation, the end points are located

$$\text{A:} \quad \begin{bmatrix} X_A \\ Y_A \\ Z_A \end{bmatrix} = \begin{bmatrix} X_{AO} \\ Y_{AO} \\ Z_{AO} \end{bmatrix} + \begin{bmatrix} U_{XA} \\ U_{XA} \\ U_{ZA} \end{bmatrix} \tag{9.65}$$

and

$$\text{B:} \quad \begin{bmatrix} X_B \\ Y_B \\ Z_B \end{bmatrix} = \begin{bmatrix} X_{BO} \\ Y_{BO} \\ Z_{BO} \end{bmatrix} + \begin{bmatrix} U_{XB} \\ U_{YB} \\ U_{ZB} \end{bmatrix} \tag{9.66}$$

The length AB is now

$$L = (X_B-X_A)^2+(Y_B-Y_A)^2+(Z_B-Z_A)^2 \tag{9.67}$$

and the new ζ-axis is determined by its unit vector

$$\vec{v}_\zeta: \begin{bmatrix}(\zeta X)\\(\zeta Y)\\(\zeta Z)\end{bmatrix} = \begin{bmatrix}(X_B-X_A)/L\\(Y_B-Y_A)/L\\(Z_B-Z_A)/L\end{bmatrix} \tag{9.68}$$

Determination of the new η-axis is not straightforward. First, the η_0-axis rotates about the ζ_0-axis by the average angle of rotation at ends A_0 and B_0 plus rotation of principal axes due to yielding of the section.

$$\bar{\theta}_{\zeta 0} = \frac{1}{2}(\theta_{\zeta OA}+\theta_{\zeta OB})+\beta \tag{9.69}$$

Thus the $\bar{\eta}$-axes is obtained as shown in Fig. 9.7.

$$\vec{v}_{\bar{\eta}}: \begin{bmatrix}(\bar{\eta}X)\\(\bar{\eta}Y)\\(\bar{\eta}Z)\end{bmatrix} = \begin{bmatrix}(\eta_o X)\cos\bar{\theta}_{\zeta o}-[(\eta_o Y)(\zeta_o Z)-(\eta_o Z)(\zeta_o Y)]\sin\bar{\theta}_{\zeta o}\\(\eta_o Y)\cos\bar{\theta}_{\zeta o}-[(\eta_o Z)(\zeta_o X)-(\eta_o X)(\zeta_o Z)]\sin\bar{\theta}_{\zeta o}\\(\eta_o Z)\cos\bar{\theta}_{\zeta o}-[(\eta_o X)(\zeta_o Y)-(\eta_o Y)(\zeta_o X)]\sin\bar{\theta}_{\zeta o}\end{bmatrix} \tag{9.70}$$

Since the direction of the η-axis coincides with the projection of $\vec{v}_{\bar{\eta}}$ on the plane perpendicular to the ζ-axis,

$$\vec{v}_\eta: \begin{bmatrix}(\eta X)\\(\eta Y)\\(\eta Z)\end{bmatrix} = \begin{bmatrix}(\eta X) - N(\zeta X)\\(\eta Y) - N(\zeta Y)\\(\eta Z) - N(\zeta Z)\end{bmatrix} /L_\eta \tag{9.71}$$

where N is the dot-product of $\vec{v}_\eta$ and $\vec{v}_\zeta$,

$$N = \vec{v}_\eta \cdot \vec{v}_\zeta = (\bar{\eta}X)(\zeta X)+(\bar{\eta}Y)(\zeta Y)+(\bar{\eta}Z)(\zeta Z) \tag{9.72}$$

and the length of the projected $\vec{v}_\eta$ is

$$L_\eta = \sqrt{[(\bar{\eta}X)-N(\zeta X)]^2+[(\bar{\eta}Y)-N(\zeta Y)]^2+[(\bar{\eta}Z)-N(\zeta Z)]^2} \tag{9.73}$$

The unit vector in the new ξ-axis, $\vec{v}_\xi$, is obtained as the cross-product of $\vec{v}_\eta$ and $\vec{v}_\zeta$,

$$v_\xi: \begin{bmatrix}(\xi Y)\\(\xi Y)\\(\xi Z)\end{bmatrix} = \begin{bmatrix}(\eta Y)(\zeta Z) & (\eta Z)(\zeta Y)\\(\eta Z)(\zeta X) - (\eta X)(\zeta Z)\\(\eta X)(\zeta Y) & (\eta Y)(\zeta X)\end{bmatrix} \tag{9.74}$$

Now, the rotation matrix of the segment AB after the deformation is determined from Eq. 9.68, Eq. 9.71, and Eq. 9.74.

$$[R(3x3)]=\begin{bmatrix}(\xi Y) & (\xi Y) & (\xi Z)\\(\eta X) & (\eta Y) & (\eta Z)\\(\zeta X) & (\zeta Y) & (\zeta Z)\end{bmatrix} \tag{9.75}$$

It is to be emphasized that this rotation matrix has been obtained taking the geometric change into consideration.

Since warping is considered only in the longitudinal direction of the column, the force vector [f(14)] and the displacement vector [u(14)] in the local system are transformed into the global system [F(14)] and [U(14)] by using the rotation matrix [R(14x14)].

$$\begin{aligned}[F(14)] &= [R^T(14x14)][f(14)]\\ [U(14)] &= [R^T(14x14)][u(14)]\end{aligned} \tag{9.76}$$

Namely

$$\begin{bmatrix} F_A(3) \\ M_A(3) \\ M_{\omega A}(1) \\ F_B(3) \\ M_B(3) \\ M_{\omega B}(1) \end{bmatrix} = \left[\begin{array}{cc|cc} R^T(3x3) & & 0 & \\ & R^T(3x3) & & \\ & & 1 & \\ \hline & & R^T(3x3) & \\ 0 & & & R^T(3x3) \\ & & & & 1 \end{array}\right] \begin{bmatrix} f_A(3) \\ m_A(3) \\ m_{\omega A}(1) \\ f_B(3) \\ m_B(3) \\ m_{\omega B}(1) \end{bmatrix} \tag{9.77}$$

and

$$\begin{bmatrix} U_A(3) \\ \theta_A(3) \\ \Omega_A(1) \\ U_B(3) \\ \theta_B(3) \\ \Omega_B(1) \end{bmatrix} = \left[\begin{array}{cc|cc} R^T(3x3) & & 0 & \\ & R^T(3x3) & & \\ & & 1 & \\ \hline & & R^T(3x3) & \\ 0 & & & R^T(3x3) \\ & & & & 1 \end{array}\right] \begin{bmatrix} u_A(3) \\ \theta_A(3) \\ \omega_A(1) \\ u_B(3) \\ \theta_B(3) \\ \omega_B(1) \end{bmatrix} \tag{9.78}$$

where $[R^T(3x3)]$ is the transpose of matrix $[R(3x3)]$ which is given by Eq. 9.75.

Now the segment stiffness relationship Eq. 9.29 is also transformed into the global system by use of Eq. 9.76.

$$[F(14)] = [R^T(14x14)][k(14x14)][R(14x14)][U(14)] \tag{9.79}$$

Stacking up this relationship for all segments, the stiffness relationship of the whole structure is obtained

$$[F(N)] = [K(NxN)][U(N)] \tag{9.80}$$

where

$$[K(NxN)] = \text{master stiffness matrix} = \Sigma[R^T][k][R]$$
$$N = 7x(\text{number of nodal points}) \tag{9.81}$$

Since the master stiffness matrix [K(NxN)] is symmetric and diagonally populated, the banded stiffness matrix [K(NxNB)] is used to save computer storage. The band width NB given by

NB = 7x(the maximum number of connected nodes)

in case of column analyses, only two nodes are connected by a segment, thus NB = 14 is sufficient.

9.5 Tangent Stiffness Approach

The master stiffness matrix [K] obtained in Eq. 9.80 is a tangent stiffness of the system, because the current geometry [R] and the instantaneous section properties were used in its computation.

Let us consider a structure which is subjected to forces $[F_A]$ and has displacements $[U_A]$. This state is shown by point A in Fig. 9.8a. When the forces are increased from $[F_A]$ to $[F_B]$, the displacements become $[U_B]$. The correct values of $[U_B]$ cannot be obtained directly because of non-linearity of the system. Thus some interative procedures must be applied. The tangent stiffness approach is one of the techniques which is used herein being somewhat modified as presented in what follows.

Since stiffness of a system is a function of the current deformation, the tangent stiffness matrix [K] changes from $[K_A]$ to $[K_B]$ during the deformation change from $[U_A]$ to $[U_B]$. In Fig. 9.8a, the stiffnesses are represented by the slopes of the load-deflection curve. In a loading state of a system, the stiffness may be assumed to decrease monotonically. Thus the secant stiffness $[\bar{K}]$ between the two states A and B is bounded by

$$|K_A| \leq |\bar{K}| \leq |K_B| \tag{9.82}$$

or using an averaging factor α, it is expressed as

$$[\bar{K}] = (1-\alpha)[K_A] + [K_B] \tag{9.83}$$

The averaging factor α is bounded by

$$0 \leq \alpha \leq 1 \tag{9.84}$$

In the extreme cases,

$$\begin{aligned} &\alpha = 0 \quad [K] = [K_A] \quad \text{upper limit} \\ &\alpha = 1 \quad [K] = [K_B] \quad \text{lower limit} \end{aligned} \tag{9.85}$$

If the factor α could be correctly estimated, the deformation $[U_B]$ would be solved directly without using laborious iterative techniques. Since it is not possible, a successive approach is applied using a fixed value for α.

Referring to Fig. 9.8b, the initial force difference is

$$[\Delta F_0] = [F_B]-[F_A] \tag{9.86}$$

Using the tangent stiffness at point A, $[K_A]$, the new deformations $[U_1]$ are calculated by

$$[U_1] = [K_A]^{-1}[\Delta F_0]+[U_A] \tag{9.87}$$

From the deformations, the tangent stiffness $[K_1]$ is obtained. The corresponding forces $[F_1]$ are calculated using Eq. 9.83 as

$$[F_1] = [(1-\alpha)K_A+K_1][U_1-U_A]+[F_A] \tag{9.88}$$

This state is shown by point P_1 in Fig. 9.8b. There is an unbalanced force of

$$[\Delta F_1] = [F_B]-[F_1] \tag{9.89}$$

Then repeat the same procedure and get the new state P_2 by

$$\begin{aligned} [U_2] &= [K_1]^{-1}[\Delta F_1]+(U_1] \\ [F_2] &= [(1-\alpha)K_A+K_B][U_2-U_1]+[F_1] \\ [\Delta F_2] &= [F_B]-[F_2] \end{aligned} \tag{9.90}$$

After n-cycles of iteration the above relations yield

$$\begin{aligned} [U_n] &= [K_{n-1}]^{-1}[\Delta F_{n-1}]+[U_{n-1}] \\ [F_n] &= [(1-\alpha)K_n+K_{n-1}][U_n-U_{n-1}]+[F_{n-1}] \\ (\Delta F_n] &= [F_B]-[F_A] \end{aligned} \tag{9.91}$$

or

$$[U_n] = \sum_{i=1}^{n} [K_{i-1}]^{-1}[\Delta F_{i-1}]+[U_A]$$
$$[\Delta F_n] = (1-\alpha) \prod_{i=1}^{n} [I]-[K_i][K_{i-1}]^{-1} \qquad (9.92)$$

where [I] = unit matrix, Σ = summation symbol, Π = multiplication symbol.

This procedure is repeated until the unbalanced forces $[\Delta F_n]$ becomes less than the prescribed tolerable limit.

The convergence and accuracy of this method are examined using Eq. 9.92. Since in the loading state, the stiffness decreases monotonically,

$$0 < |[I]-[K_i][K_{i-1}]^{-1}| < 1 \qquad (9.93)$$

thus the unbalanced force $[\Delta F_n]$ converges to zero in the order of at least $(1-\alpha)^n$. Accuracy of the solution can be improved as much as needed by decreasing the loading steps. In an extreme case as

$$[K_i][K_{i-1}]^{-1} = [I] \qquad (9.94)$$

the upper solution and the lower solution coincide with each other.

9.6 Numerical Examples

9.6.1 Large Deflection of Elastic Column

In order to examine effect of segment size and load steps on convergence and accuracy of the solution in a non-linear problem, the large deflection of an elastic column with an initial imperfection is discussed in what follows.

As shown in Fig. 9.9, the column is simply supported at its ends and has an initial deflection of sinusoidal form,

$$U = U_o \sin\frac{\pi Z}{L} \tag{9.95}$$

The exact solution of this problem with a parabolic imperfection case is presented in Appendix 11.4.

(a) Effect of Segment Size

Using a column with initial deflection of $U_o/L = 0.02$, the effect of segment size on the load deflection relation is examined in three examples with different numbers of segments NS.

Example A-1: two segments (NS = 2)

Example A-2: four segments (NS = 4)

Example A-3: eight segments (NS = 8)

The solutions obtained by using the averaged stiffness matrices ($\alpha = 0.5$) are plotted in Fig. 9.9. The dotted line is the exact solution. The columns with more than four segments give almost the same results, thus the use of four segments is considered to be small enough to analyse elastic columns.

(b) Effect of Averaging Factor

Since all above solutions are not close to the exact one as shown in Fig. 9.9, the averaging factor α of the stiffness matrix must

be examined. The upper and the lower solutions for the same column were examined in six different examples,

Example B-1: NS = 2
Example B-2: NS = 4
Example B-3: NS = 8
} α = 0 (lower solution)

Example C-1: NS = 2
Example C-2: NS = 4
Example C-3: NS = 8
} α = 1 (upper solution)

The results are plotted in Fig. 9.10. Refinement of segment size has little effect on the upper bound solution but it improves the lower bound solutions very much, and the lower bound solution approaches the exact solution.

(c) Effect of Load Steps

Using the same column with an initial deflection of U_o/L=0.02, six examples were calculated with different load steps (ΔP),

Example D: P/P_E=0, 0.5, 0.8, 0.9, 0.95, 0.98, 0.99

D-1 α= 0.0
D-2 α= 0.5
D-3 α= 1.0
} NS = 8

Example E: P/P_E = 0, 0.25, 0.5, 0.65, 0.8, 0.85, 0.9, 0.925, 0.95, 0.965, 0.98, 0.985, 0.99, 0.995

E-1 $\alpha = 0.0$
E-2 $\alpha = 0.5$
E-3 $\alpha = 1.0$
} NS = 8

The results are plotted in Fig. 9.11 which shows that load steps affect only the upper bound solution. The lower bound solutions are almost identical in both Examples D-1 and E-1.

(d) Effect of Initial Imperfection

From the above discussion it may be concluded that the lower bound solution (α=0) with four segments (NS = 4) gives good results in the analysis of elastic columns. In order to check this conclusion, three other examples were calculated for a column with different initial imperfection.

Example F-1: $U_o/L = 0.01$
F-2: $U_o/L = 0.02$
F-3: $U_o/L = 0.05$
} NS = 4, α = 0

As shown in Fig. 9.12, good agreement was observed with the exact solutions in all three cases.

9.6.2 In-Plane Beam-Column with a Lateral Load

As an inelastic beam-column example, an in-plane beam-column with a concentrated lateral load at its mid-span was studied as shown in Fig. 9.13.

The wide-flange section W8x31 with residual stress was used. Five different slenderness ratios were selected:

Example E-1	L/r = 20		
E-2	40		
E-3	60	NS = 8	
		α = 0	
E-4	80		
E-5	100		

The beam-column was cut into eight segments two of which were short segments (ℓ = 1 inch) located under the lateral load. The axial force P was kept constant ($P/P_y = 0.4$) while the lateral load R was increased, which is nondimensionalized by the fraction to

$$R_{pc} = \frac{4M_{pc}}{L} \tag{9.96}$$

Fig. 9.13 shows numerical results of an end rotation angle θ in radians. Open circles represent the present solutions and the solid lines are results reported by Lu and Kamalvand in Ref. 9. Although only loading states were calculated good agreement was observed in the two analyses.

9.6.3 Biaxially Loaded Column

Fig. 9.14 shows a numerical results of a column which is subjected to axial thrust P with the symmetric eccentricities of both ends.

Example F

Section:	5x6H (without residual stress)
Length:	L = 96 in.
Material:	σ_y = 36 ksi E = 30000 ksi G = 11500 ksi
Eccentricities:	e_x = 0.89 in. e_y = 2.28 in.
Warping:	restrained at both ends

The mid-height displacement U_{Xm}, U_{Ym} and the rotation angle θ_{Zm} were computed using eight segments (NS = 8) and the lowest stiffness factor (α = 0). Since the loading was symmetric, two small segments (ℓ = 1 inch) were installed at the mid-height. In Fig. 9.14, the solutions by the present analysis are plotted by solid lines. Open circles and broken lines show experimental results and theoretical results reported by Birnstiel in Ref. 15, respectively.

The experiment shows a sudden increment of rotation angle θ_{Zm} after onset of yielding. The present solution does not follow this large rotation and thus gives a higher value for the ultimate strength. This is considered to be resulted from the assumption in the present analysis that contribution of shear stress on yielding was neglected.

9.6.4 Space Frame

The present method is directly applicable to analysis of space structures if warping deformation is perfectly free or perfectly restrained at all junctions of members. This condition is satisfied at joints of a space frame at which a maximum of three members meet at right angles, because no bi-moments exist at those joints.

As a numerical example, the space frame which had been studied by Morino and Lu in Ref. 26 was selected here. The frame is composed of four columns and four beams as shown in Fig. 9.15a.

Example G

Columns: W10x60, L = 144 in.

Beams: W18x60, L = 144 in.

Material: σ_y = 34 ksi, E = 30000 ksi, G = 11500 ksi

Eighteen segments and eighteen nodal points were used. Nodal points were numbered so that band width NB of the master stiffness matrix [K] might be the smallest (in this example NB = 7x4 = 28). Eight short segments (ℓ = 1 inch) were selected where plastic hinges were expected to be formed.

Four vertical loads and a horizontal load were applied proportionally as shown in Fig. 9.15a. Fig. 9.15b shows horizontal displacement Δ at point where the horizontal force H was applied.

Open circles are the solutions obtained by the present analysis. The dotted horizontal line represents the lowest value of H for which the system was found to be unstable. The solid lines are results reported by Morino and Lu in Ref. 26. Although a solution was not obtained in the large deflection portion, good agreement was observed in elastic portion and for the ultimate strength.

9.7 Summary

A method to solve biaxially loaded columns was presented. The column was treated as a space structure after segmentation. The sections were cut into finite elements only in the segments where yielding was expected. The segment stiffness relationships were computed using the direct stiffness method. Nonlinearity due to material plasticity and geometrical change was overcome by a modified tangent stiffness approach. Numerical Examples were presented on large deflection of an elastic column, an in-plane beam-column with a lateral load, a biaxially loaded column and a space frame. Although the cross section was limited in wide-flange shapes in the present analysis, loads including bi-moment could be applied at any point on the column.

All numerical results were compared with other reported values. In most cases, good agreements were observed. For a predominant torsional deformation, this analysis procedure indicated a higher value for the ultimate strength. This indication was considered to be

related to the simpler yield criterion assumed. This method would be improved by accounting for shear stress in the yield condition. Further, space structures could be solved more generally by treating warping and bi-moment as three dimensional vectors at intersections of members.

10. SUMMARY AND CONCLUSIONS

This dissertation presents two analyses of in-plane beam-columns:

1. The column-Curvature Curve Method (Chapter 2 and Chapter 3)
2. Simple interaction equations (Chapter 4),

two analyses of biaxially loaded sections:

1. Interaction relation (Chapter 5 and Chapter 6)
2. General behavior of sections (Chapter 8)

and two analyses of biaxially loaded columns:

1. Ultimates strength (Chapter 7)
2. General behavior (Chapter 9).

In Chapter 2, the Column Curvature Curve (CCC) method is introduced to solve symmetrically as well as unsymmetrically loaded in-plane beam-columns using analytically developed curvature curves.

The CCC method is then extended to solve an in-plane beam-column of general material in Chapter 3. As an application, an eccentrically loaded concrete wall is investigated.

In Chapter 4, the averaged plastic hinge concept is proposed to calculate the ultimate strength of in-plane beam-columns. Simple maximum strength interaction equations for a beam-column under various loading conditions are presented.

Two methods to obtain the exact interaction relations for a biaxially loaded cross section are developed: one for doubly symmetric sections (Chapter 5) and the other for general sections (Chapter 6).

The exactness of the solution is proved analytically by the upper and lower bound techniques of limit analysis..

Combination of the averaged plastic-hinge concept introduced for in-plane beam-columns in Chapter 4 and simple interaction equations developed in Chapter 5 for biaxially loaded wide-flange sections makes it possible to obtain the ultimate strength of biaxially loaded columns for symmetrical as well as unsymmetrical loadings.

The general behavior of a biaxially loaded section is studied in Chapter 8. Bi-moment and warping deformation are included in the generalized stresses and the generalized strains, respectively. Strain hardening and elastic unloading are taken into consideration. Subsequent yield surfaces and the hysteresis response of a biaxially loaded cross section are investigated.

Using the results obtained in Chapter 8 for the behavior of a biaxially loaded section, a method of analysis for a biaxially loaded column is presented in Chapter 9. In this analysis, the column is treated as a space structure which is composed of several segments. Nonlinearity due to material plasticity and geometric change of the column is overcome by the successive tangent stiffness approach.

Factors taken into account in the analysis are

1. Plasticity, strain hardening and elastic unloading of material,
2. Warping deformation and residual stress, and
3. Initial imperfections and second order effects in column deflection.

The major conclusion of the dissertation is that several analyses for inelastic beam-column problems are presented. Their validity is shown in numerical examples. Some are exact solutions and the others are approximate solutions in simple forms.

11. APPENDICES

11.1 Proof of Equivalent Column

Consider a beam-column ACB subjected to axial thrust P, shear force V, and bending moments M_A and M_B as shown in Fig. 11.1a. At section C curvature and, hence, moment are maximum.

$$\left.\frac{dM(x)}{dx}\right|_c = 0 \tag{11.1}$$

Moment M(x) may be expressed in terms of deflection W(x):

$$M(x) = P\,W(x) + Vx + M_A \tag{11.2}$$

Hence,

$$\frac{dM(x)}{dx} = P\,\frac{dW(x)}{dx} + V \tag{11.3}$$

From Eqs. 11.1 and 11.2, at section C

$$\left.\frac{dM(x)}{dx}\right|_c = P\left.\frac{dW(x)}{dx}\right|_c + V = 0$$

$$\therefore \tan\theta_c = \left.\frac{dW(x)}{dx}\right|_c = -\frac{V}{P}$$

Thus, the slope at the section of maximum curvature ($\tan\theta_c$) is parallel to the resultant force of thrust P and shear V.

The part CB of the beam-column can therefore be replaced by a cantilever beam subjected to horizontal thrust $P^* = \sqrt{P^2 + V^2}$ and moment M_A at its free end as shown in Fig. 11.1b. The length of this

cantilever beam may be increased without altering the thrust, resulting in another cantilever beam D*C* which is subjected to horizontal thrust $P^* = \sqrt{P^2 + V^2}$ only and produces exactly the same state of stress over the original cantilever AC, Fig. 11.1c. This proves that the beam-column AC is a part of the equivalent column D*C*. Similarly, the entire beam-column ACB is a part of the simple column D*C*E* subjected to thrust P* only (Fig. 2.3).

The thrust on the equivalent column is the resultant of P and V

$$P^* = \sqrt{P^2 + V^2} = \sqrt{P^2 + \left(\frac{M_B - M_A}{L}\right)^2} \tag{11.4}$$

For this equivalent column the unknown length L* must be determined using Eqs. 2.22 to 2.35 which account for equilibrium and boundary conditions.

11.2 Computation of Slope and Deflection by CCC-Method

From a knowledge of the curvature distribution, the rotation and deflection of a beam-column at any section can be computed by integration of the curvature diagram once and twice, respectively. The curvature distribution φ is not expressed explicitly as a function of x. Instead, kx is expressed as a function of φ (Eqs. 2.22 to 2.25). Therefore, curvature φ needs to be obtained by numerical integration.

Consider half waves of CCC-s for a cantilever beam as shown in Fig. 11.2. First, one chooses n + 1 points on the curvature axis:

$$\varphi_o \ (= 0), \ \varphi_1, \ \varphi_2, \ \ldots \ \varphi_N \ (= \varphi_m^*) \tag{11.5}$$

Corresponding kx values are computed using Eqs. 2.22 to 2.35:

$$kx_o \left(= \frac{kL^*}{2} \right), \; kx_1 \; kx_2, \; \ldots \; kx_N \; (= 0) \tag{11.6}$$

The Fourier Series for the curvature function is

$$\varphi = \sum_{j=1}^{N} C_j \cos \frac{(2j - 1)\pi}{2L^*} kx \tag{11.7}$$

Substituting for kx_i and φ_i $(i = 1, 2, \ldots, N)$, one gets n-simultaneous equations:

$$\begin{bmatrix} \varphi_1 \\ \varphi_2 \\ \varphi_N \end{bmatrix} = \begin{bmatrix} A_{11} & A_{12} & .. & A_{1N} \\ & & & \\ A_{N1} & ..... & & A_{NN} \end{bmatrix} \begin{bmatrix} C_1 \\ C_2 \\ C_N \end{bmatrix} \tag{11.8}$$

where

$$A_{ij} = \cos \frac{(2j - 1)\pi}{2L^*} kx_i \tag{11.9}$$

The coefficients C_j of the Fourier Series are obtained by premultiplying the φ-matrix by the inverse of the A-matrix, that is

$$[C] = [A]^{-1} [\varphi] \tag{11.10}$$

The rotation angle at point x of the cantilever is, from Eq. 2.48,

$$\Theta^* = \int_o^x \Phi^* \, dx$$

$$= \Phi_y \int_o^x \varphi \, dx \tag{11.11}$$

$$= \Phi_y \sum_{j=1}^{N} C_j \frac{2L^*}{(2j - 1)\pi k} \sin \frac{(2j - 1)\pi}{2L^*} kx$$

A non-dimensional rotation is defined by

$$\theta^* = k\Theta^*/\Phi_y$$

$$= \sum_{j=1}^{N} C_j \frac{2L^*}{(2j - 1)\pi} \sin \frac{(2j - 1)\pi}{2L^*} kx \tag{11.12}$$

The deflection at point x is

$$W^* = \int_o^x = \Theta^* \, dx$$

$$= \frac{\Phi_y}{k} \sum_{j=1}^{N} C_j \frac{2L^*}{(2j - 1)\pi} \int_o^x \sin \frac{(2j - 1)\pi}{2L^*} kx \, dx \tag{11.13}$$

$$= \frac{\Phi_y}{k} \sum_{j=1}^{N} C_j \left[\frac{2L^*}{(2j - 1)\pi}\right]^2 \left(1 - \cos \frac{(2j - 1)\pi}{2L^*} kx\right)$$

The non-dimensional deflection is defined by

$$w^* = k^2 W^*/\Phi_y$$

$$= \sum_{j=1}^{N} C_j \left[\frac{2L^*}{(2j - 1)\pi}\right]^2 \left(1 - \cos \frac{(2j - 1)\pi}{2L^*} kx\right) \tag{11.14}$$

Now, consider rotations at ends A and B of a beam-column shown in Fig. 11.3a. Maximum curvature occurs at section C with

$$\overline{AC} = \ell_A \quad , \quad \overline{CB} = \ell_B \tag{11.15}$$

Rotation angles at sections A and B with respect to the tangent at point C are

$$\Theta_A^* = \frac{\Phi_y}{k} \theta_A^* \quad , \quad \Theta_B^* = \frac{\Phi_y}{k} \theta_B^* \tag{11.16}$$

Deflections at sections A and B with respect to the tangent at point C are

$$W_A^* = \frac{\Phi_y}{k^2} w_A^* \quad , \quad W_B = \frac{\Phi_y}{k^2} w_B^* \tag{11.17}$$

Member rotation R is expressed by

$$R = \frac{W_B^* - W_A^*}{\ell_A + \ell_B} = \frac{\Phi_y}{k} \frac{w_B^* - w_A^*}{kL} \tag{11.18}$$

Then, rotation angles at A and B of the beam-column are

$$\Theta_A = \Theta_A^* + R = \frac{\Phi_y}{k} \left(\theta_A^* + \frac{w_B^* - w_A^*}{kL} \right) \tag{11.19}$$

$$\Theta_B = \Theta_B^* - R = \frac{\Phi_y}{k} \left(\theta_B^* - \frac{w_B^* - w_A^*}{kL} \right) \tag{11.20}$$

Non-dimensional rotations are obtained by

$$\theta_A = \frac{k}{\Phi_y} \Theta_A = \Theta_A^* + \frac{w_B^* - w_A^*}{kL} \tag{11.21}$$

$$\theta_B = \frac{k}{\Phi_y} \Theta_B = \theta_B^* - \frac{w_B^* - w_A^*}{kL} \tag{11.22}$$

Even if the maximum curvature does not occur inside the beam-column as shown in Fig. 11.3(b), the expressions for end rotations are the same as given by Eqs. 2.62 and 2.63.

11.3 General Solution of Elastic Beam-Columns

Consider a member which is subjected to a thrust P, end moments M_A and M_B, and partly distributed uniform load w as shown in Fig. 11.4. The governing equations for this elastic beam-column problem are

$$\frac{d^4y_1}{dx^4} + k^2 \frac{d^2y_1}{dx^2} = 0 \qquad (0 \leq x \leq x_1)$$

$$\frac{d^4y_2}{dx^4} + k^2 \frac{d^2y_2}{dx^2} = \frac{w}{EI} \qquad (x_1 \leq x \leq x_2) \tag{11.23}$$

$$\frac{d^4y_3}{dx^4} + k^2 \frac{d^2y_3}{dx^2} = 0 \qquad (x_2 \leq x \leq \ell)$$

where
$$k^2 = P/EI \tag{11.24}$$

The general solutions are obtained in the following forms:

$$y_i = A_i \cos(kx) + B_i \sin(kx) + C_i x + D_i + f_i(x) \qquad (i = 1, 2, 3) \tag{11.25}$$

where $f_i(x)$ are particular solution of the above differential equations and

$$f_1(x) = f_3(x) = 0 \qquad f_2(x) = \frac{w}{2k^2EI} x^2 \tag{11.26}$$

The twelve integration constants A_i, B_i, C_i, D_i are solved from the following twelve boundary conditions:

$$x = 0 : \quad y_1 = 0, \quad y_1'' = -\frac{M_A}{EI}$$

$$x = x_1 : \quad y_1 = y_2, \quad y_1' = y_2', \quad y_1'' = y_2'', \quad y_1''' = y_2''' \tag{11.27}$$

$$x = x_2 : \quad y_2 = y_3, \quad y_2' = y_3', \quad y_2'' = y_3'', \quad y_2''' = y_3'''$$

$$x = \ell : \quad y_3 = 0, \quad y_3'' = -\frac{M_A}{EI}$$

These conditions become twelve simultaneous equations as follows:

$$
\left[\begin{array}{cccc|cccc|cccc}
1 & 0 & 0 & 1 & & & & & & & & \\
-1 & 0 & 0 & 0 & & & & & & & & \\
\hline
C_1 & S_1 & x_1 & 1 & -C_1 & -S_1 & -x_1 & -1 & & & & \\
-S_1 & C_1 & \frac{1}{k} & 0 & S_1 & -C_1 & -\frac{1}{k} & 0 & & & & \\
-C_1 & -S_1 & 0 & 0 & C_1 & S_1 & 0 & 0 & & & & \\
S_1 & -C_1 & 0 & 0 & -S_1 & C_1 & 0 & 0 & & & & \\
\hline
 & & & & C_2 & S_2 & x_2 & 1 & -C_2 & -S_2 & -x_2 & -1 \\
 & & & & -S_2 & C_2 & \frac{1}{k} & 0 & S_2 & -C_2 & -\frac{1}{k} & 0 \\
 & & & & -C_2 & -S_2 & 0 & 0 & C_2 & S_2 & 0 & 0 \\
 & & & & S_2 & -C_2 & 0 & 0 & -S_2 & C_2 & 0 & 0 \\
\hline
 & & & & & & & & C_\ell & S_\ell & \ell & 1 \\
 & & & & & & & & -C_\ell & -S_\ell & 0 & 0
\end{array}\right]
\left[\begin{array}{c}
A_1 \\ B_1 \\ \hline C_1 \\ D_1 \\ \hline A_2 \\ B_2 \\ \hline C_2 \\ D_2 \\ \hline A_3 \\ B_3 \\ \hline C_3 \\ D_3
\end{array}\right]
=
\left[\begin{array}{c}
0 \\ -\frac{1}{k^2}\frac{MA}{EI} \\ \hline \frac{1}{2k^2}\frac{w}{EI}x_1^2 \\ \frac{1}{k^3}\frac{w}{EI}x_1 \\ \frac{1}{k^4}\frac{w}{EI} \\ 0 \\ \hline -\frac{1}{2k^2}\frac{w}{EI}x_2^2 \\ -\frac{1}{k^3}\frac{w}{EI}x_2 \\ -\frac{1}{k^4}\frac{w}{EI} \\ 0 \\ \hline 0 \\ -\frac{1}{k^2}\frac{MB}{EI}
\end{array}\right]
\qquad (11.28)
$$

where

$$C_1 = \cos(kx_1) \qquad S_1 = \sin(kx_1)$$

$$C_2 = \cos(kx_2) \qquad S_2 = \sin(kx_2) \tag{11.29}$$

$$C_\ell = \cos(k\ell) \qquad S_\ell = \sin(k\ell)$$

The constants are solved as follows:

$$A_1 = \frac{M_A}{k^2 EI}$$

$$B_1 = \frac{1}{k^2 EI} \frac{M_B - M_A \cos k\ell}{\sin k\ell} - \frac{w}{k^4 EI} \frac{\cos k(\ell - x_1) - \cos k(\ell - x_2)}{\sin k\ell}$$

$$C_1 = \frac{M_A - M_B}{k^2 \ell EI} - \frac{w}{2k^2 \ell EI} (x_2 - x_1)(2\ell - x_1 - x_2)$$

$$D_1 = \frac{1}{k^2} \frac{M_A}{EI} \tag{11.30}$$

$$A_2 = \frac{M_A}{k^2 EI} + \frac{w}{k^4 EI} \cos kx_1$$

$$B_2 = \frac{1}{k^2 EI} \frac{M_B - M_A \cos k\ell}{\sin k\ell} - \frac{w}{k^4 EI} \frac{\cos kx_1 \cos k\ell - \cos k(\ell - x_2)}{\sin k\ell}$$

$$C_2 = \frac{M_A - M_B}{k^2 \ell EI} - \frac{w}{2k^2 \ell EI} (x_1^2 + 2x_2\ell - x_2^2)$$

$$D_2 = \frac{M_A}{k^2EI} - \frac{w}{k^4EI}\left(1 - \frac{k^2x_1^2}{2}\right)$$

$$A_3 = \frac{M_A}{k^2EI} + \frac{w}{k^4EI}(\cos kx_1 - \cos kx_2)$$

$$B_3 = \frac{1}{k^2EI}\frac{M_B - M_A \cos k\ell}{\sin k\ell} - \frac{w}{k^4EI}(\cos kx_1 - \cos kx_2)\cot k\ell \qquad (11.31)$$

$$C_3 = \frac{M_A - M_B}{k^2\ell EI} - \frac{w}{2k^2\ell EI}(x_1^2 - x_2^2)$$

$$D_3 = \frac{M_A}{k^2EI} + \frac{w}{2k^2EI}(x_1^2 - x_2^2)$$

Let them be expressed in the following form:

$$A_i = \frac{M_{mc}}{k^2EI}(a_{im} + q\, a_{iw})$$

$$B_i = \frac{M_{mc}}{k^2EI}(b_{im} + q\, b_{iw}) \qquad (11.32)$$

$$C_i = \frac{M_{mc}}{k^2{}_1EI}(c_{im} + q\, c_{iw})$$

$$D_i = \frac{M_{mc}}{k^2EI}(d_{im} + q\, d_{iw})$$

Where

$$q = w/k^2 \, M_{mc} \tag{11.33}$$

Location of the maximum bending moment $x = x_i^*$ for each portion is obtained from the condition

$$\frac{d^3 y_i}{dx^3} = A_i k^3 \sin (kx_i^*) - B_i k^3 \cos (kx_i^*) = 0 \tag{11.34}$$

or

$$kx_i^* = \tan^{-1} \frac{B_i}{A_i} = \tan^{-1} \frac{b_{im} + qb_{iw}}{a_{im} + qa_{iw}} \tag{11.35}$$

The ultimate state is obtained when the maximum bending moment reaches the plastic moment of the member M_{mc}, ie,

$$\left.\frac{d^2 y}{dx^2}\right|_{x = x^*} = -A_i k^2 \cos (kx^*) - B_i k^2 \sin (kx^*) + f_i'' (x^*) = -\frac{M_{mc}}{EI} \tag{11.36}$$

or

$$A_i \cos (kx^*) + B_i \sin (kx^*) = \frac{M_{mc}}{k^2 EI} - \frac{1}{k^2} f_i'' (x^*) \tag{11.37}$$

Elimination of x* from Eq. 11.35 and Eq. 11.37 gives the ultimate load q_o. There are five possible cases in the ultimate state according to the location of the plastic hinge (Fig. 11.5):

Case-I The plastic hinge in the left portion

$$x^* = x_1^* \quad (x_1^* < x_1,\ x_2^* < x_1,\ x_3^* < x_2)$$

$$q_o = \frac{1}{b_{1w}} \left(\sqrt{1 - a_{1m}^2} - b_{1m}\right) \tag{11.38}$$

Case-II The plastic hinge at the left boundary

$$x^* = x_1 \quad (x_1^* > x_1,\ x_2^* < x_1,\ x_3^* < x_2)$$

$$q_o = \frac{1}{b_{1w}} \left[\frac{1 - a_{1m}\cos(kx_1)}{\sin(kx_1)} - b_{1m}\right] \tag{11.39}$$

Case-III The plastic hinge in the middle portion

$$x^* = x_2^* \quad (x_1^* > x_1,\ x_1 < x_2^* < x_2,\ x_3^* < x_2)$$

$$q_o = -\frac{1-a_{2m}\,a_{2w}-b_{2m}\,b_{2w}}{1-a_{2m}^2-b_{2m}^2} - \sqrt{\left(\frac{1-a_{2m}\,a_{2w}-b_{2m}\,b_{2w}}{1-a_{2m}^2-b_{2m}^2}\right)^2 - \frac{1-a_{2m}^2-b_{2m}^2}{1-a_{2w}^2-b_{2w}^2}} \tag{11.40}$$

Case-IV The plastic hinge at the right boundary

$$x^* = x_2 \quad (x_1^* > x_1,\ x_2^* > x_2,\ x_3^* < x_2)$$

$$q_o = \frac{1 - a_{3m}\cos(kx_2) - b_{3m}\sin(kx_2)}{a_{3w}\cos(kx_2) + b_{3w}\sin(kx_2)} \tag{11.41}$$

Case-V The plastic hinge in the right portion

$$x^* = x_3^* \quad (x_1^* > x_1,\ x_2^* > x_2,\ x_3^* > x_2)$$

$$q_o = -\frac{a_{3m}\,a_{3w} + b_{3m}\,b_{3w}}{a_{3w}^2 + b_{3w}^2} + \sqrt{\left(\frac{a_{3m}\,a_{3w} + b_{3m}\,b_{3w}}{a_{3w}^2 + b_{3w}^2}\right)^2 + \frac{1 - a_{3m}^2 - b_{3m}^2}{a_{3w}^2 + b_{3w}^2}} \tag{11.42}$$

The location of the plastic hinge x^*_i (Eq. 11.35) and the ultimate load q_o (Eqs. 11.38 to 42) are functions of each other. Therefore, they have to be solved by iteration. A computer program was made for this purpose.

11.4 Large Deflection of Elastic Beam-Columns

Let us consider an elastic column of length L and bending rigidity EI as shown in Fig. 11.6. The s-coordinate is taken along the

deflected configuration.

The initial deflection $u_o(s)$ is assumed to be small and expressed in the parabolic form

$$u_o(s) = \frac{4\,\Delta_o}{L^2}\, s\,(L - S) \tag{11.43}$$

Thus, the initial curvature $\varphi_0(s)$ is constant throughout the column

$$\varphi_0(s) = \frac{8\,\Delta_o}{L^2} \tag{11.44}$$

The deflection increases due to the application of axial compression P and end moments M_0. The total deflection is denoted by u(s). The slope $\theta(s)$ and the curvature $\varphi(s)$ are given by

$$\sin\theta = \frac{du}{ds} \tag{11.45}$$

$$\varphi = -\frac{d\theta}{ds} \tag{11.46}$$

The equilibrium condition between the bending moment M(s) and the thrust P is

$$\frac{dM}{ds} - P\sin\theta = 0 \tag{11.47}$$

Since the bending moment M(s) is proportional to the curvature change,

$$M = -EI\,(\varphi - \varphi_o) \tag{11.48}$$

or using Eq. 11.44 and Eq. 11.46

$$M = EI\left(\frac{d\theta}{ds} - \frac{8\,\Delta_o}{L^2}\right) \tag{11.49}$$

The governing equation is obtained from Eq. 11.47 and Eq. 11.49:

$$\frac{d^2\theta}{ds^2} + \frac{P}{EI}\sin\theta = 0 \tag{11.50}$$

Eq. 11.50 can be integrated once

$$\frac{1}{2}\left(\frac{d\theta}{ds}\right)^2 - \frac{P}{EI}\cos\theta = C \tag{11.51}$$

The integral constant C is determined from the end condition:

$$M = M_0, \quad u = \alpha \quad \text{at } s = 0 \tag{11.52}$$

where α is the slope angle at the end.

Evaluate Eq. 11.49 at s = 0,

$$\left.\frac{d\theta}{ds}\right|_{s=0} = \frac{M_o}{EI} + \frac{8\,\Delta_o}{L^2} \tag{11.53}$$

Substitute Eq. 11.53 into Eq. 11.51 and get

$$C = \frac{1}{2}\left(\frac{M_o}{EI} + \frac{8\,\Delta_o}{L^2}\right)^2 - \frac{P}{EI}\cos\alpha \tag{11.54}$$

Now Eq. 11.51 becomes

$$\frac{d\theta}{ds} = -\sqrt{4\,\frac{P}{EI}\left(\sin^2\frac{\alpha}{2} - \sin^2\frac{\theta}{2}\right) + \left(\frac{M_o}{EI} + \frac{8\,\Delta_o}{L^2}\right)^2} \tag{11.55}$$

Integrate Eq. 11.55 along the half length,

$$\frac{L}{2} = \int_0^{L/2} ds = \int_0^{\alpha} \frac{d\theta}{\sqrt{4\,\frac{P}{EI}\left(\sin^2\frac{\alpha}{2} - \sin^2\frac{\theta}{2}\right) + \left(\frac{M_o}{EI} + \frac{8\,\Delta_o}{L^2}\right)^2}} \tag{11.56}$$

or

$$1 = \int_0^{\alpha} \frac{d\theta}{\sqrt{\pi^2\,\frac{P}{P_E}\left(\sin^2\frac{\alpha}{2} - \sin^2\frac{\theta}{2}\right) + \left(\frac{\pi^2}{2}\,\frac{M_o}{P_E L} + 4\,\frac{\Delta_o}{L}\right)^2}} \tag{11.57}$$

where P_E is the Euler's Buckling Load:

$$P_E = \frac{\pi^2\,EI}{L^2} \tag{11.58}$$

In Eq. 11.57, the end slope angle α is the only unknown, which is to be solved numerically.

Using the obtained α, the maximum deflection at mid-span Δ is calculated. From Eq. 11.45,

$$du = \sin\theta \frac{ds}{d\theta} d\theta \tag{11.59}$$

Substituting Eq. 11.55 and integrating, one gets

$$\frac{\Delta}{L} = \frac{1}{2} \int_0^{\alpha} \frac{\sin\theta \, d\theta}{\sqrt{\pi^2 \frac{P}{P_E} (\sin^2 \frac{\alpha}{2} - \sin^2 \frac{\theta}{2})^2 + \left(\frac{\pi^2}{2} \frac{M_o}{P_E L} + 4 \frac{\Delta_o}{L}\right)^2}} \tag{11.60}$$

As numerical results, the relationships between P/P_E and Δ/L are plotted for several initial deflections Δ_o/L in Fig. 11.7. The end moments M_0 are neglected here.

When there are neither initial imperfection Δ_o nor end moments M_0, Eq. 11.57 is expressed in simple form using the elliptic integral:

$$K(\alpha) = \int_0^{\frac{\pi}{2}} \frac{d\omega}{\sqrt{1 - \sin^2 \alpha \cos^2 \omega}} \tag{11.61}$$

Thus the axial force P/P_E and the maximum deflection Δ/L are solved as functions of the end slope angle α:

$$\frac{P}{P_E} = \frac{4}{\pi^2} K^2 (\frac{\alpha}{2}) \tag{11.62}$$

$$\frac{\Delta}{L} = \frac{\sin \frac{\alpha}{2}}{K(\frac{\alpha}{2})} \tag{11.63}$$

This relation is shown by the uppermost curve in Fig. 11.7.

According to the small deflection theory, a load P greater than the buckling load can not be applied and the load-deflection

curves approach the horizontal line $P = P_E$ asymptotically as shown by dotted lines in Fig. 11.7. These relations are expressed approximately by

$$\frac{P}{P_E} = 1 - \frac{\Delta_o}{\Delta} \tag{11.64}$$

12. NOTATIONS

12.1 Notations for Chapter 2

A = area of section

a, b, c, f = constants which define m-φ-p relationship

E = modulus of elasticity

e_A, e_B = eccentricities of the thrust at ends A and B

h = depth of section

I = moment of inertia of section

k^2 = P^*/EI

L = length of beam-column

L^* = length of equivalent column

$M, (m)$ = bending moment, $(m = M/M_y)$

$M_A, M_B, (m_A, m_B)$ = moment at ends A and B, $(m_A = M_A/M_y, m_B = M_B/M_y)$

$M_{pc}, (m_{pc})$ = full-plastic moment of section, $(m_{pc} = M_{pc}/M_y)$

m_1, m_2 = bending moment at initial and secondary yield

$\bar{M}_A, \bar{M}_B, (\bar{m}_A, \bar{m}_B)$ = constant bending moments at ends A and B, $(\bar{m}_A = \bar{M}_A/\bar{M}_y, \bar{m}_B = \bar{M}_B/\bar{M}_y)$

$P, (p)$ = axial thrust of beam-column $(p = P/P_y)$

$P^*, (p^*)$ = axial thrust of equivalent column, $(p^* = P^*/P_y)$

P_y = axial yield load

r = radius of gyration of section

S = elastic section modulus

V = shear force

W^*, (w^*) = deflection with respect to tangent at the point of maximum curvature (see Fig. 2.21), $(w^* = W^* k^2/\Phi_y)$

x = longitudinal coordinate axis

y = transverse coordinate axis

α, β = coefficients of bending moment due to eccentric thrust at ends A and B (Eq. 2.38)

γ = S/AL

ϵ_y = strain at yield point

κ = M_B/M_A

ρ_1 = location of initial yield point

ρ_2 = location of secondary yield point

λ = $\frac{L}{r}\sqrt{\frac{\sigma_y}{E}}$

σ_y = yield stress

Φ, (φ) = curvature, $(\varphi = \Phi/\Phi_y)$

Φ_m, (φ_m) = maximum curvature of beam-column, $(\varphi_m = \Phi_m/\Phi_y)$

Φ_m^*, (φ_m^*) = maximum curvature of equivalent column, $(\varphi_m^* = \Phi_m^*/\Phi_y)$

Φ_y = curvature at initial yielding for pure bending

φ_1 = curvature at initial yielding with bending and thrust

φ_2 = curvature at secondary yielding with bending and thrust

12.2 Notations for Chapter 3

a, b, c, f, m_{pc} = constants which determine m-φ-p relationship

e = eccentricity of axial thrust P

E = modulus of elasticity

f_1, f_2, f_3, g = functions which determine CCC (Eq. 3.43)

h = height of wall

I = moment of interia of cross section ($= \frac{t^3}{12}$)

k = $\sqrt{P^*/EI} = \sqrt{12\ \varepsilon_y\ P^*}/t$

L = length of beam-column

L^* = length of equivalent column

L_{AB} = computed distance between A and B

M, (m) = bending moment ($m = M/M_y$)

$M_A, M_B, (m_A, m_B)$ = end moments ($m_A = M_A/M_y$, $m_B = M_B/M_y$)

M_y = initial yield moment ($= \sigma_y\ t^2/6$)

P, (p) = axial thrust ($p = -P/P_y$)

P_y = yield thrust ($= \sigma_y\ t$)

P^*, (p^*) = thrust in equivalent column ($p^* = P^*/P_y$)

t = thickness of wall

V = shear force in beam-column

x, y = coordinate along and across wall height

x_m = location of maximum curvature

y_{ty}, y_{cy} = boundary of yielding in tension and compression

ε, $(\bar{\varepsilon})$ = axial strain ($\bar{\varepsilon} = \varepsilon/\varepsilon_y$)

$\varepsilon_{ty}, \varepsilon_{cy}$ = yield strain in tension and compression

$\varepsilon_{to}, \varepsilon_{co}$ = limit strains (cracking and crushing)

ε_y = yield strain (= σ_y/E)

ε_m = mean strain

χ = M_B/M_A

μ = $-\sigma_{ty}/\sigma_{cy}$

σ, $(\bar{\sigma})$ = axial stress ($\bar{\sigma} = \sigma/\sigma_y$)

σ_{ty}, σ_{cy} = yield stress in tension and compression

σ_y = yield stress (= σ_{cy})

$\varphi_{et}, \varphi_{ec}, \varphi_{tc}, \varphi_{ct}$ = boundary curvatures

φ_1, φ_2 = boundary curvatures

φ_{to}, φ_{co} = ultimate curvatures due to strain limit

φ_m, φ_m^* = maximum curvatures in wall and in equivalent column

φ_A, φ_B = end curvatures

Φ, (φ) = curvature ($\varphi = \Phi/\Phi_y$)

Φ_y = initial yield curvature (= $2\varepsilon_y/t$)

12.3 Notations for Chapter 4

c = width of uniform load

e = eccentricity of lateral load

EI = bending rigidity

f, f_1, f_2, f_3 = averaging factor and its coefficients

k = $\sqrt{P/EI}$

L, L_A, L_B = column length

L/r = slenderness ratio

M_{mc} = averaged flow moment

M_o = ultimate end moment

M_{pc}, M_p = plastic moment with and without P

M_{yc}, M_y = initial yield moment with and without P

N = power factor for f_1

P = axial thrust

P_y = yield axial thrust

Q = lateral load

Q_o = ultimate lateral load

w = uniformly distributed load

φ = curvature

λ = constant due to support condition

λ' = eccentricity of plastic hinge

12.4 Notations for Chapter 5

A, A_i = areas

A_p = area contributing to axial force

b, b_o, b_1, b_2, B = widths (Fig. 5.6)

d, d_o, d_1, D = depths (Fig. 5.6)

e, e_{xi}, e_{yi} = distances (Fig. 5.5)

M_x, M_y = bending moments

M_{px}, M_{py} = plastic moments

m_x, m_y = M_x/M_{px}, M_y/M_{py}

P = axial force

P_y = axial force at yielding

p = P/P_y

Q_x, Q_y = static moments of section

r, r_o, r_i = radii

S_x, S_y = elastic section moduli

t_f, t_w = thickness (Fig. 5.6)

Z_x, Z_y = plastic section moduli

$\alpha, \beta, \lambda, \delta, \mu, \nu$ = constants

$\dot{e}, \dot{e}_o$ = rates of strain

$\dot{\kappa}, \dot{\kappa}_x, \dot{\kappa}_y$ = rates of curvature

σ_y = yield stress

θ = angle between N.A. and x-axis (Fig. 5.1)

η = distance from N.A.

12.5 Notations for Chapter 6

A_o = area of section

A_i = area of i-th element

$\bar{A}$ = area of function

$\dot{D}_I$ = rate of internal energy dissipation

e_{xi}, e_{yi} = central coordinate of i-th element

M_x, M_y = bending moments acting on a section

M_{xi}, M_{yi} = moment contribution of i-th element

M_{px}, M_{py} = plastic limit moments

m_x, m_y = $M_x/M_{px}, M_y/M_{py}$

N.A. = neutral axis

P, p = axial force ($p = P/P_y$)

P_y = axial force at yielding

P_i = axial force contribution of i-th element

Q_{xi}, Q_{yi} = static moments of inertia of i-th element

$\bar{Q}_x$, $\bar{Q}_y$ = static moment of inertia functions

$\dot{W}_E$ = rate of external work done

Z_x, Z_y = plastic section moduli

α, β = parameters for the N.A.

$\dot{\varepsilon}$ = strain rate

$\dot{\chi}$ = curvature rates

η = distance from the N.A.

η_i = centroidal distance of i-th element

σ_y = yield stress

12.6 Notations for Chapter 7

A	= area of section
a, b, c, d	= constants in interaction of wide flange sections
A_i, B_i, C_i	= coefficients of deflection functions ($i = 0, 1, 2$)
[D]	= deflection coefficient vector
E, G	= moduli of elasticity
[F]	= external force vector
F_{st}	= stability function
F_y, F_A, F_p	= initial averaged and fully plastic yield functions for cross section
F_c	= interaction function of column
$f_{s\xi}$, $f_{s\eta}$	= shape factors of section
I_ξ, I_η	= bending moments of inertia of section
I_ω	= warping moment of inertia of section

K_T	= St. Venant torsion constant
$\bar{K}$	= see Eq. 7.3.
$[K]$	= stiffness matrix
L	= length of column
M	= moment
m	= moment non-dimensionalized by $M_{p\xi}$, $M_{p\eta}$, $M_{p\xi}$
$M_{p\xi}$, $M_{p\eta}$, $M_{p\xi}$	= full-plastic moments of section
M_ξ, M_η, M_ξ	= moments acting on section
M_{xo}, M_{xL}, M_{yo}, M_{yL}, M_{zo}, M_{zL}	= end moments
m_ξ^*, m_η^*, m_ξ^*	= moments on critical section
$m_{\xi a}$, $m_{\eta a}$	= averaged moments
$m_{\xi \ell}$, $m_{\eta \ell}$	= initial yield moments in uniaxial bending
$m_{\xi u}$, $m_{\eta u}$	= full plastic moments in uniaxial bending
P, p	= axial force ($p = P/P_y$)
P_y	= axial force at yielding
P_E	= Euler's buckling load
$\nu_{\omega o}$, $\nu_{\omega L}$	= warping restraint factors
r_1, r_2	= warping restraint constants - Eq. 7.23
U, V, u, v	= deflection of column ($u = U/L$, $v = V/L$)
X, Y, Z, x, y, z	= global coordinates ($x = X/L$, $y = Y/L$, $z = Z/L$)
α, β	= averaging factors in interaction of section
Θ, θ	= rotation angle of column
σ	= normal stress
σ_y, τ_y	= yield stresses
ξ, η, ζ	= local coordinates on section

12.7 Notations for Chapter 8

$A, \bar{A}$ = area ($\bar{A} = \int dxdy$)

B, D = width and depth of cross section

$E, E_H, \bar{E}_H$ = elastic modulus, strain hardening modulus ($\bar{E}_H = E_H/E$)

$f, \dot{f}$ = (generalized stress) generalized stress increment

$I_x, \bar{I}_x, I_y, \bar{I}_y$ = moment of inertia ($\bar{I}_x = \int y^2\, dxdy$, $\bar{I}_y = \int x^2\, dxdy$)

$I_w, \bar{I}_w$ = warping moment of inertia ($\bar{I}_w = \int x^2\, y^2\, dxdy$)

K, K_o = stiffness matrix, elastic stiffness matrix (unit matrix)

M_x, m_x, M_y, m_y = bending moment ($m_x = M_x/M_{px}$, $m_y = M_y/M_{py}$)

M_w, m_w = bi-moment ($m_w = M_w/M_{pw}$)

M_{px}, M_{py} = initial yield moment ($I_x\, \sigma_y/(D/2)$, $I_y\, \sigma_y/(B/2)$)

M_{pw} = initial yield bi-moment ($I_\omega\, \sigma_y/(BD/4)$)

m, n = number of elements

P, p = axial force ($p = P/P_y$)

P_y = initial yield axial force ($A\, \sigma_y$)

X, Y, x, y = axes of principal coordinates ($x = \frac{X}{B/2}$, $y = \frac{Y}{D/2}$)

$\Delta, \delta, \dot{\delta}$ = generalized strain, generalized strain increment

$\epsilon, \bar{\epsilon}$ = axial strain ($\bar{\epsilon} = \epsilon/\epsilon_y$)

$\epsilon_o, \bar{\epsilon}_o$ = strain at centroid of the cross section ($\bar{\epsilon}_o = \epsilon_o/\epsilon_y$)

$\epsilon_1, \epsilon_1', \epsilon_2, \epsilon_2'$ = elastic strain limits, plastic strain limits

$\epsilon_y, \epsilon_H, \bar{\epsilon}_H$ = initial yield strain, initial hardening strain ($\bar{\epsilon}_H = \epsilon_H/\epsilon_y$)

$\sigma, \bar{\sigma}$ = axial stress ($\bar{\sigma} = \sigma/\sigma_y$)

σ_y = initial yield stress level

$\sigma_r, \sigma_{rc}, \sigma_{rt}$ = residual stresses

$\varphi_x, \bar{\varphi}_x, \varphi_y, \bar{\varphi}_y$ = curvature ($\bar{\varphi}_x = \varphi_x/\varphi_{px}$, $\bar{\varphi}_y = \varphi_y/\varphi_{py}$)

$\varphi_{px}, \varphi_{py}$ = initial yield curvature ($\epsilon_y/(D/2)$, $\epsilon_y/(B/2)$)

$\omega, \bar{\omega}$ = warping ($\bar{\omega} = \omega/\omega_p$)

ω_p = initial yield warping ($\epsilon_y/(BD/4)$)

12.8 Notations for Chapter 9

A, A_o = elastic area, initial area

A_ξ, A_η = shear resistance areas

b, d, t_f, t_w = dimensions of wide-flange section

b_i = elastic width of flange plate

$C(c_{\xi o}, c_{\eta o})$ = centroid of elastic portion of section

E, G = elastic moduli

E_t, G_t = tangent moduli

F, f = forces

$[F], [f]$ = force vectors

$I_\xi, I_\eta, I_{\xi\eta}, I_{\xi o}, I_{\eta o}, I_{\xi\eta o}$ = moments of inertia of section

I_ω = warping moment of inertia

K_T = St. Venant torsion constant

$\bar{K}$ = (See Eq. 9.24)

$[K], [k]$ = tangent stiffness matrices

k_ξ, k_η, k_ζ = (See Eq. 9.40, Eq. 9.47 and Eq. 9.55)

L = length of segment

M, m = moments

m_ξ, m_η = bending moments

m_ζ = twisting moment

M_ω, m_ω = bi-moments

P = axial compression

$Q_\xi, Q_\eta, Q_{\xi o}, Q_{\eta o}$ = static moments of inertia of section

$[R]$ = rotation matrix

$S(s_{\xi o}, S_{\eta o})$ = shear center of elastic portion of section

U, u = displacements

$[U], [u]$ = displacement vectors

$\vec{v}_\xi, \vec{v}_\eta, \vec{v}_\zeta$ = unit vectors in ξ, η, ζ directions

x, y, z = global coordinates

α = stiffness averaging factor

β = rotation angle of principal axes

ν_ξ, ν_η = shear deflection constants (Eq. 9.52)

Δ = deflection

$[\Delta F]$ = unbalanced force vector

$\epsilon, \epsilon_o, (\dot{\epsilon})$ = normal strains (rate)

$\epsilon_c, (\dot{\epsilon}_c)$ = normal strain (rate) at centroid

$\theta_\xi, \theta_\eta (\dot{\theta}_\xi, \dot{\theta}_\eta)$ = bending rotation angles (rates)

$\theta_\zeta, (\dot{\theta}_\zeta)$ = twisting angle (rate)

ξ, η, ζ = local coordinates on segment

ρ_1, ρ_2, ρ_3 = distance from shear center

$\varphi_\xi, \varphi_\eta (\dot{\varphi}_\xi, \dot{\varphi}_\eta)$ = bending curvatures (rates)

$\varphi_\omega (\dot{\varphi}_\omega)$ = warping curvature (rate)

ω_o, ω_η = warping distributed on section

Ω, ω = warping deformations

13. TABLES

Table 2.1 Length of Equivalent Column kL* for a Rectangular Section

φ_m^* \ p^*	0.1	0.2	0.3	0.4	0.5	0.6	0.7	0.8	0.9
0.1	1.57	1.57	1.57	1.57	1.57	1.57	1.57	1.57	1.57
0.2	1.57	1.57	1.57	1.57	1.57	1.57	1.57	1.57	1.48
0.3	1.57	1.57	1.57	1.57	1.57	1.57	1.57	1.54	1.36
0.4	1.57	1.57	1.57	1.57	1.57	1.57	1.55	1.48	1.28
0.5	1.57	1.57	1.57	1.57	1.57	1.56	1.52	1.42	1.21
0.6	1.57	1.57	1.57	1.57	1.56	1.54	1.48	1.36	1.15
0.7	1.57	1.57	1.57	1.57	1.55	1.51	1.44	1.32	1.10
0.8	1.57	1.57	1.57	1.55	1.53	1.48	1.40	1.28	1.06
0.9	1.57	1.57	1.56	1.54	1.50	1.45	1.36	1.24	1.03
1.0	1.57	1.56	1.54	1.52	1.48	1.42	1.33	1.21	1.00
1.1	1.56	1.55	1.53	1.50	1.45	1.39	1.30	1.18	0.976
1.2	1.55	1.54	1.51	1.48	1.43	1.36	1.28	1.15	0.953
1.3	1.54	1.52	1.49	1.46	1.41	1.34	1.25	1.13	0.932
1.4	1.53	1.51	1.48	1.44	1.38	1.32	1.23	1.10	0.912
1.5	1.51	1.49	1.46	1.42	1.36	1.30	1.21	1.08	0.895
1.6	1.50	1.48	1.44	1.40	1.34	1.28	1.19	1.07	0.879
1.7	1.48	1.46	1.43	1.38	1.33	1.26	1.17	1.05	0.864
1.8	1.47	1.45	1.41	1.36	1.31	1.24	1.15	1.03	0.850
1.9	1.46	1.44	1.40	1.35	1.29	1.22	1.13	1.02	0.837
2.0	1.44	1.42	1.39	1.34	1.28	1.27	1.12	1.00	0.825
2.1	1.43	1.41	1.37	1.32	1.26	1.19	1.10	0.989	0.813
2.2	1.42	1.40	1.36	1.31	1.25	1.18	1.09	0.976	0.803

← Secondary Plastic | Primary Plastic →

Elastic →

← Primary Plastic

$$P^* = \left[P^2 + \left(\frac{M_B - M_A}{L} \right)^2 \right]^{1/2}$$

$$p^* = P^*/P_y$$

$$k = \sqrt{P^*/EI}$$

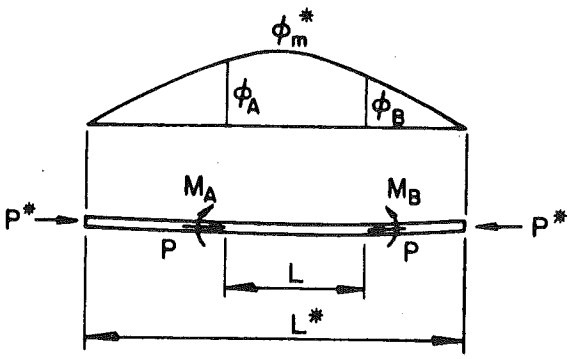

Table 3.1 Cases of Numerical Examples

EXAMPLE	MATERIAL		LOAD		RESULTS
	μ	$\epsilon_y = \sigma_y/E$	m_A/p	m_B/p	Figure Number
AO	0	0.001215	1.0	1.0	3.10 11 12 13 14
A1	0.1				3.12
A2	0.2				3.12
A5	0.5				3.12
A10	1.0				3.12
BO	0		1.0	0	3.13
CO			1.0	-1.0	3.13
DO			2.0	2.0	3.14
AO'		0.001944	1.0	1.0	3.14
DO'			2.0	2.0	3.14

Table 7.1 Ultimate Strength of Columns

No.	Size	Interaction Constants of Sections (Eq. 63) a	b	c	d	Yield Stress σ_y	Length L	Eccentricities e_{xo}, e_{xL}	e_{yo}, e_{yL}	Ultimate Load Experiment*	Syal & Sharma	Present Sol.
1	H6x6	2.339	1.553	2.738	1.365	33	96	1.61	2.78	92.8	93.1	102.7
2	W5x18.5	2.372	1.539	2.660	1.308	36	96	1.60	3.21	54.1	50.75	49.4
3	W5x18.5	2.365	1.528	2.641	1.297	36	120	0.80	2.63	62.7	60.84	55.3
4	W6x25	2.432	1.331	2.767	1.329	36	96	1.66	2.95	86.3	84.35	84.9
5	H5x5	2.327	1.516	2.716	1.353	36	96	2.36	3.17	49.6	50.20	46.2
6	H5x5	2.327	1.516	2.716	1.353	36	120	2.38	2.51	47.9	47.76	39.6
7	H5x6	2.427	1.212	2.879	1.373	36	96	0.89	2.82	76.6	80.16	75.7
8	H5x6	2.427	1.212	2.879	1.373	36	96	0.34	1.87	109.4	110.10	110.6
10	I4x8	2.610	1.035	3.466	1.566	36	96	0.19	2.60	85.0	78.70	79.5
12	W5x18.5	2.365	1.491	2.667	1.314	36	120	0.77	2.78	51.0	56.23	53.3
13	W4x13	2.399	1.343	2.810	1.366	65	120	0.42	2.72	46.1	47.24	45.6
14	W4x13	2.399	1.343	2.810	1.366	65	120	0.83	2.35	38.7	40.12	44.1
B1	W12x79	2.427	1.313	2.689	1.282	33	180	6.00	12.00		150.95	155.9
H1	W14x43	2.566	1.070	3.128	1.392	33	264.6	0.50 0.00	5.00 0.00	152.0	144.19 (0.34)	143.8 (0.37)

( ) location of critical section from the top.
* experimental results are due to Birnstiel (Ref. 6).

Table 8.1 Stress-Strain Relationships Including Hysteresis

	strain ε	stress σ	change in strain limits $\varepsilon_1, \varepsilon_1'$ $\varepsilon_2, \varepsilon_2'$	tangent modulus E_t $\dot{\varepsilon} > 0$ $\dot{\varepsilon} < 0$
tension	strain-hardening	$E\frac{\varepsilon_1-\varepsilon_1'}{2} + E_H(\varepsilon - \frac{\varepsilon_2-\varepsilon_2'}{2})$	$\varepsilon_1 = \varepsilon$ $\varepsilon_2 = \varepsilon$ $\varepsilon_1' = \varepsilon - 2\,\varepsilon_y$ $\varepsilon_2' = \varepsilon - 2\,\varepsilon_H$	E_H E
	plastic	$E\frac{\varepsilon_1-\varepsilon_1'}{2} + E_H\frac{\varepsilon_2+\varepsilon_2'}{2}$	$\varepsilon_1 = \varepsilon$ no change $\varepsilon_1' = \varepsilon - 2\,\varepsilon_y$	0 E
	elastic	$E(\varepsilon - \frac{\varepsilon_1+\varepsilon_1'}{2}) + E_H\frac{\varepsilon_2+\varepsilon_2'}{2}$	no change	E E
compression	plastic	$E\frac{\varepsilon_1'-\varepsilon_1}{2} + E_H\frac{\varepsilon_2'+\varepsilon_2}{2}$	$\varepsilon_1' = \varepsilon$ no change $\varepsilon_1 = \varepsilon + 2\,\varepsilon_y$	E 0
	strain-hardening	$E\frac{\varepsilon_1'-\varepsilon_1}{2} + E_H(\varepsilon - \frac{\varepsilon_2'-\varepsilon_2}{2})$	$\varepsilon_1' = \varepsilon$ $\varepsilon_2' = \varepsilon$ $\varepsilon_1 = \varepsilon + 2\,\varepsilon_y$ $\varepsilon_2 = \varepsilon + 2\,\varepsilon_H$	E E_H

Table 8.2 Numerical Examples

Ex.	Section	Loading	Note	Fig. No.
A	W 8 x 31	$\begin{pmatrix}0\\0\\0\end{pmatrix}^* \longrightarrow \begin{pmatrix}0.3\\0.6\\0.6\end{pmatrix}^* \rightleftharpoons \begin{pmatrix}-0.3\\-0.6\\-0.6\end{pmatrix}^*$	Proportional Loading	8.7
B1, B2, B3, B4	W 8 x 31	$\begin{pmatrix}0\\0\\0\end{pmatrix}^* \longrightarrow \begin{pmatrix}0.3\\0.6\\0.6\end{pmatrix}^*$; $\begin{pmatrix}0\\0\\0\end{pmatrix}^* \longrightarrow \begin{pmatrix}0.3\\0.6\\0\end{pmatrix}^* \longrightarrow \begin{pmatrix}0.3\\0.6\\0.6\end{pmatrix}^*$; $\begin{pmatrix}0\\0\\0\end{pmatrix}^* \longrightarrow \begin{pmatrix}0.3\\0\\0\end{pmatrix}^* \longrightarrow \begin{pmatrix}0.3\\0\\0.6\end{pmatrix}^* \longrightarrow \begin{pmatrix}0.3\\0.6\\0.6\end{pmatrix}^*$; $\begin{pmatrix}0\\0\\0\end{pmatrix}^* \longrightarrow \begin{pmatrix}0\\0.6\\0\end{pmatrix}^* \longrightarrow \begin{pmatrix}0\\0.6\\0.6\end{pmatrix}^* \longrightarrow \begin{pmatrix}0.3\\0.6\\0.6\end{pmatrix}^*$	Different Loading Paths	8.8
C6	W 8 x 31	$\begin{pmatrix}0\\0\\0\end{pmatrix} \longrightarrow \begin{pmatrix}0.3\\0.4\\0.6\end{pmatrix} \overset{9}{\longleftrightarrow} \begin{pmatrix}0.3\\0.4\\-0.6\end{pmatrix}$	Cyclic Loading	8.9
C8	W 8 x 31	$\begin{pmatrix}0\\0\\0\end{pmatrix} \longrightarrow \begin{pmatrix}0.3\\0.4\\0.8\end{pmatrix} \overset{9}{\longleftrightarrow} \begin{pmatrix}0.3\\0.4\\-0.8\end{pmatrix}$		
C9	W 8 x 31	$\begin{pmatrix}0\\0\\0\end{pmatrix} \longrightarrow \begin{pmatrix}0.3\\0.4\\0.9\end{pmatrix} \overset{9}{\longleftrightarrow} \begin{pmatrix}0.3\\0.4\\-0.9\end{pmatrix}$		
C10	W 8 x 31	$\begin{pmatrix}0\\0\\0\end{pmatrix} \longrightarrow \begin{pmatrix}0.3\\0.4\\1.0\end{pmatrix} \overset{9}{\longleftrightarrow} \begin{pmatrix}0.3\\0.4\\-1.0\end{pmatrix}$		
C11	W 8 x 31	$\begin{pmatrix}0\\0\\0\end{pmatrix} \longrightarrow \begin{pmatrix}0.3\\0.4\\1.1\end{pmatrix} \overset{9}{\longleftrightarrow} \begin{pmatrix}0.3\\0.4\\-1.1\end{pmatrix}$		
D1	W 8 x 31	$\begin{pmatrix}0\\0\\0\end{pmatrix} \longrightarrow \begin{pmatrix}0\\0.4\\0.8\end{pmatrix} \longleftrightarrow \begin{pmatrix}0\\0.4\\-0.8\end{pmatrix}$	Subsequent Yield Surface	8.10
D2	W 8 x 31	$\begin{pmatrix}0\\0\\0\end{pmatrix} \longrightarrow \begin{pmatrix}0.3\\0.4\\0.8\end{pmatrix} \longleftrightarrow \begin{pmatrix}0.3\\0.4\\-0.8\end{pmatrix}$		
D3	W 8 x 31	$\begin{pmatrix}0\\0\\0\end{pmatrix} \longrightarrow \begin{pmatrix}0.3\\0.4\\1.1\end{pmatrix} \longleftrightarrow \begin{pmatrix}0.3\\0.4\\-1.1\end{pmatrix}$		8.11
E1	W 14 x 176	$\begin{pmatrix}0\\0\\0\end{pmatrix} \longrightarrow \begin{pmatrix}0\\1.129\\0\end{pmatrix} \rightleftharpoons \begin{pmatrix}0\\1.120\\0\end{pmatrix}$	Comparison With Others	8.12
E2	W 14 x 176	$\begin{pmatrix}0\\0\\0\end{pmatrix} \longrightarrow \begin{pmatrix}0.5024\\0.6452\\0\end{pmatrix} \rightleftharpoons \begin{pmatrix}-0.5024\\-0.6452\\0\end{pmatrix}$		

$\begin{pmatrix}p\\m_x\\m_y\end{pmatrix}$ $\longrightarrow$ oneway loading
$\rightleftharpoons$ bothway loading
$\overset{N}{\longleftrightarrow}$ cyclic loading (N cycles)

*non-dimensionalized by M_{px}, M_{py}

14. FIGURES

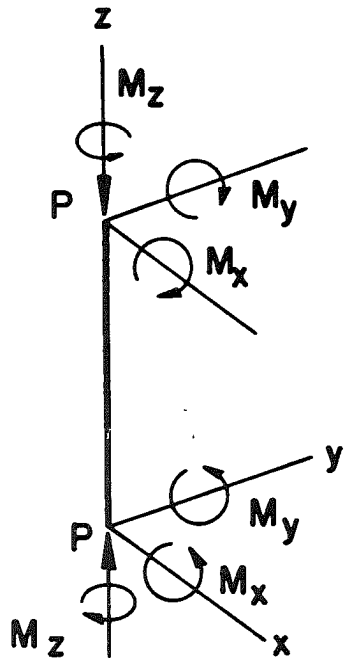

(a) Isolated Column

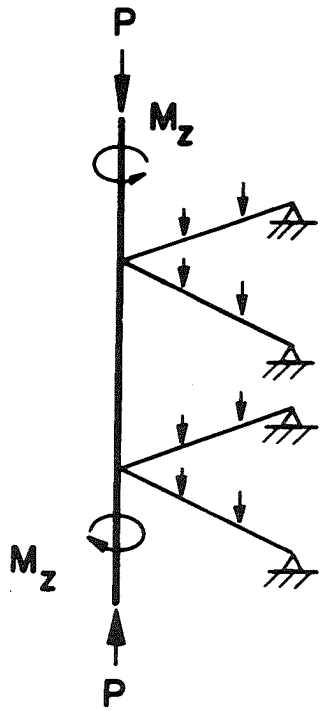

(b) Elastically Restrained Column

Fig. 1.1 Columns Subjected to Biaxial Loading and Twisting Moment

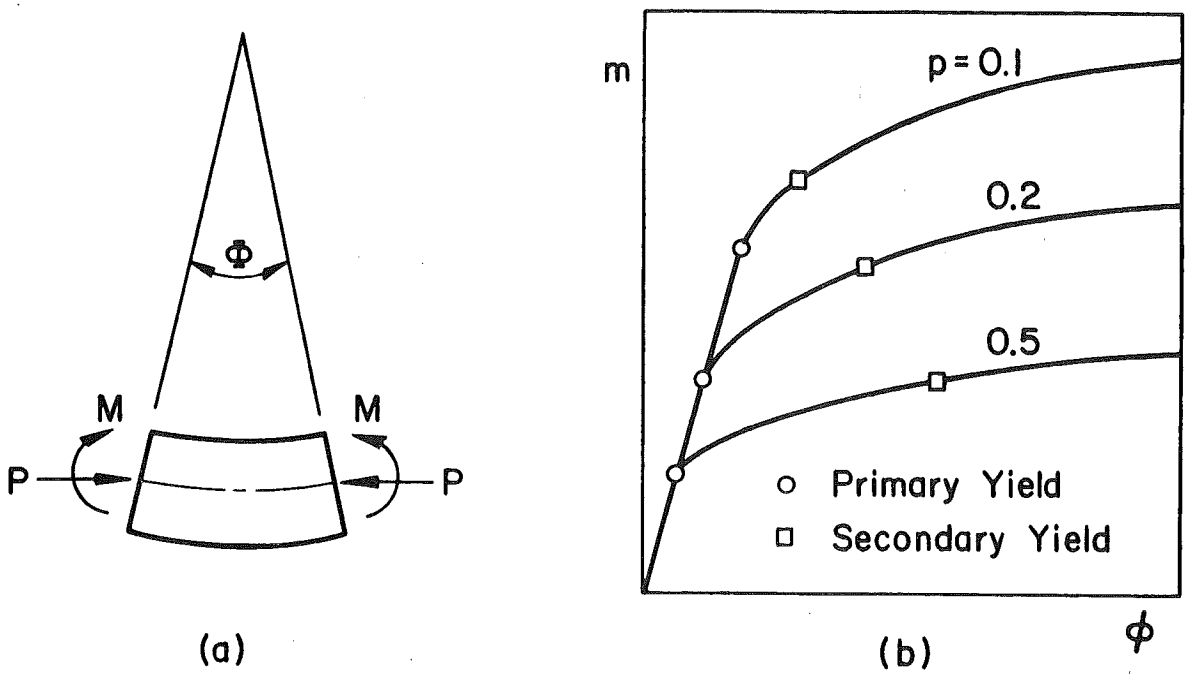

Fig. 2.1 Moment-Curvature-Thrust Relationship

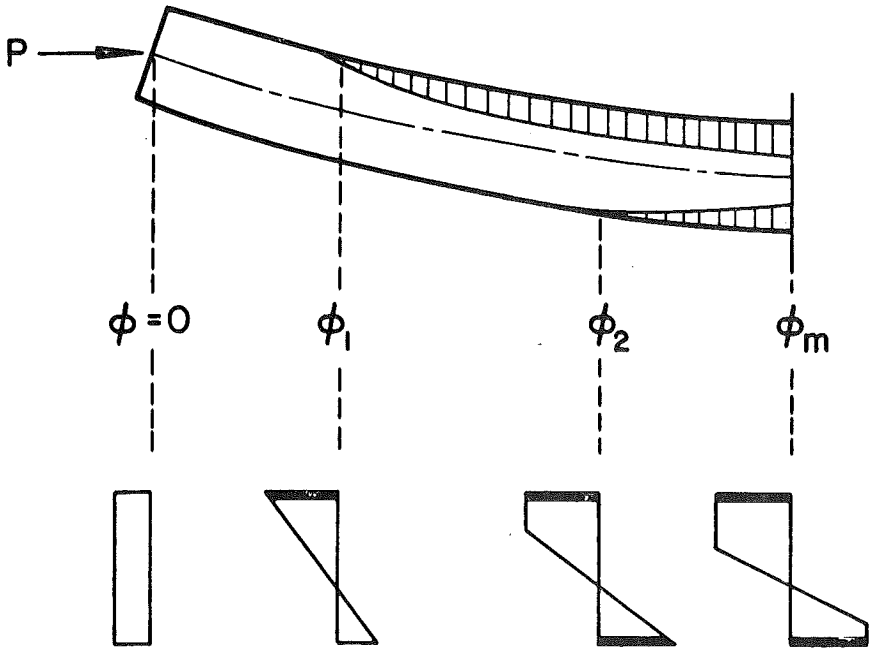

Fig. 2.2 Regime of Curvature

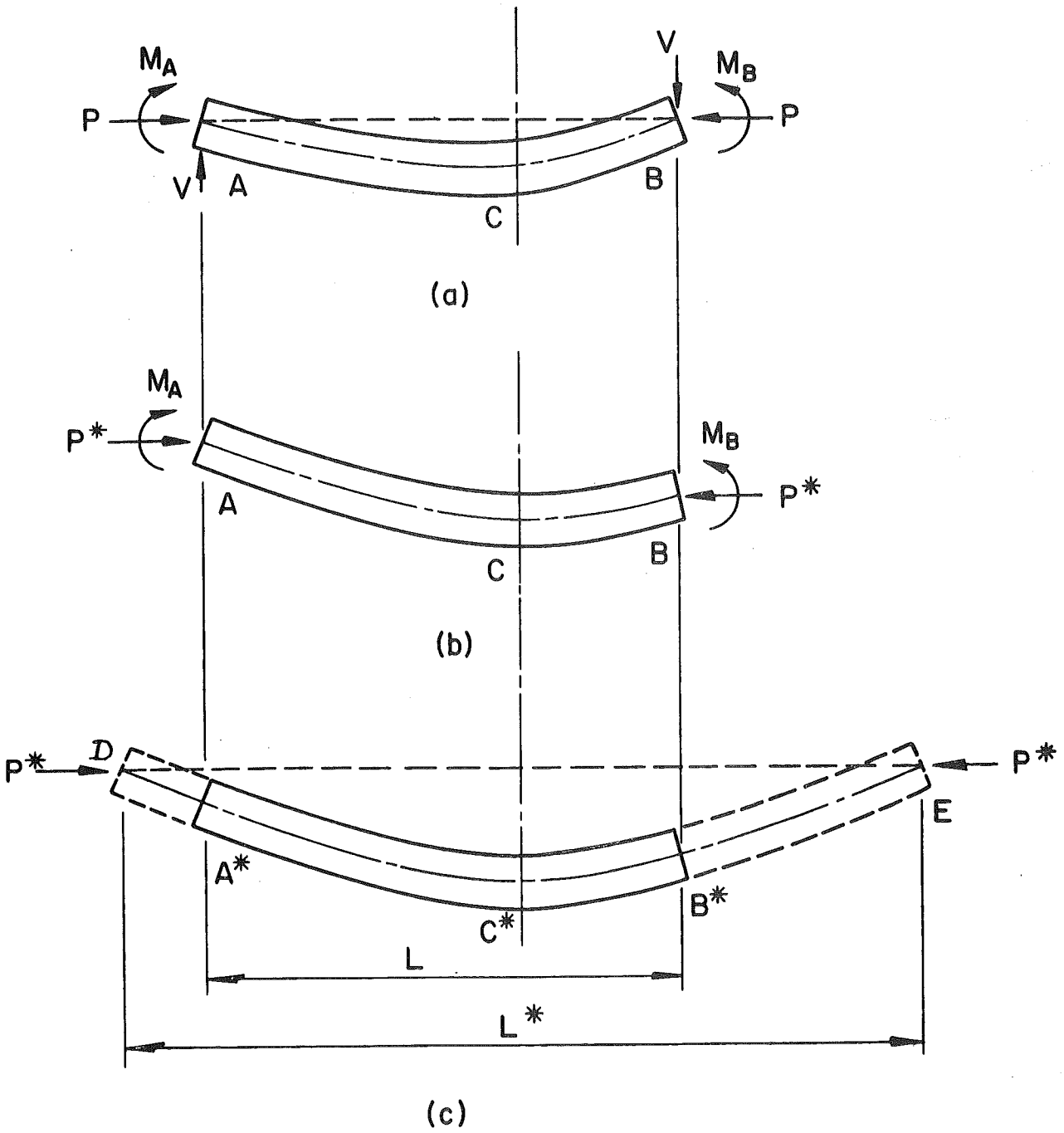

Fig. 2.3 Beam-Column and Its Equivalent Column

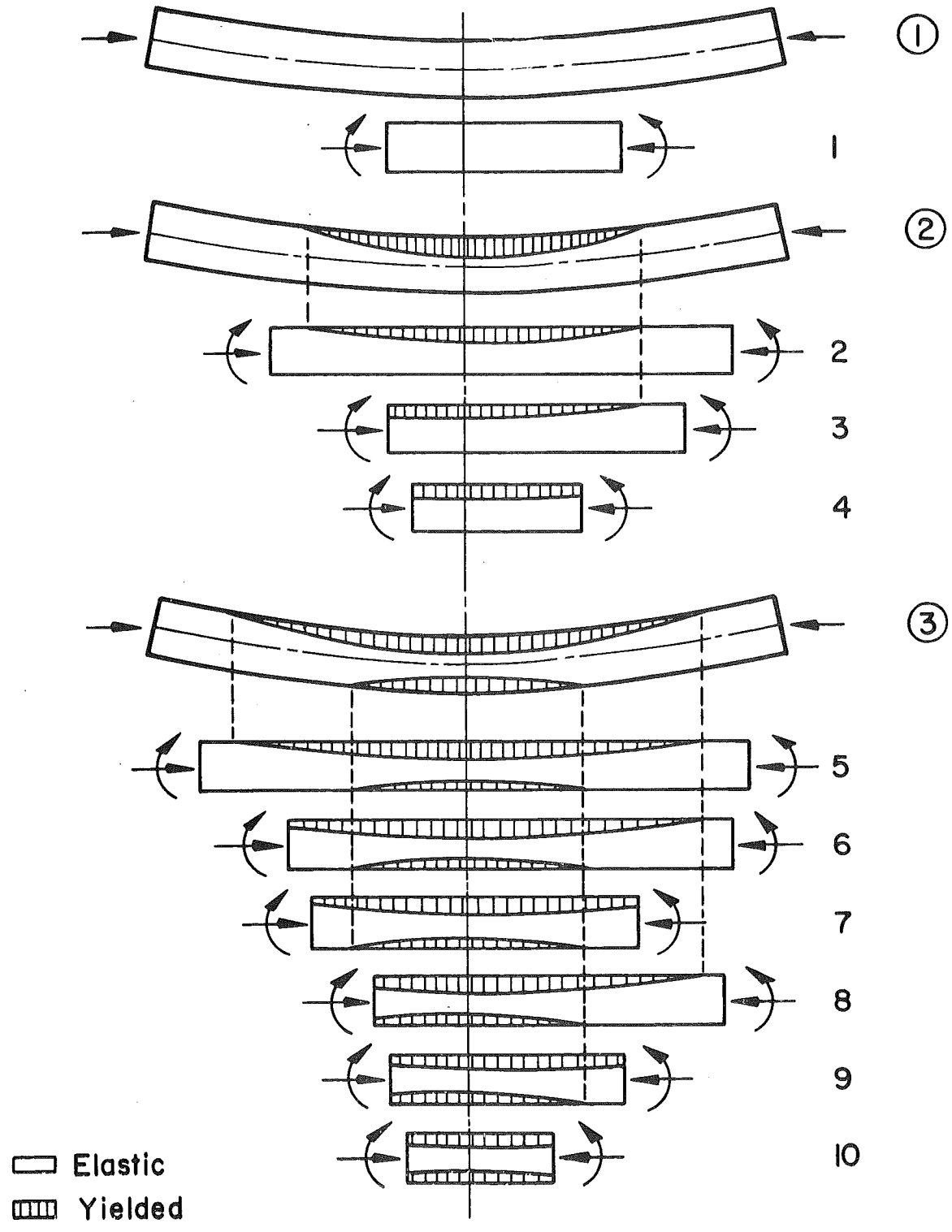

Fig. 2.4 Types of Elastic Beam-Columns

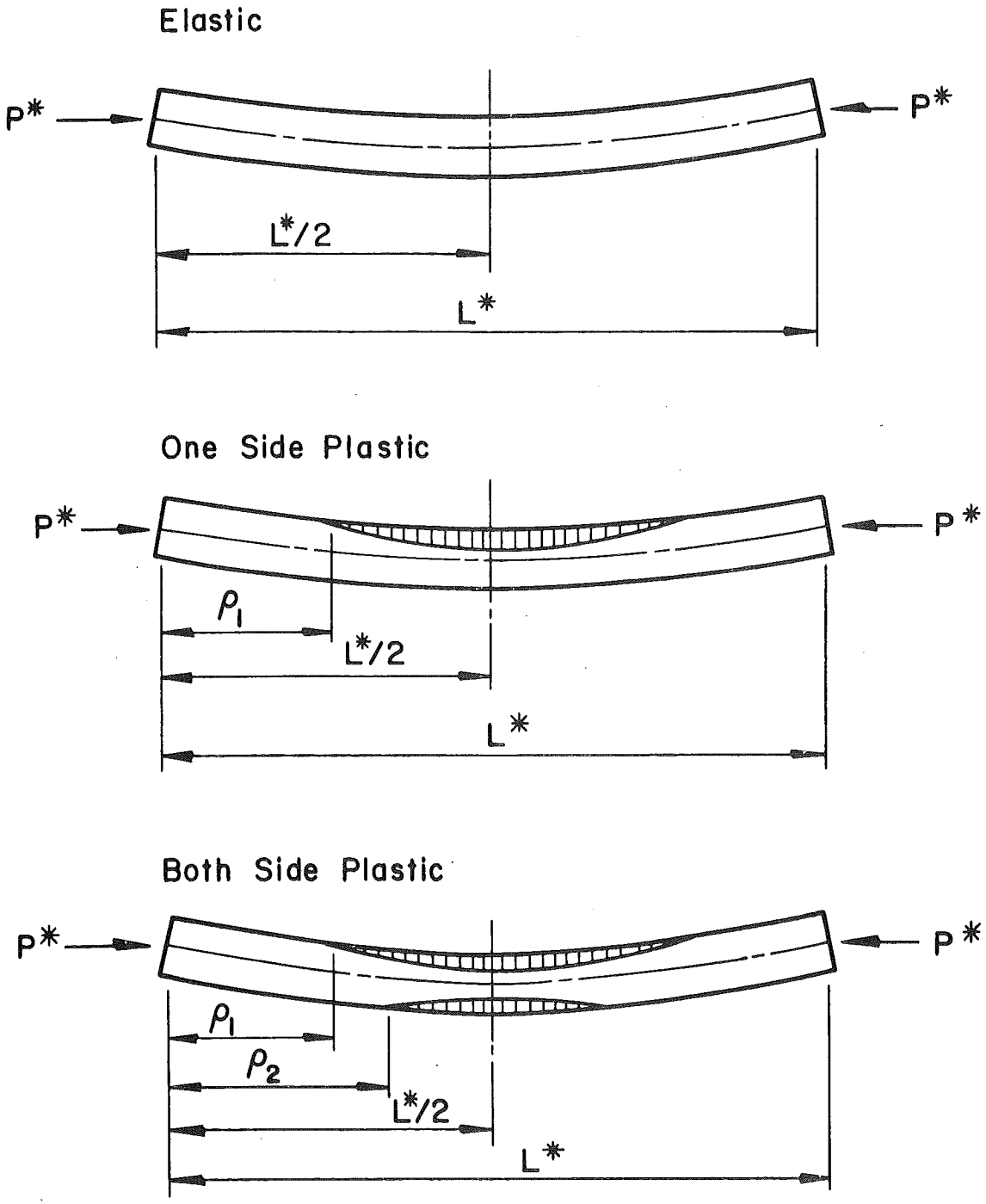

Fig. 2.5 Types of Equivalent Columns

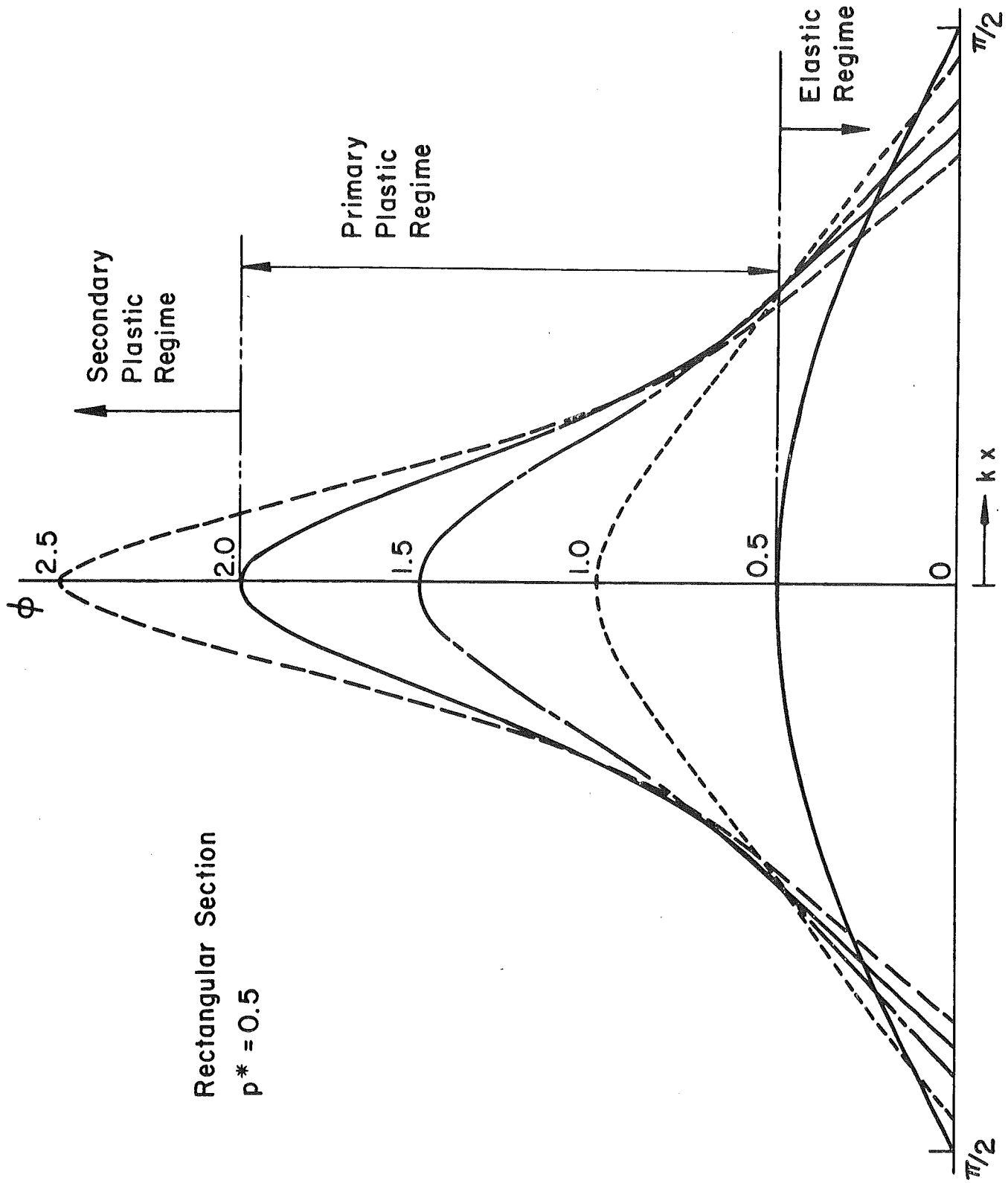

Fig. 2.6 An Example of Column Curvature Curves

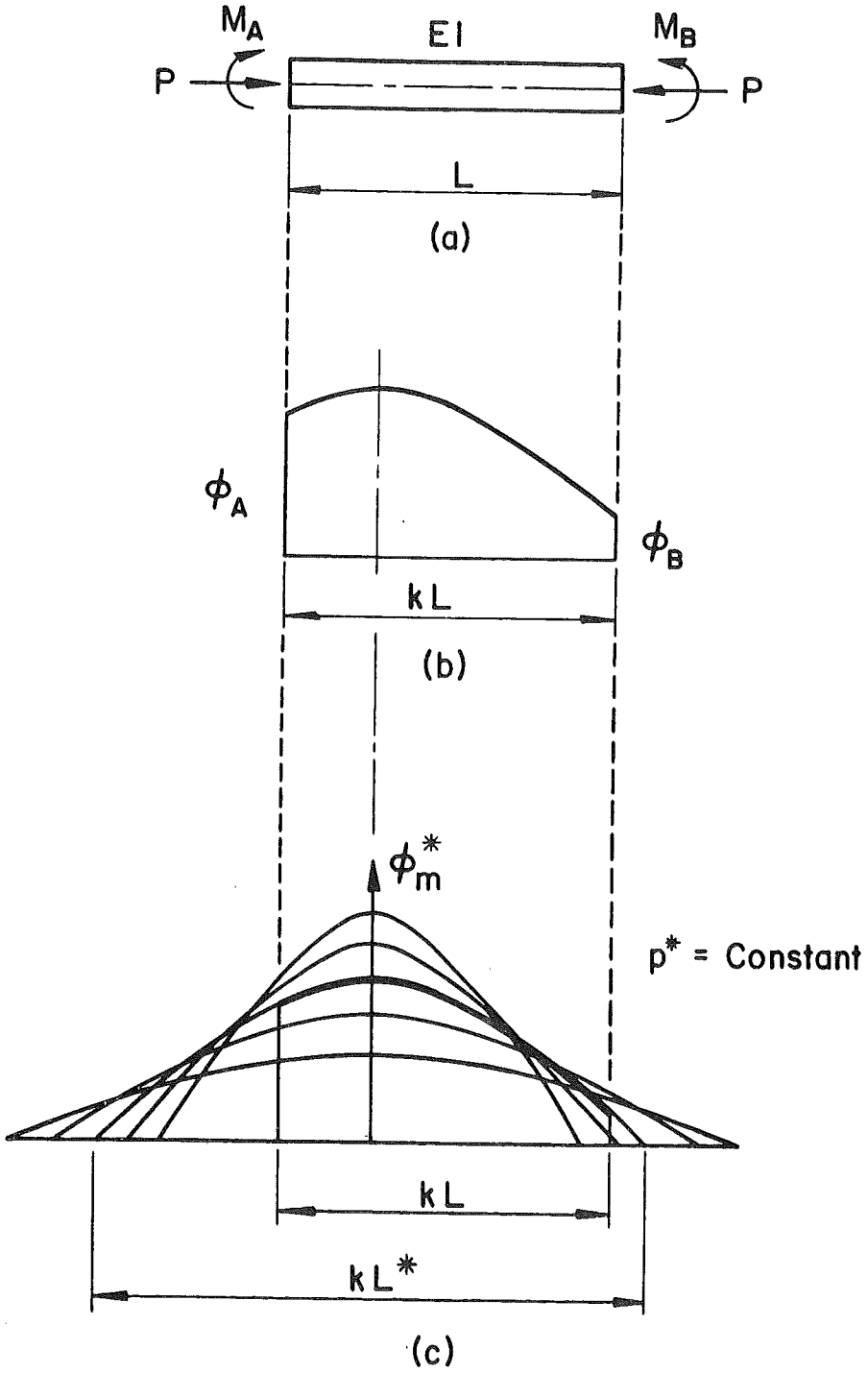

Fig. 2.7 Application of Column Curvature Curves

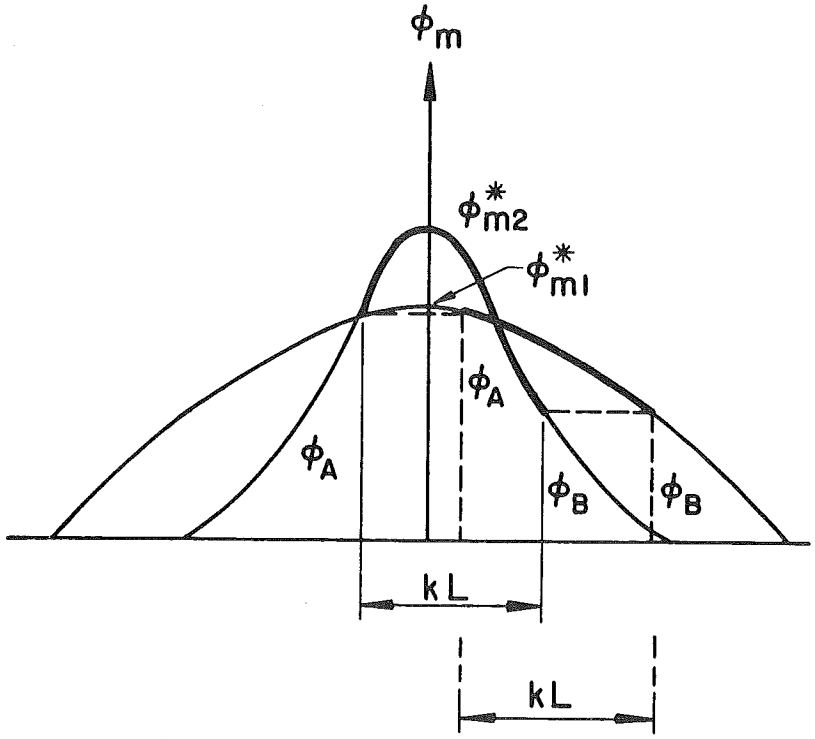

(a)

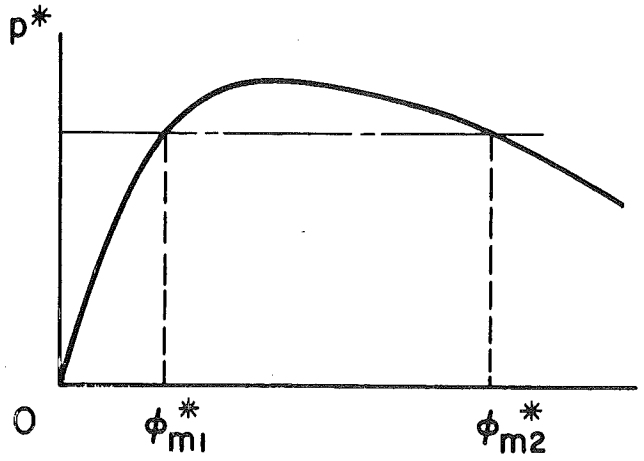

(b)

Fig. 2.8 Loading and Unloading

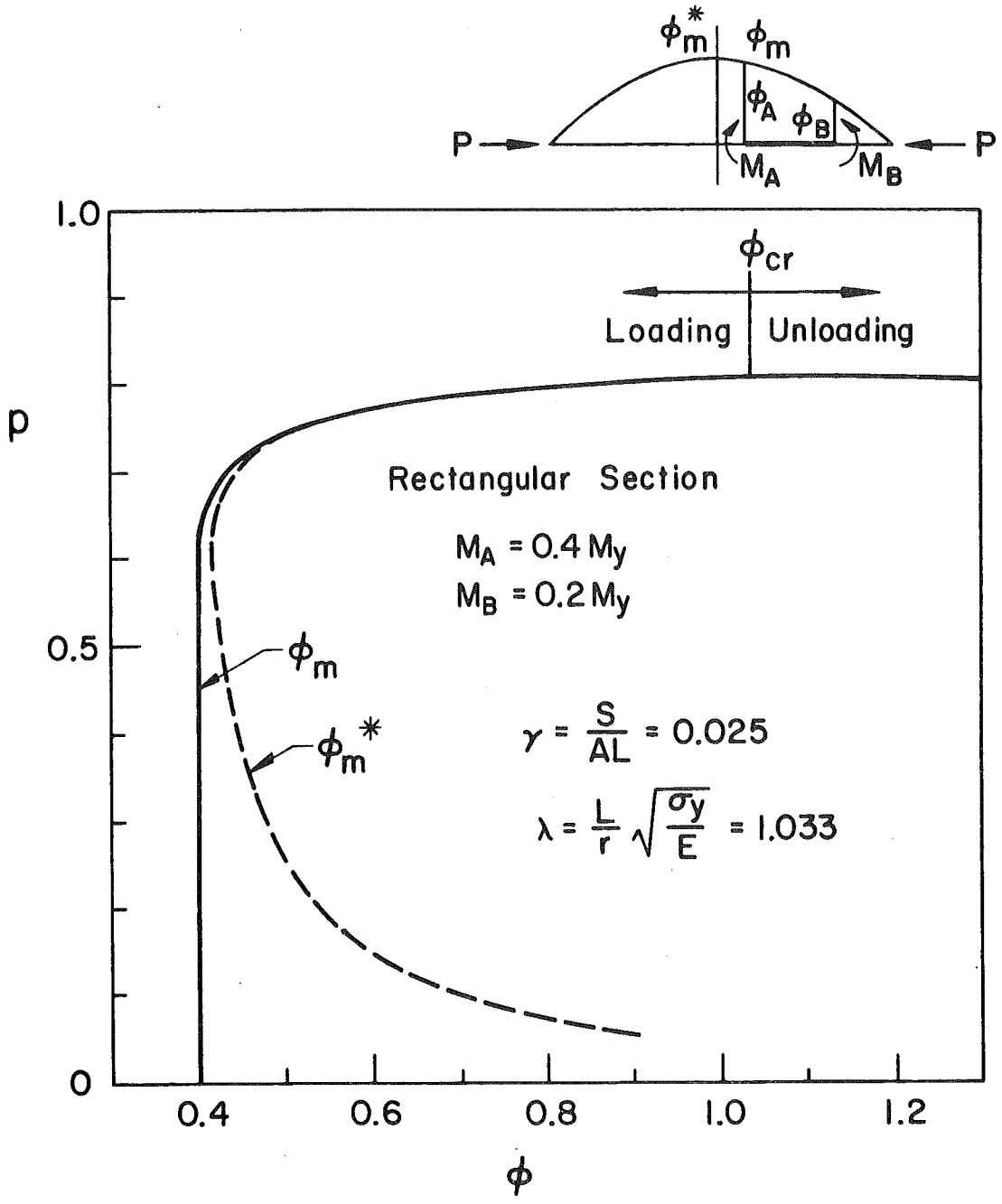

Fig. 2.9 Comparison of Maximum Curvatures φ_m and φ_m^*

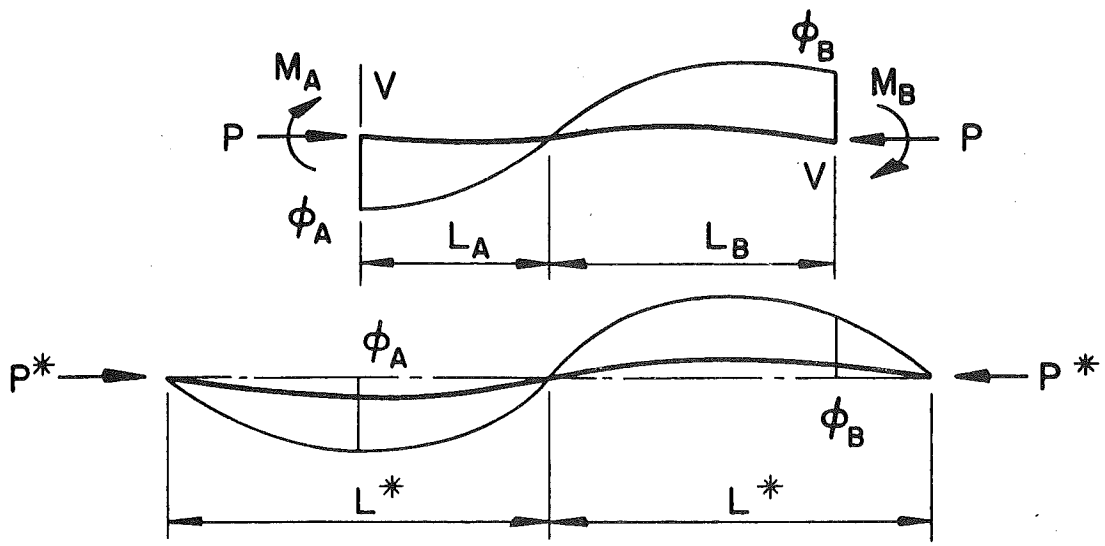

Fig. 2.10 Beam-Column with Double Curvature

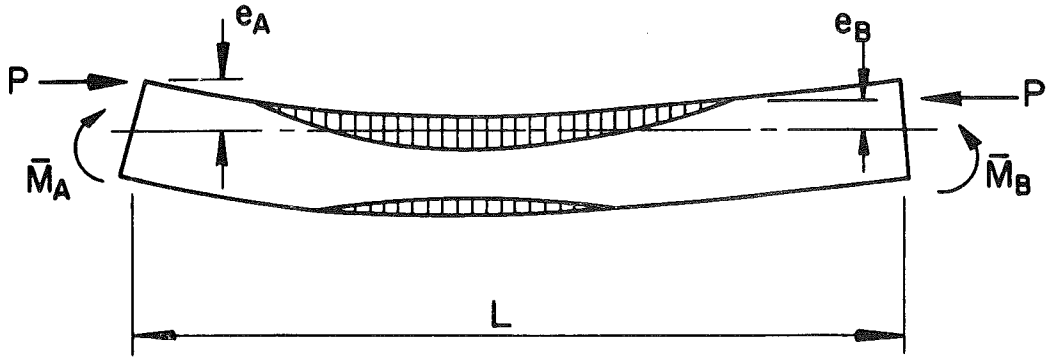

Fig. 2.11 Loading Condition of Beam-Column

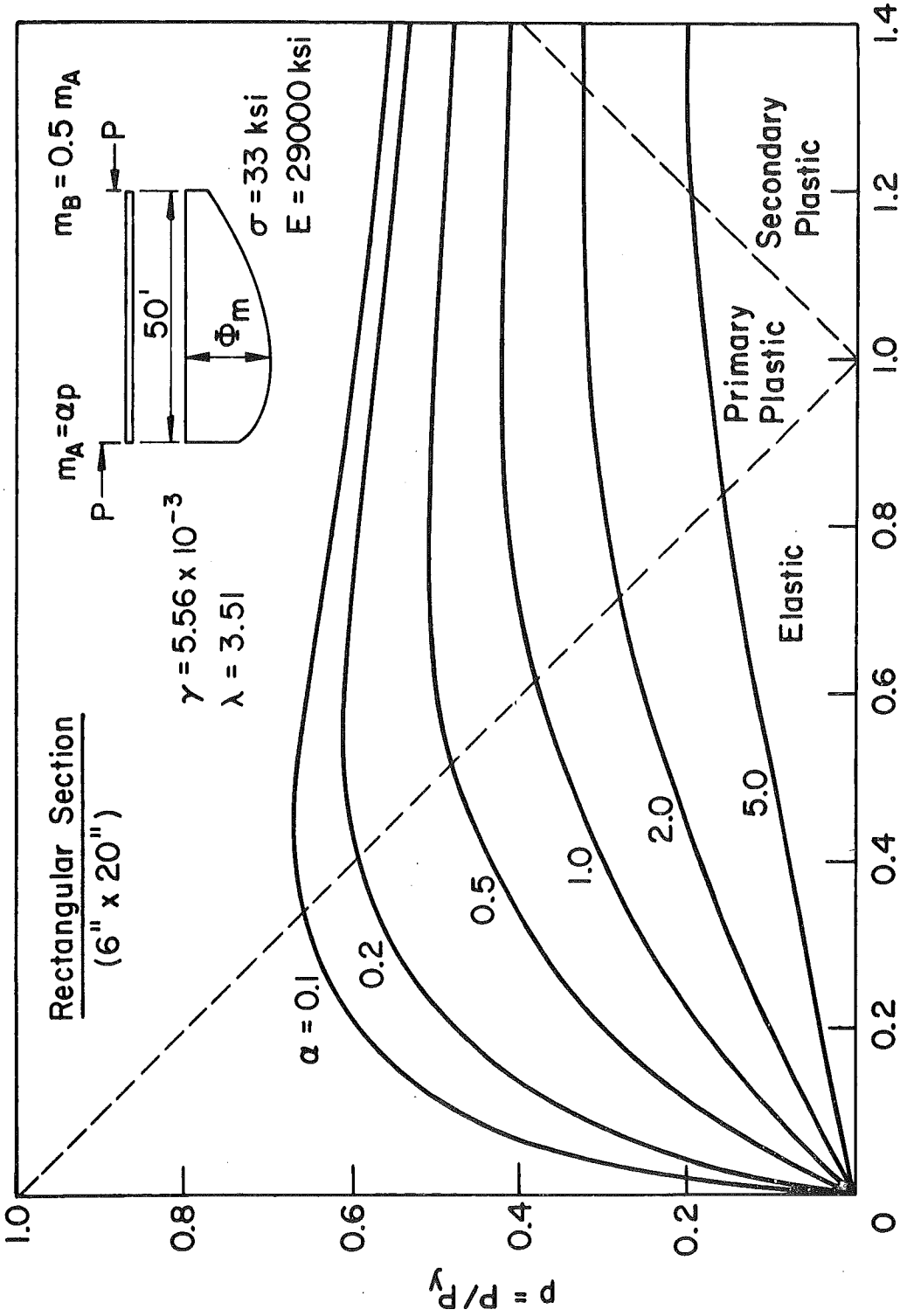

Fig. 2.12 Maximum Curvature (Rectangular Section)

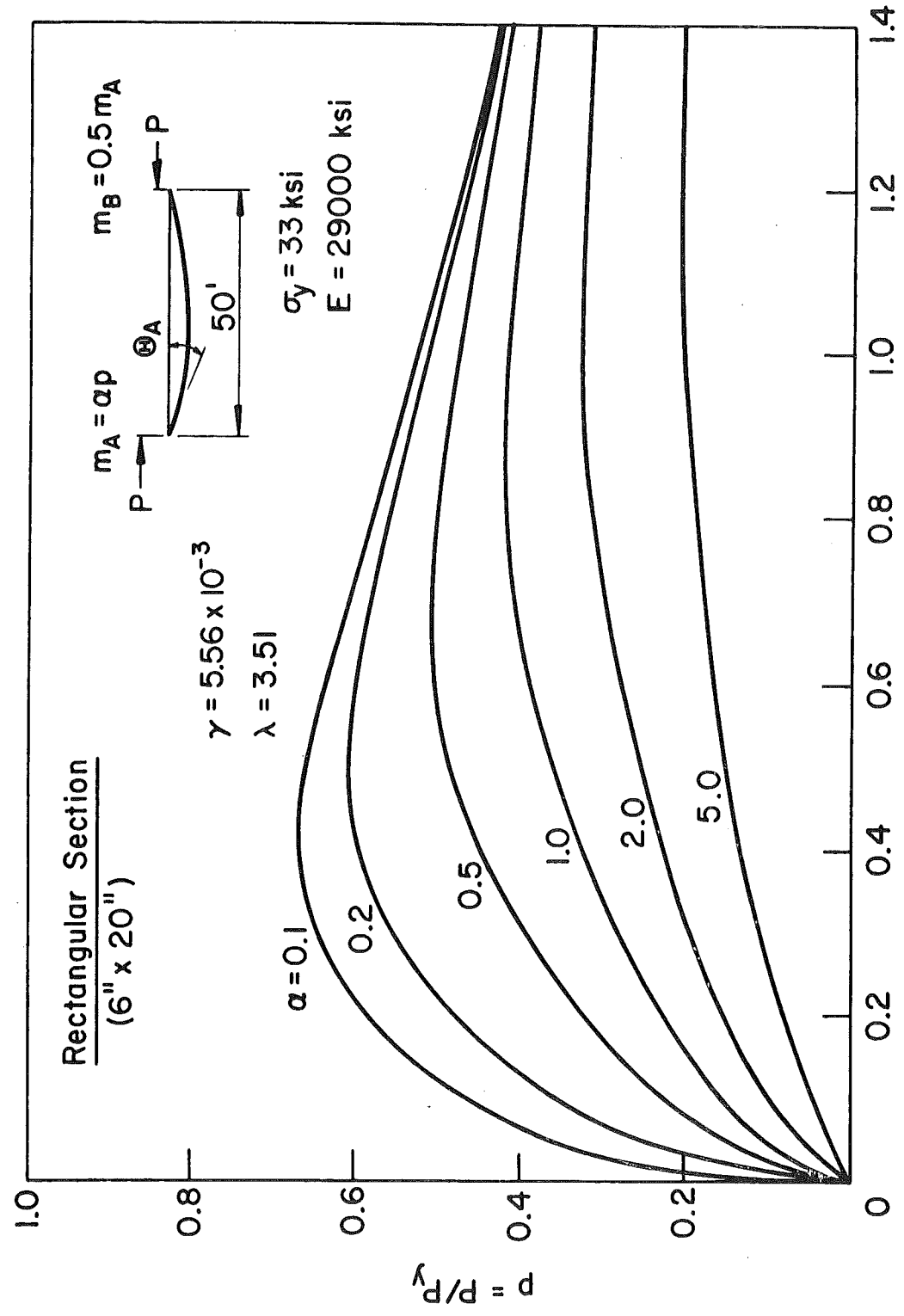

Fig. 2.13 End Rotation (Rectangular Section)

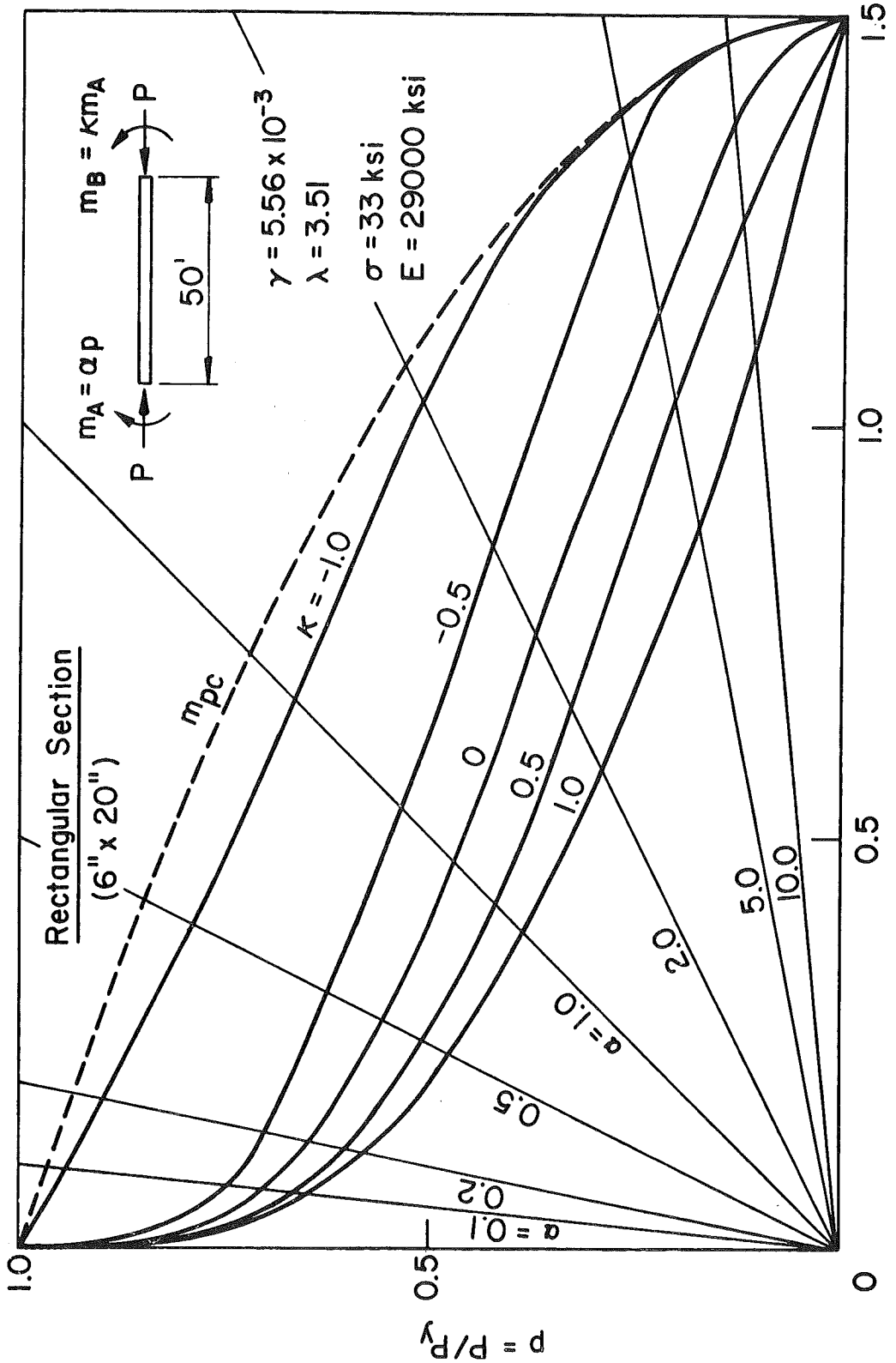

Fig. 2.14 Interaction Curves (Rectangular Section)

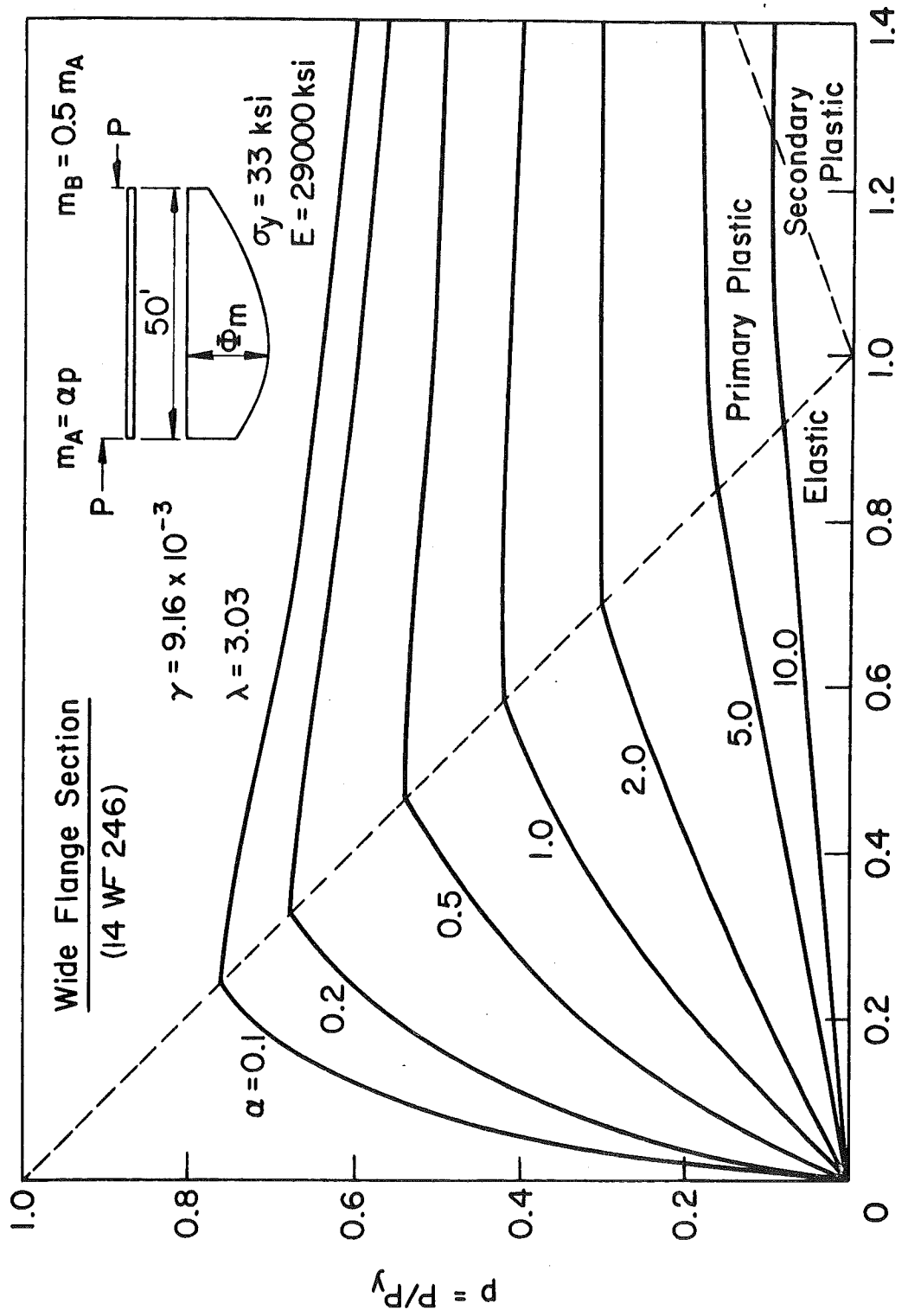

Fig. 2.15 Maximum Curvature (Wide-Flange Section)

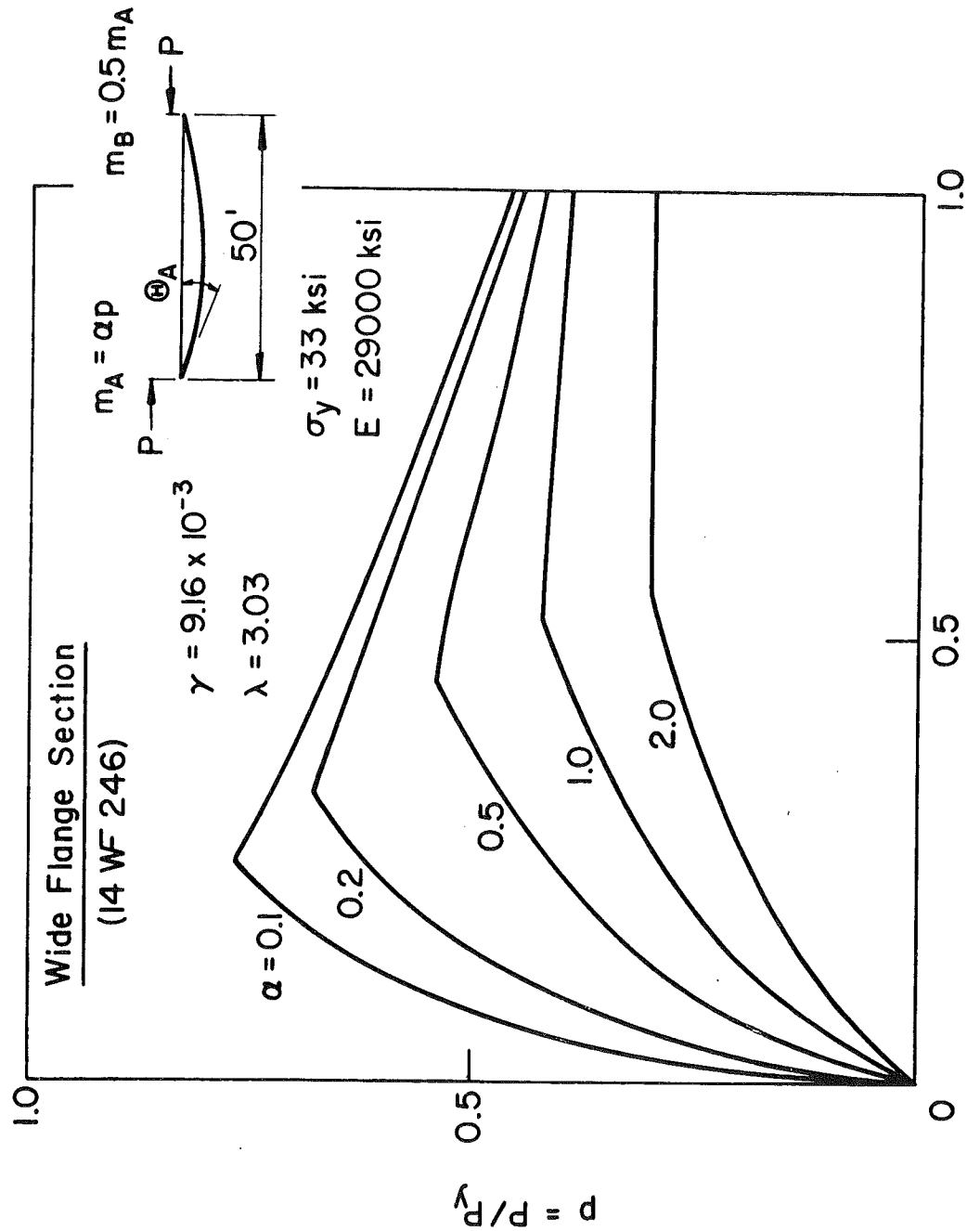

Fig. 2.16 End Rotation (Wide-Flange Section)

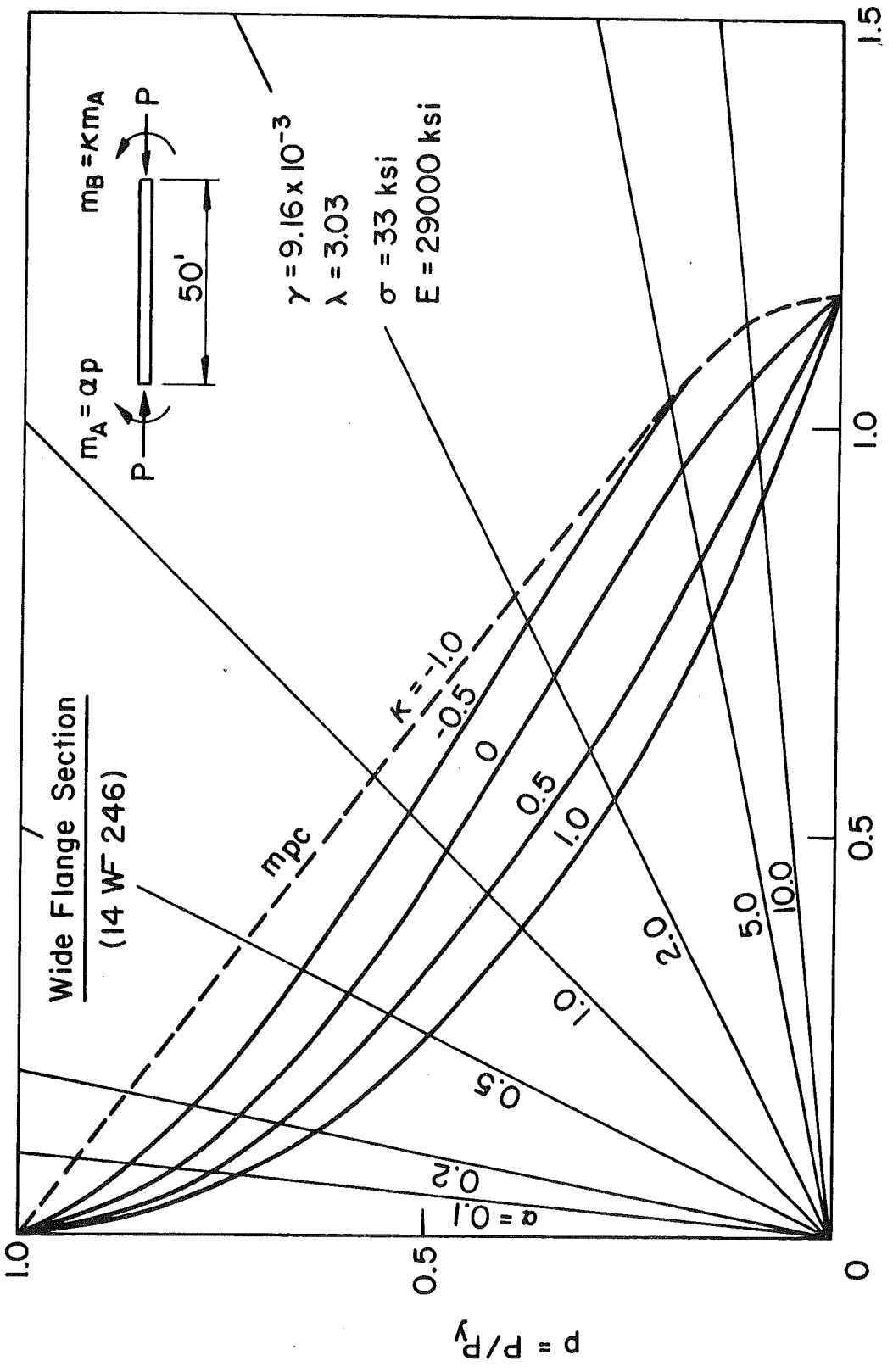

Fig. 2.17 Interaction Curves (Wide-Flange Section)

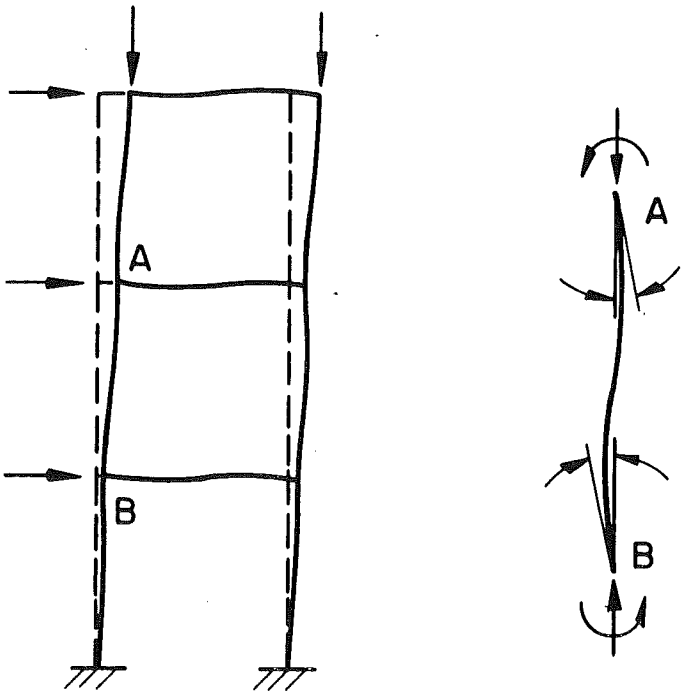

Fig. 2.18 Beam-Columns as Members of a Frame

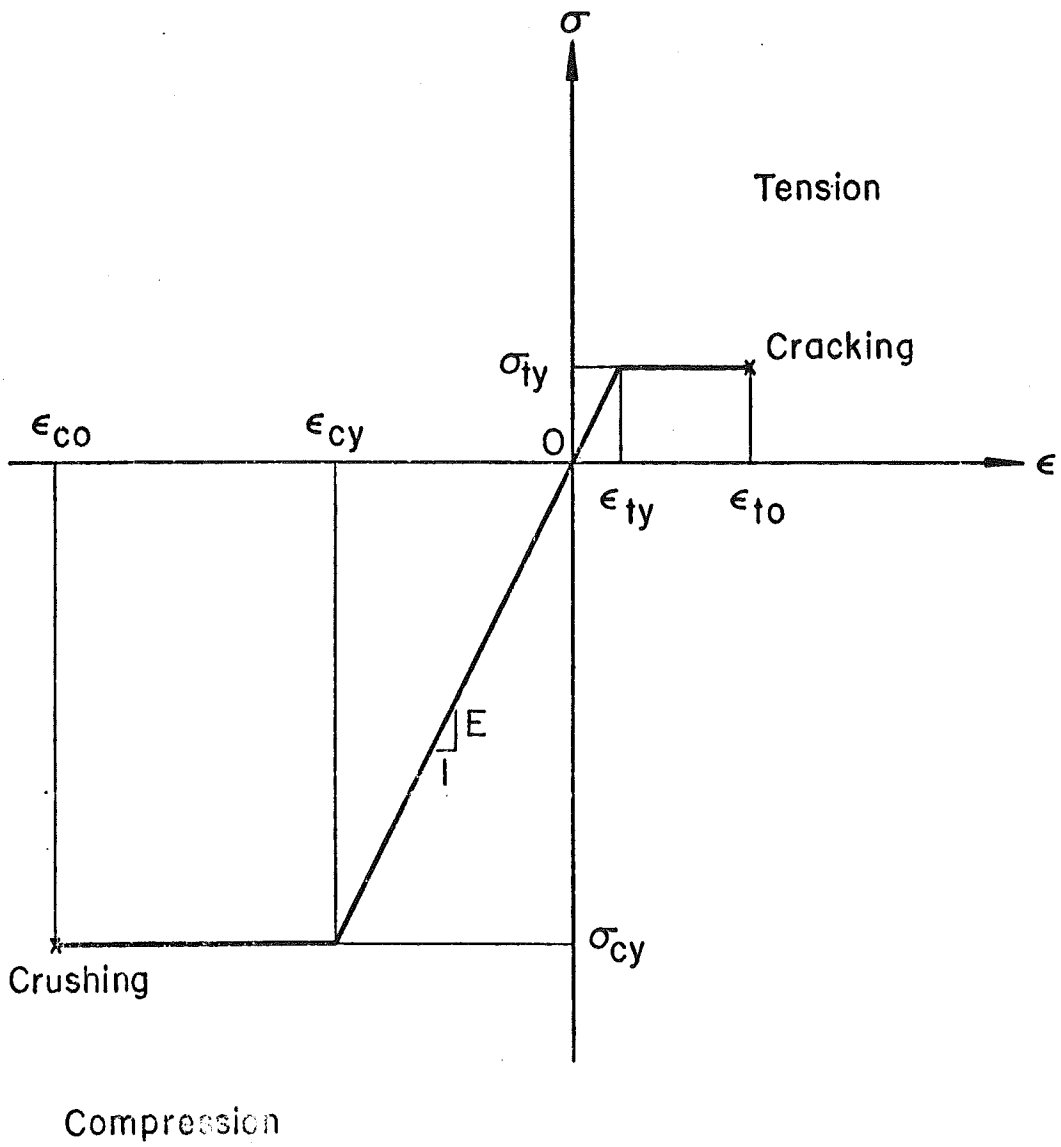

Fig. 3.1 Idealized Stress-Strain Relationship

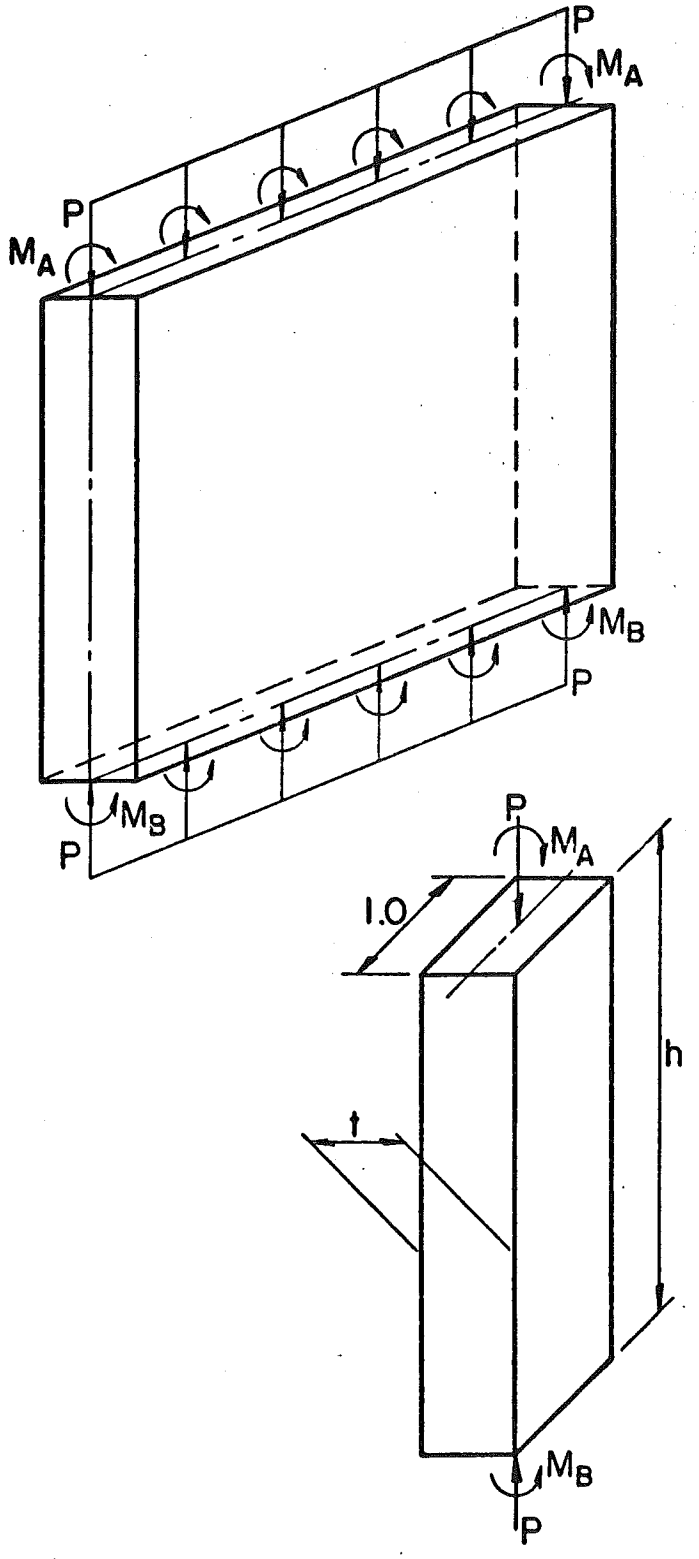

Fig. 3.2 Wall and Beam-Column

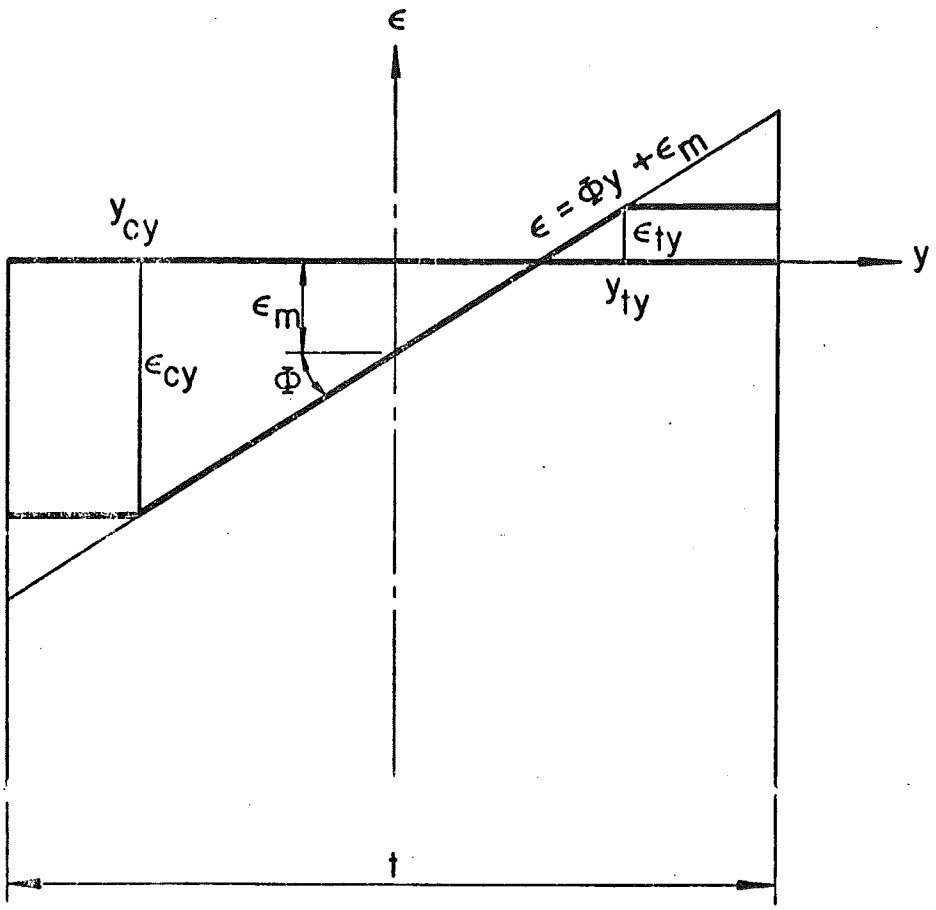

Fig. 3.3 Linear Distribution of Strain

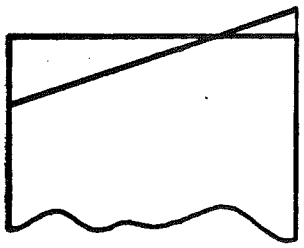

(a) Elastic Regime

$(\phi \le \phi_{et} \quad \phi \le \phi_{ec})$

$m = \phi$

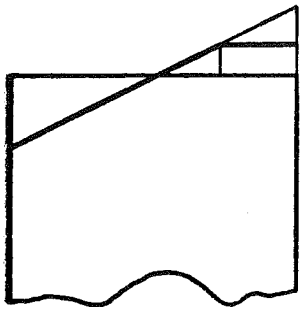

(b) Tension Yield Regime

$(\phi_{et} < \phi_{ec} \quad \phi_{et} \le \phi_{tc})$

$$m = 3(\mu + p) - 2\sqrt{\frac{(\mu + p)^3}{\phi}}$$

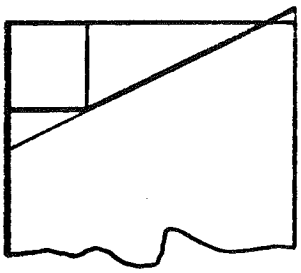

(c) Compression Yield Regime

$(\phi_{ec} < \phi_{ec} \quad \phi_{ec} < \phi \le \phi_{ct})$

$$m = 3(1 - p) - 2\sqrt{\frac{(1-p)^3}{\phi}}$$

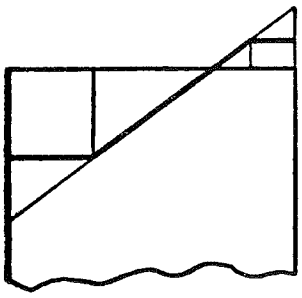

(d) Combined Yield Regime

$(\phi_{tc} < \phi \text{ or } \phi_{ct} < \phi)$

$$m = \frac{3(1-p)(\mu+p)}{1+\mu} - \frac{(1+\mu)^3}{16\phi^2}$$

Fig. 3.4 m-φ-p Equations in Regimes

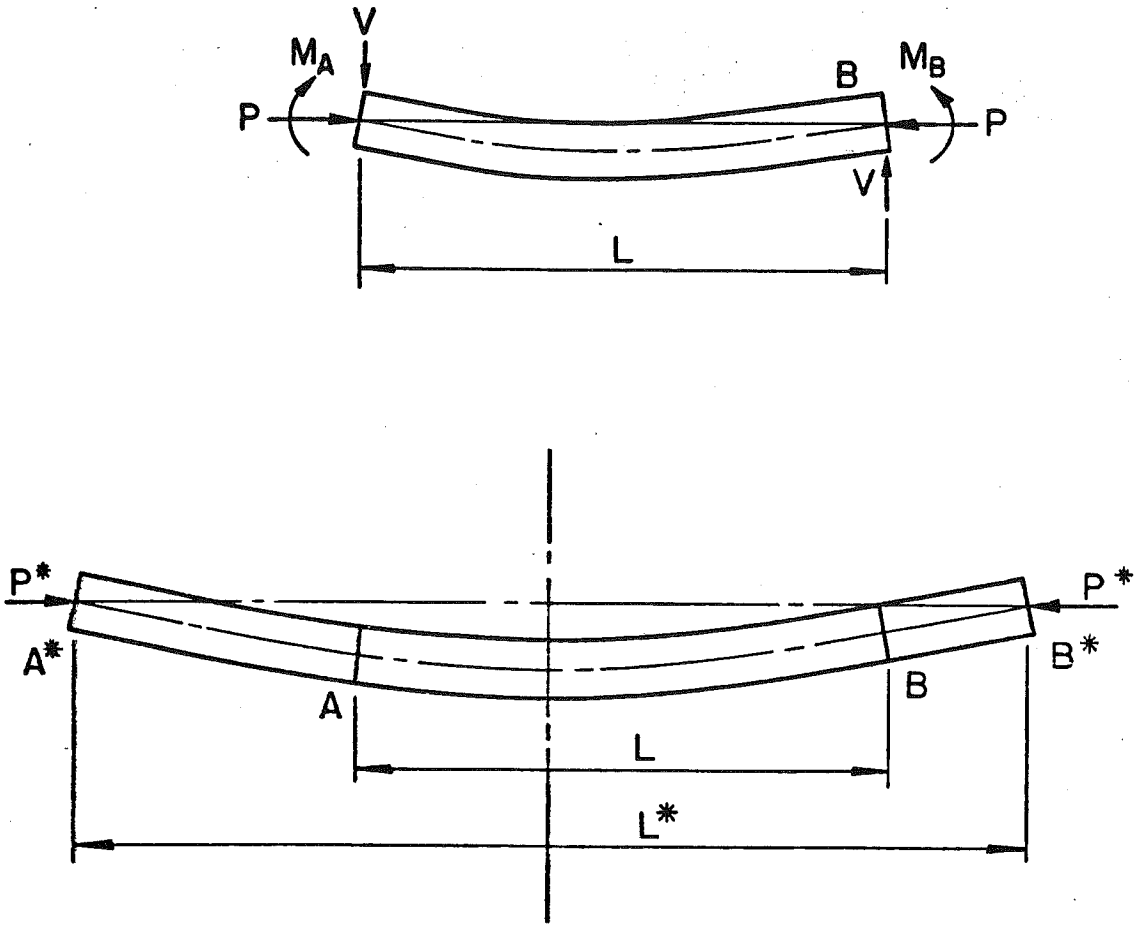

Fig. 3.5 Beam-Column and Its Equivalent Column

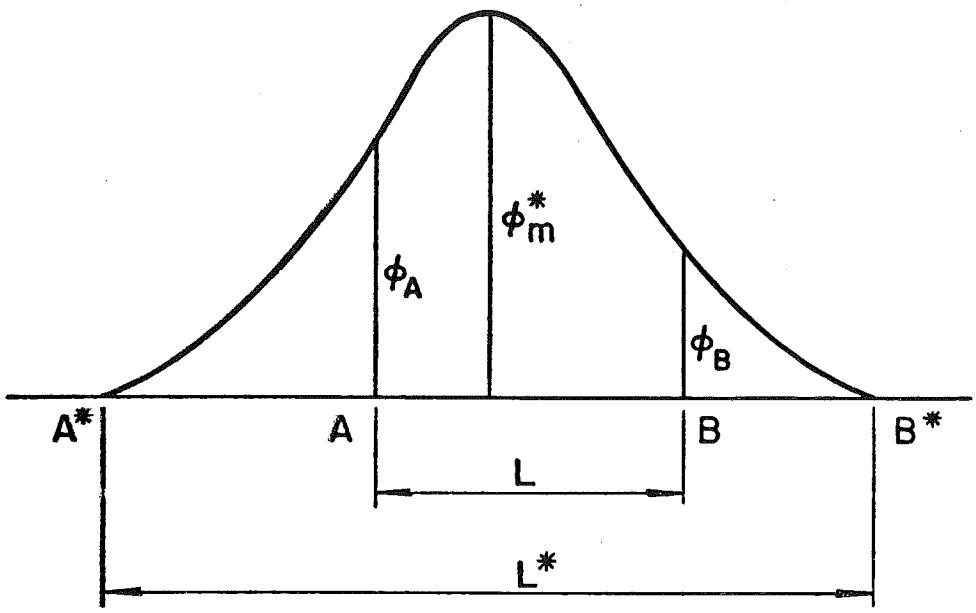

Fig. 3.6 Curvature of Beam-Column AB

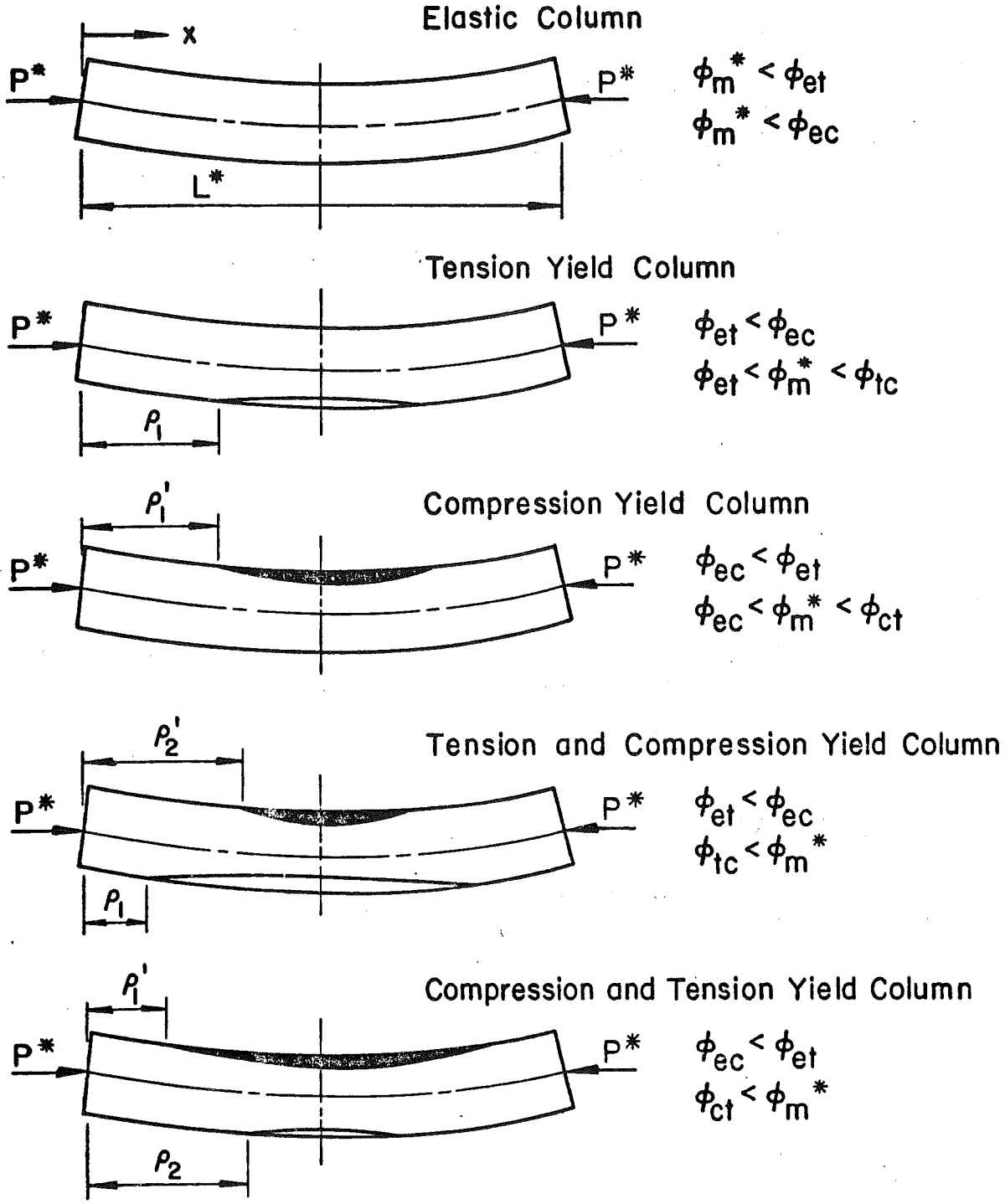

Fig. 3.7 Five Types of Equivalent Column

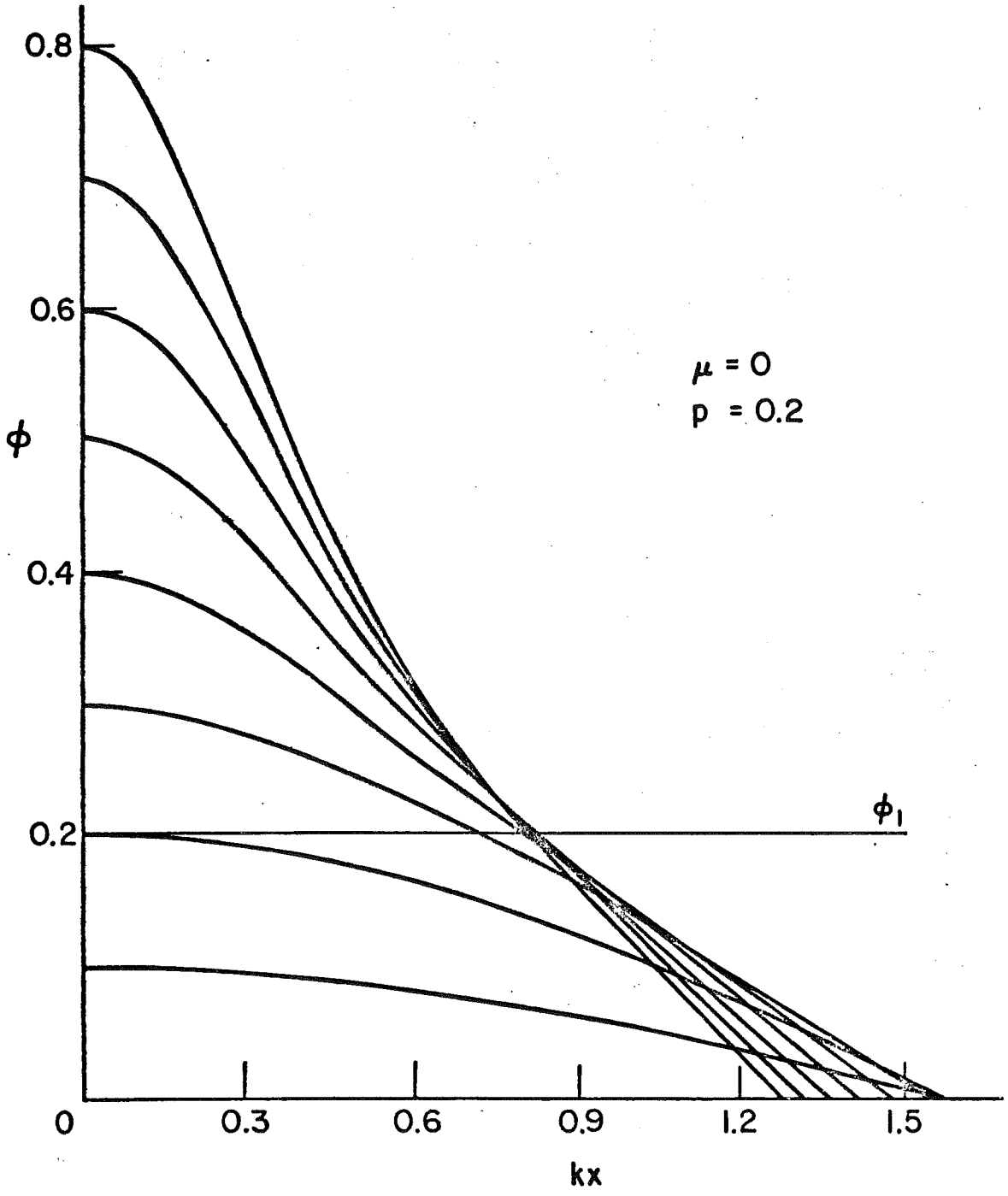

Fig. 3.8 Column Curvature Curves

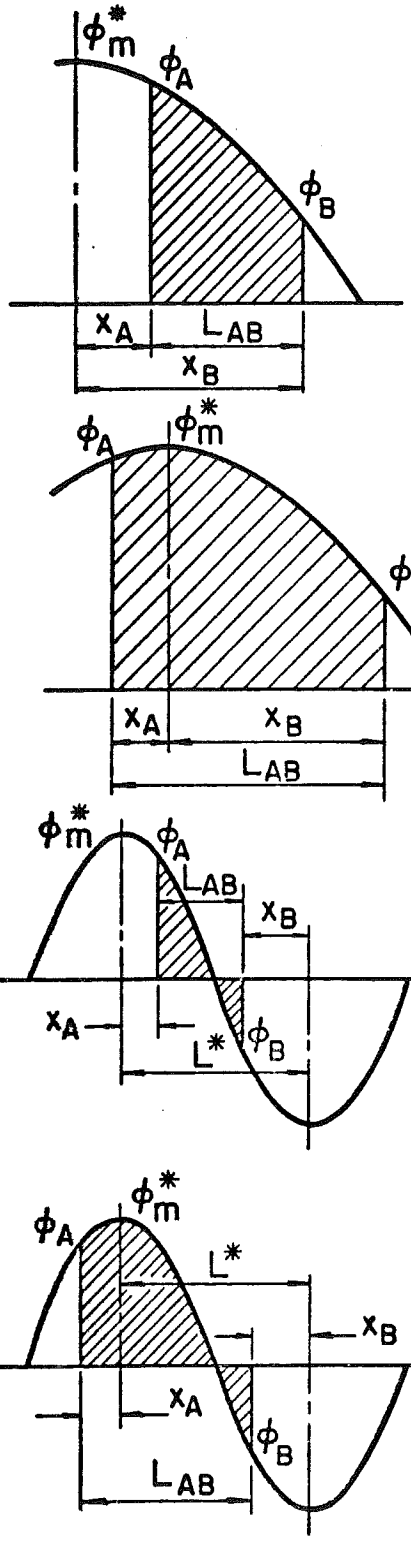

Single Curvature ($\phi_A \phi_B \geq 0$)

Type 1

$L_{AB} = x_B - x_A$

$\phi_m = \phi_A$, $x_m = 0$

Type 2

$L_{AB} = x_A + x_B$

$\phi_m = \phi_m^*$, $x_m = x_A$

Double Curvature ($\phi_A \phi_B < 0$)

Type 1

$L_{AB} = L^* - x_A - x_B$

$\phi_m = \phi_A$, $x_m = 0$

Type 2

$L_{AB} = L^* + x_A - x_B$

$\phi_m = \phi_m^*$, $x_m = x_A$

Fig. 3.9 Computation of Column Length L_{AB}

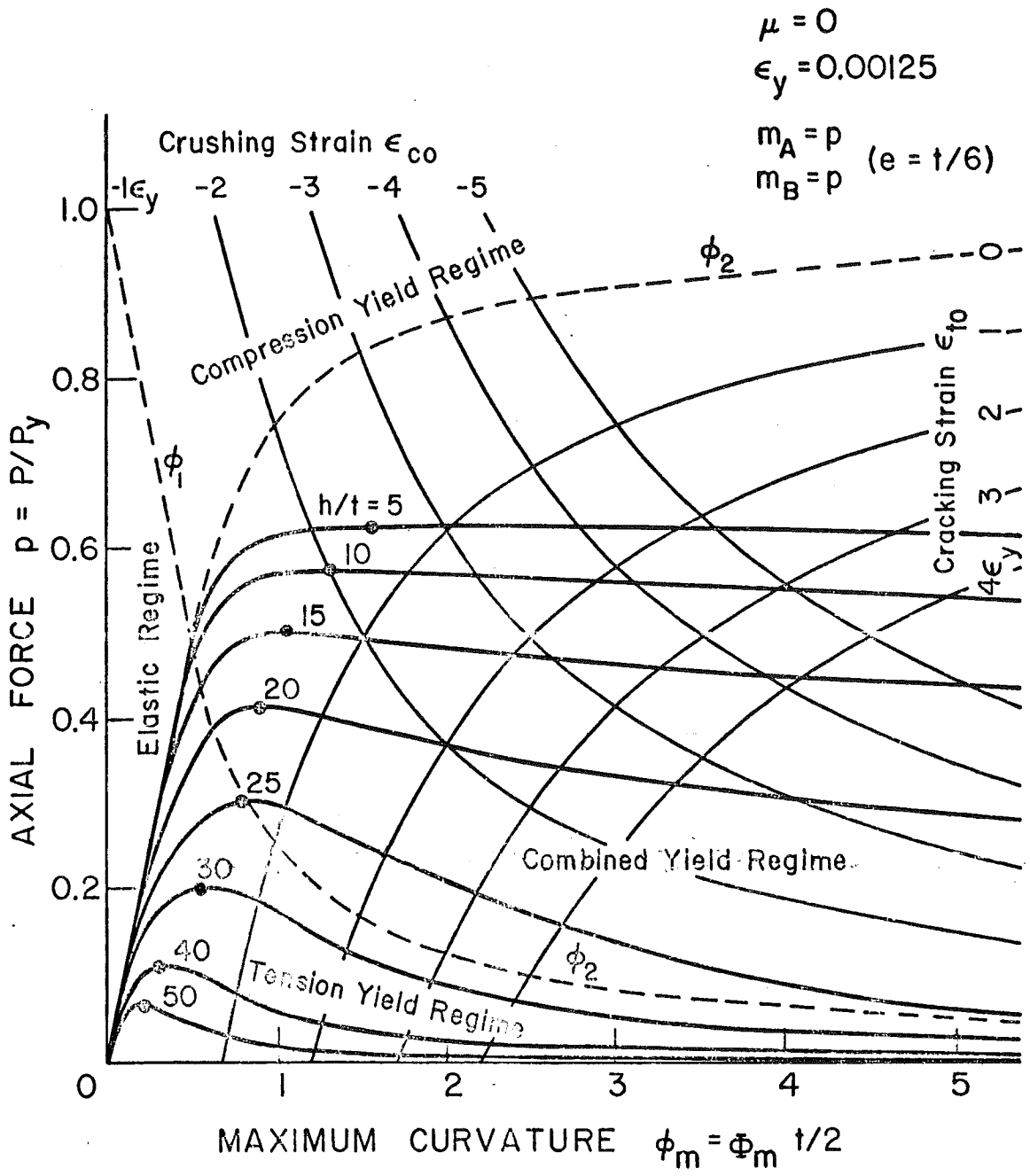

Fig. 3.10 Load-Curvature Curves of Masonry Wall

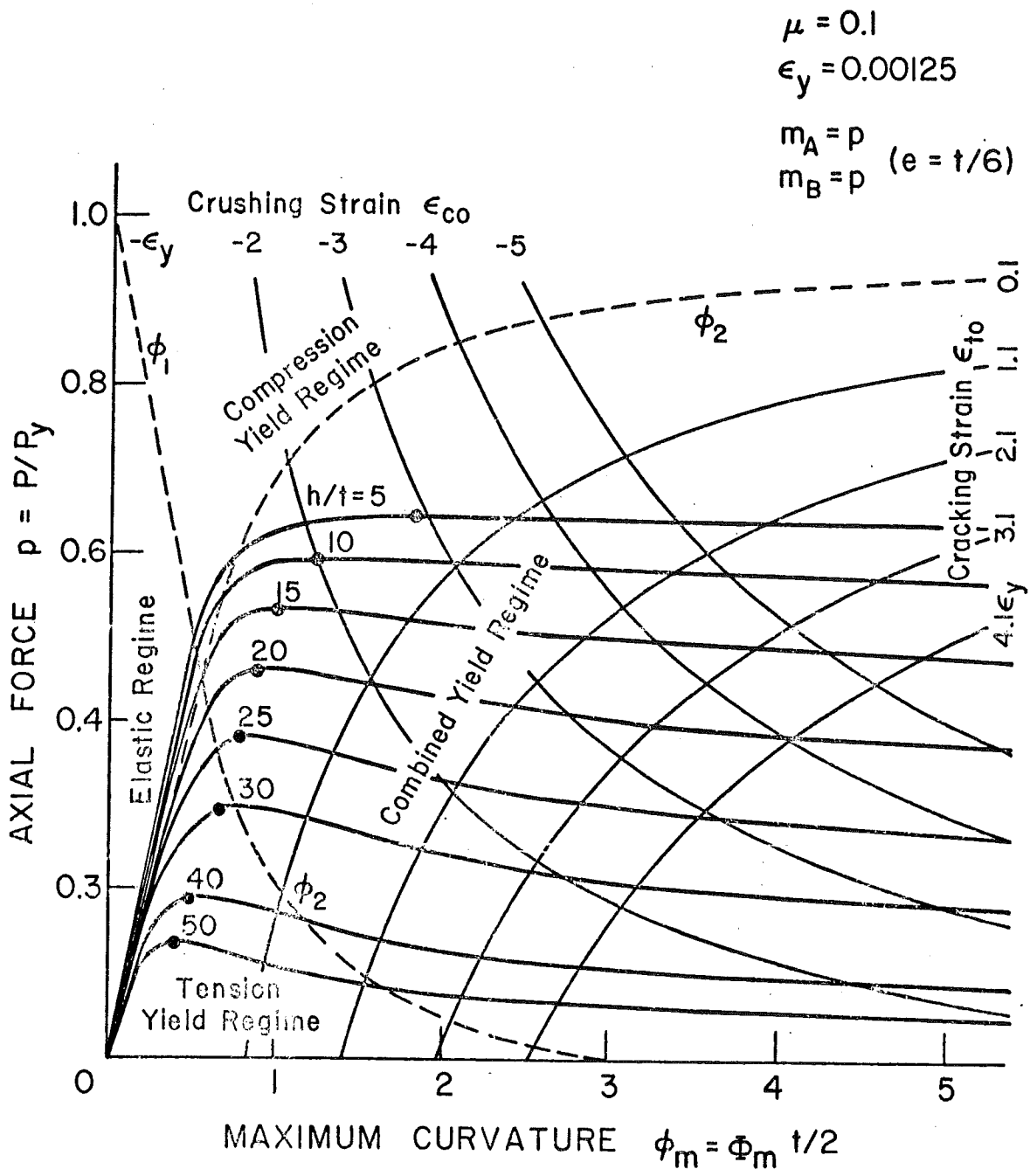

Fig. 3.11 Load Curvature Curves of Concrete Wall

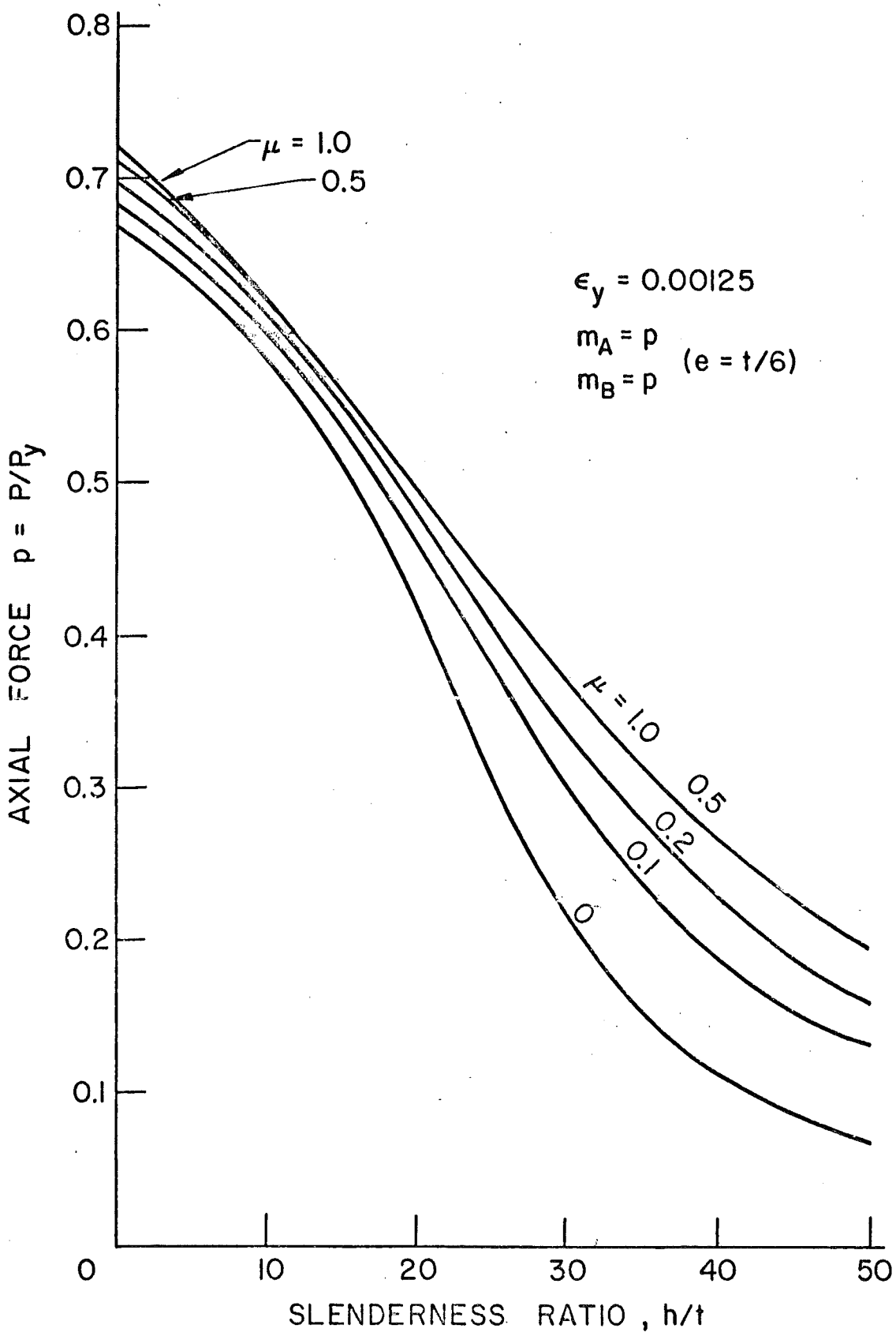

Fig. 3.12 Strength of Wall with Various Materials

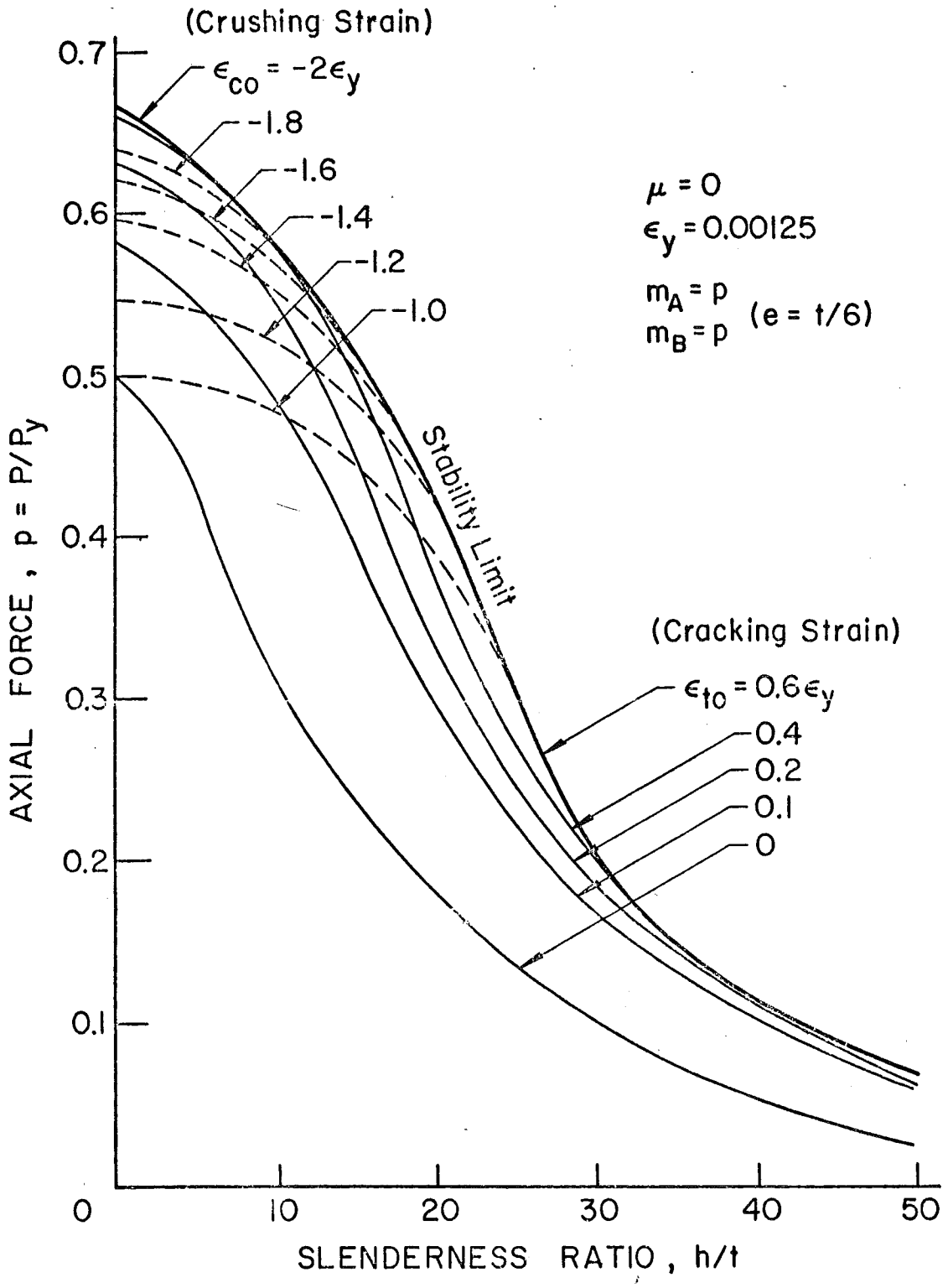

Fig. 3.13 Ultimate Strength of Masonry Wall

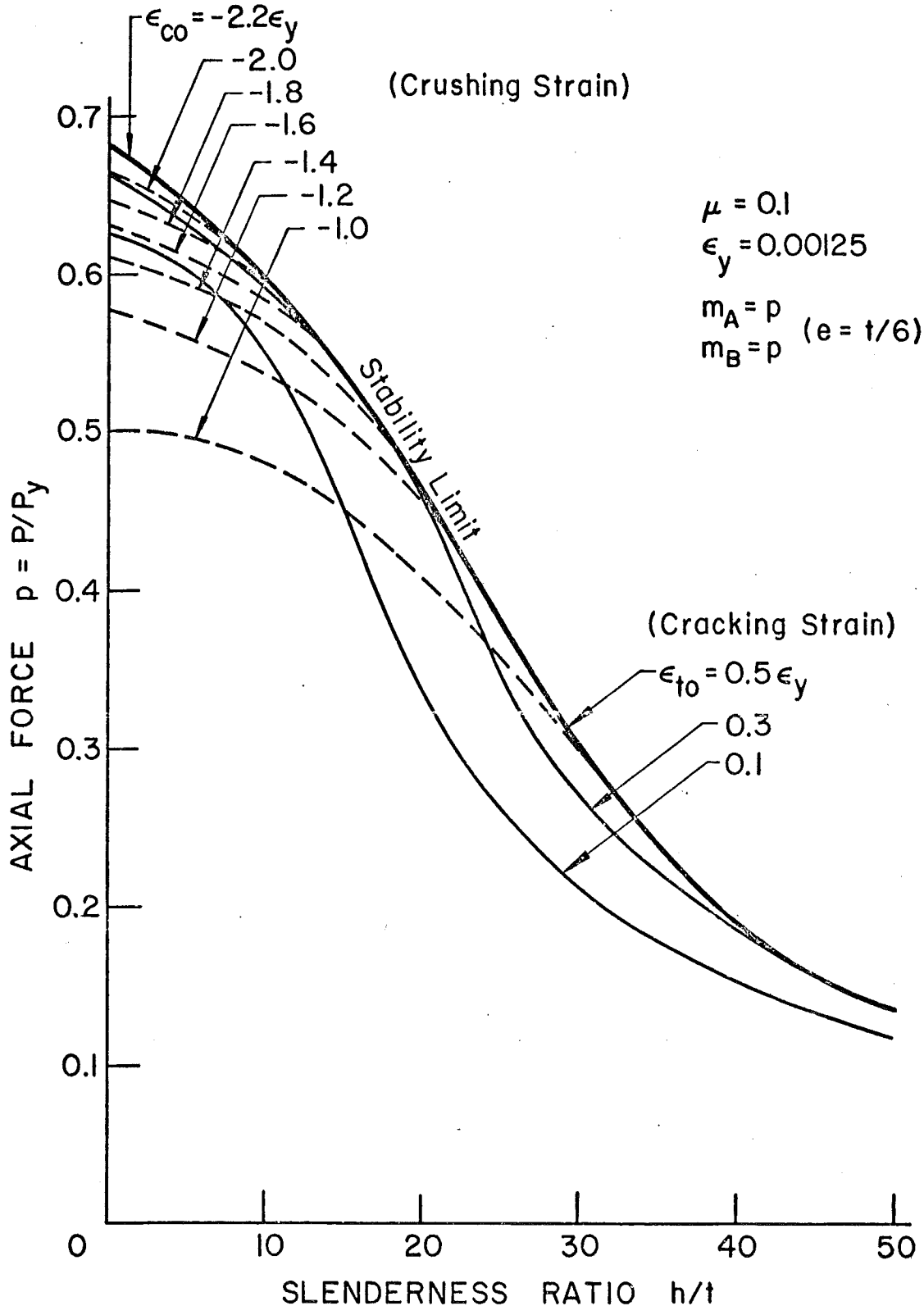

Fig. 3.14 Ultimate Strength of Concrete Wall

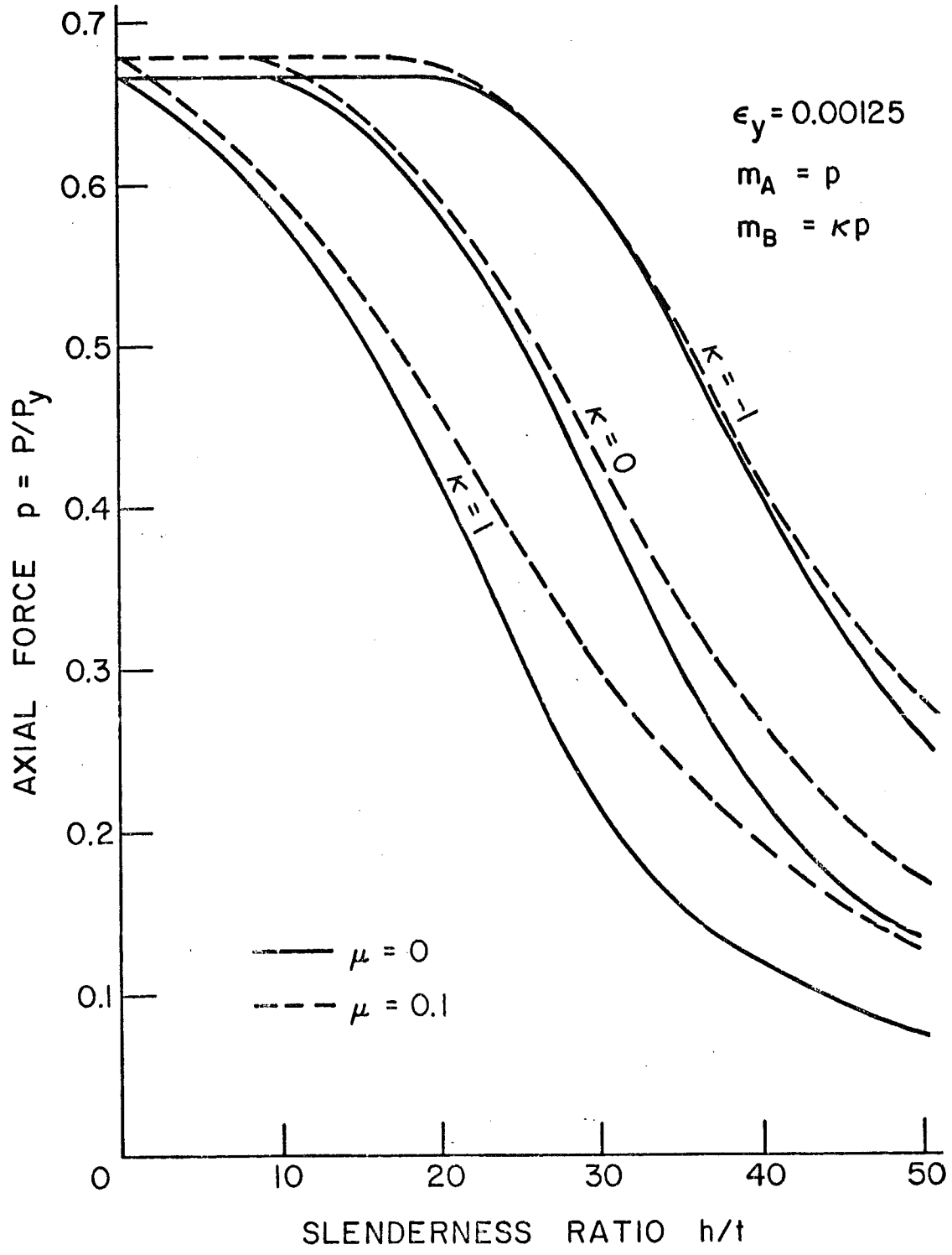

Fig. 3.15 Strength of Wall Against Various Load

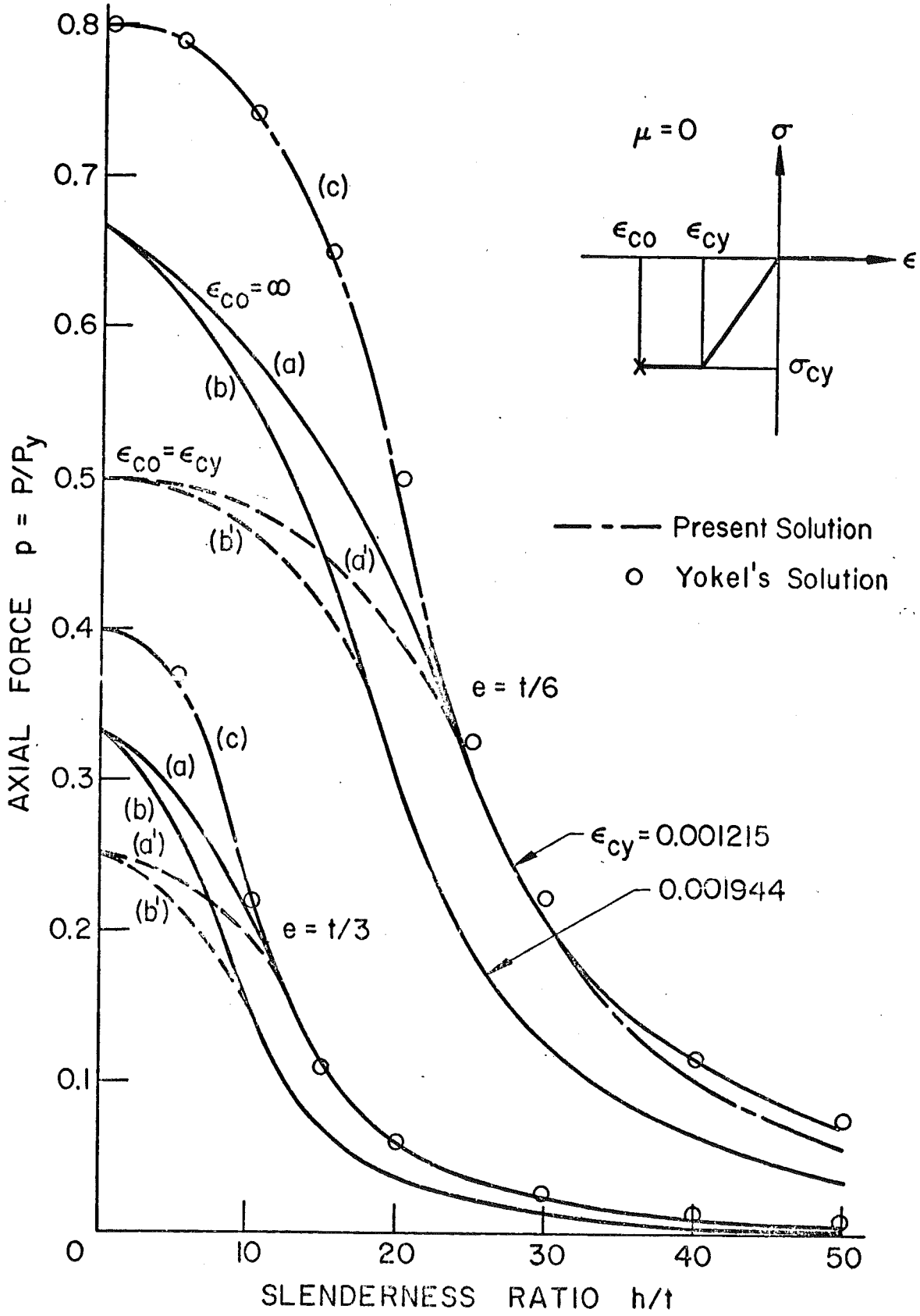

Fig. 3.16 Comparison with Reported Results (Ref. 10)

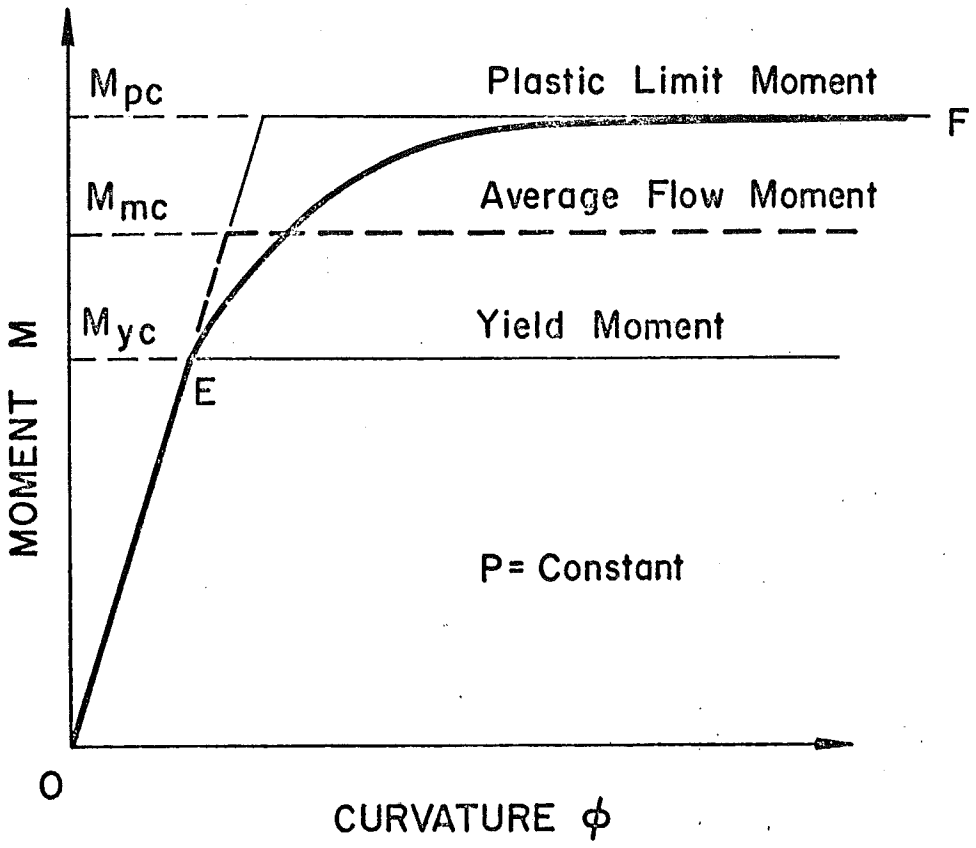

Fig. 4.1 Idealization of Moment Curvature Relation

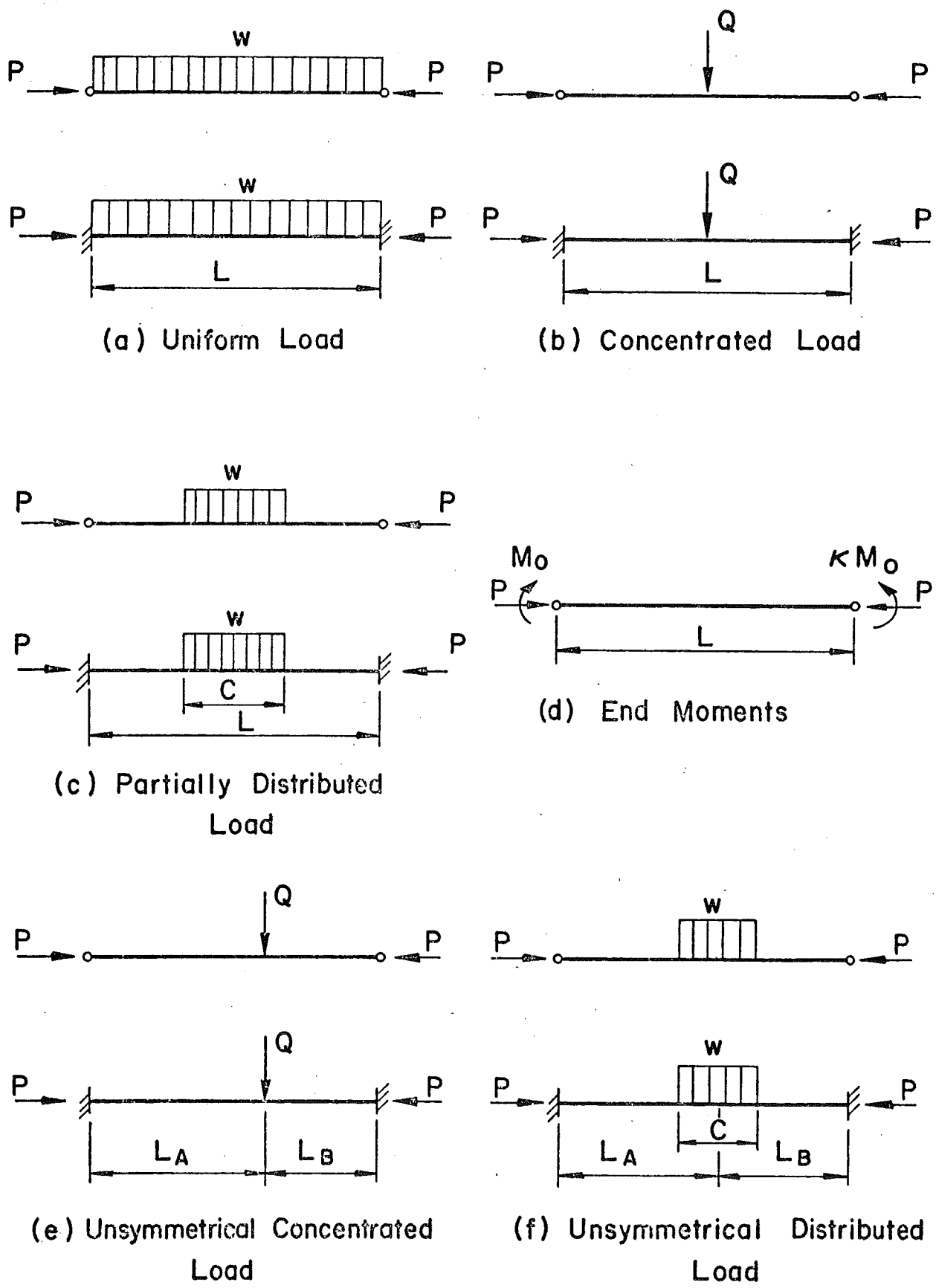

Fig. 4.2 Laterally Loaded Beam-Columns

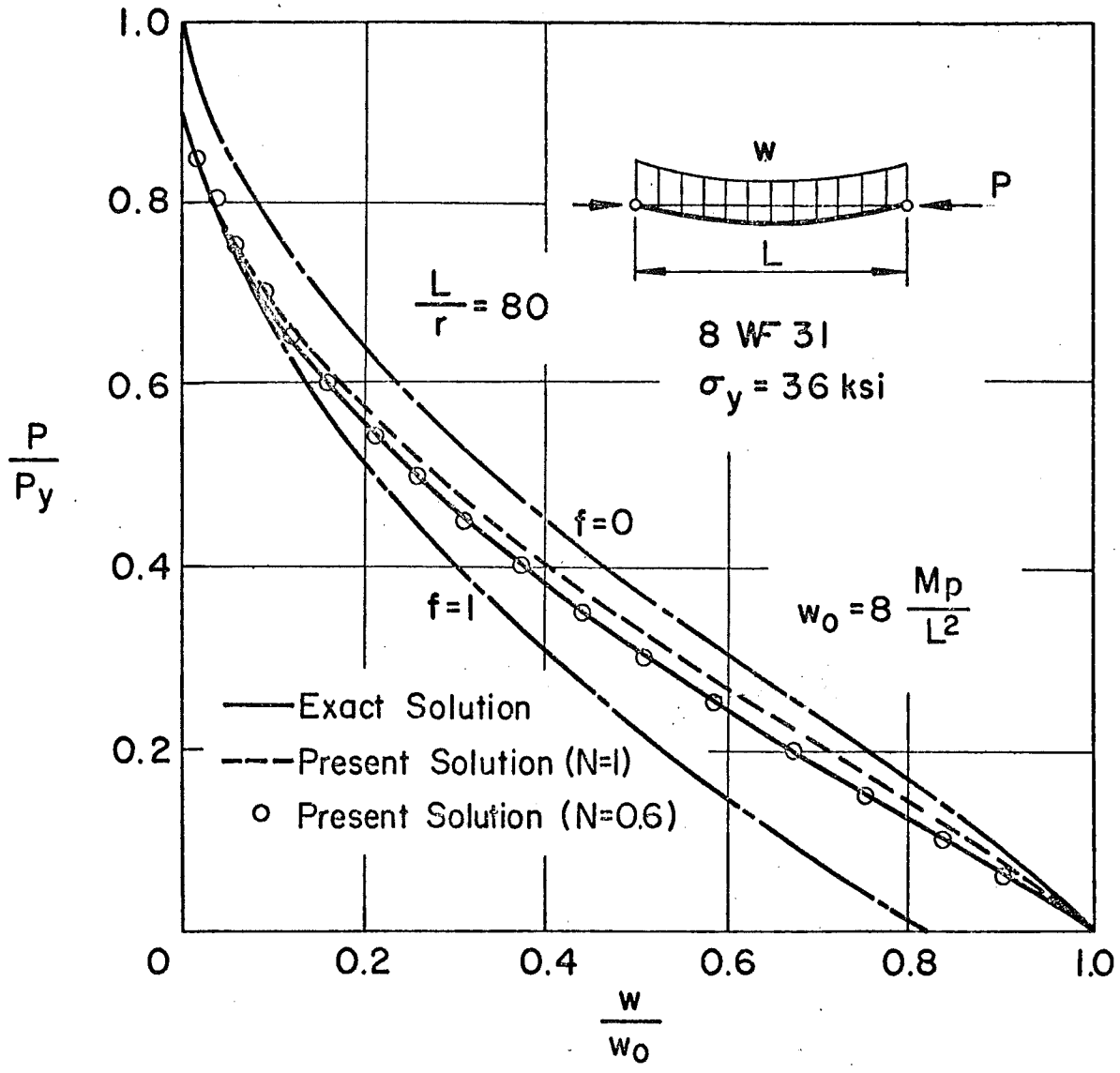

Fig. 4.3 Bounded Solution of Beam-Column

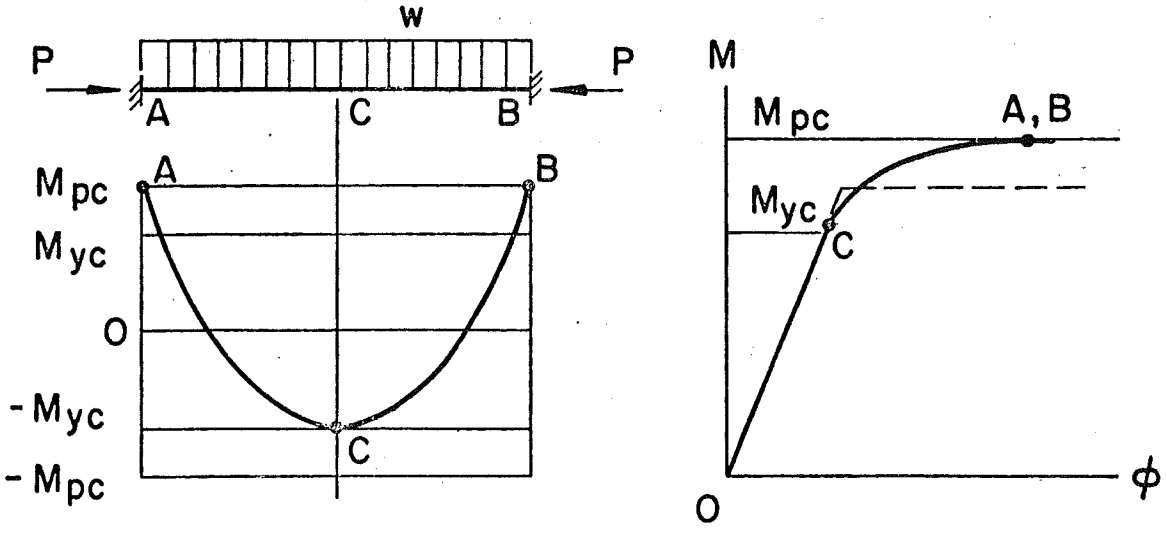

(a) Uniform Load

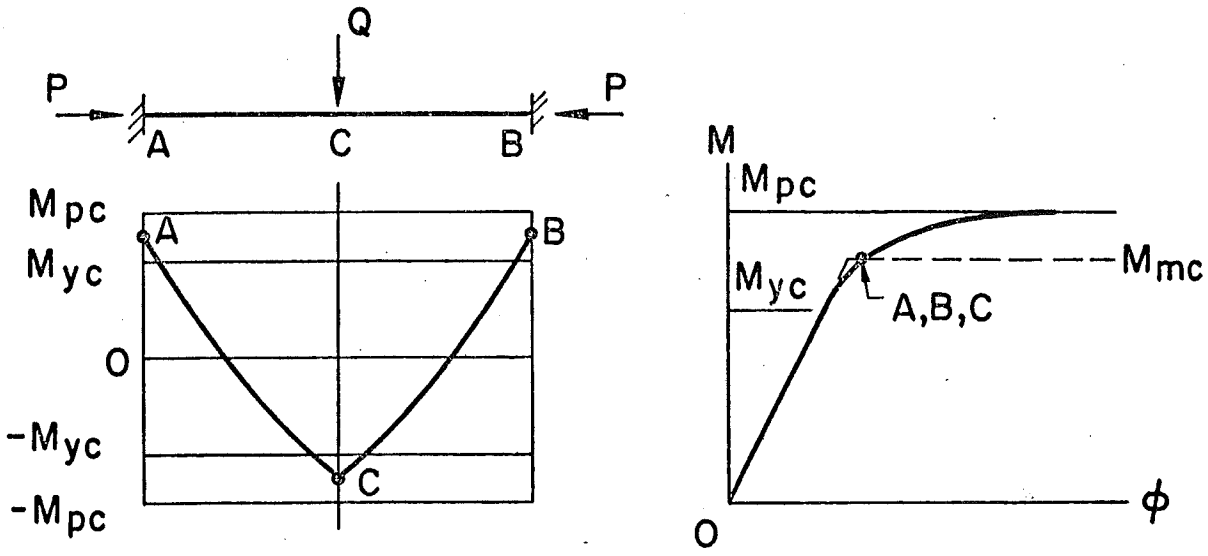

(b) Concentrated Load

Fig. 4.4 Average Flow Moment of Fixed Beam-Columns

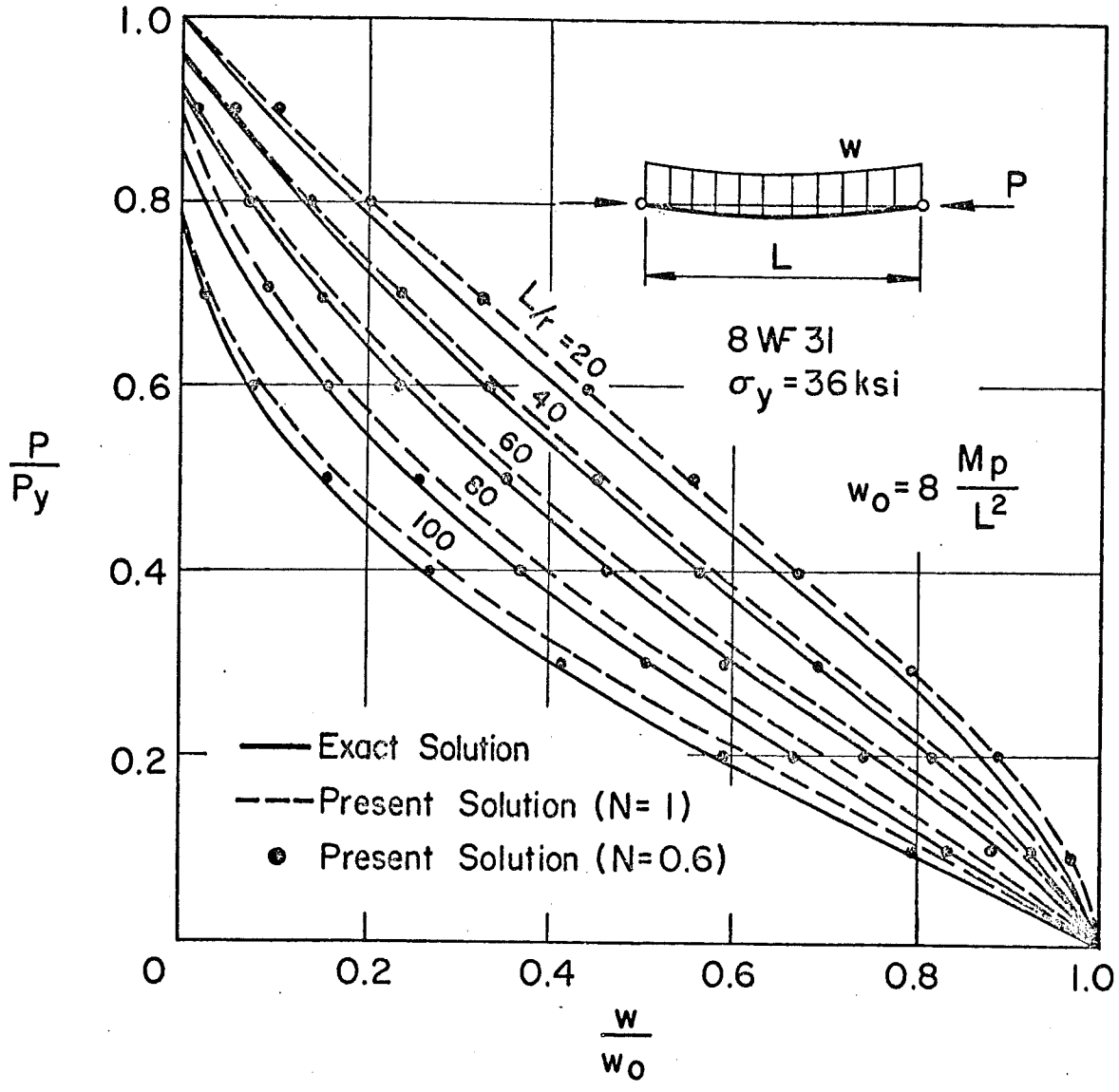

Fig. 4.5 Simple Beam-Column with Uniform Load (Ref. 9)

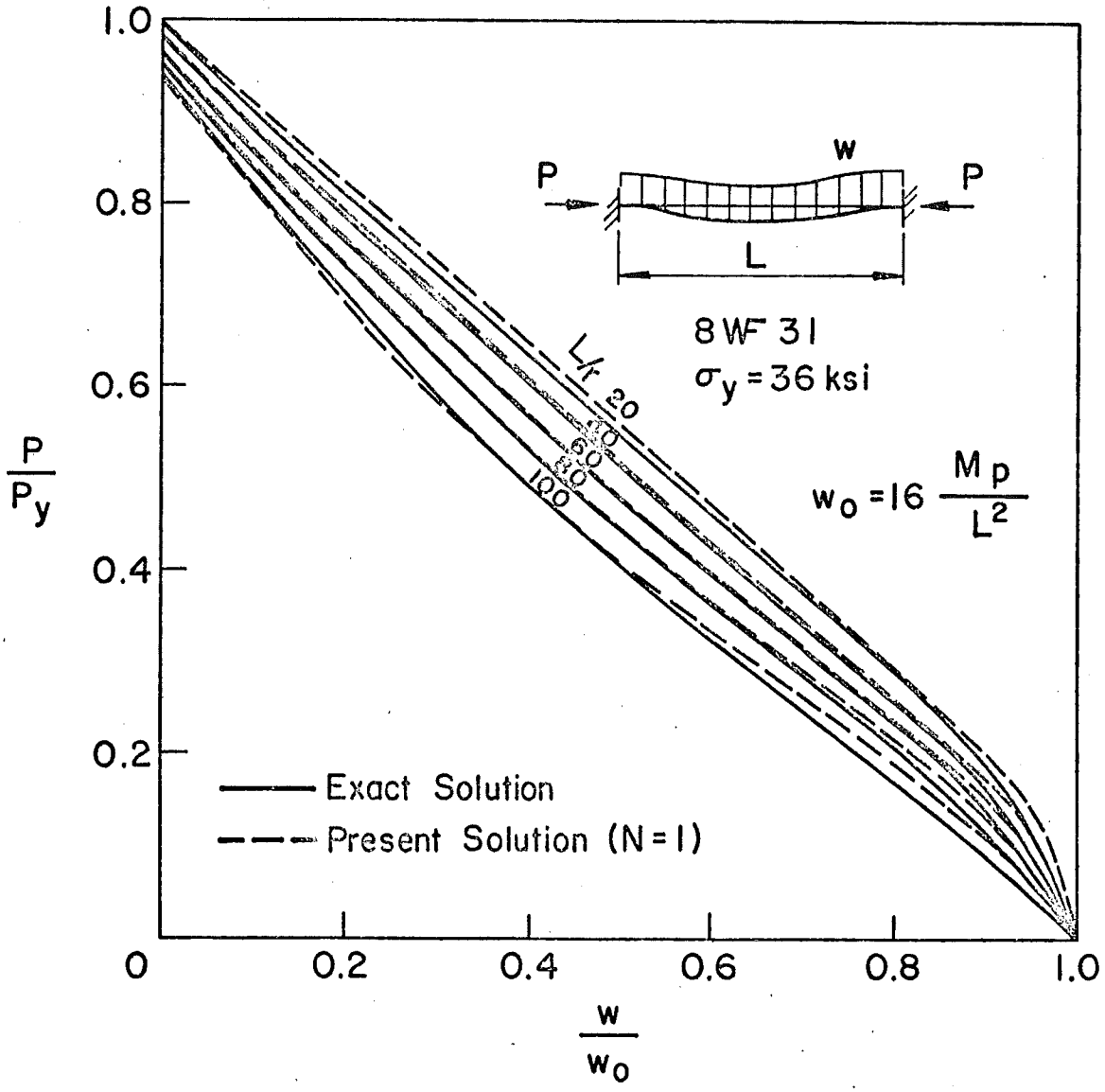

Fig. 4.6 Fixed Beam-Column with Uniform Load (Ref. 9)

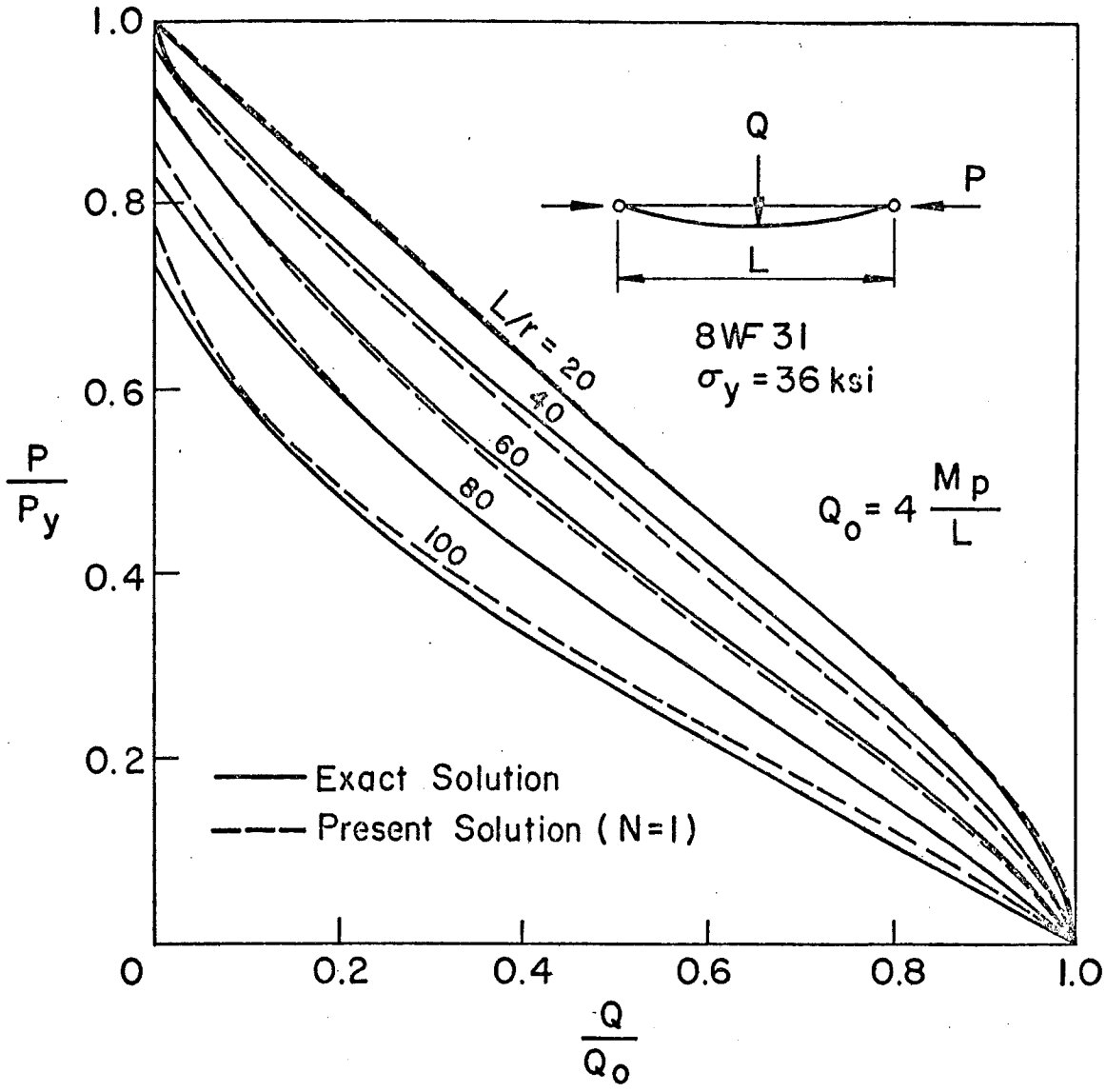

Fig. 4.7 Simple Beam-Column with Concentrated Load (Ref. 9)

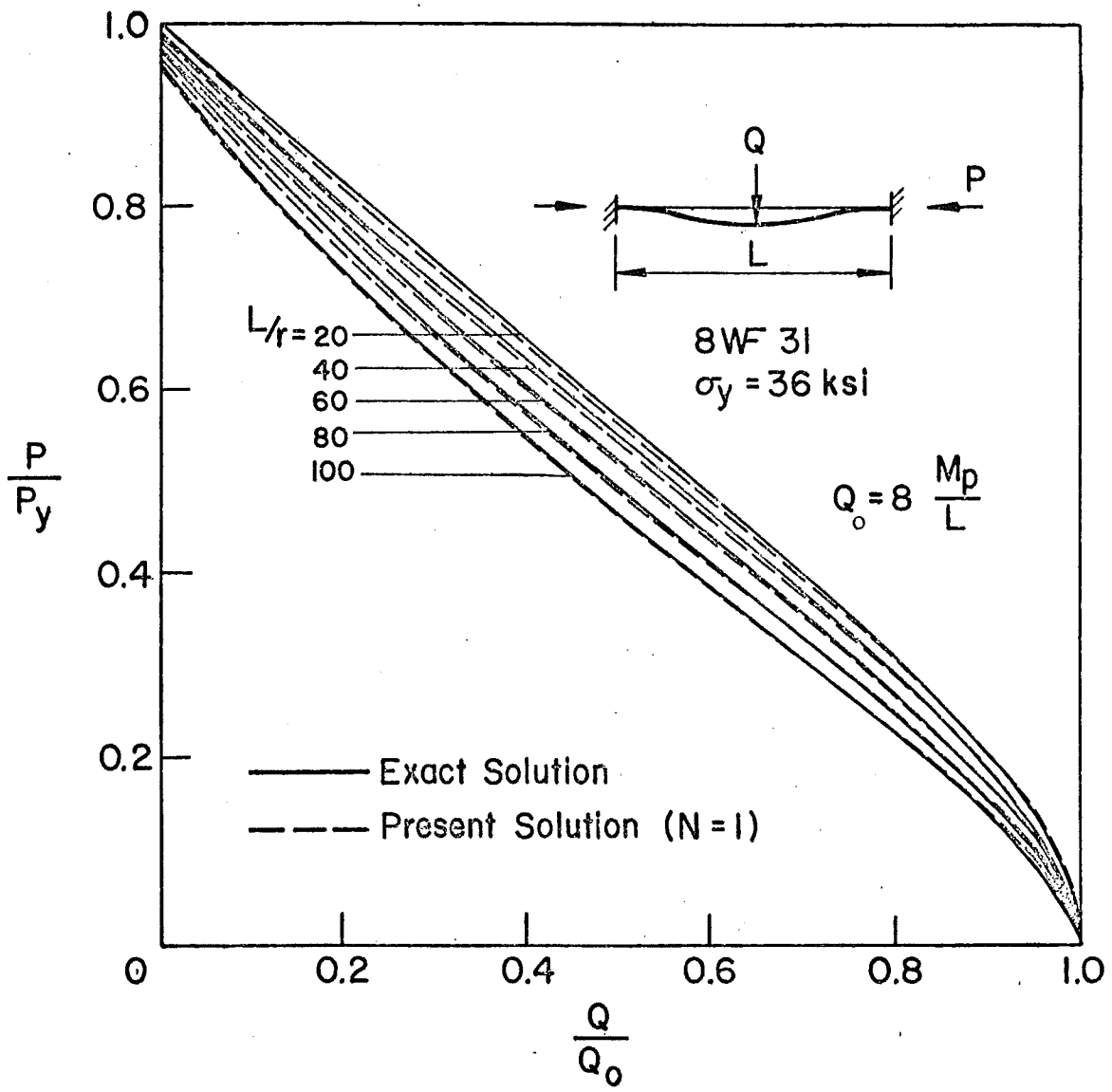

Fig. 4.8 Fixed Beam-Column with Concentrated Load (Ref. 9)

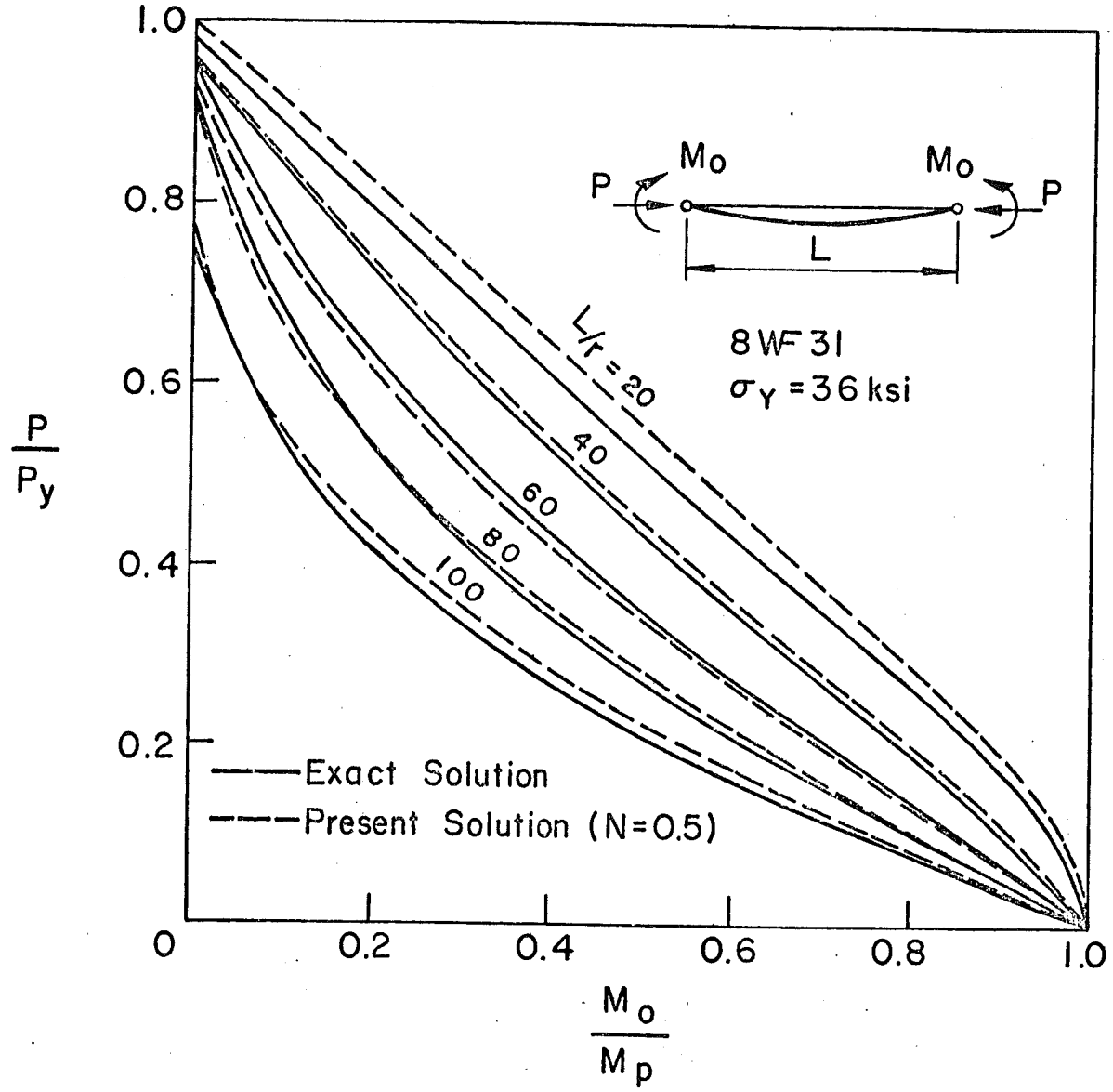

Fig. 4.9 Beam-Column with End-Moments

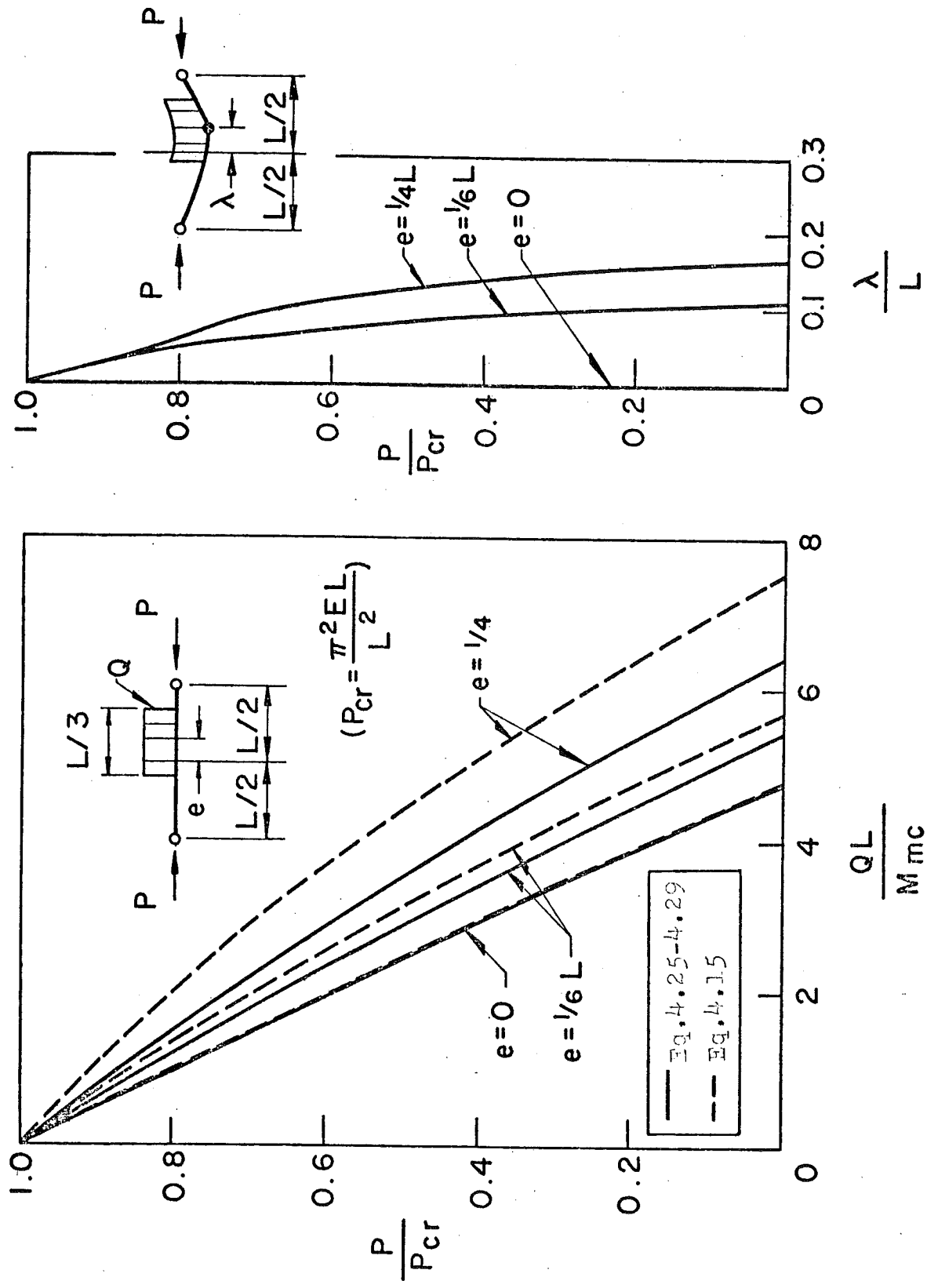

Fig. 4.10 Accuracy of Eq. 4.15 (Uniform Load on Simple Beam-Column)

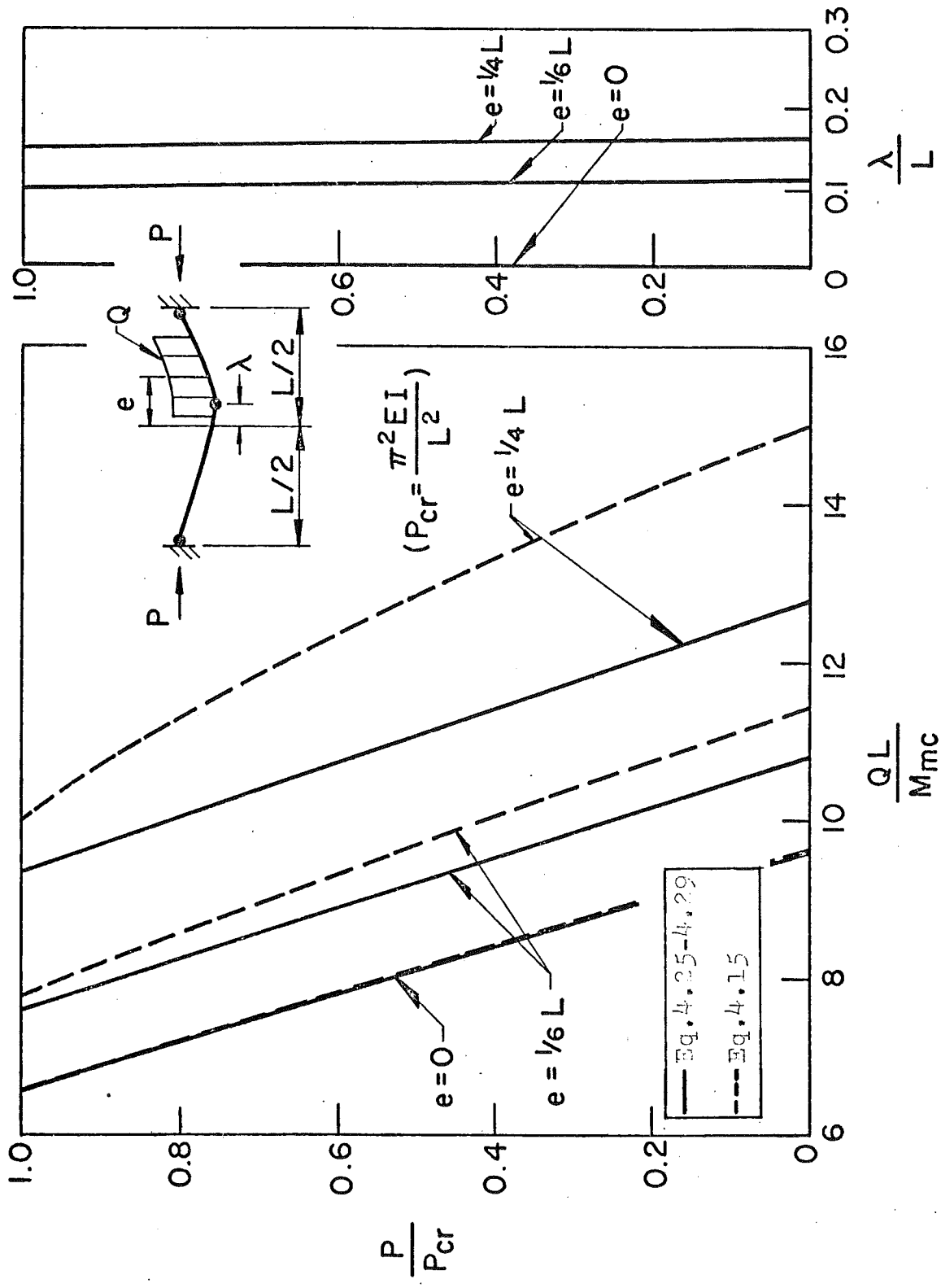

Fig. 4.11 Accuracy of Eq. 4.15 (Uniform Load on Fixed Beam-Column)

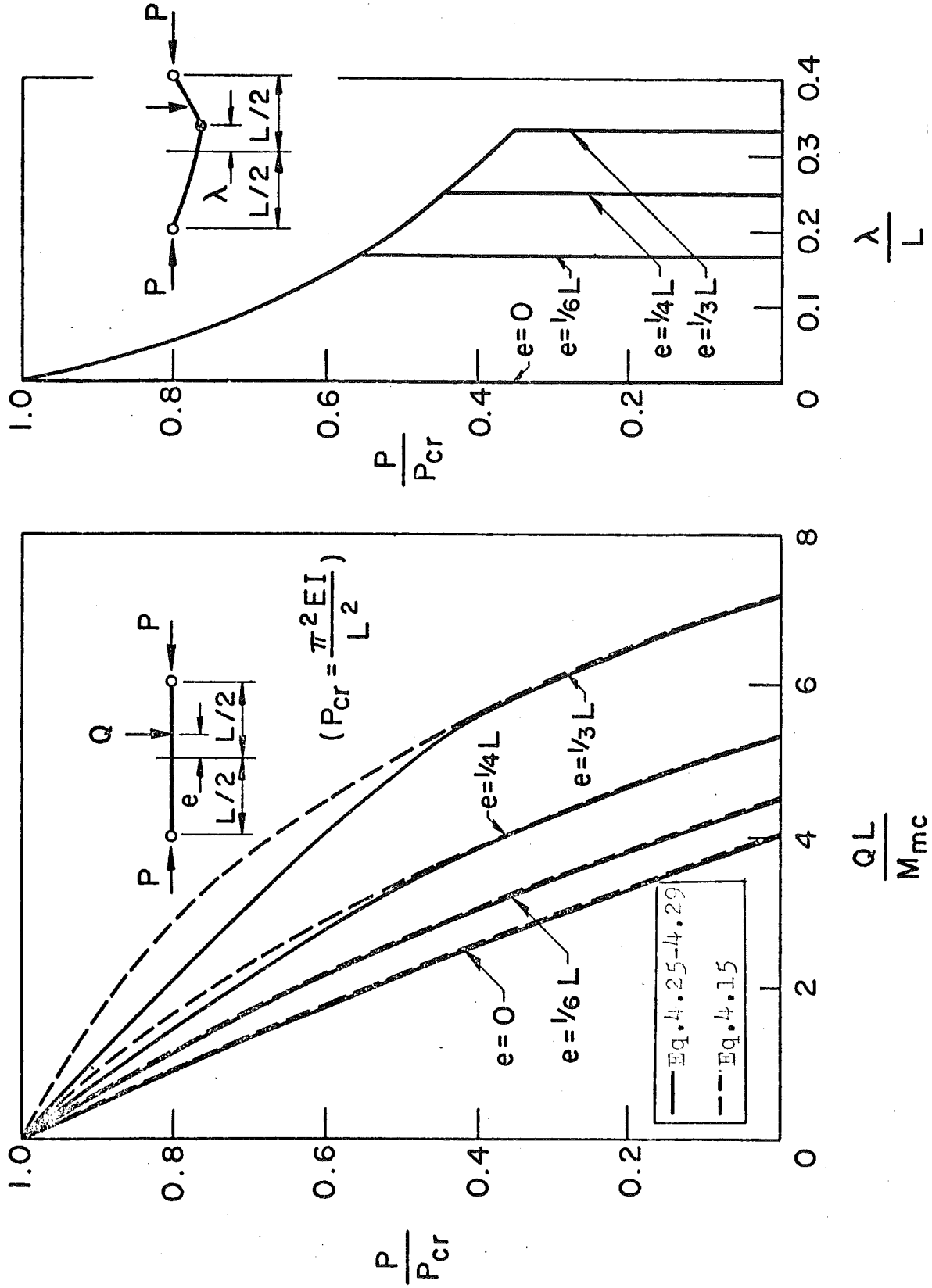

Fig. 4.12 Accuracy of Eq. 4.15 (Concentrated Load on Simple Beam-Column)

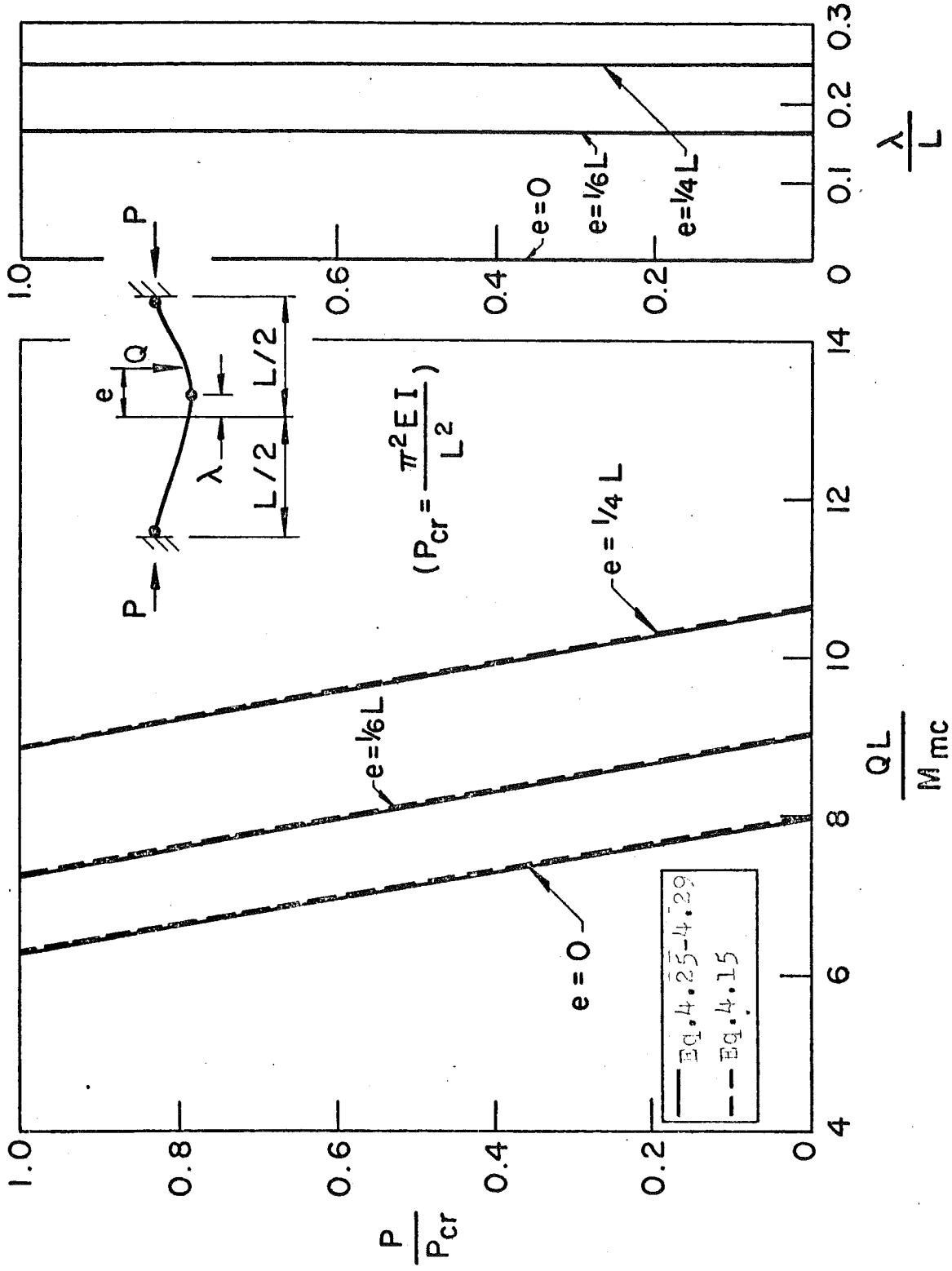

Fig. 4.13 Accuracy of Eq. 4.15 (Concentrated Load on Fixed Beam-Column)

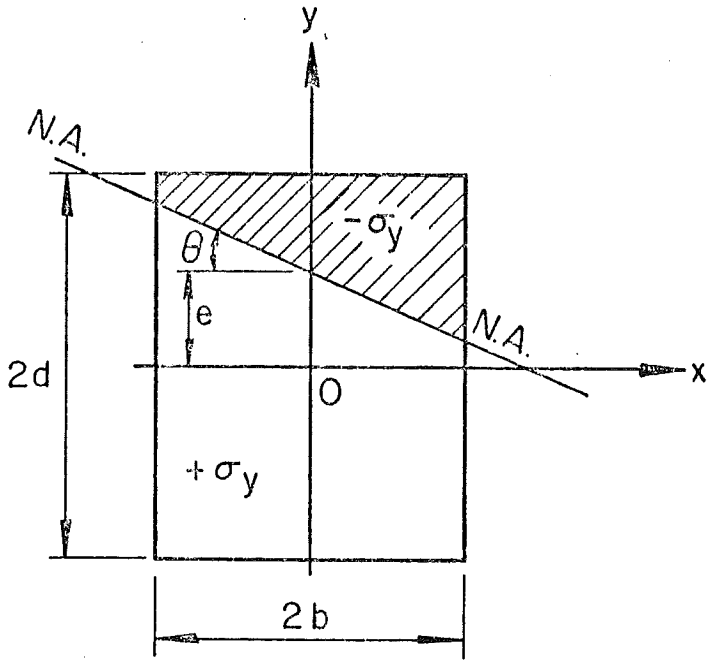

Fig. 5.1 Rectangular Section and Neutral Axis

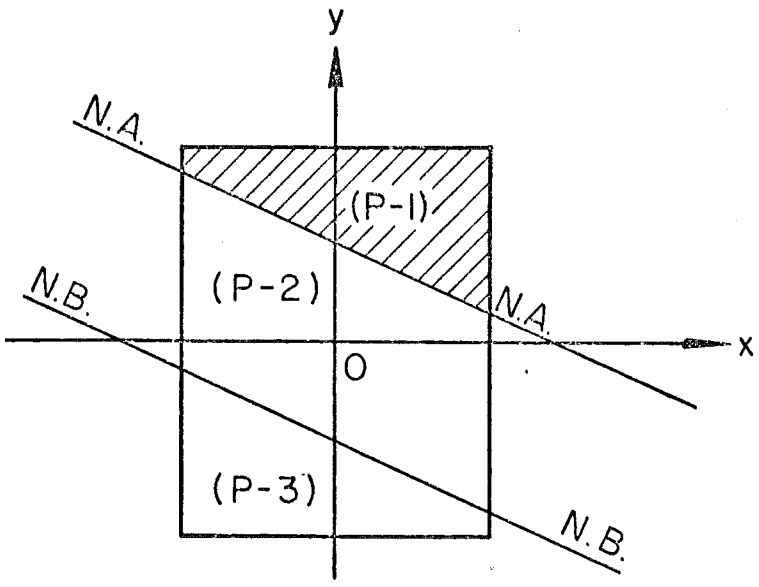

Fig. 5.2 Partitioning of Rectangular Section

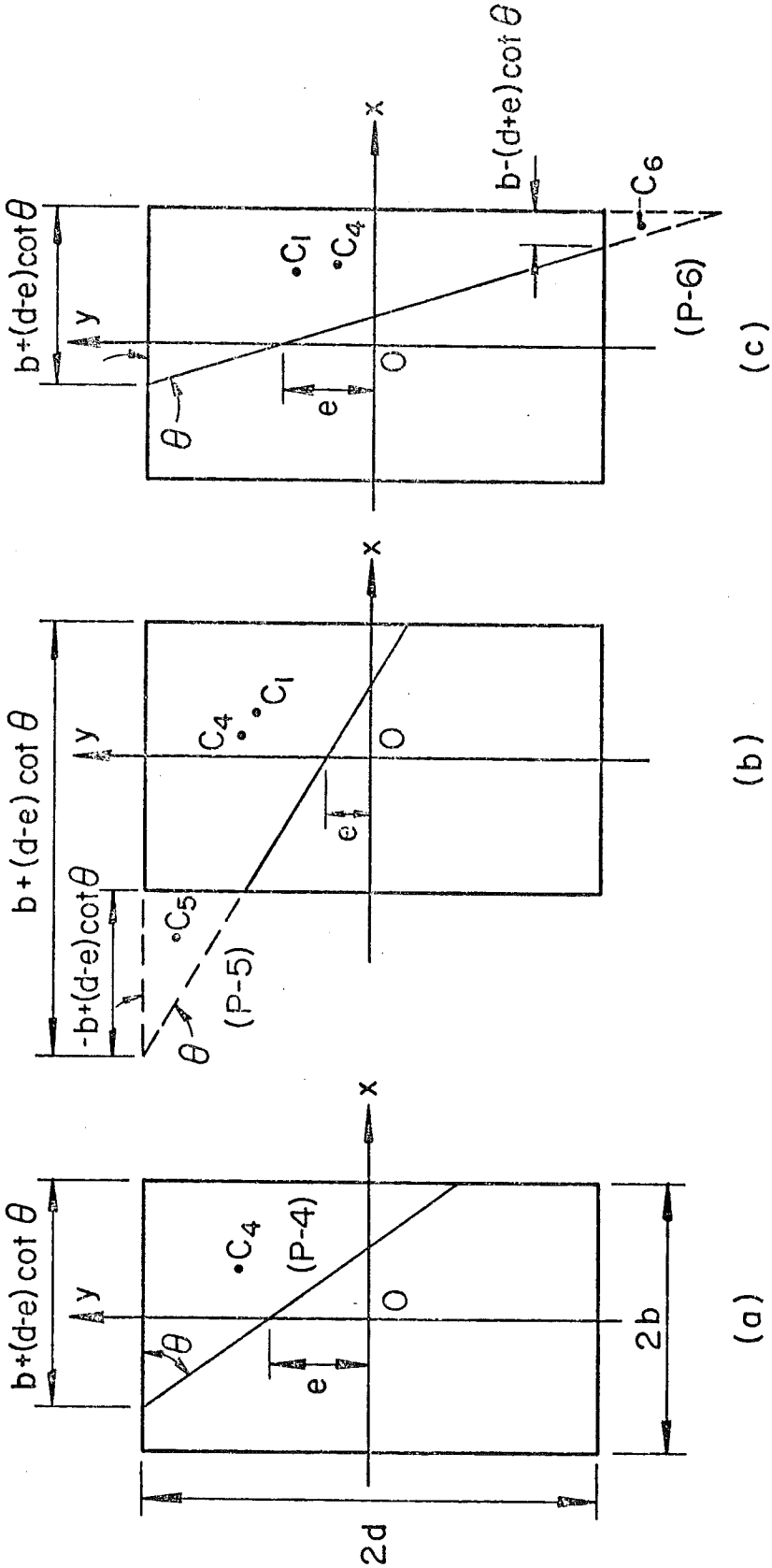

Fig. 5.3 Possible Locations of Neutral Axis

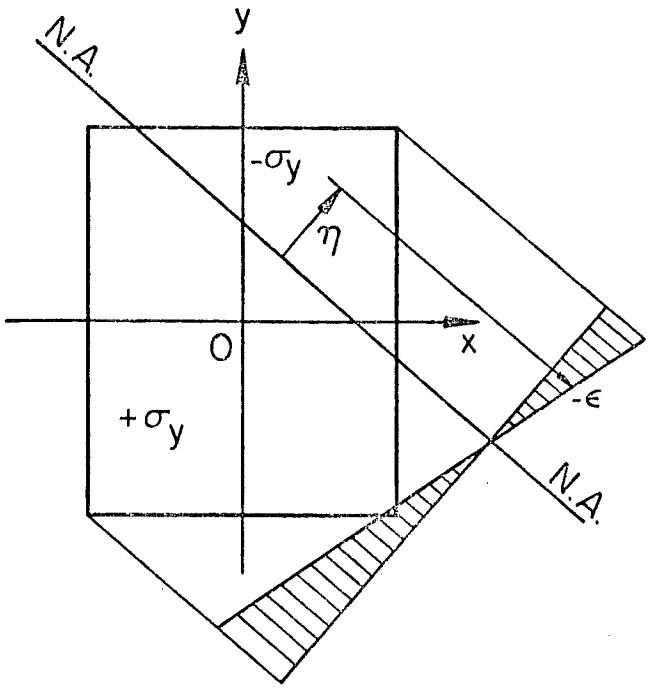

Fig. 5.4 Distribution of Strain Rate

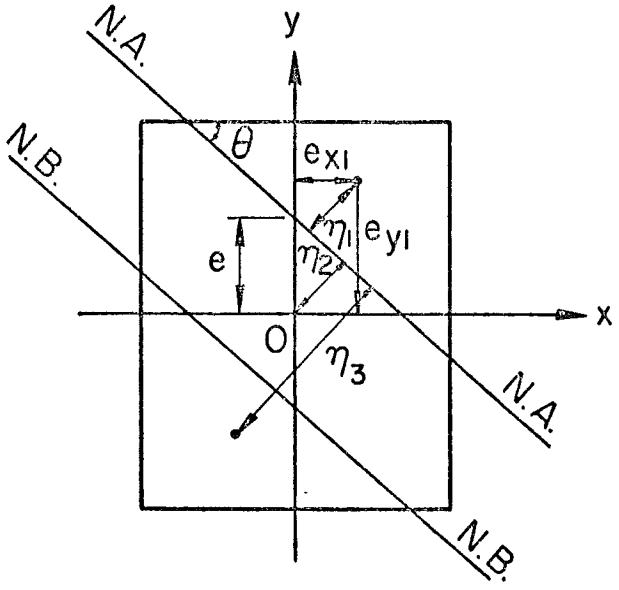

Fig. 5.5 Geometry of Centroidal Points

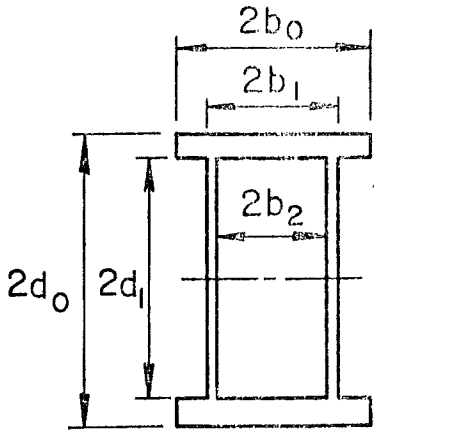

Double Web Section

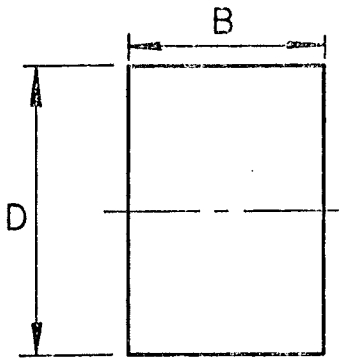

Rectangular Section

$$b_0 = b_1 = \frac{1}{2} B, \quad b_2 = 0$$

$$d_0 = \frac{1}{2} D, \quad d_1 = 0$$

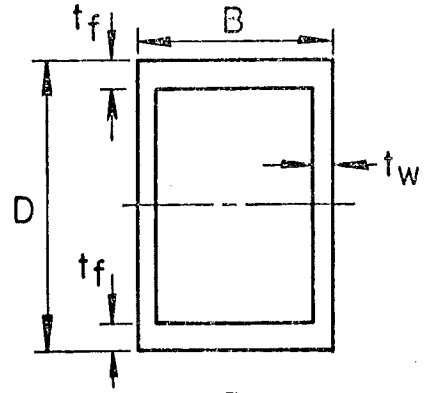

Box Section

$$b_0 = b_1 = \frac{1}{2} B, \quad b_2 = \frac{1}{2} B - t_w$$

$$d_0 = \frac{1}{2} D, \quad d_1 = \frac{1}{2} D - t_f$$

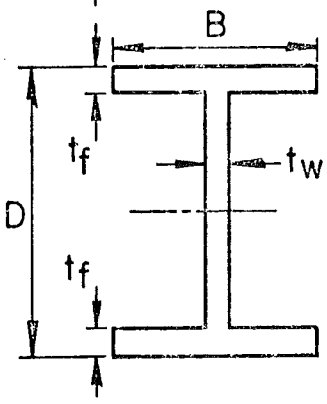

Wide Flange Section

$$b_0 = \frac{1}{2} B, \quad b_1 = \frac{1}{2} t_w, \quad b_2 = 0$$

$$d_0 = \frac{1}{2} D, \quad d_1 = \frac{1}{2} D - t_f$$

Fig. 5.6 Particular Cases of Double Web Section

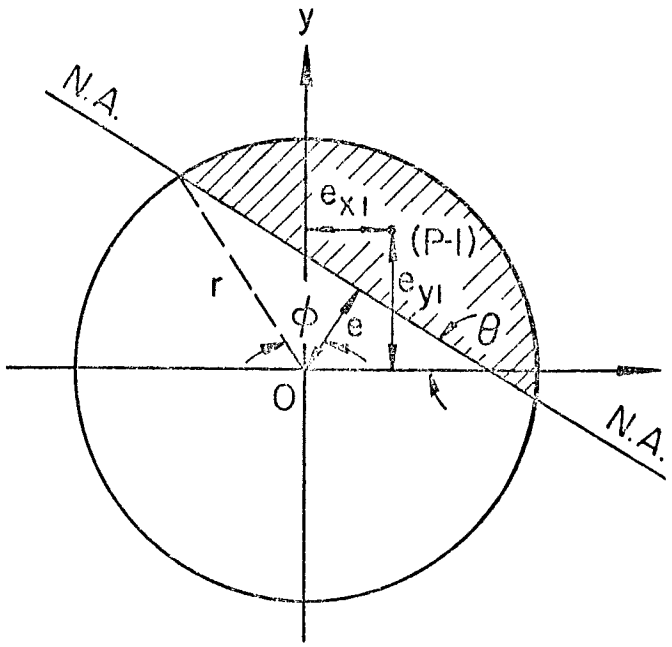

Fig. 5.7 Solid Circular Section

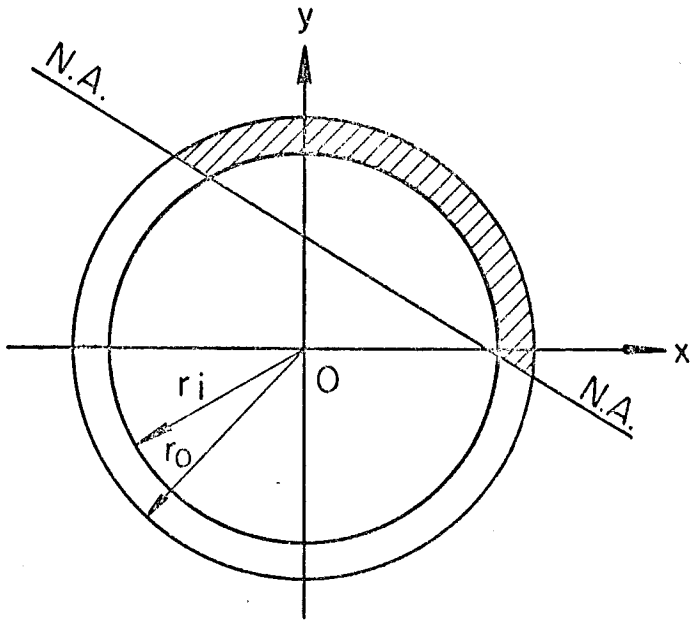

Fig. 5.8 Hollow Circular Section

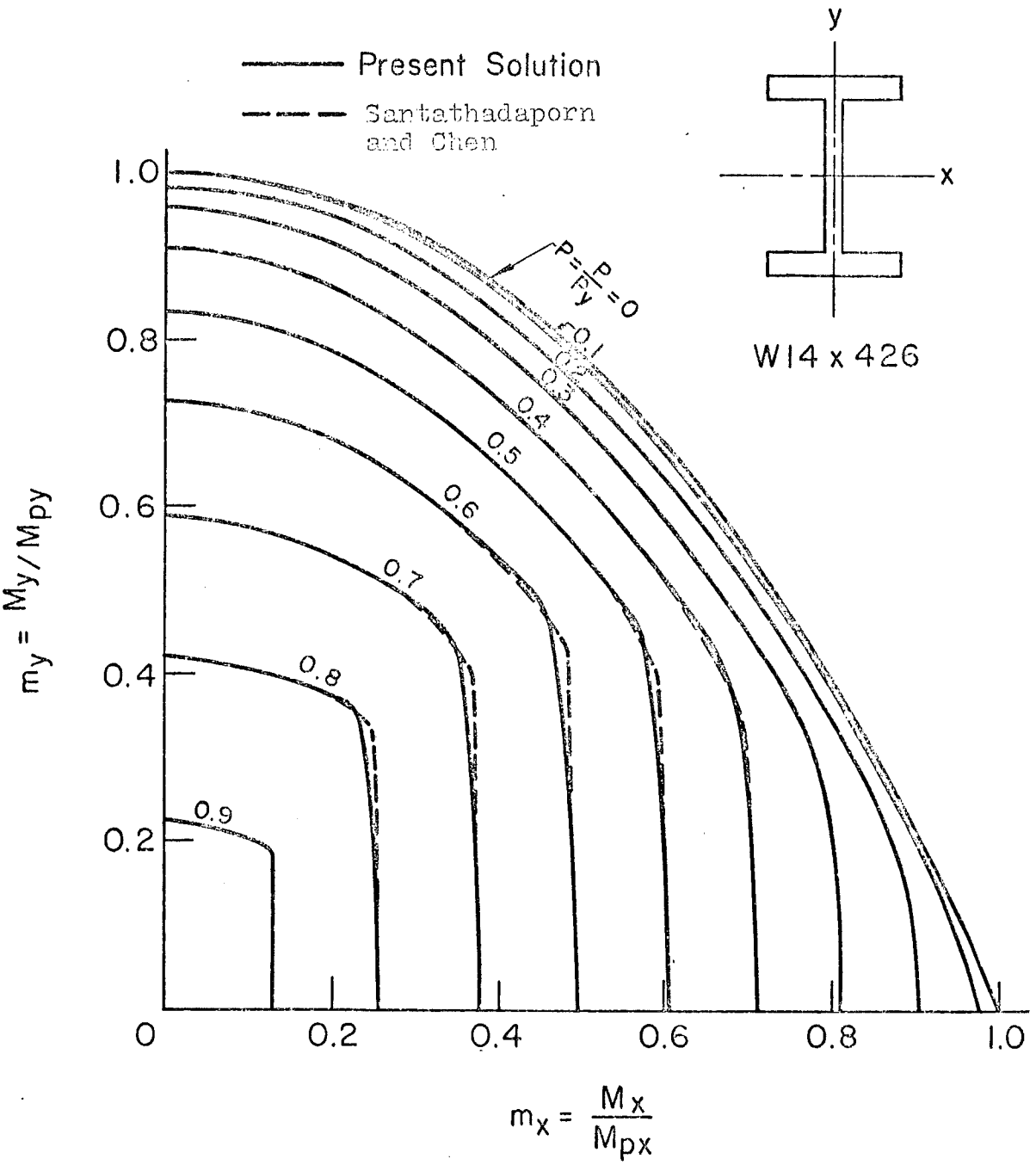

Fig. 5.9 Interaction Curves for a Wide Flange Section

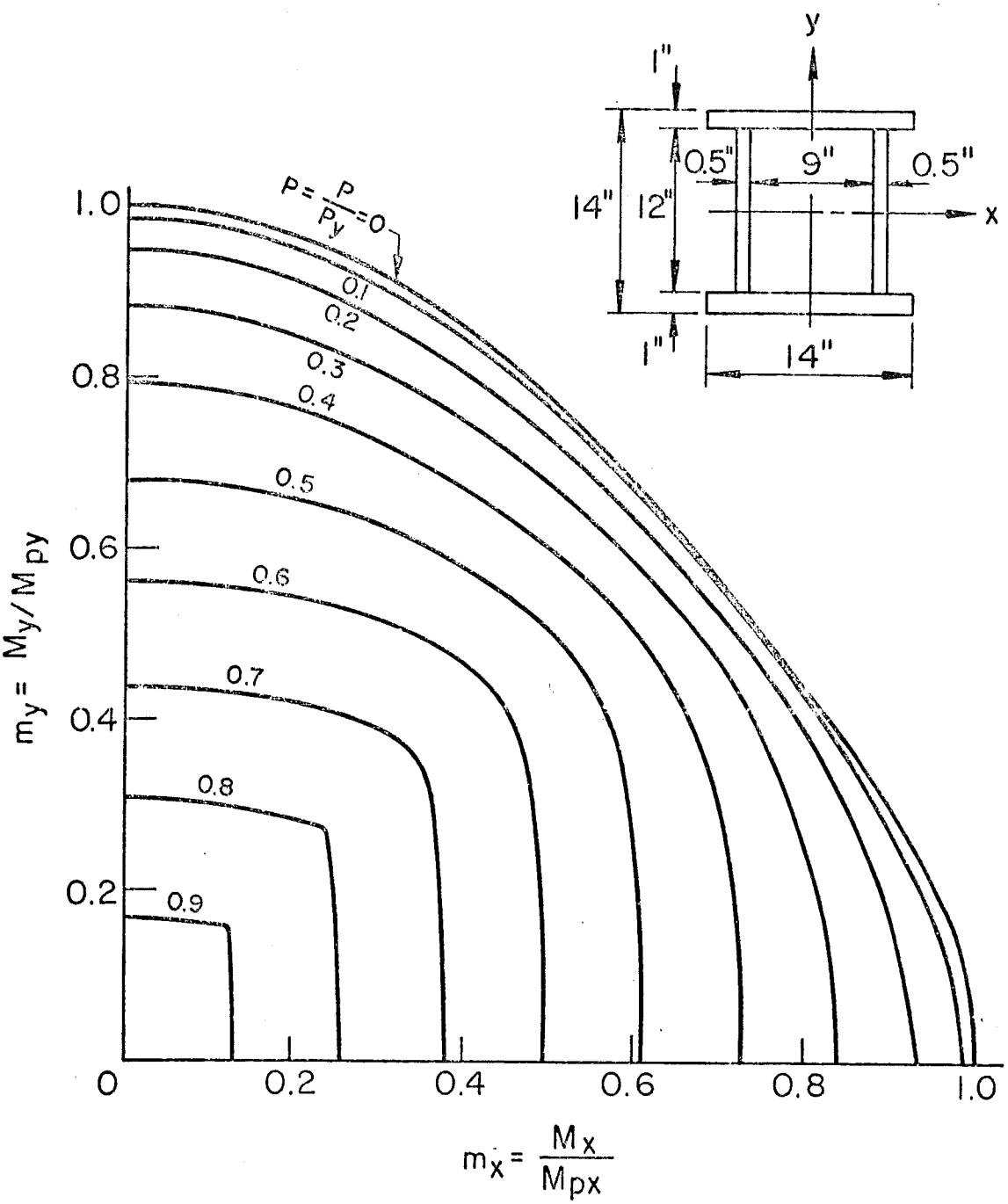

Fig. 5.10 Interaction Curves for a Double Web Section

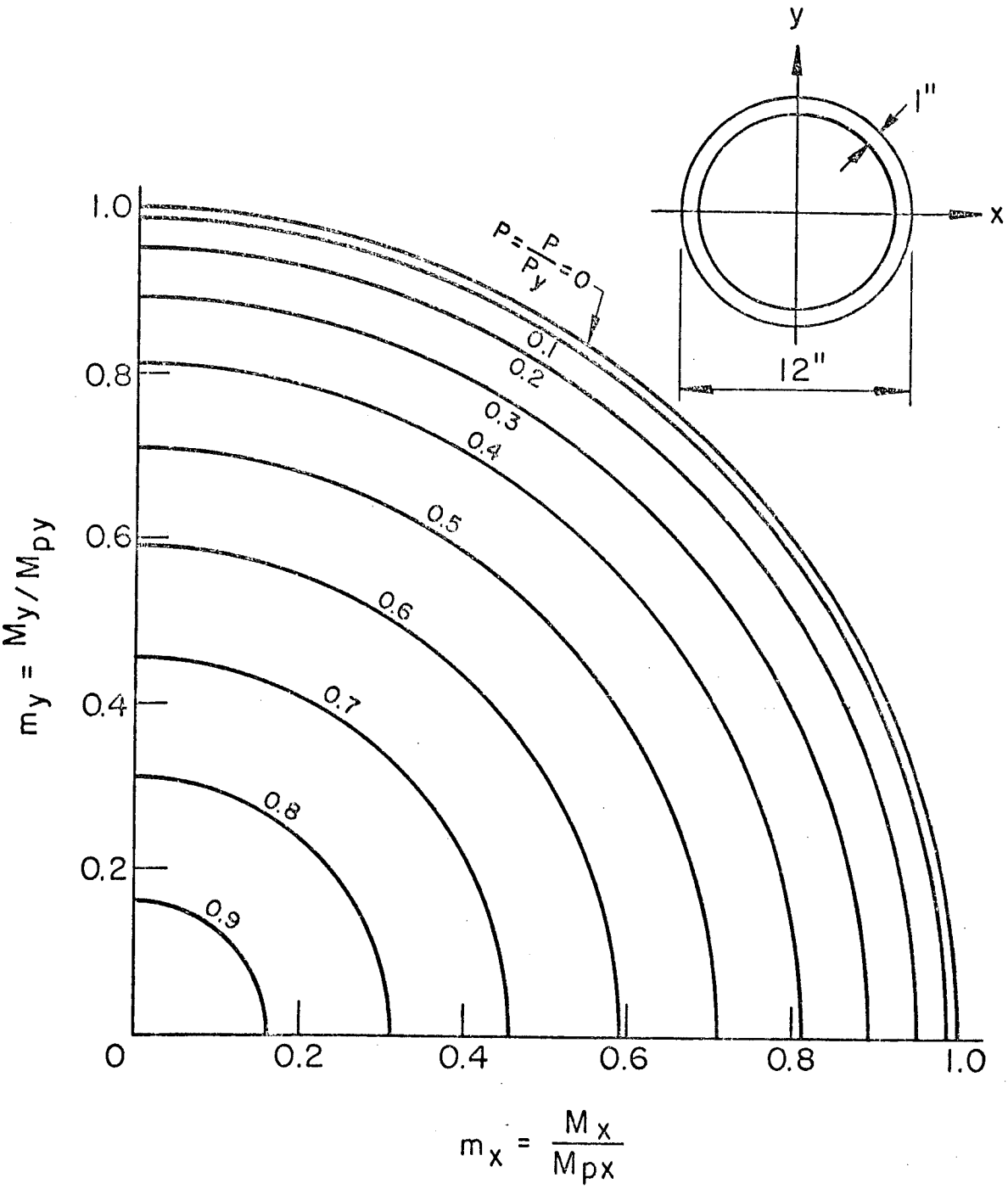

Fig. 5.11 Interaction Curves of a Hollow Circular Section

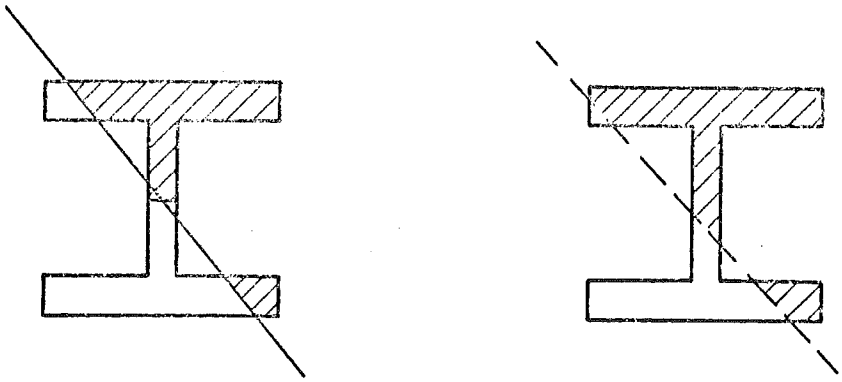

(a) Idealized Section with Approximate N.A.
(Santathadaporn and Chen)

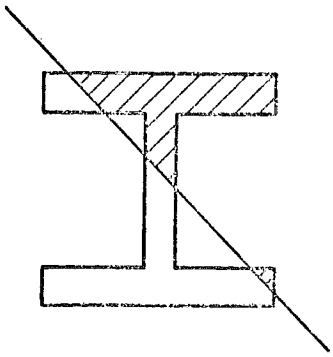

(b) Idealized Section with Exact N.A. (Present Solution)

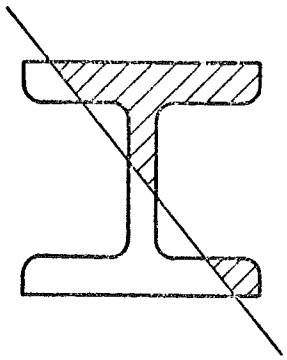

(c) Actual Section with Exact N.A.

Fig. 5.12 Wide Flange Sections and Neutral Axes

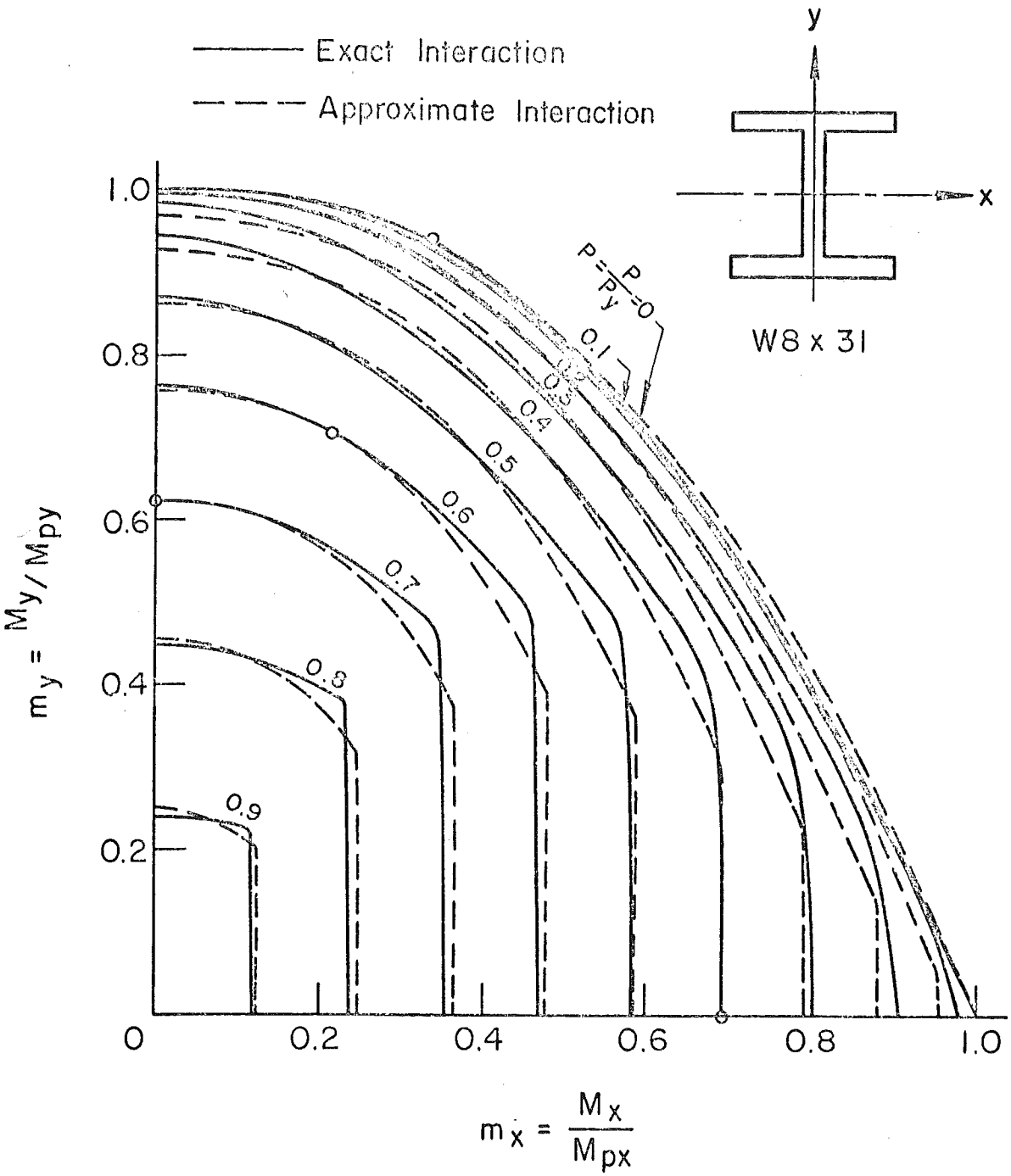

Fig. 5.13 Interaction Curves of Wide Flange Section (W8x31)

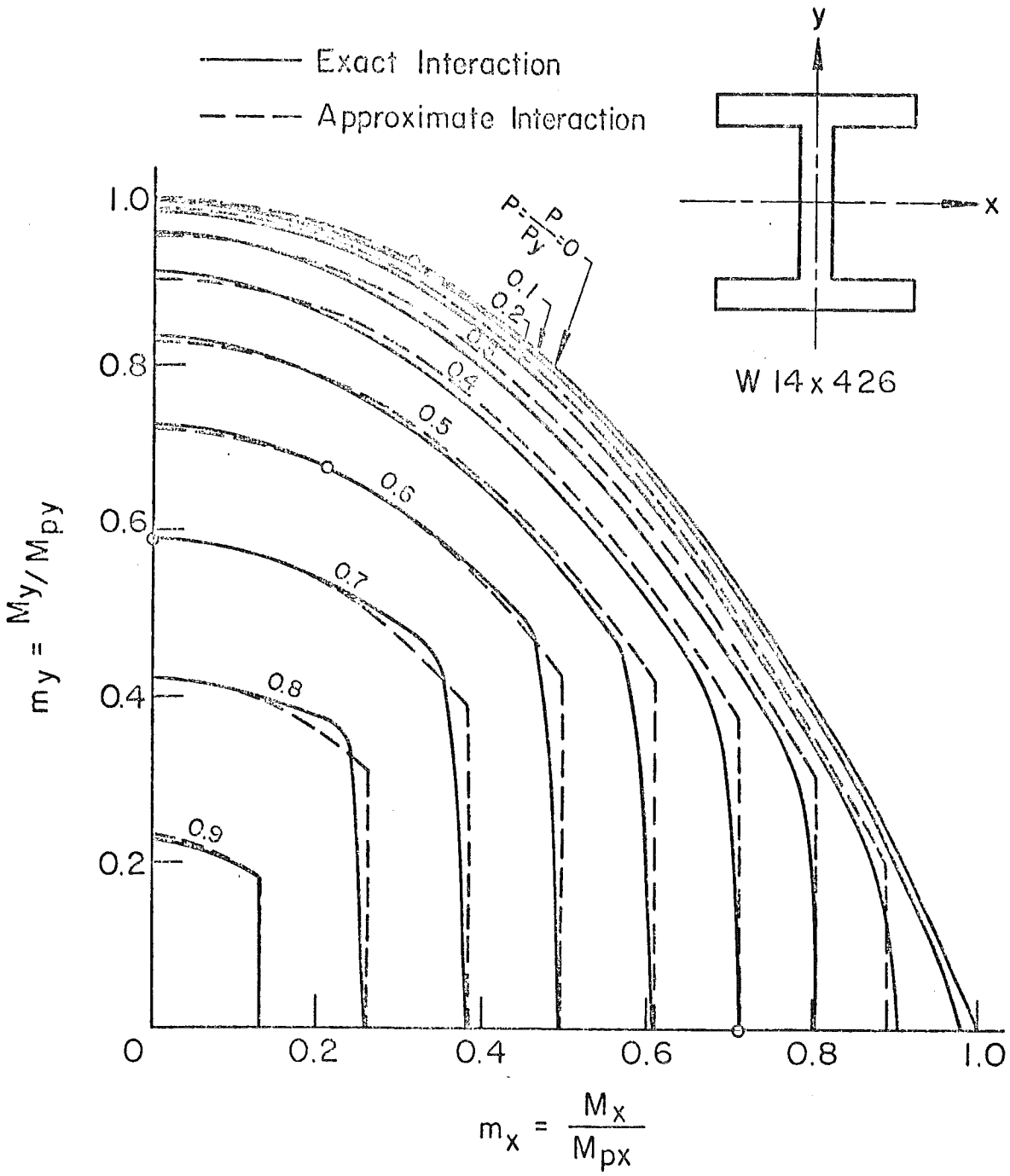

Fig. 5.14 Interaction Curves of Wide Flange Section (W14x426)

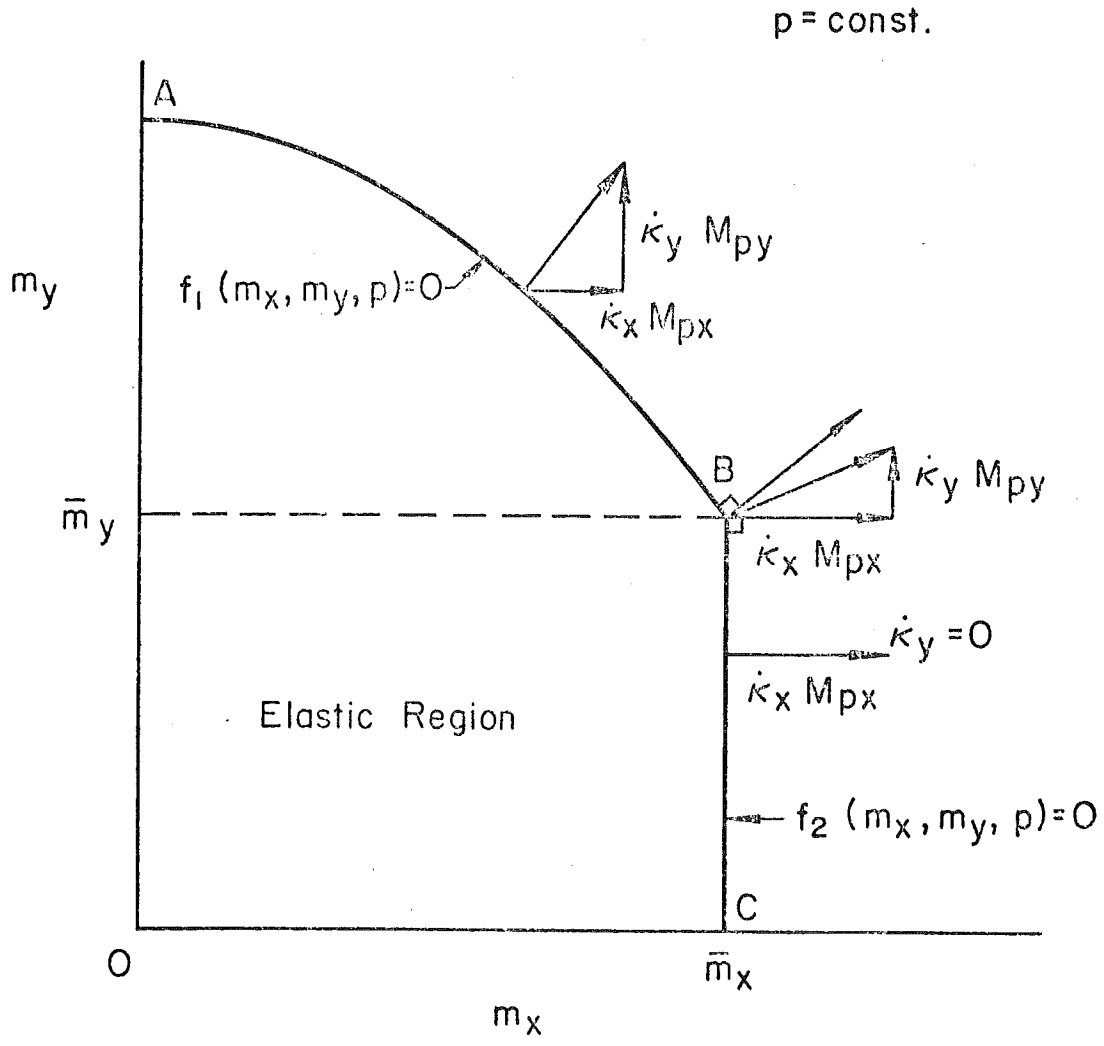

Fig. 5.15 Yield Surface and Strain Vectors

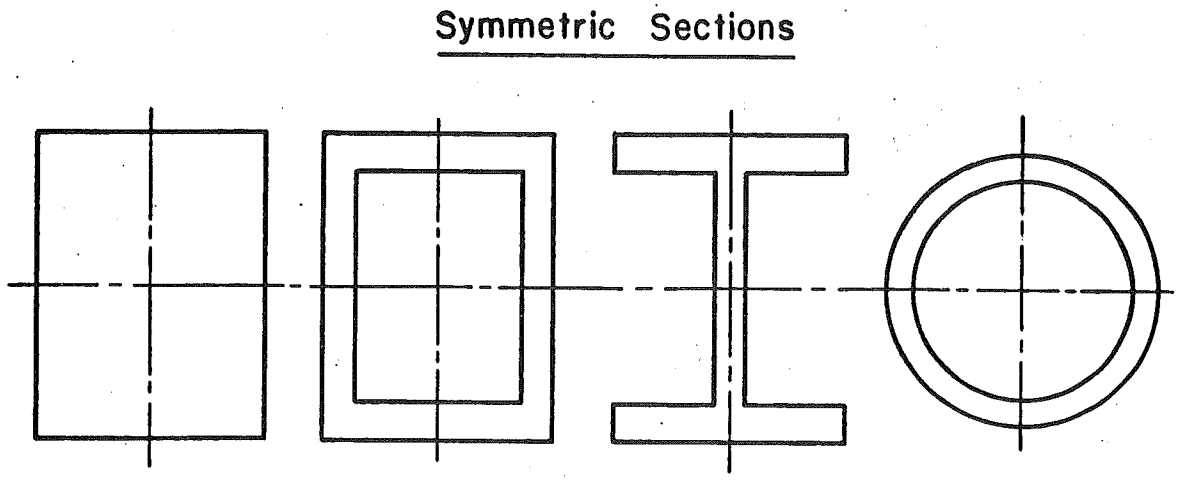

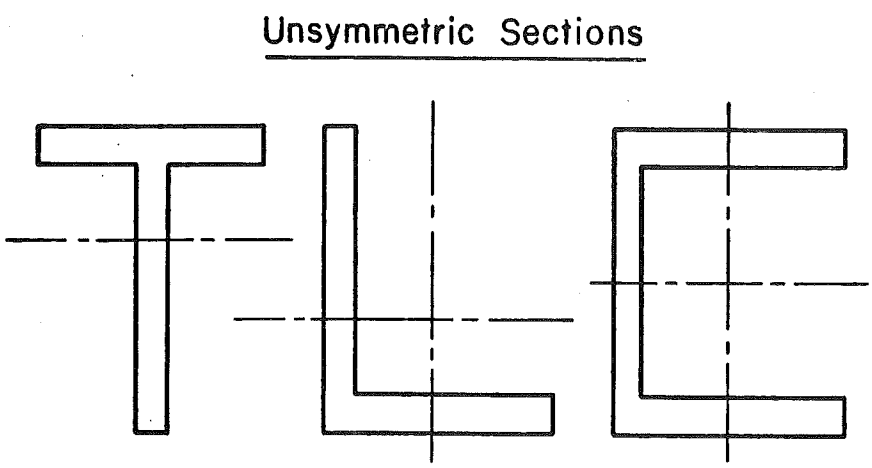

Fig. 6.1 Structural Steel Sections

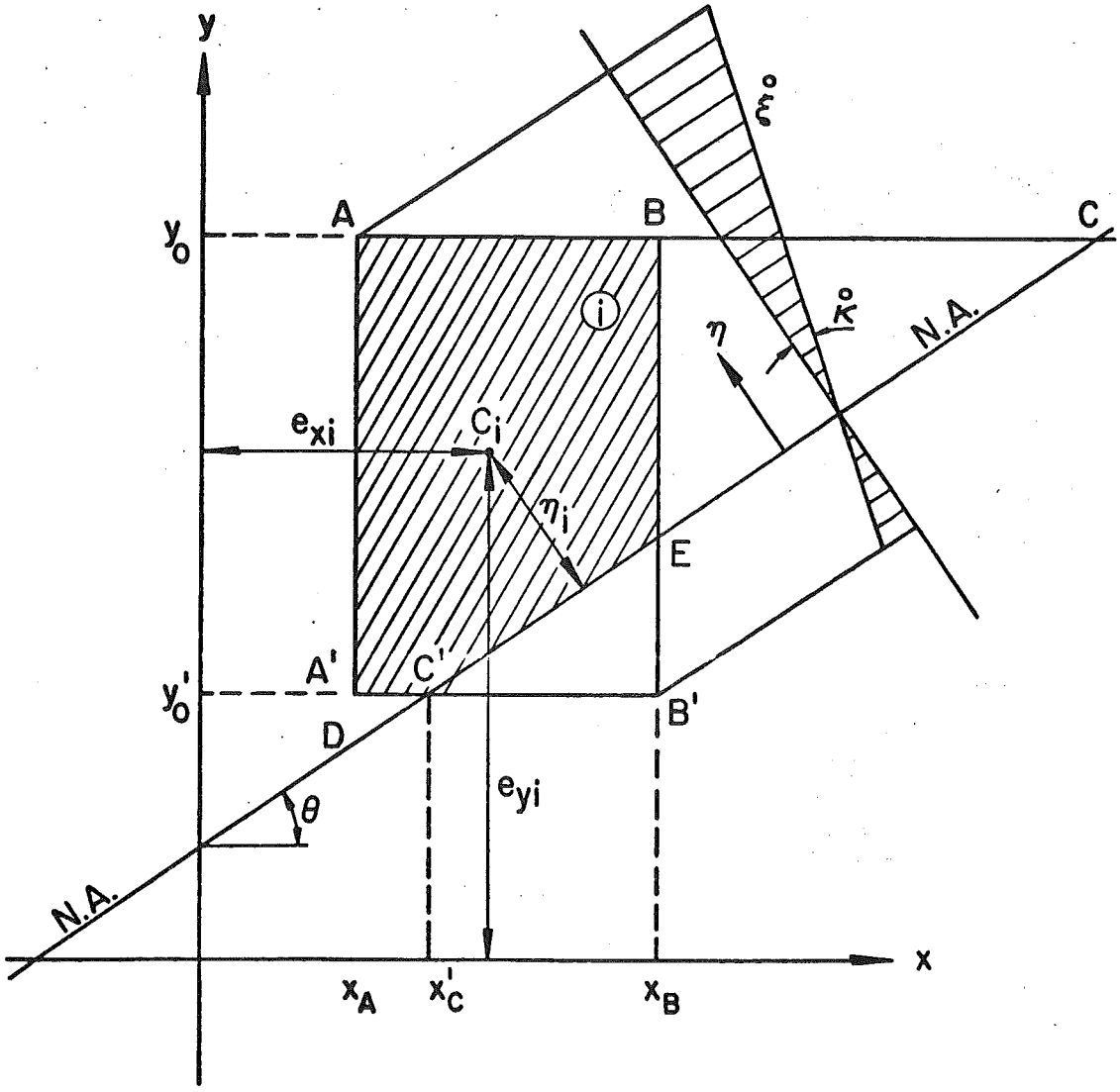

Fig. 6.2 A Rectangular Element of Section

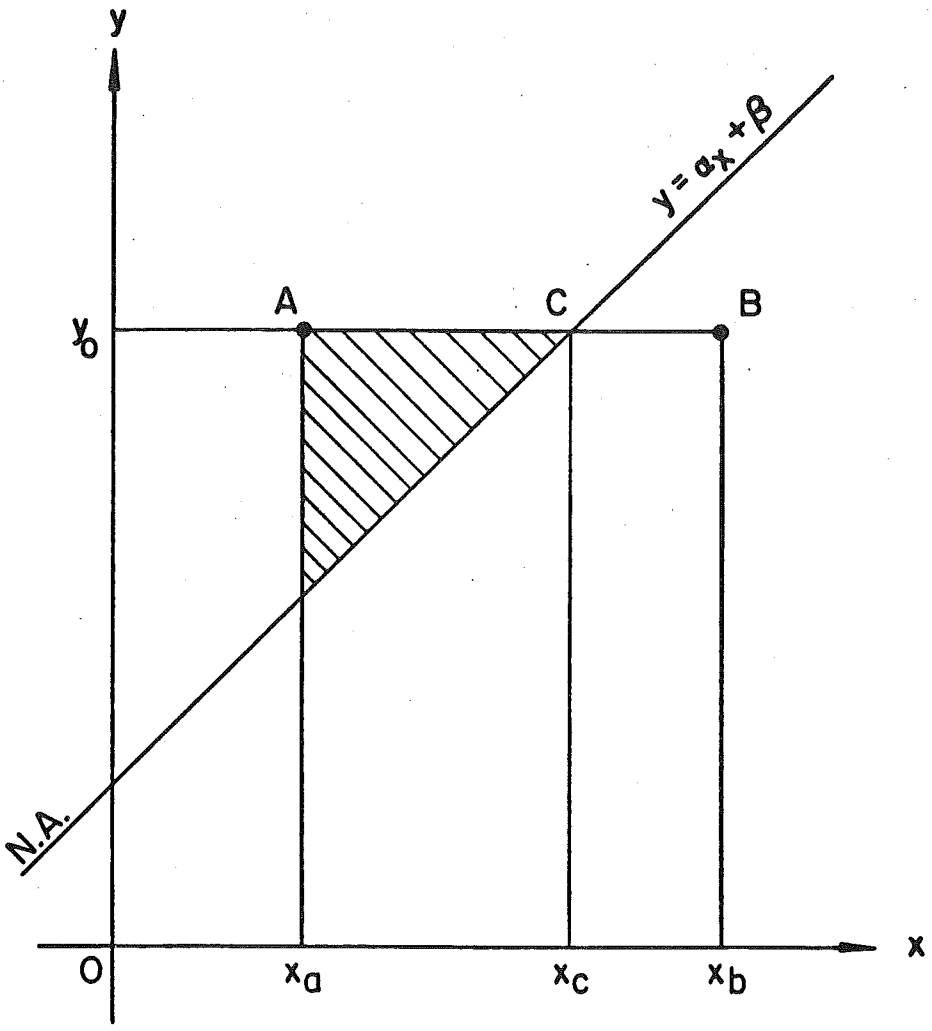

Fig. 6.3 A Line Element and the Neutral Axis

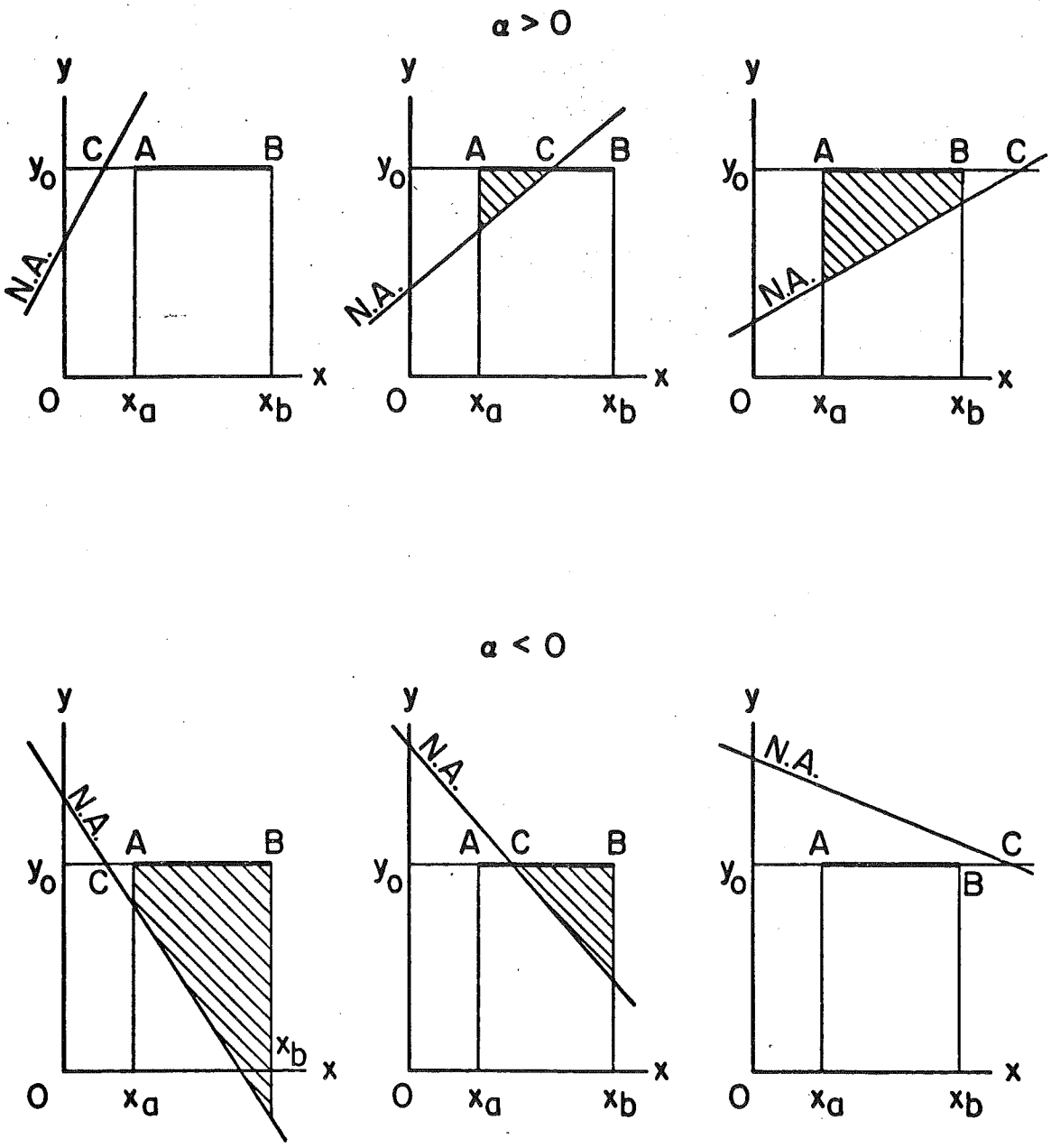

Fig. 6.4 Different Positions of the Neutral Axis

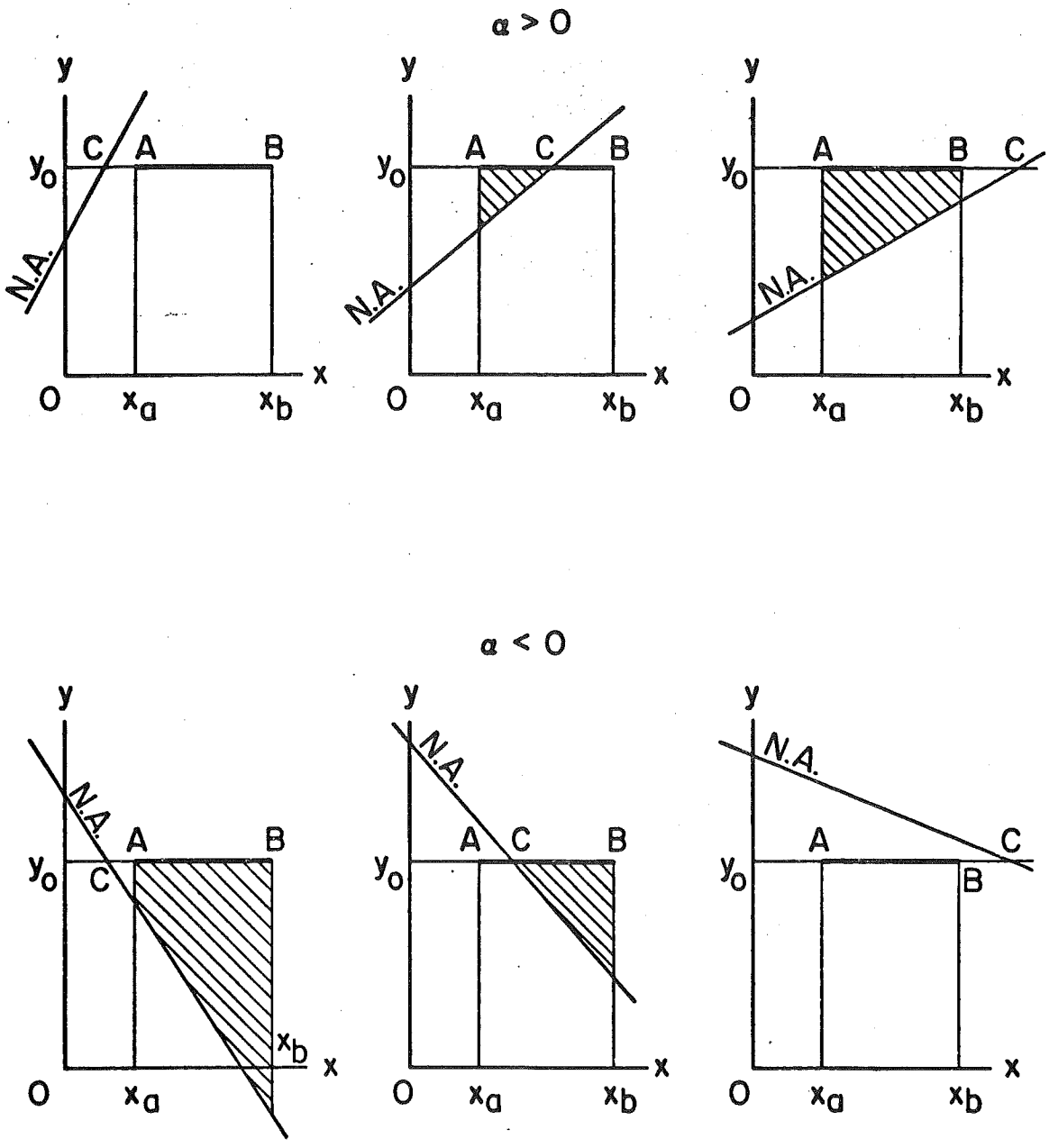

Fig. 6.4 Different Positions of the Neutral Axis

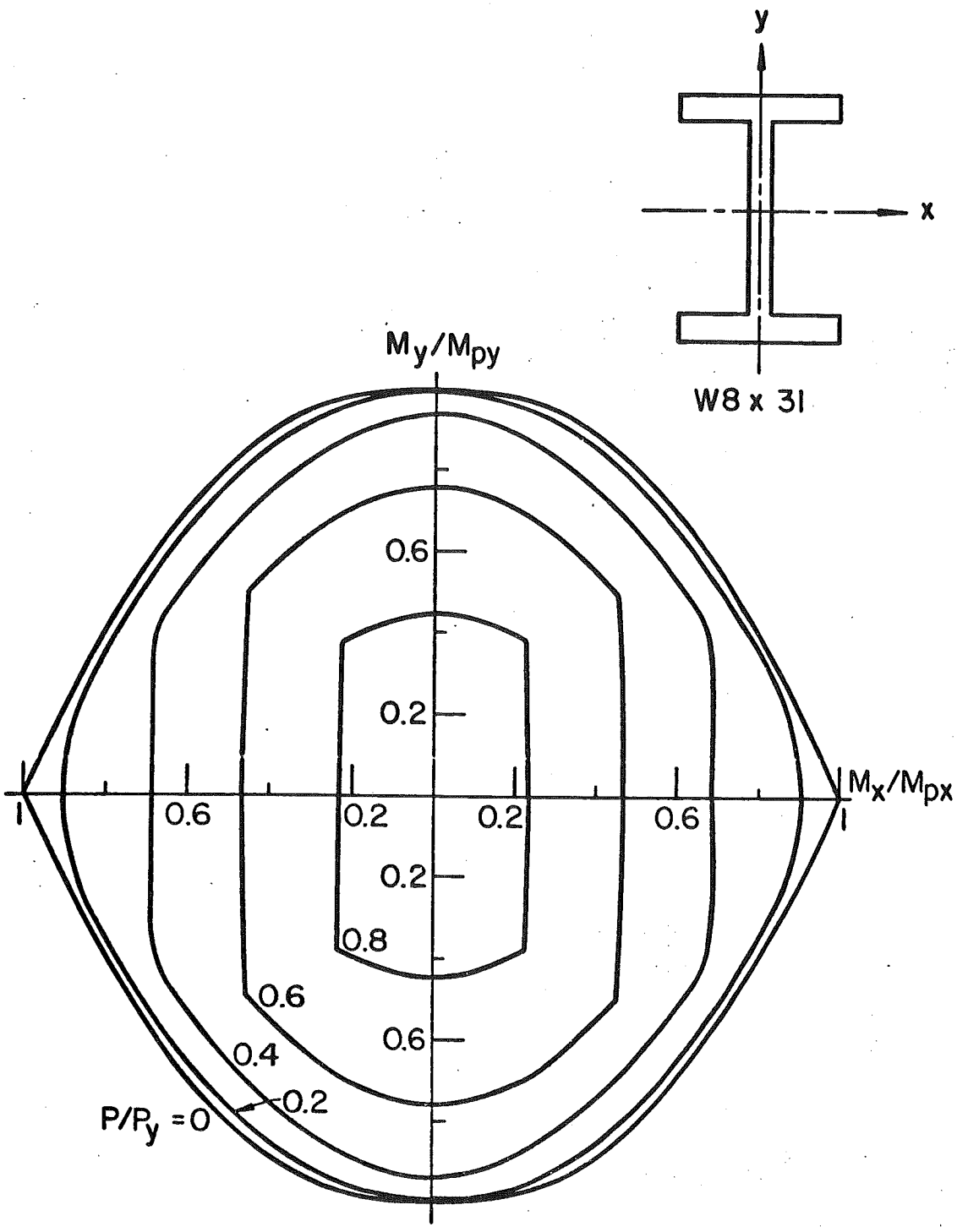

Fig. 6.5 Interaction Curves of a Wide Flange Section

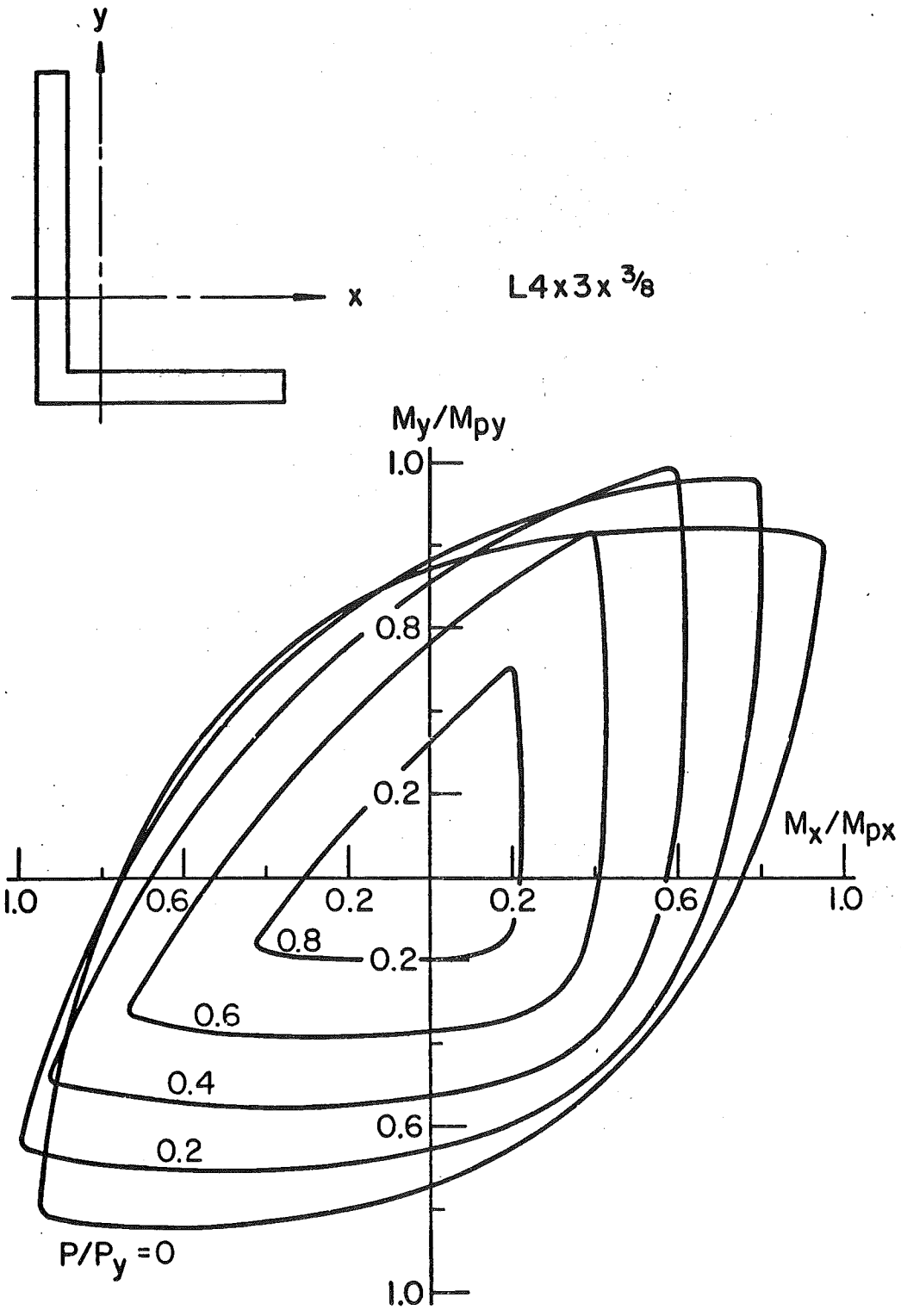

Fig. 6.6 Interaction Curves of an Angle Section

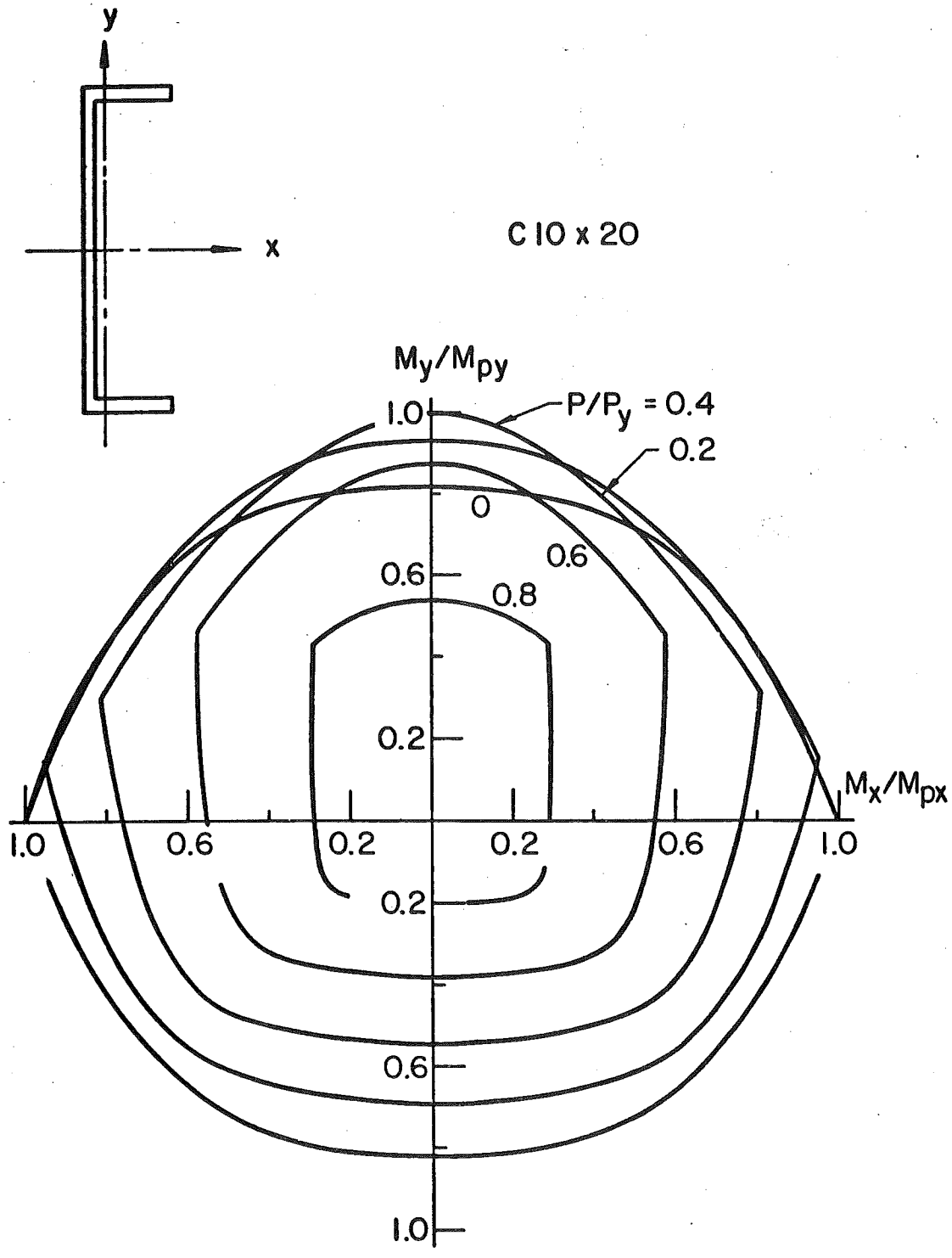

Fig. 6.7 Interaction Curves of a Channel Section

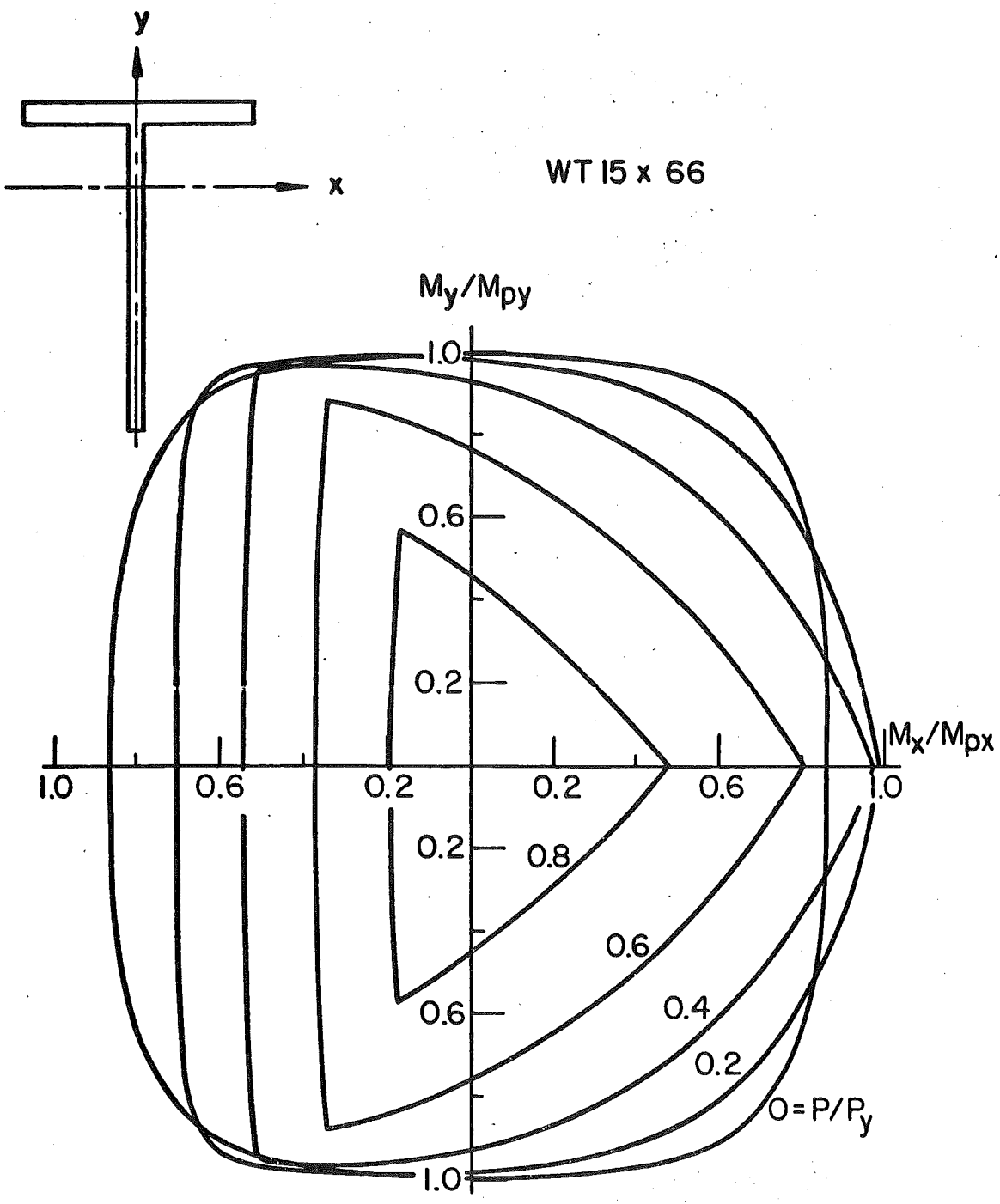

Fig. 6.8 Interaction Curves of a Structural Tee Section

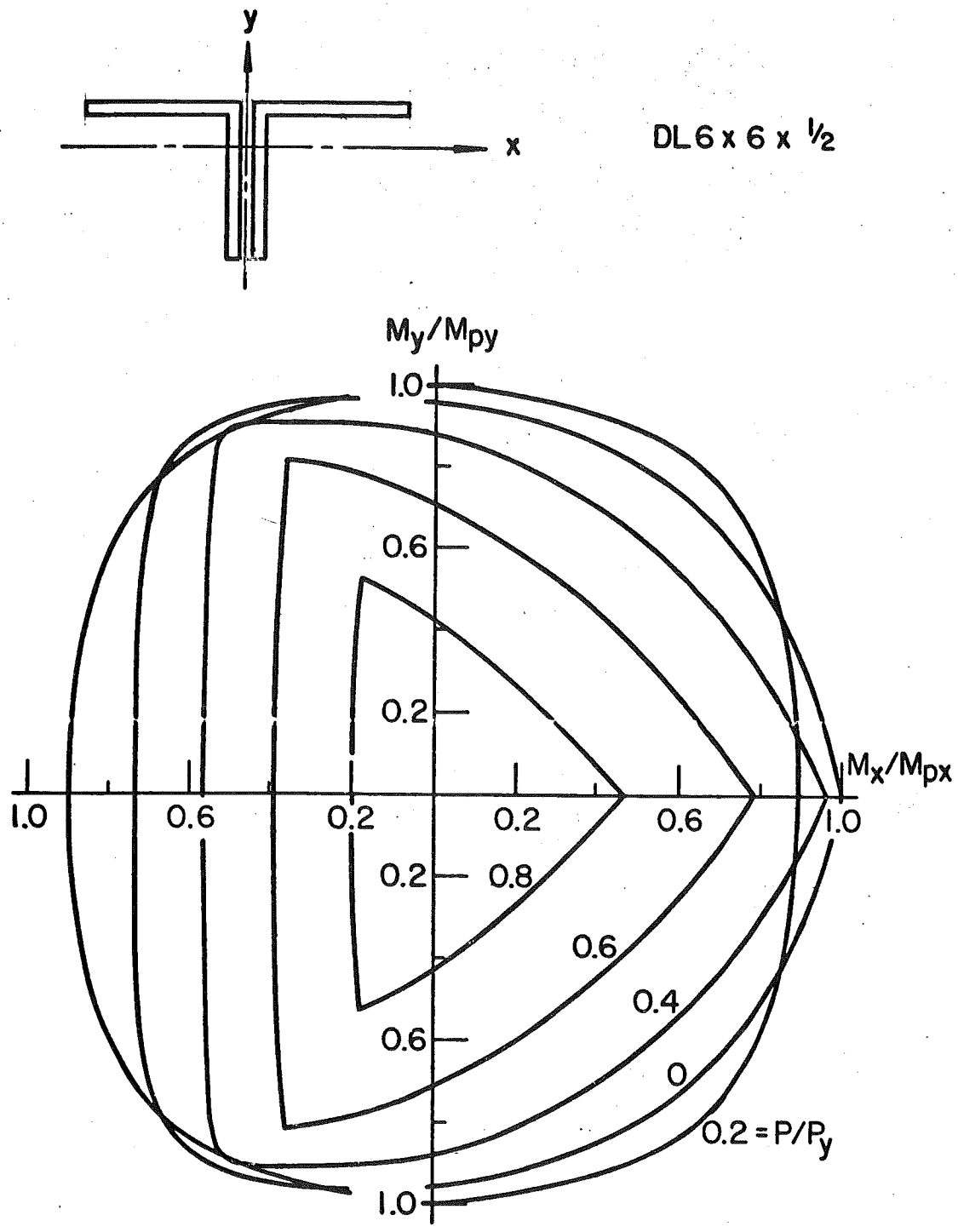

Fig. 6.9 Interaction Curves of a Double-Angle Section

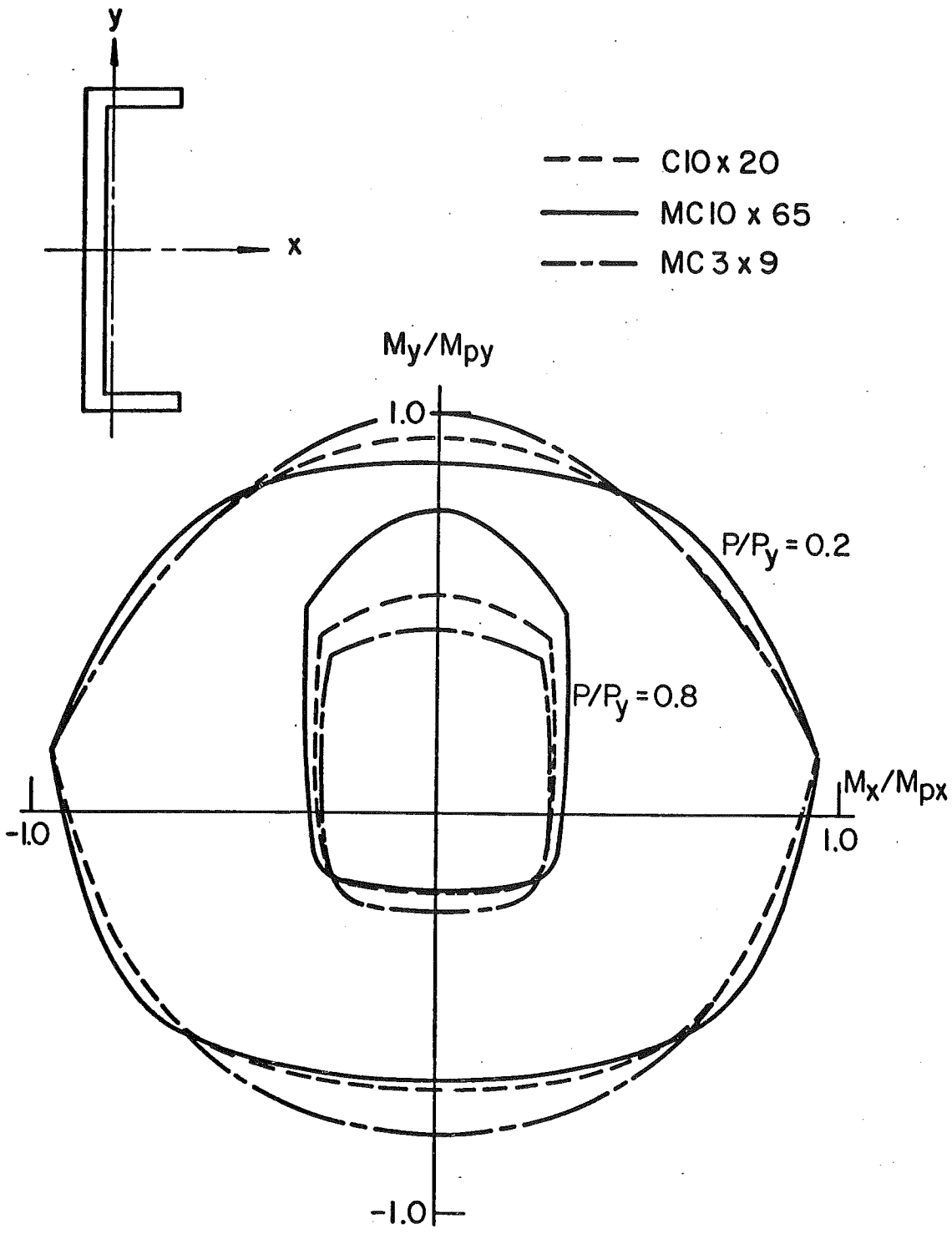

Fig. 6.10 Interaction Curves for Various Channel Sections

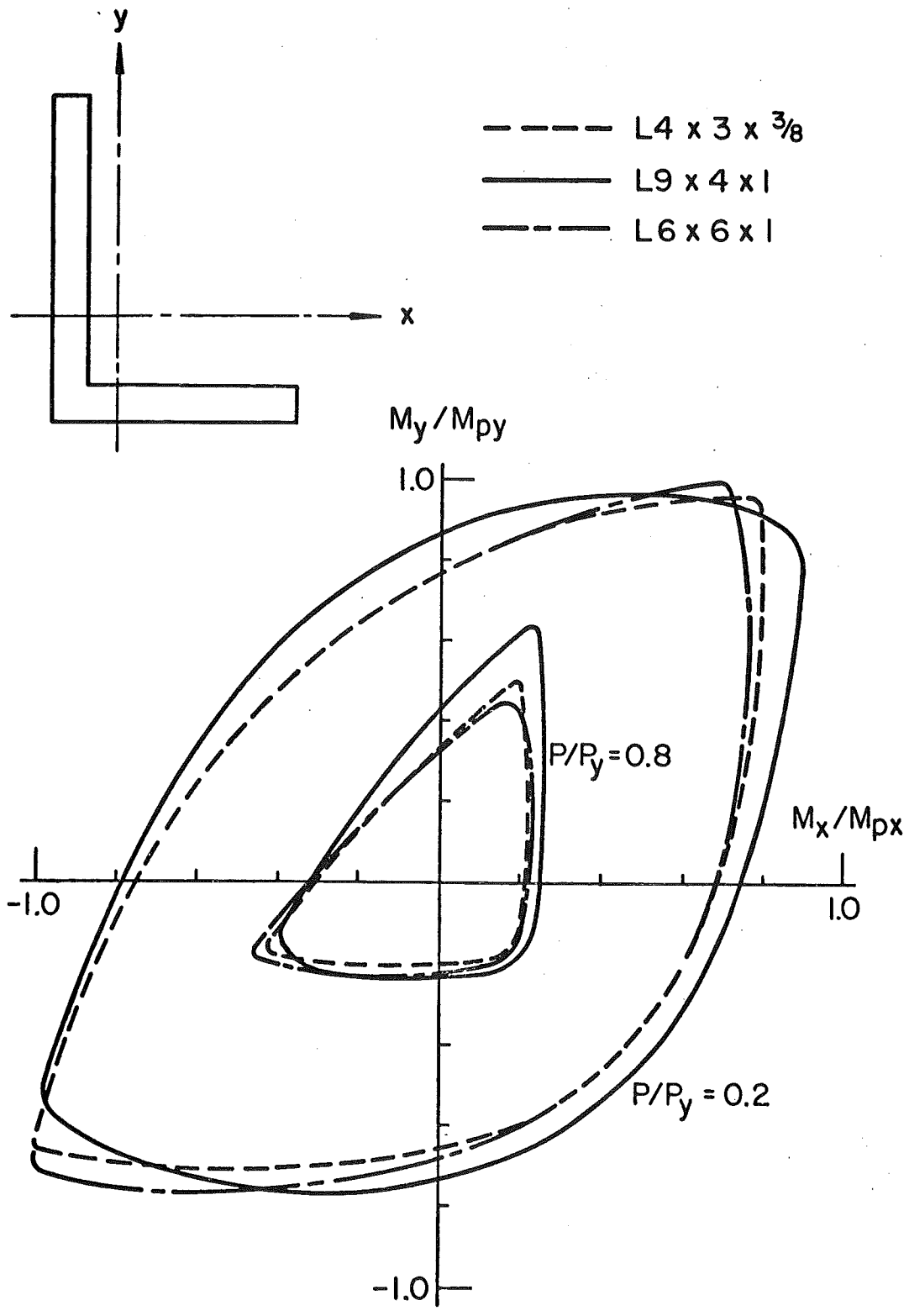

Fig. 6.11 Interaction Curves for Various Angle Sections

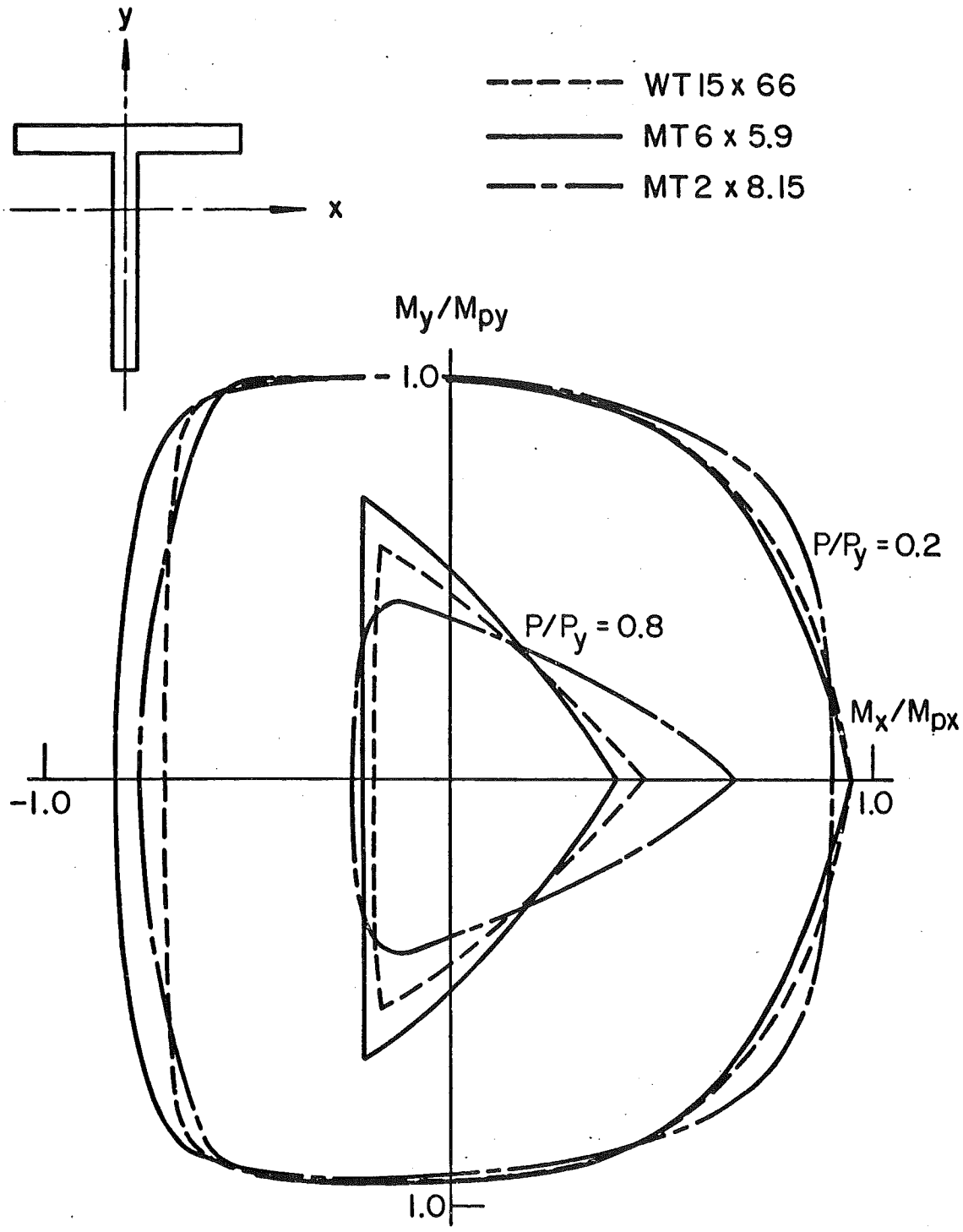

Fig. 6.12 Interaction Curves for Various Angle Sections

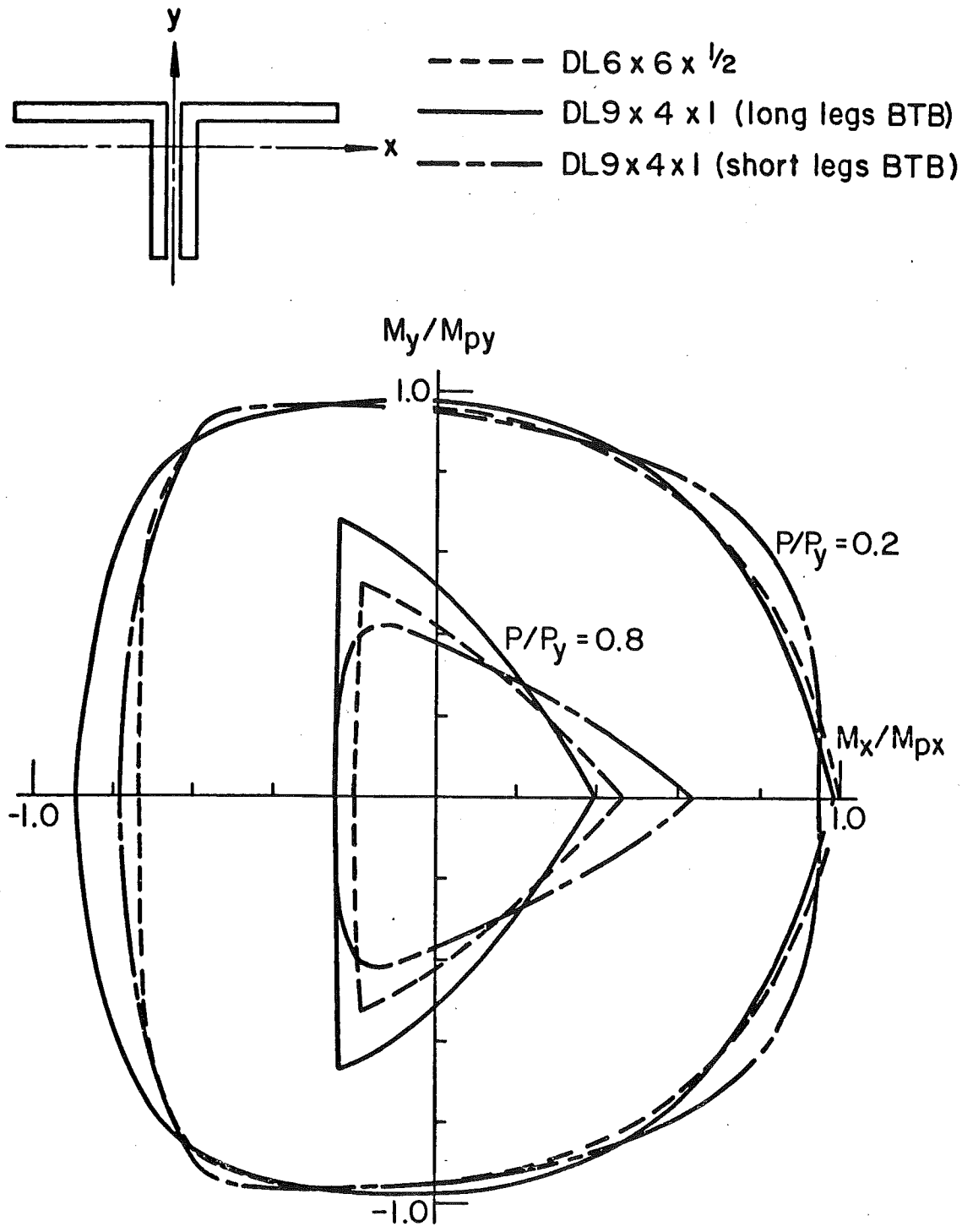

Fig. 6.13 Interaction Curves for Various Double-Angle Sections

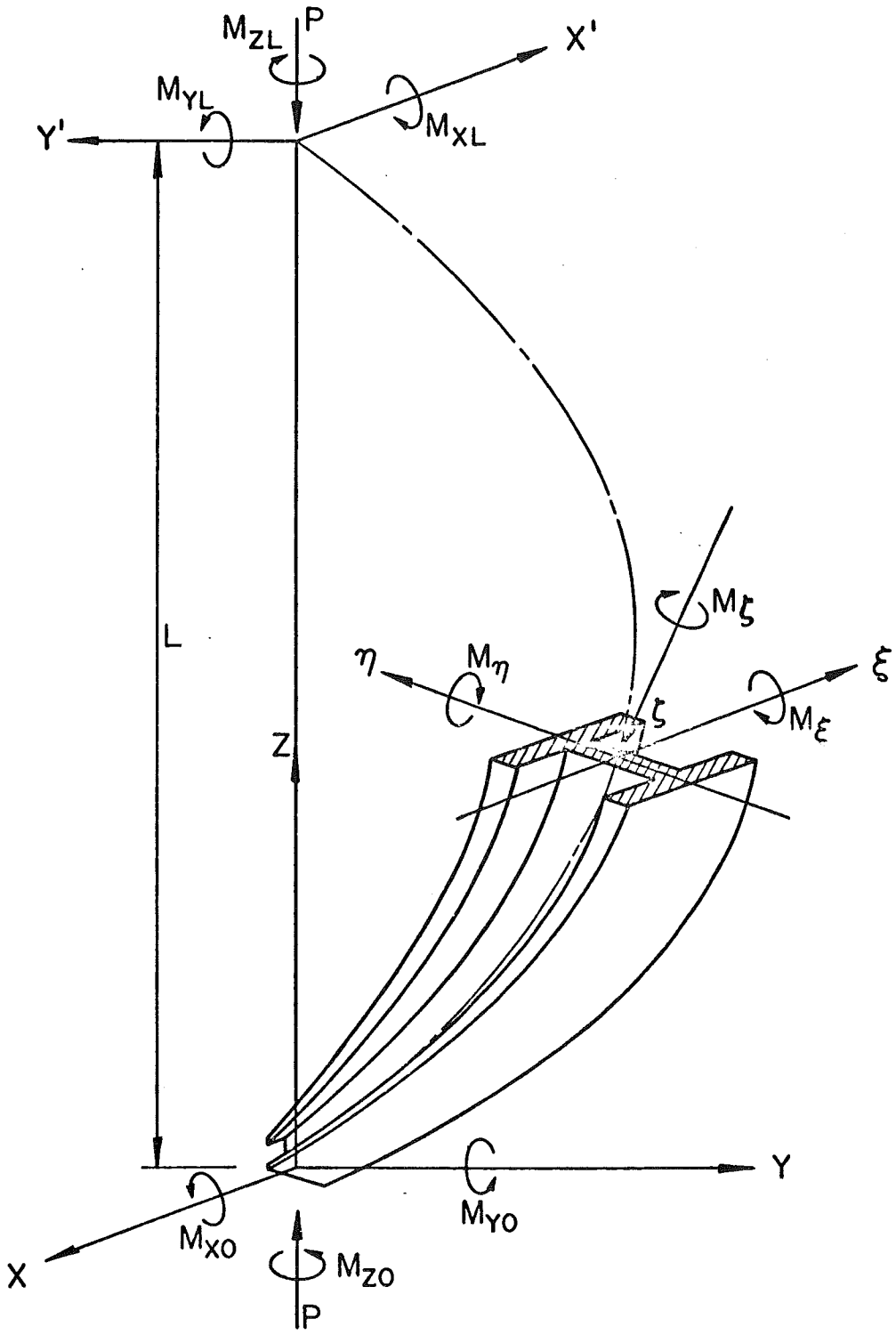

Fig. 7.1 Internal Forces and External Forces

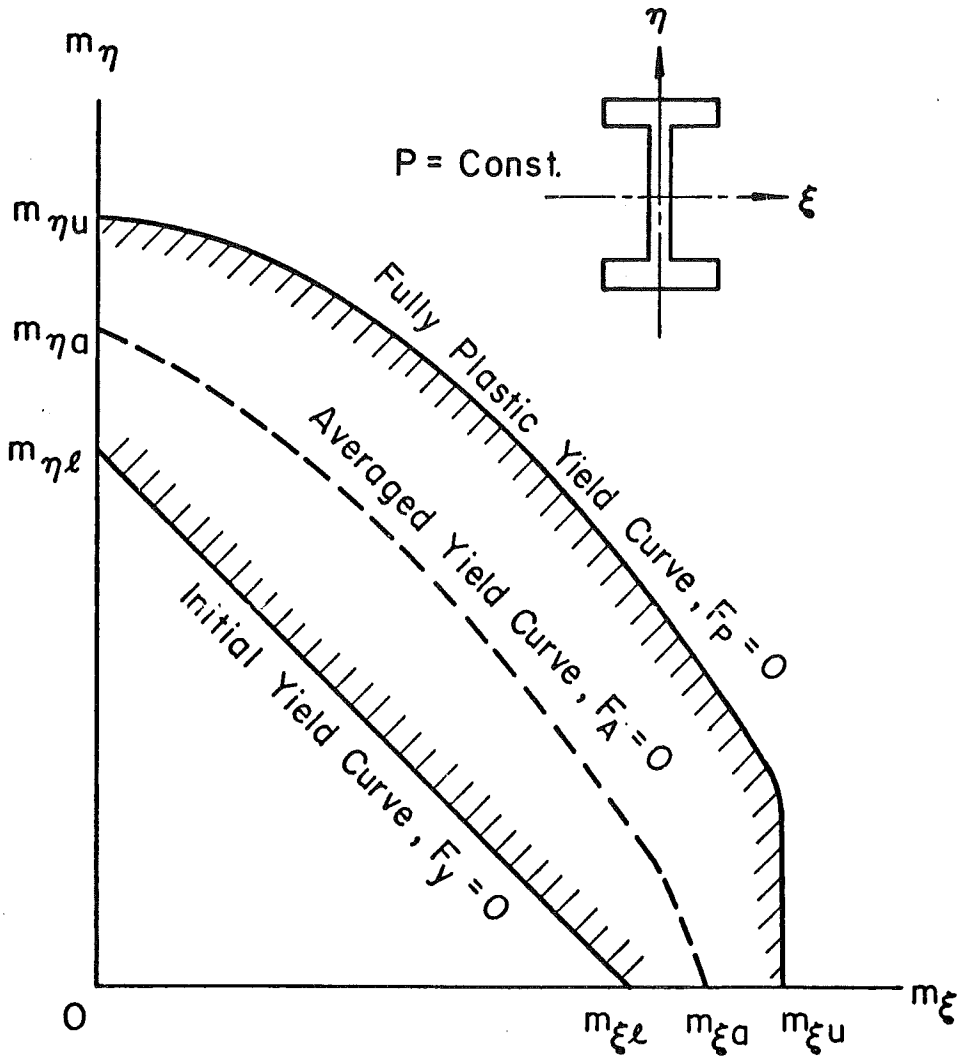

Fig. 7.2 Averaged Interaction Section

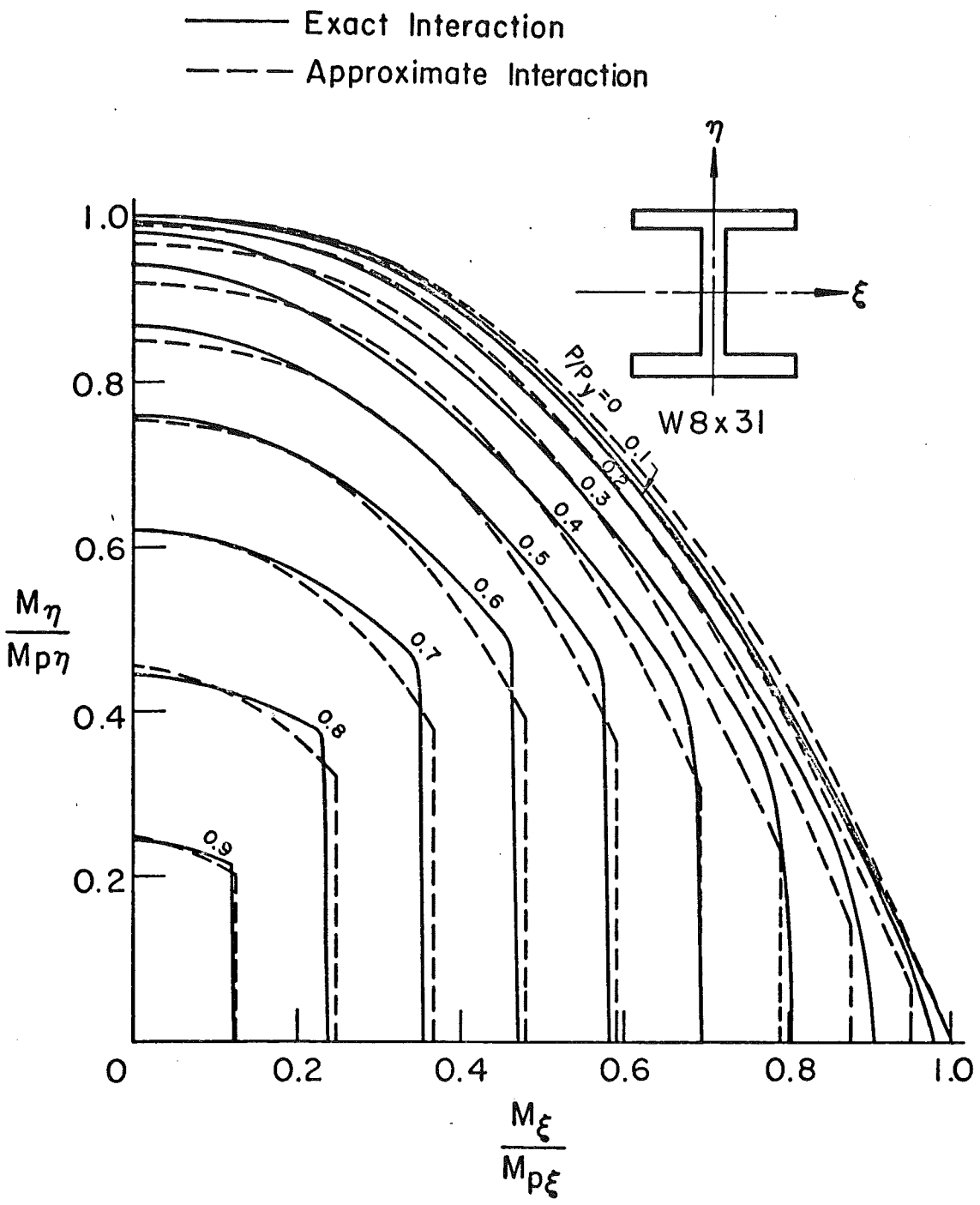

Fig. 7.3 Interaction of a Wide-Flange Section

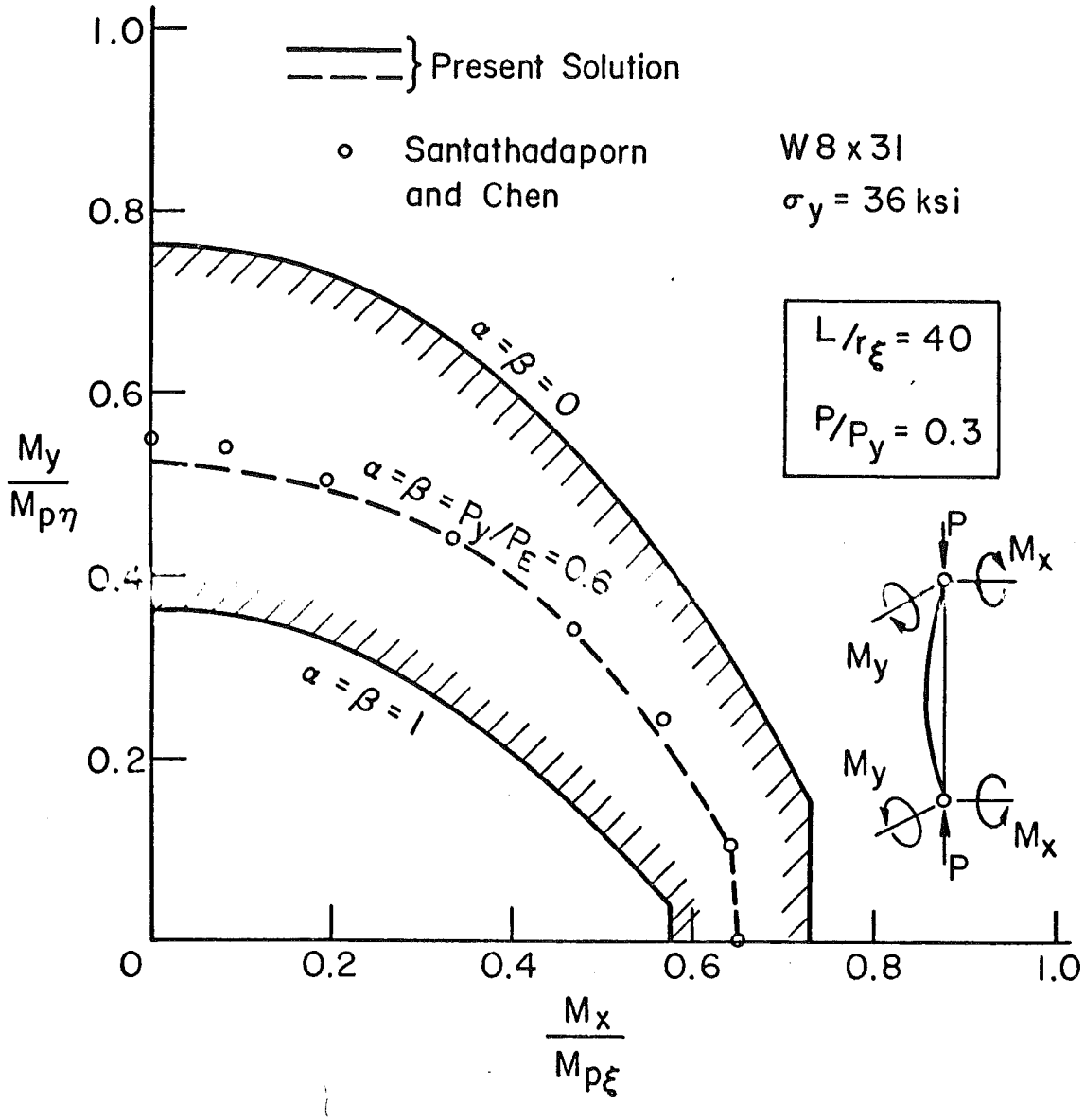

Fig. 7.4 Bounded Interaction Curve of Column (Ref. 20)

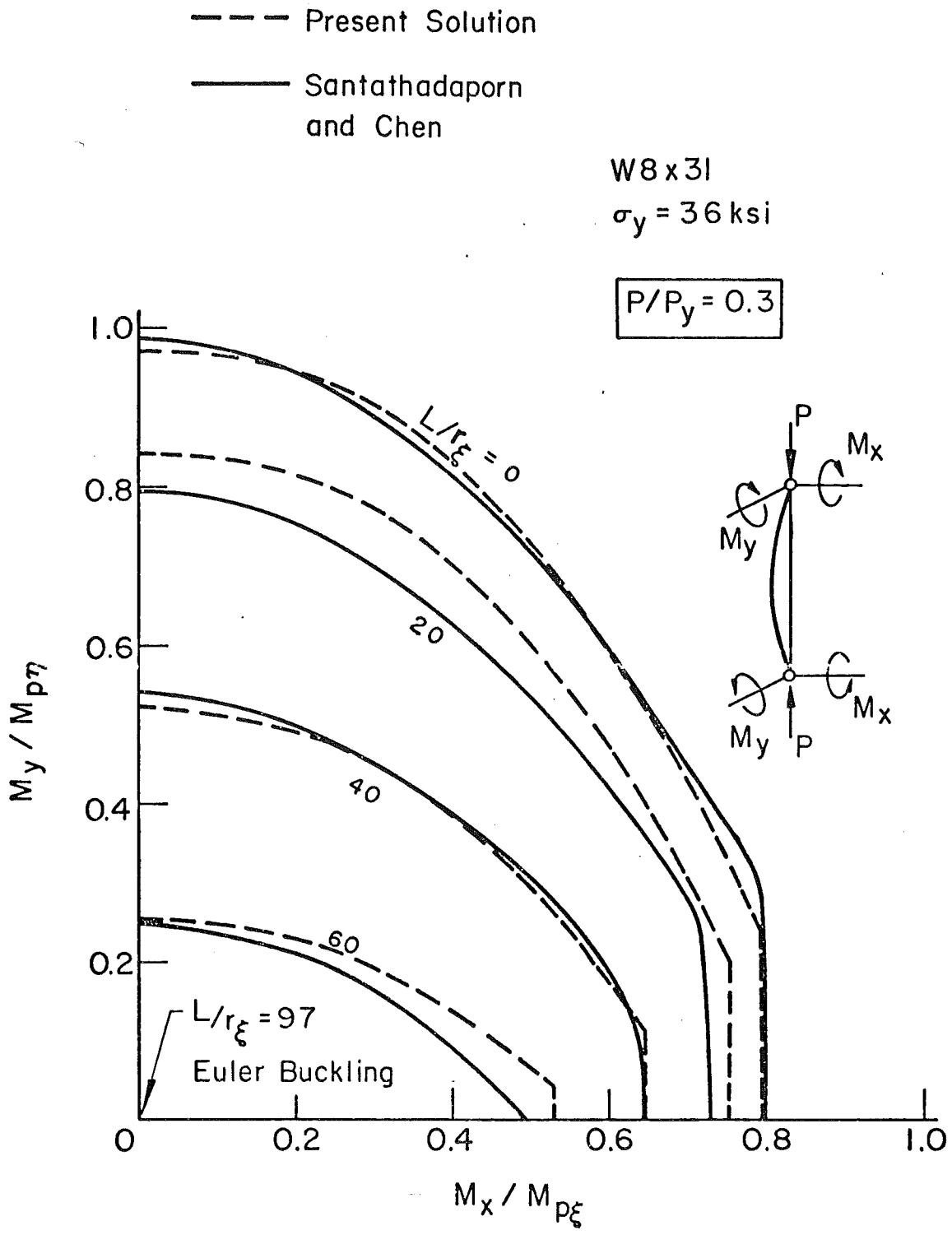

Fig. 7.5 Comparison in Symmetric Loading Cases (Ref. 20)

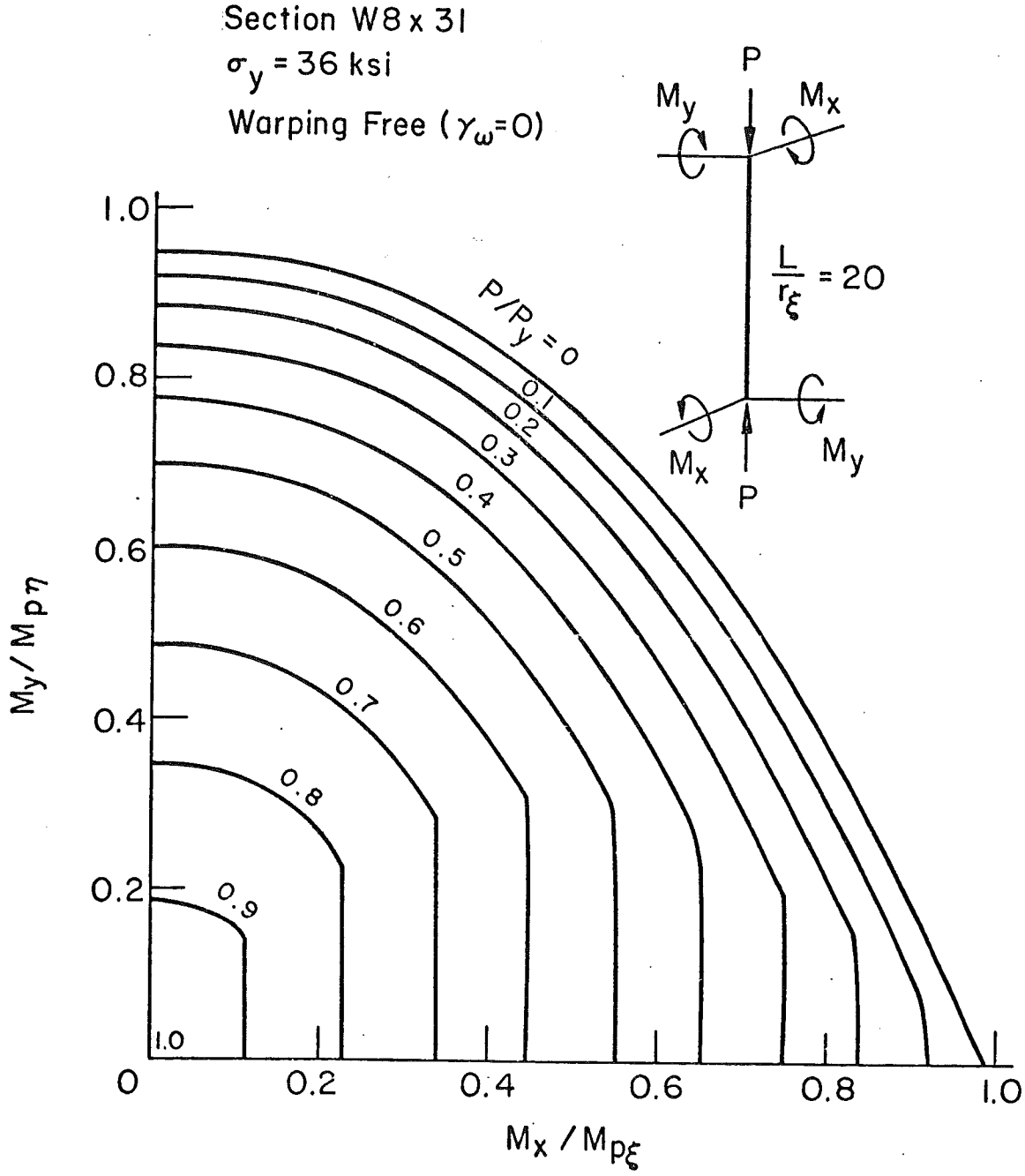

Fig. 7.6 Interaction of Symmetric Column (L/r_ξ = 20)

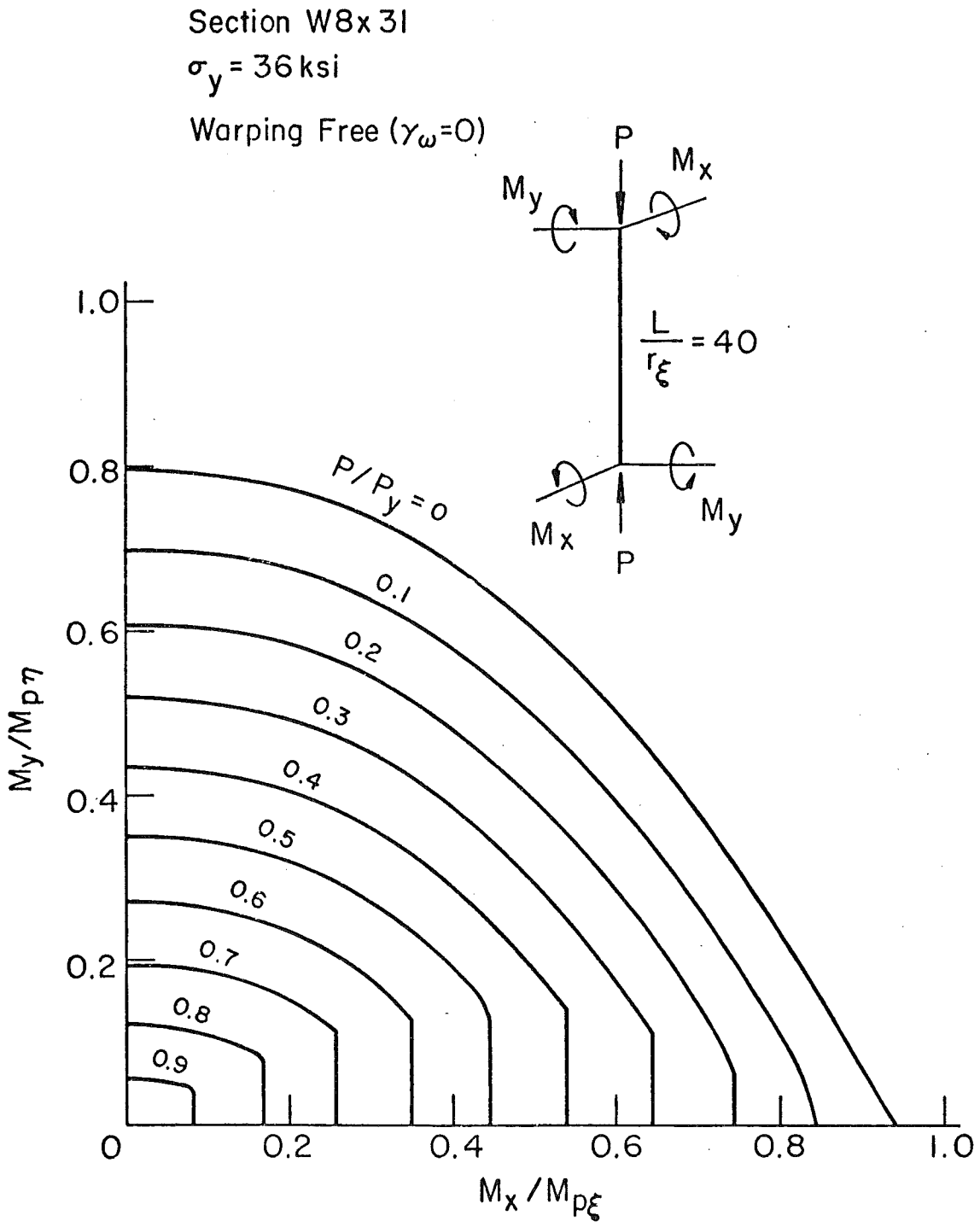

Fig. 7.7 Interaction of Symmetric Column (L/r_ξ = 40)

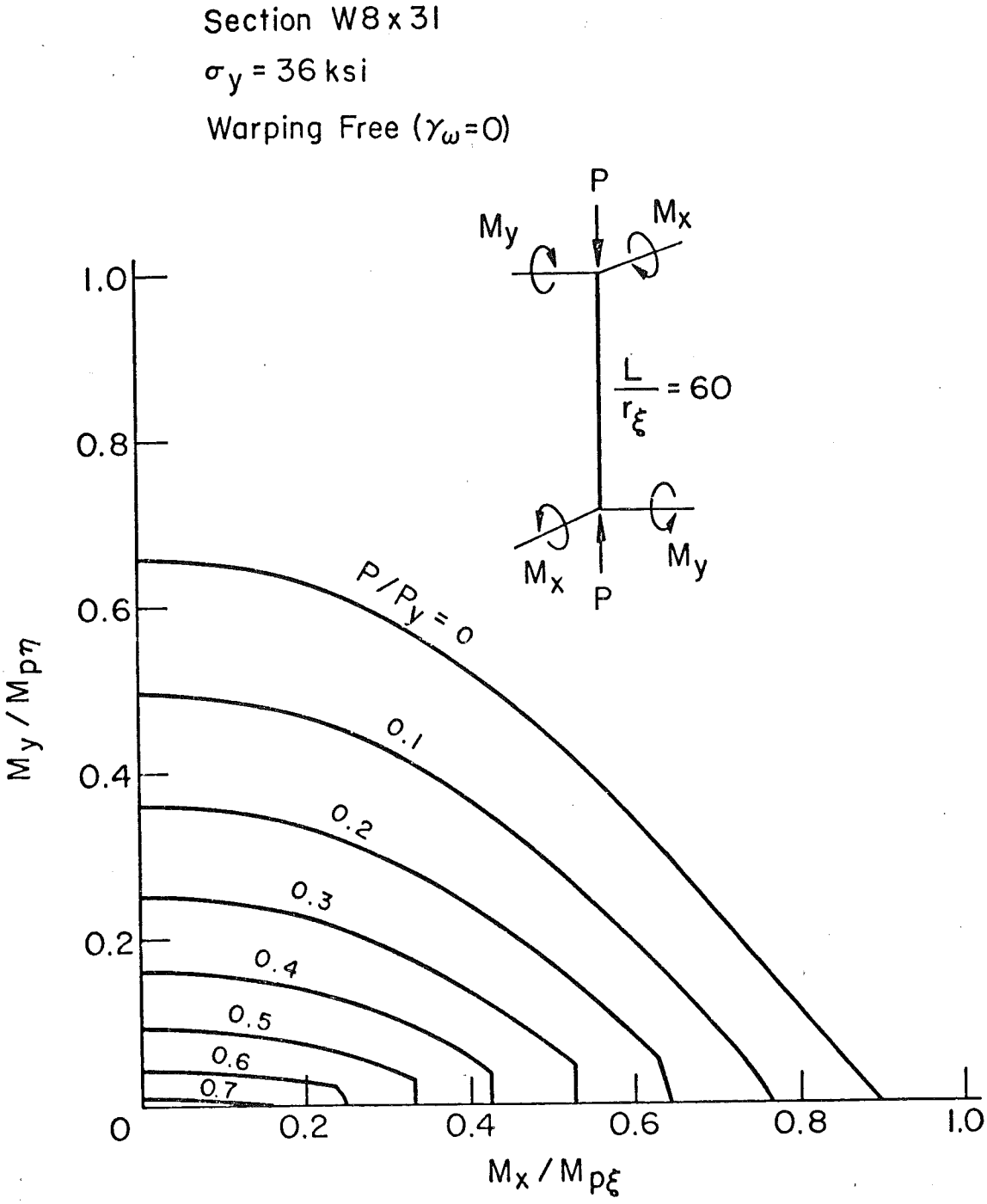

Fig. 7.8 Interaction of Symmetric Column (L/r_ξ = 60)

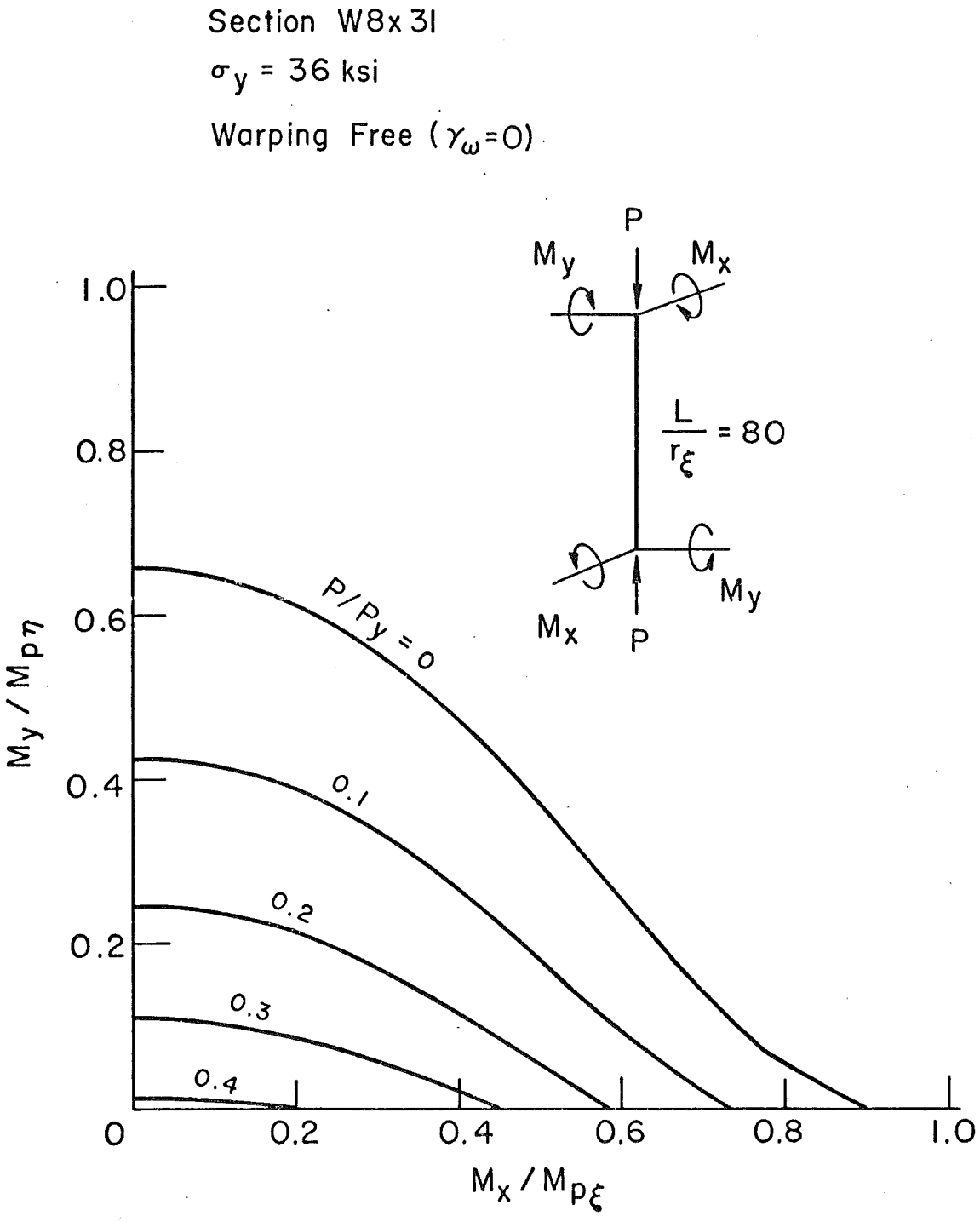

Fig. 7.9 Interaction of Symmetric Column (L/r_ξ = 80)

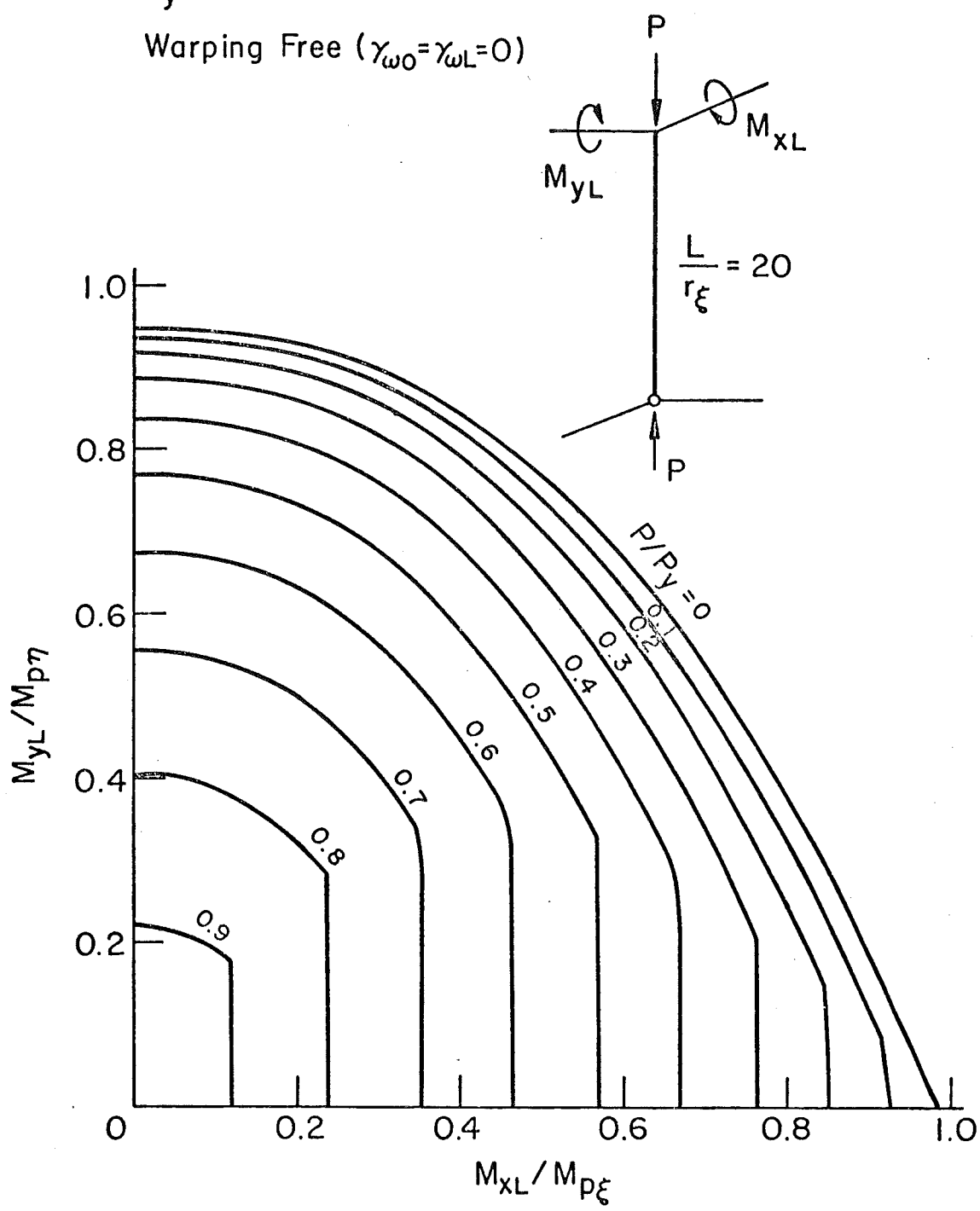

Fig. 7.10 Interaction of Unsymmetric Column (L/r_ξ = 20)

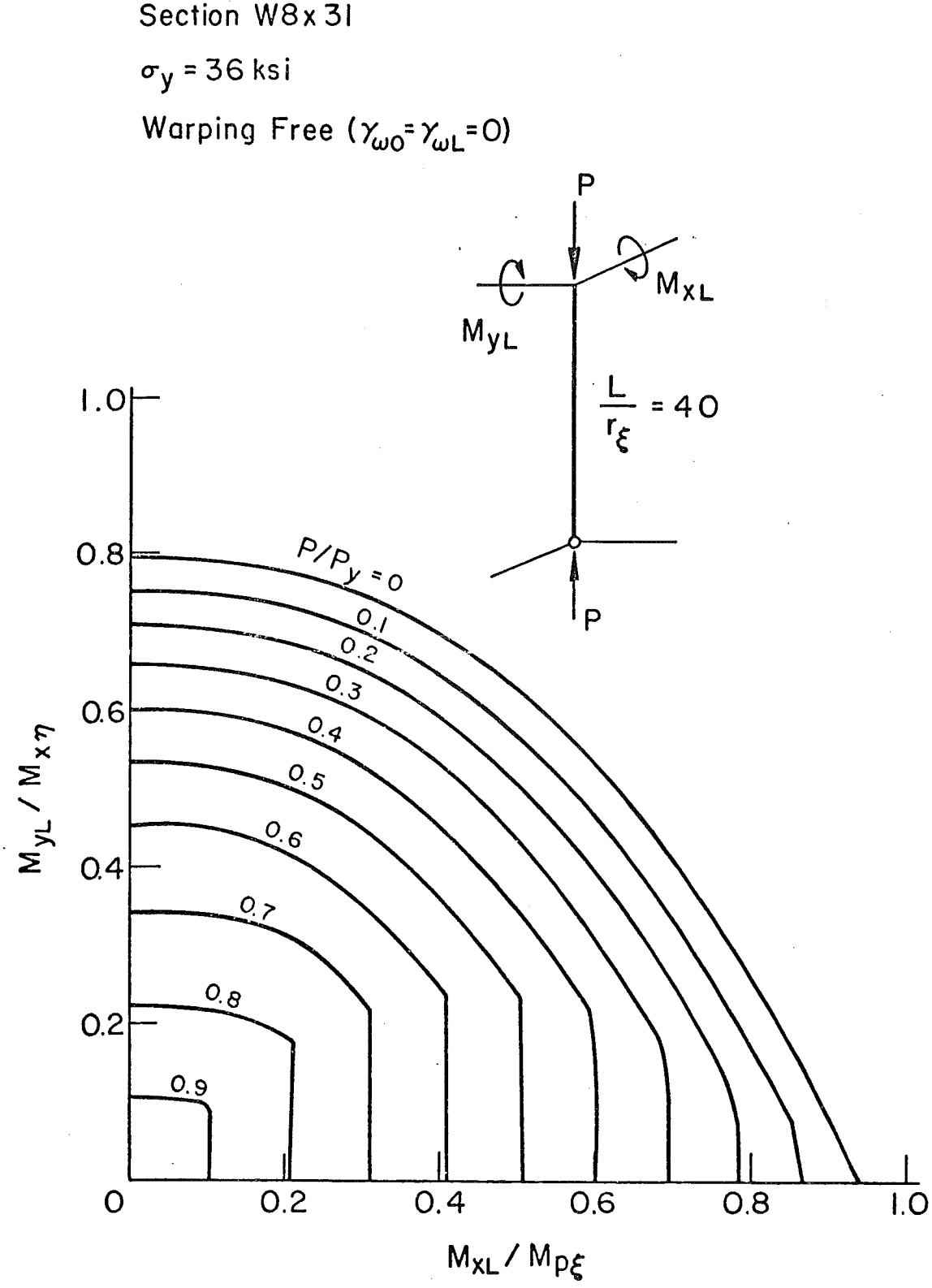

Fig. 7.11 Interaction of Unsymmetric Column (L/r_ξ = 40)

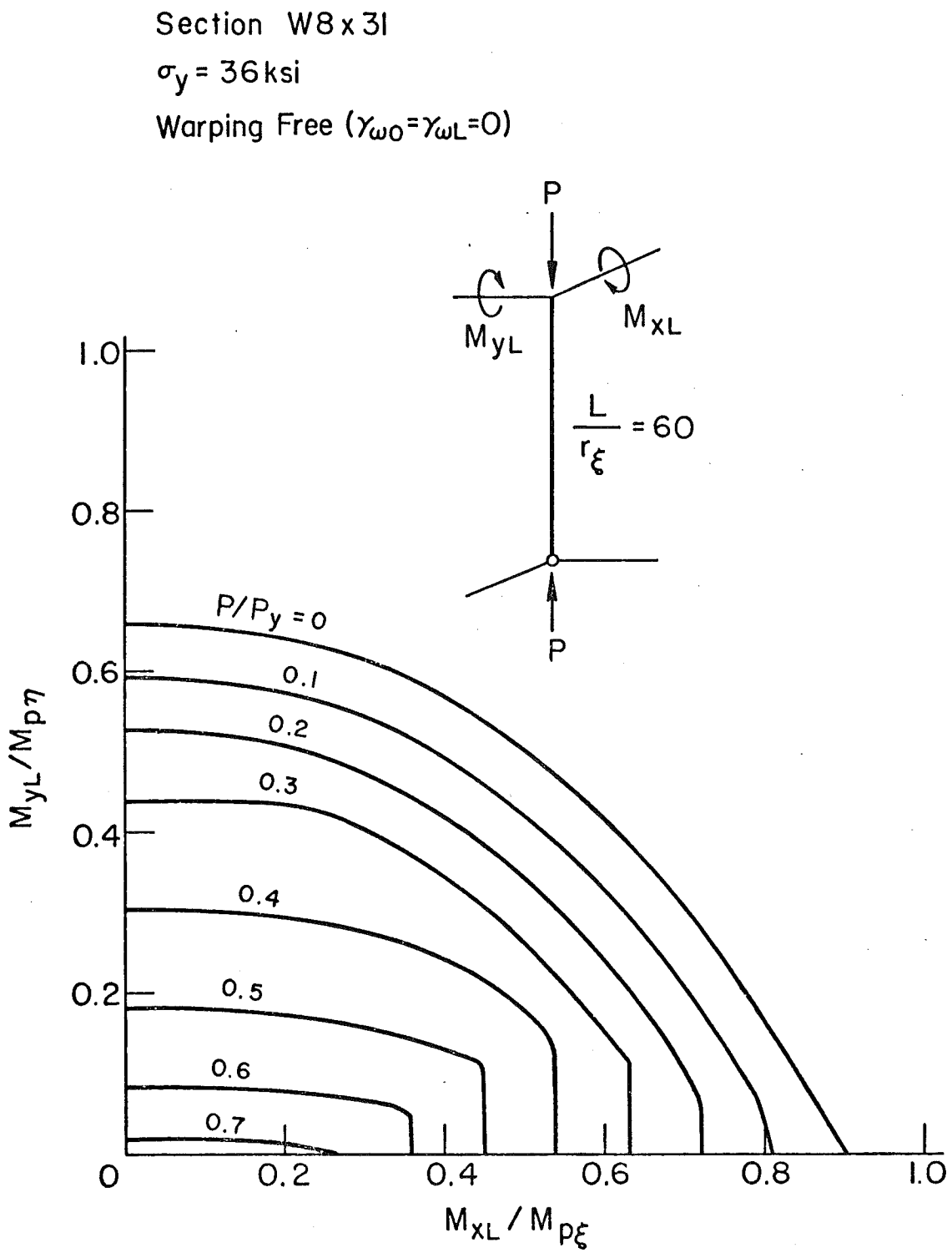

Fig. 7.12 Interaction of Unsymmetric Column (L/r_ξ = 60)

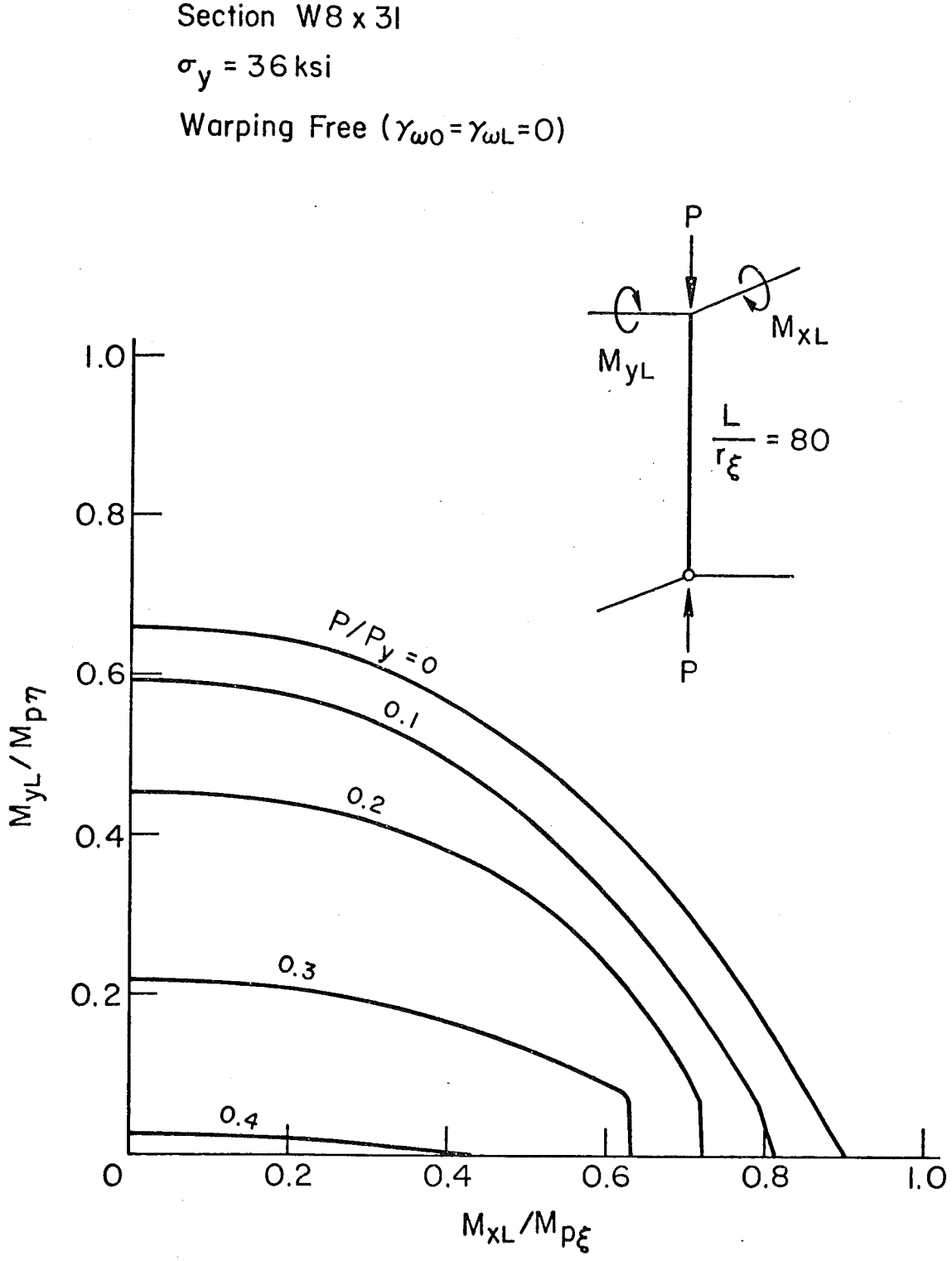

Fig. 7.13 Interaction of Unsymmetric Column (L/r_ξ = 80)

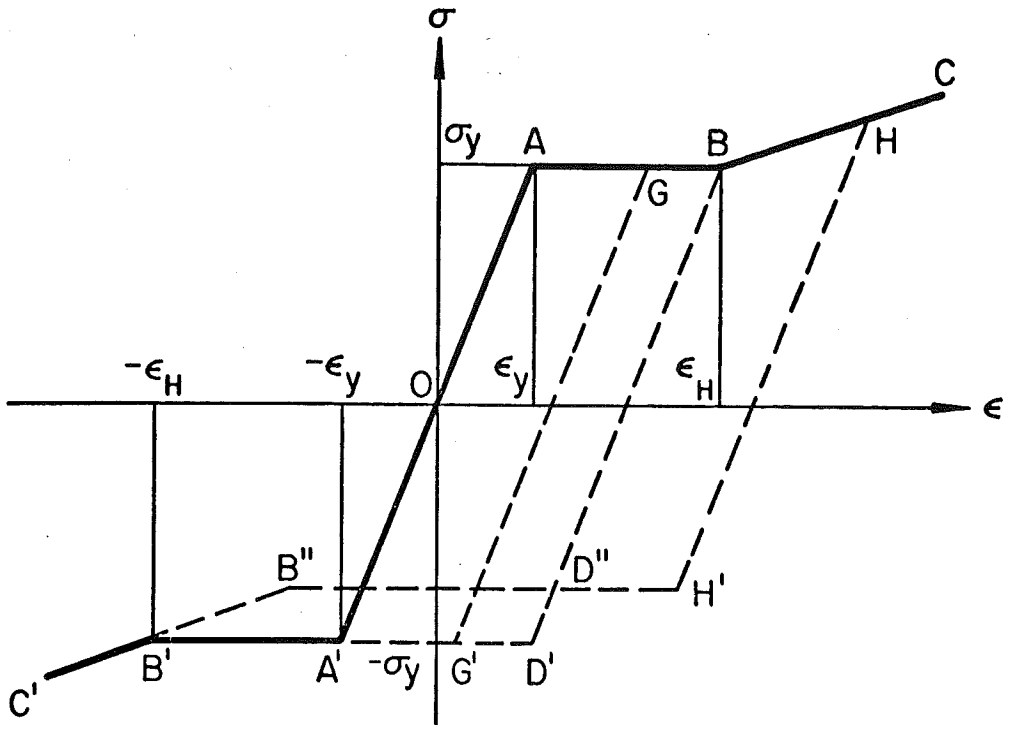

(a) Initial State of Stress-Strain

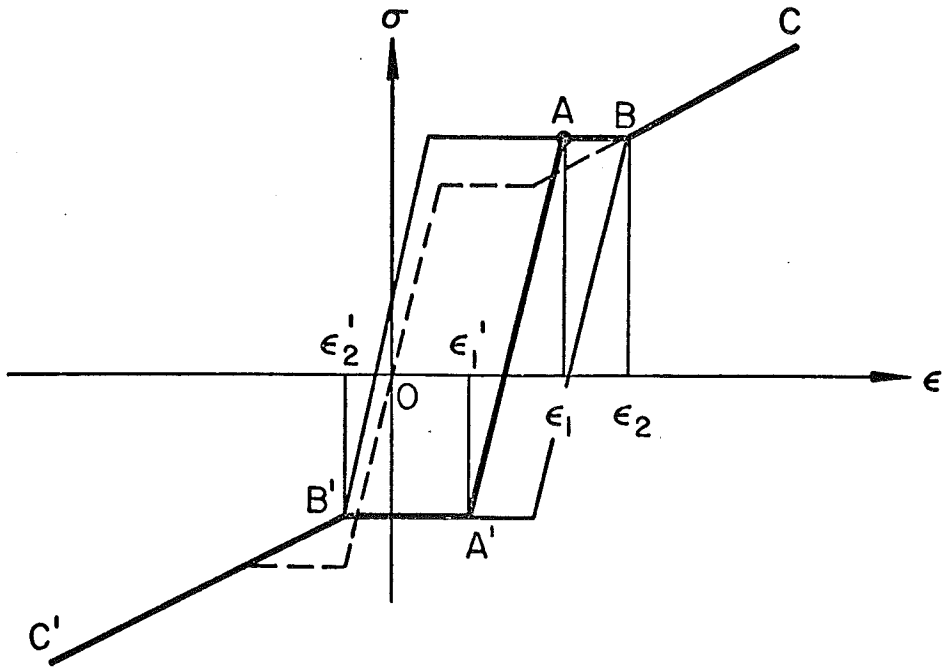

(b) Subsequent State of Stress-Strain

Fig. 8.1 An Idealized Stress-Strain Relationship

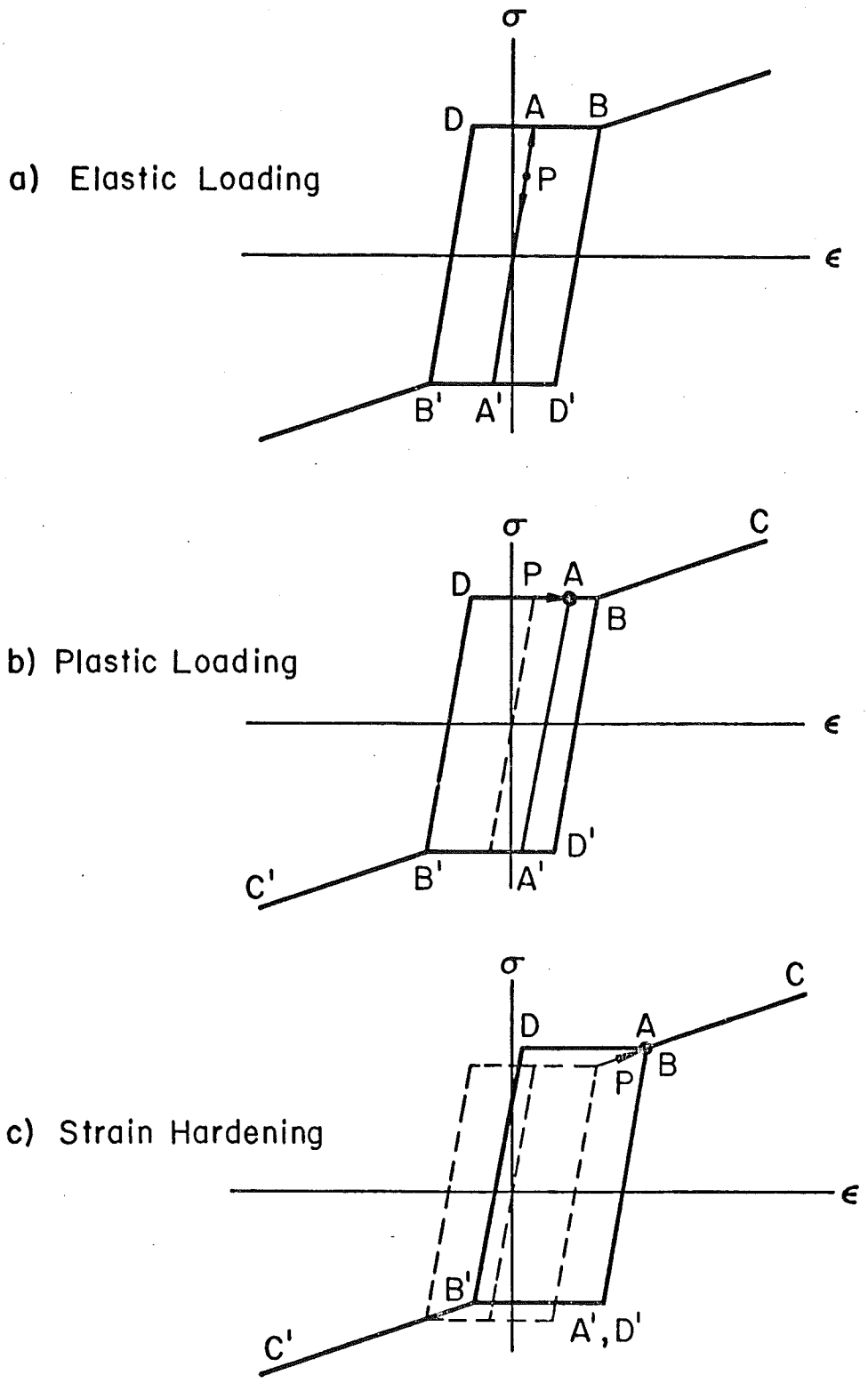

Fig. 8.2 Mechanical Model of Stress-Strain

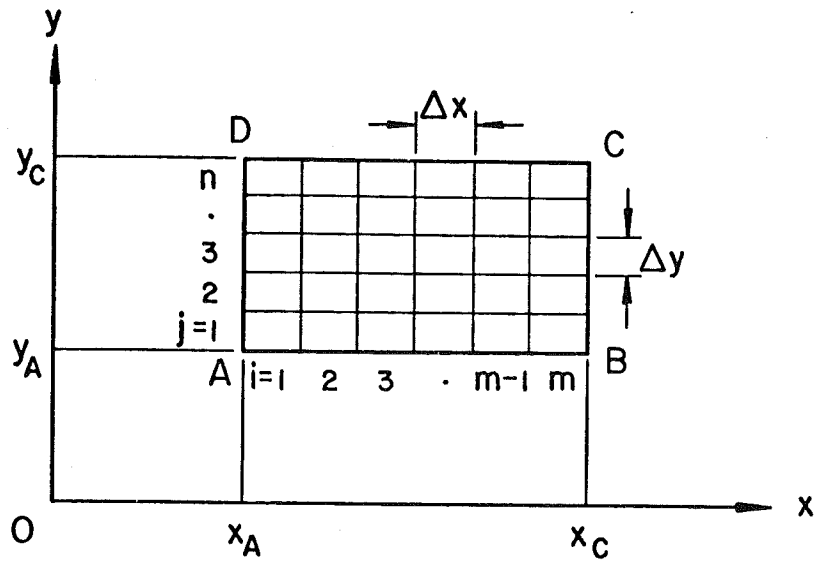

Fig. 8.3 Partitioning of Rectangular Element

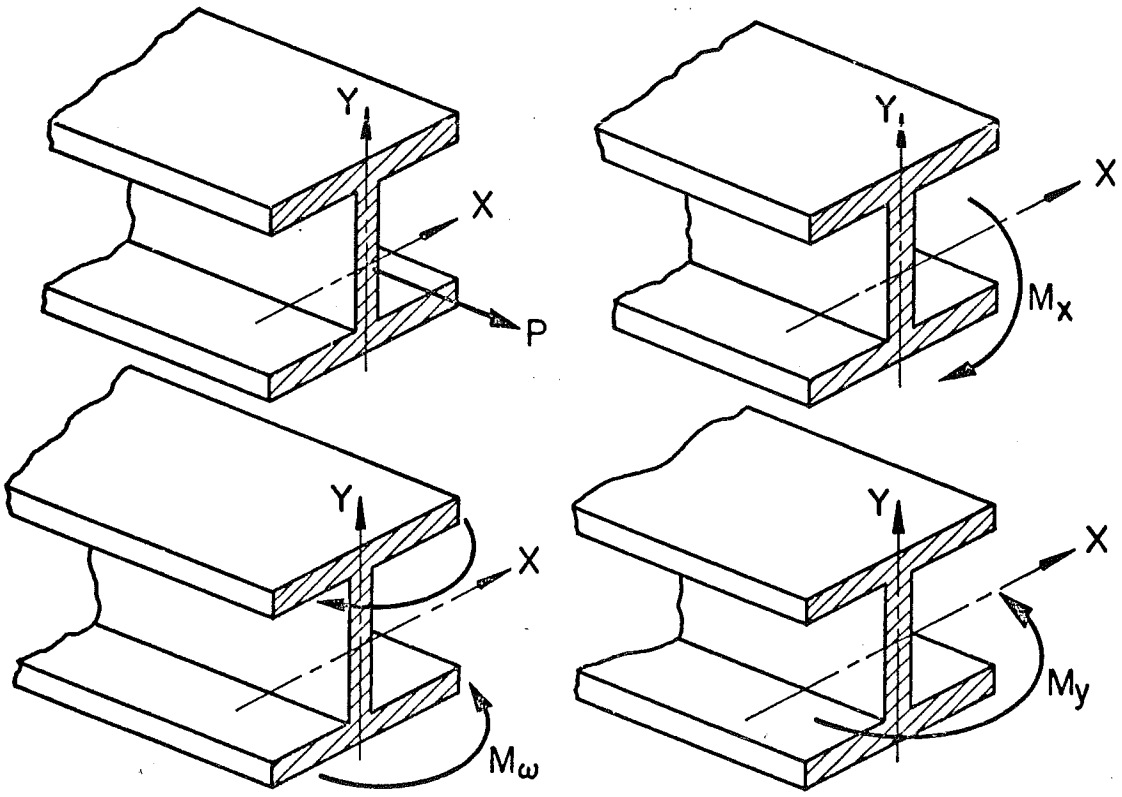

Fig. 8.4 Generalized Stresses

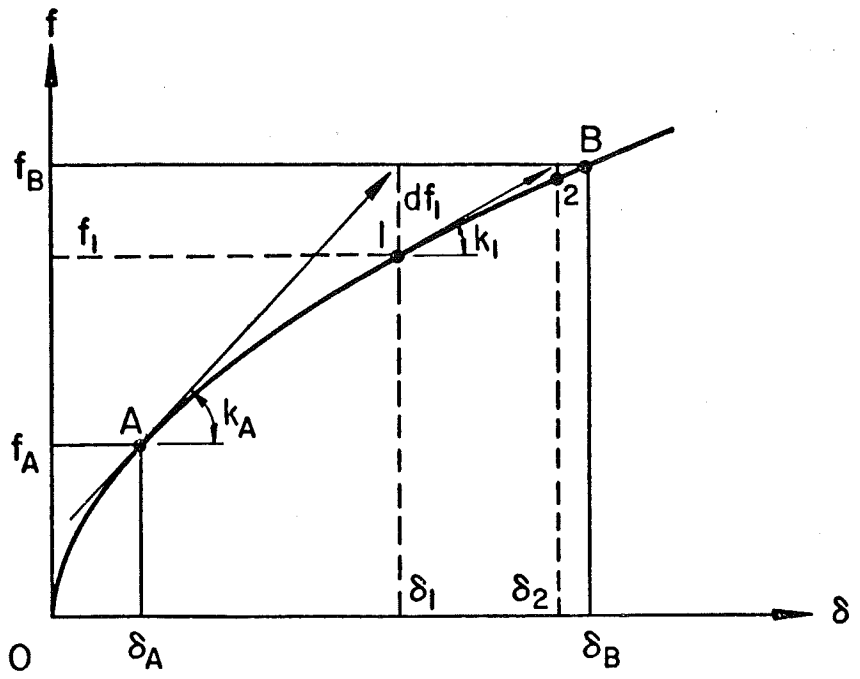

Fig. 8.5 Tangent Stiffness Method

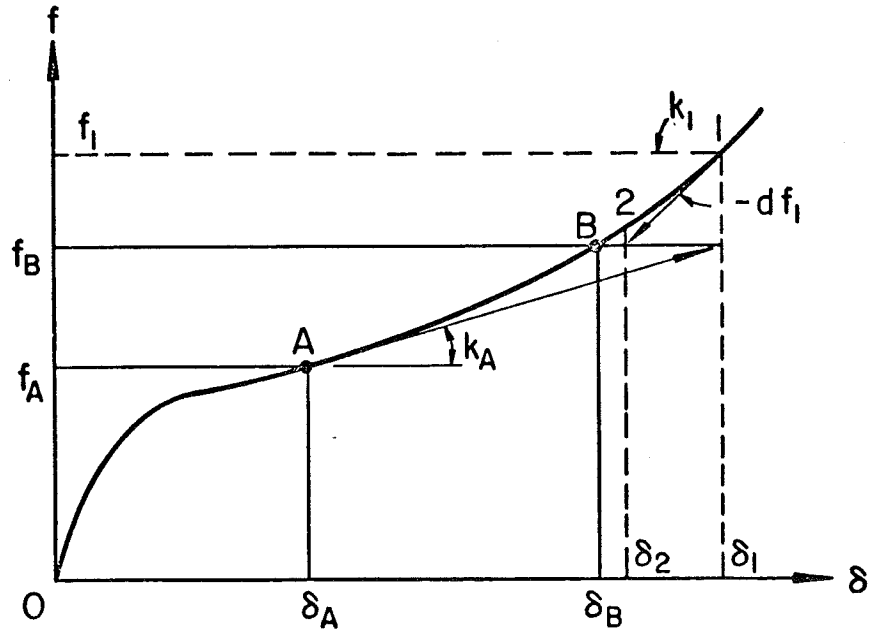

Fig. 8.6 Tangent Stiffness with Strain Hardening

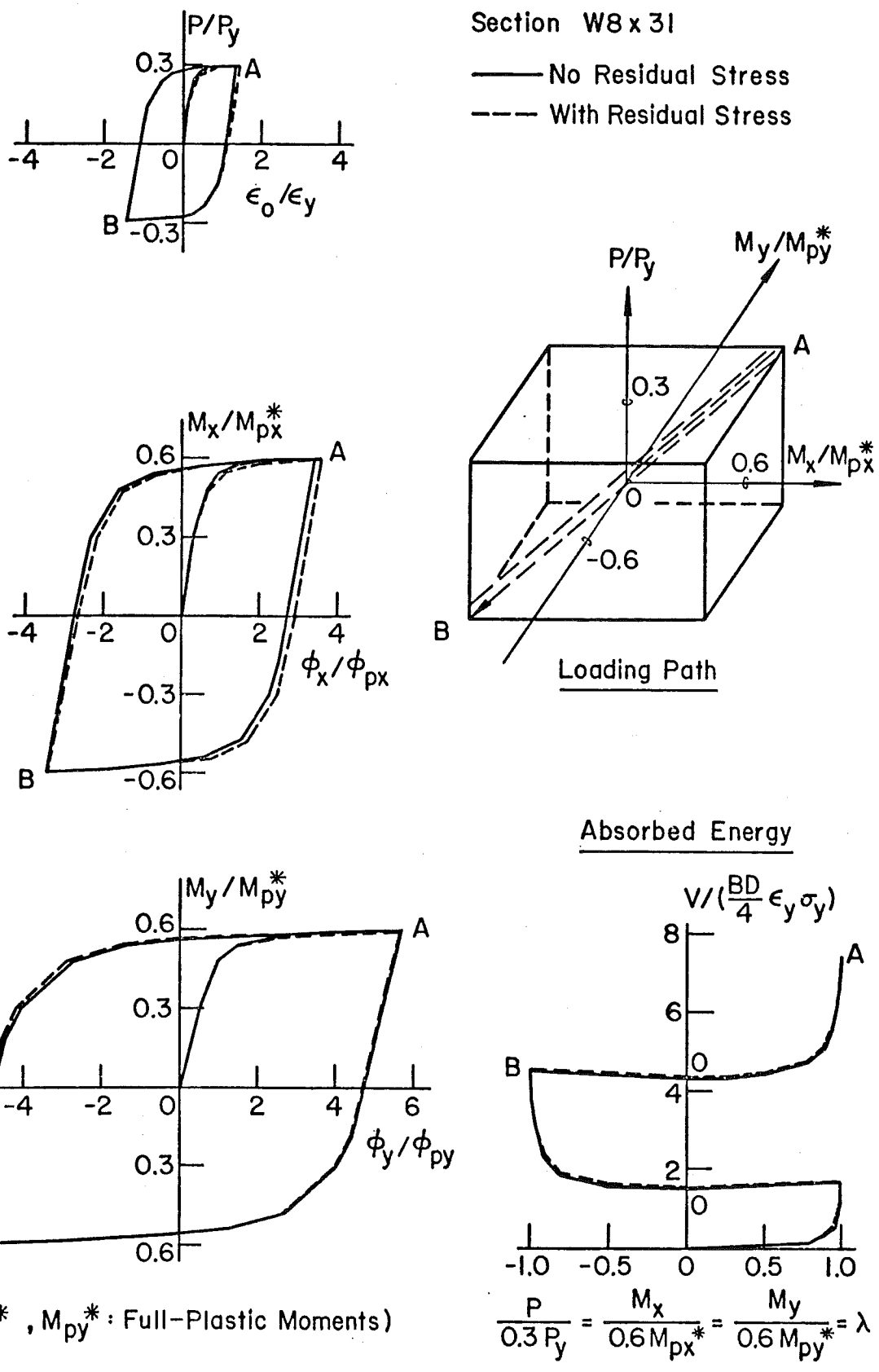

Fig. 8.7 Proportional Loading

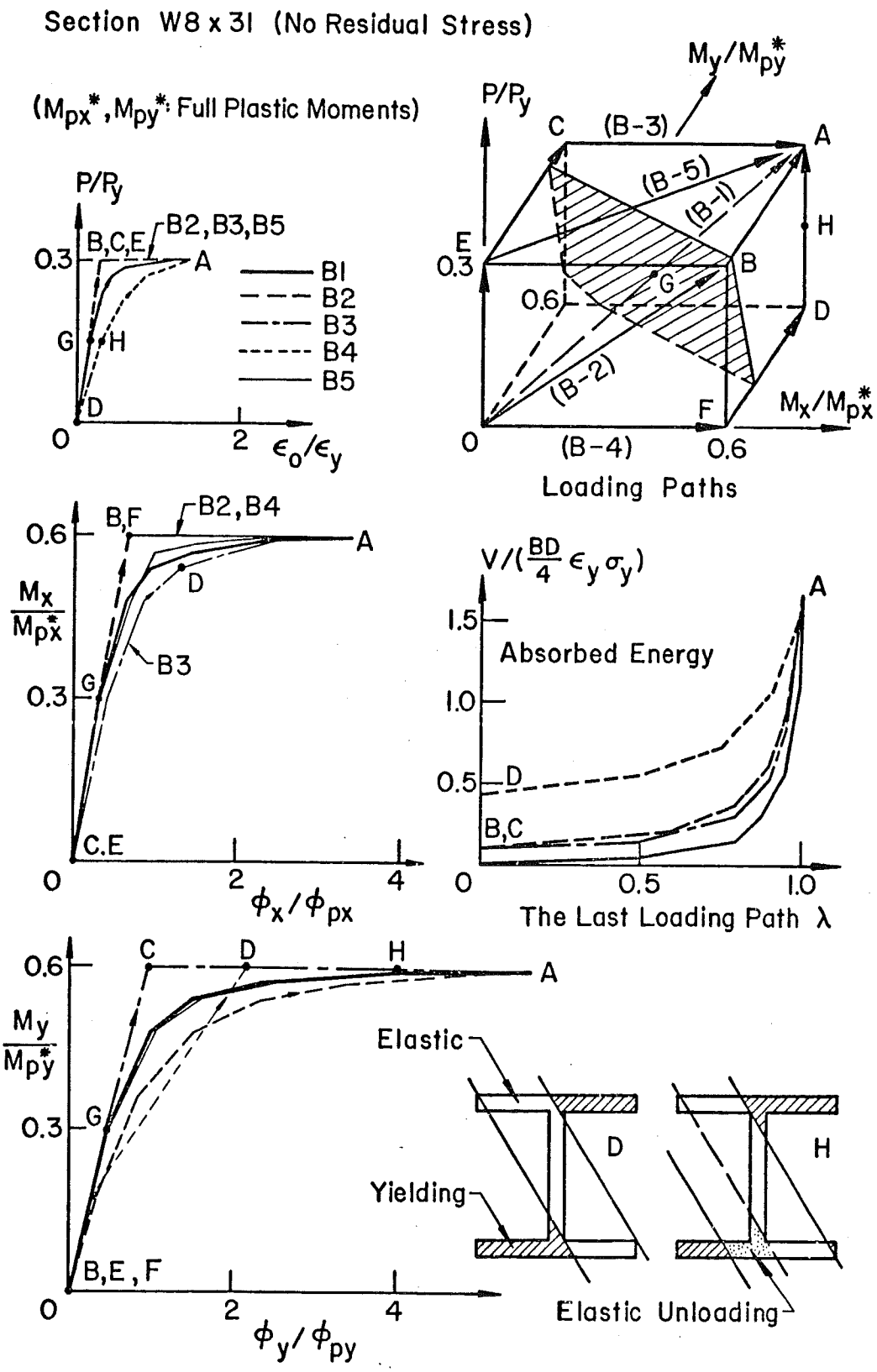

Fig. 8.8 Effect of Loading Paths

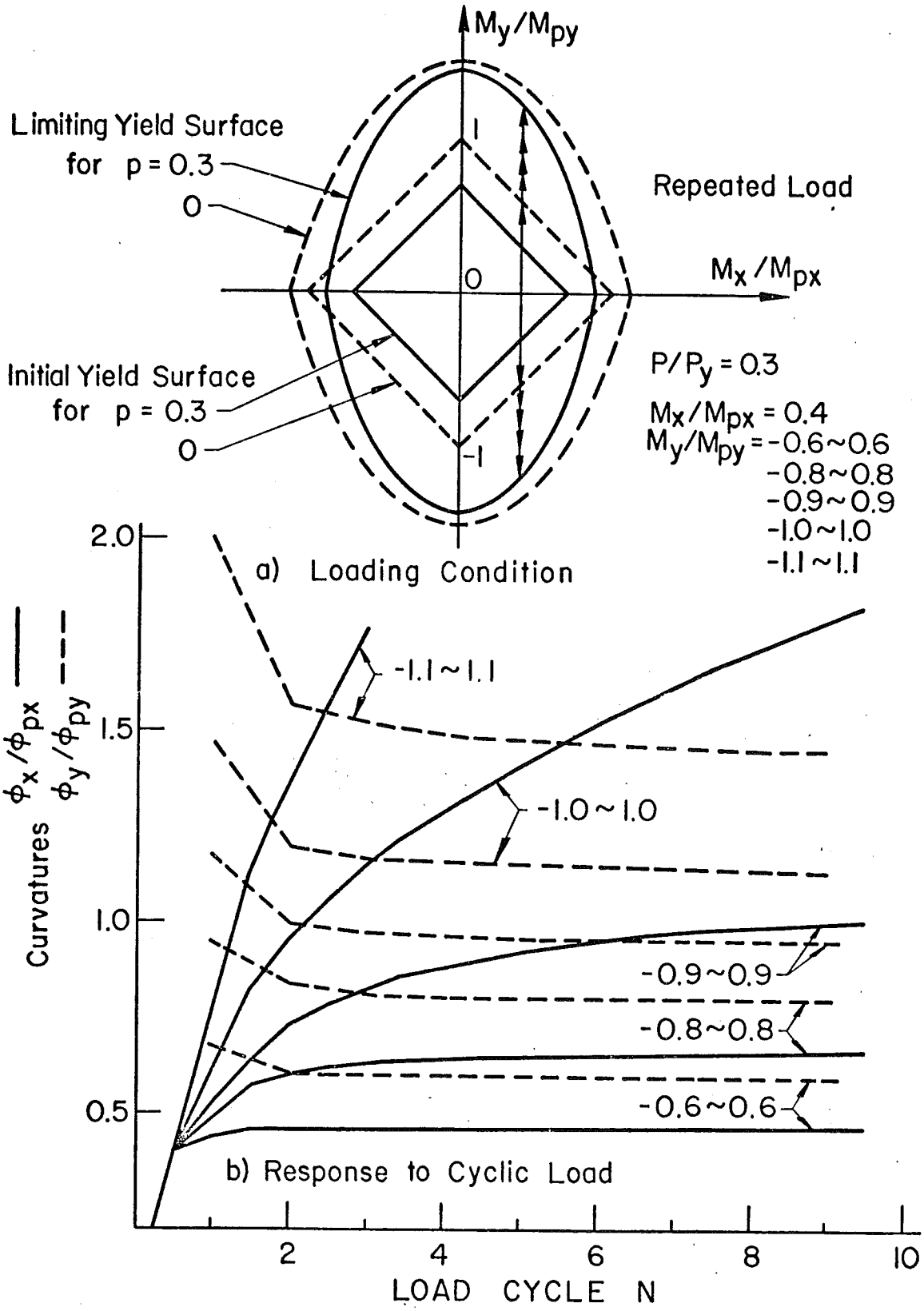

Fig. 8.9 Repeated Loading

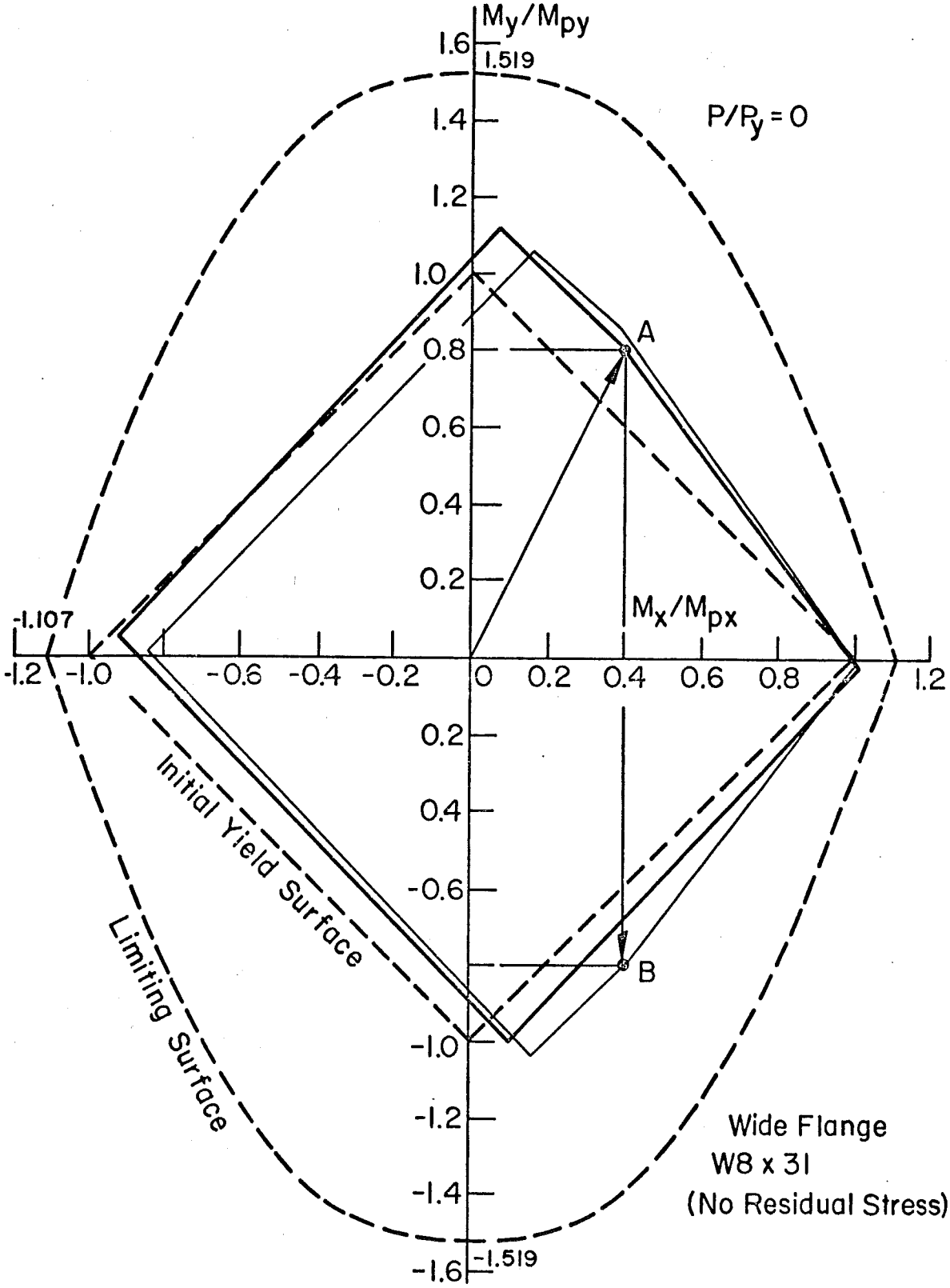

Fig. 8.10 Subsequent Yield Surface

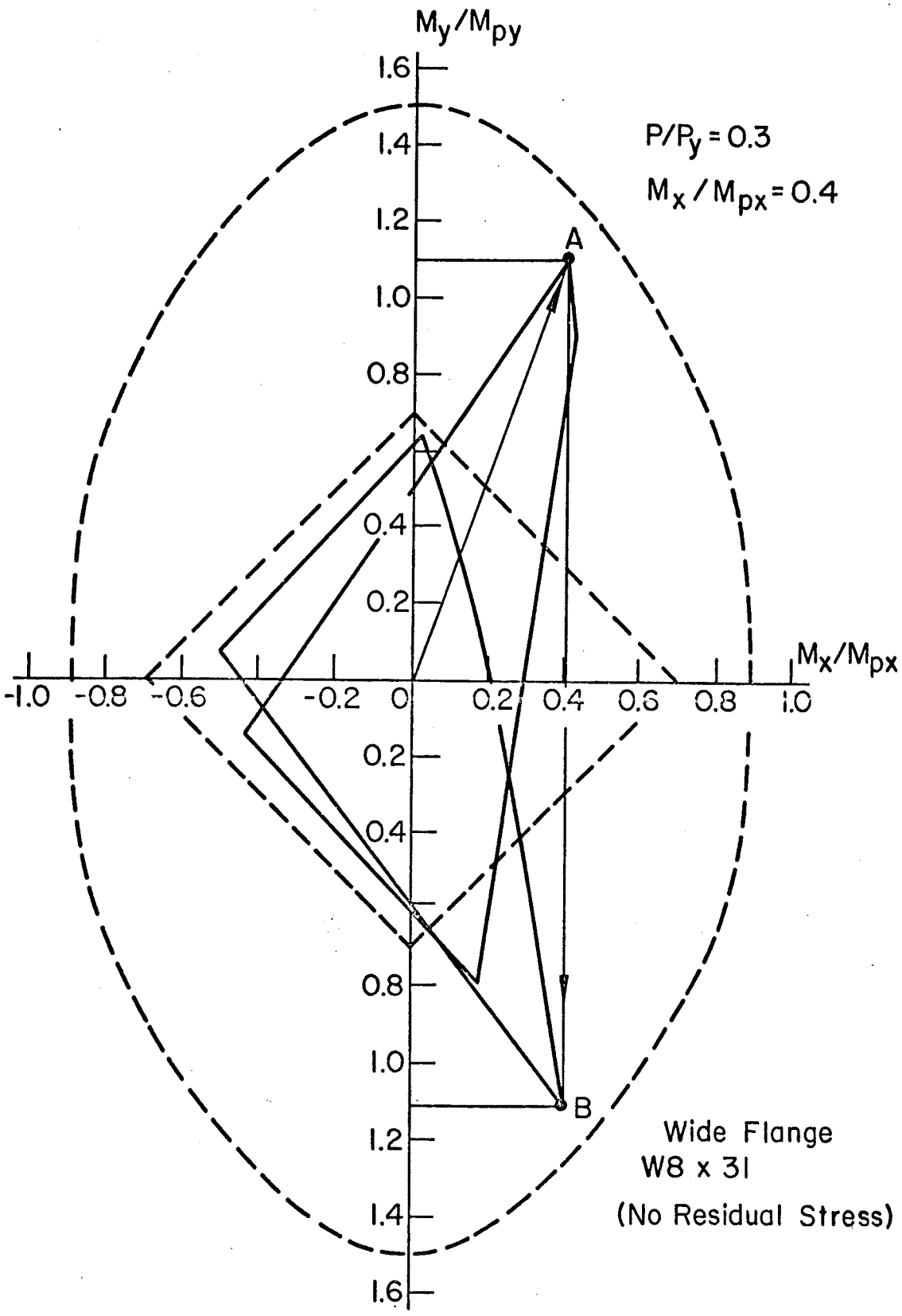

Fig. 8.11 Transformation of Subsequent Yield Surface

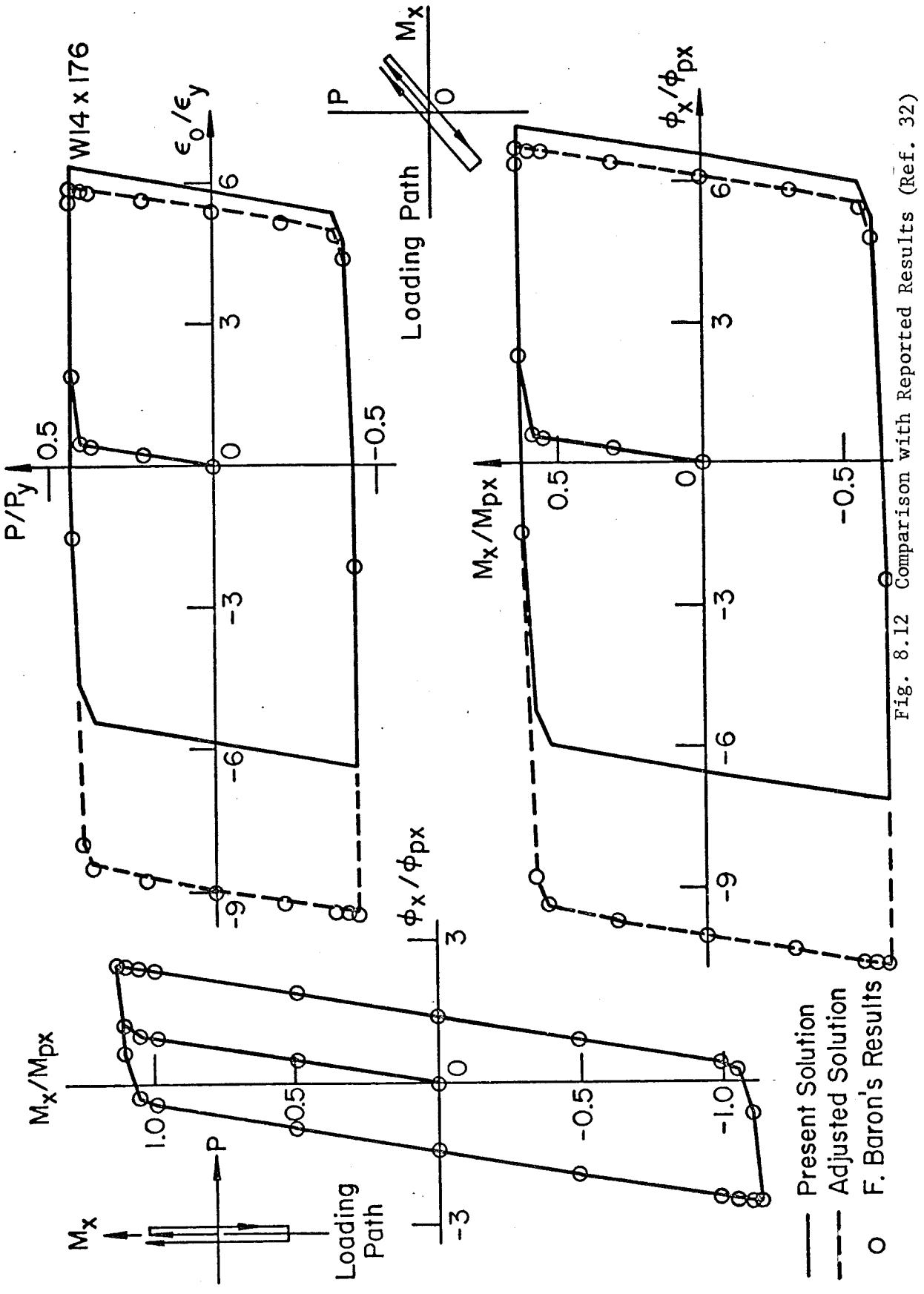

Fig. 8.12 Comparison with Reported Results (Ref. 32)

(C: Farthest Point from $\overline{OA}$)

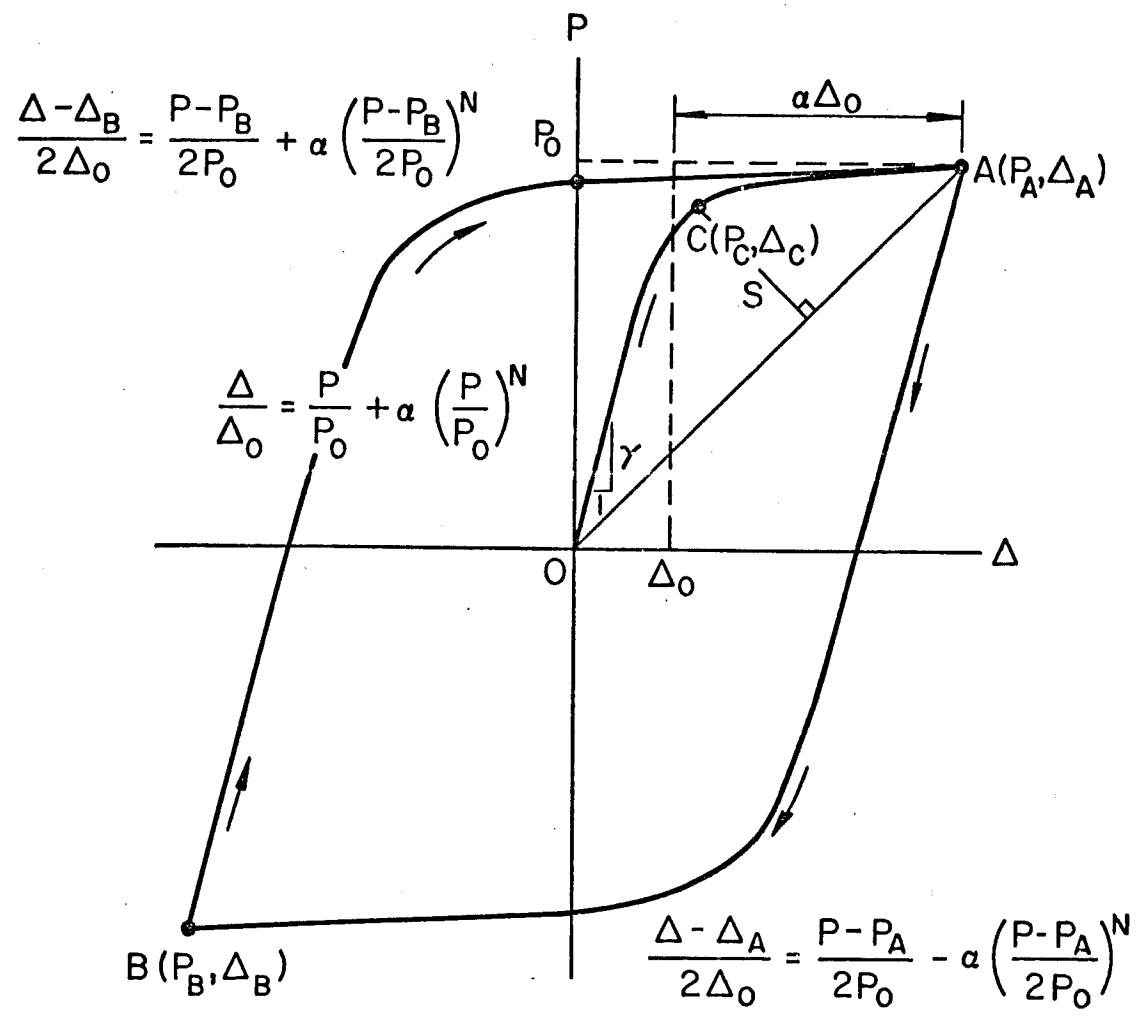

Fig. 8.13 Curve Fitting by a Ramberg-Osgood Function (Ref. 33)

$$\frac{\phi_x}{\phi_{xo}} = \frac{M_x}{M_{xo}} + \alpha\left(\frac{M_x}{M_{xo}}\right)^N$$

$\alpha = 4.38$ $\quad \phi_{xo} = 0.636\ \phi_{px}$

$N = 21$ $\quad M_{xo} = 0.594\ M_{px}$

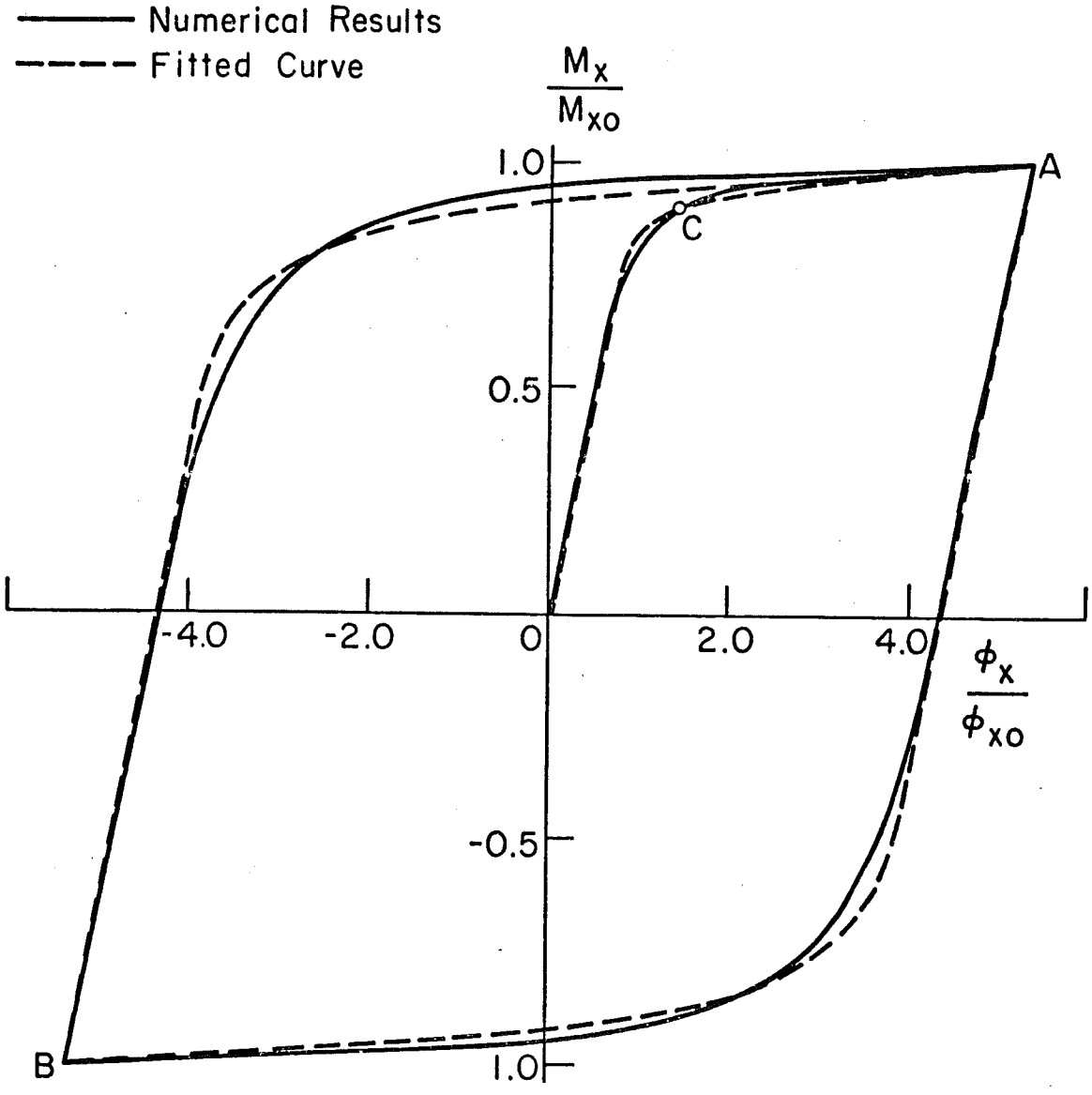

Fig. 8.14 Moment-Curvature Curve Fitting

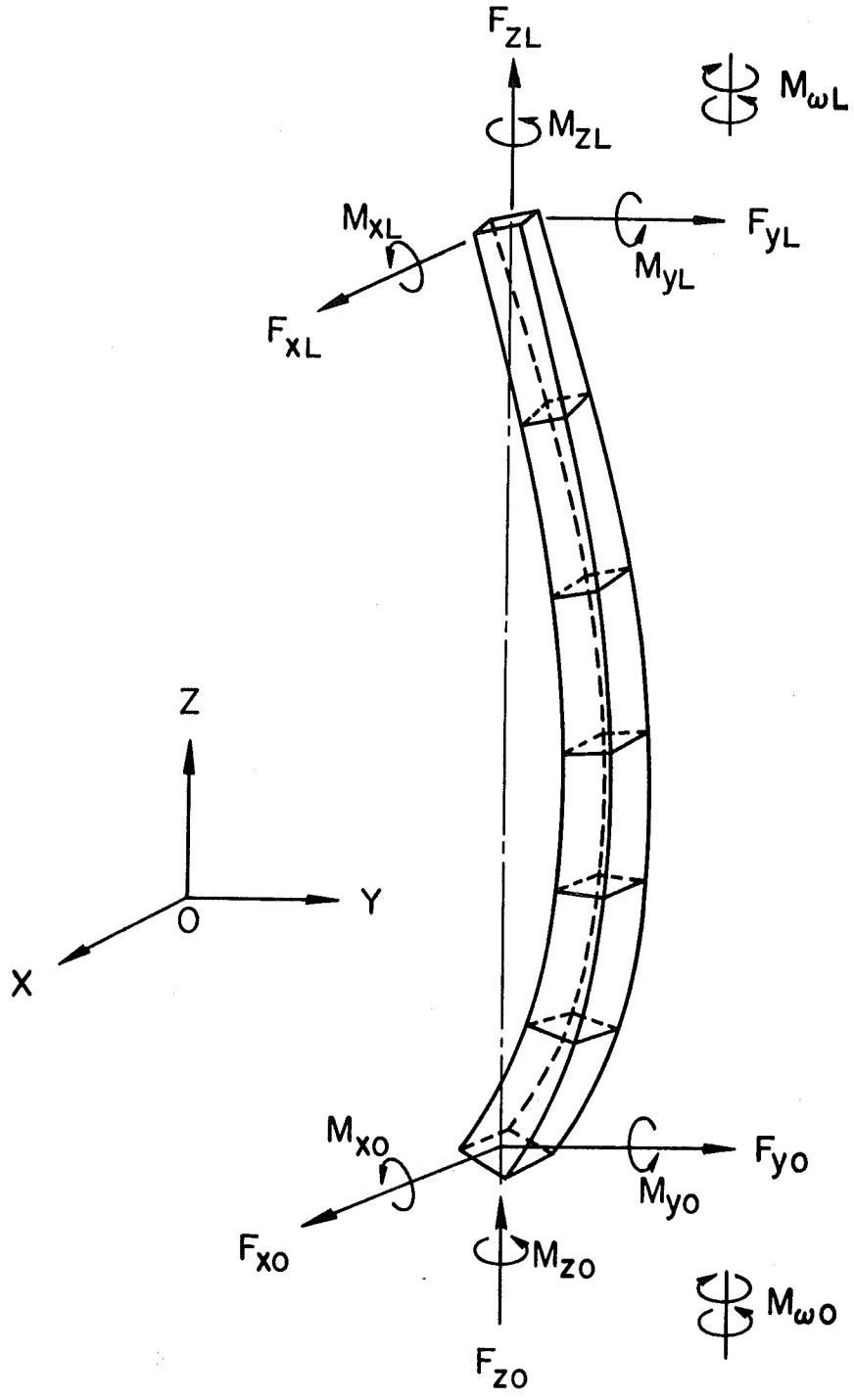

Fig. 9.1 Segmentation of Biaxially Loaded Column

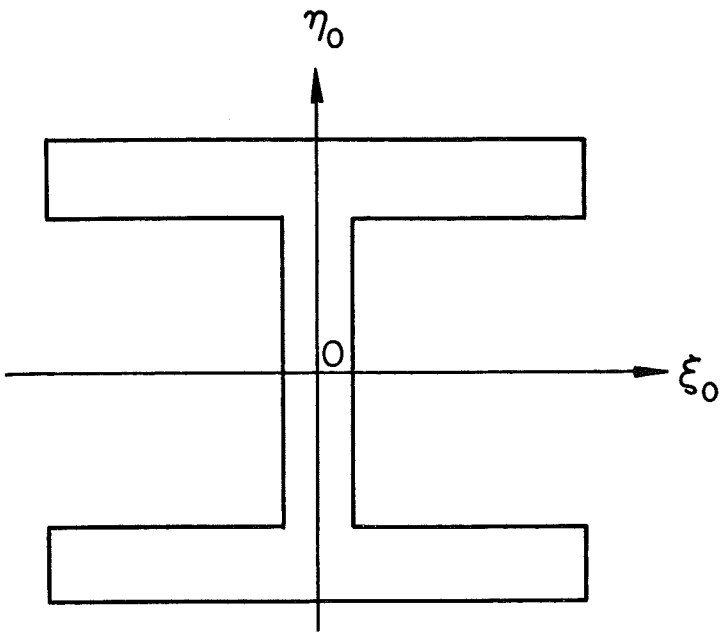

a) Initial Elastic State

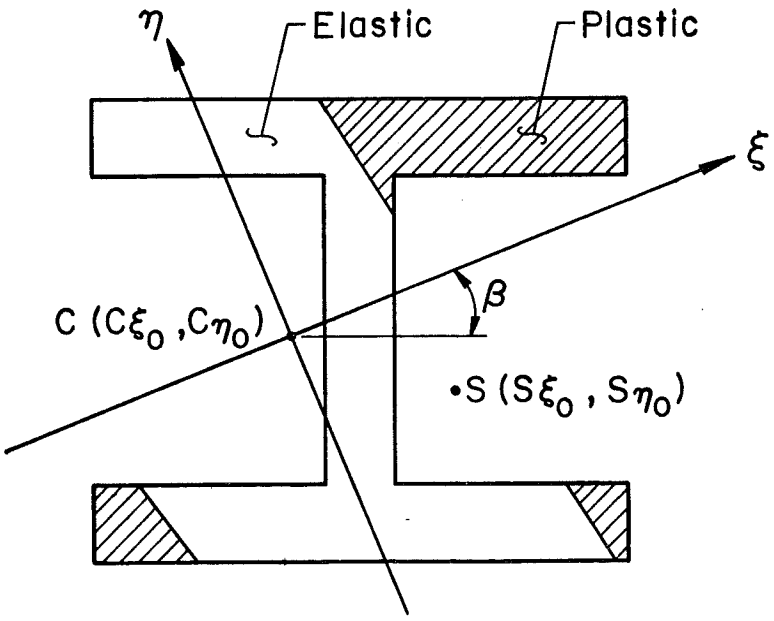

b) Elastic Plastic State

Fig. 9.2 Wide Flange and its Principal Axes

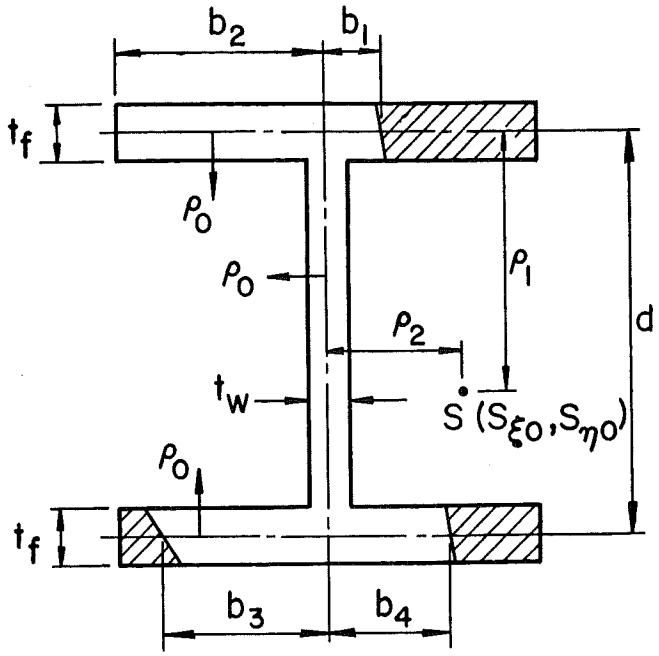

a) Idealization of Elastic Portion

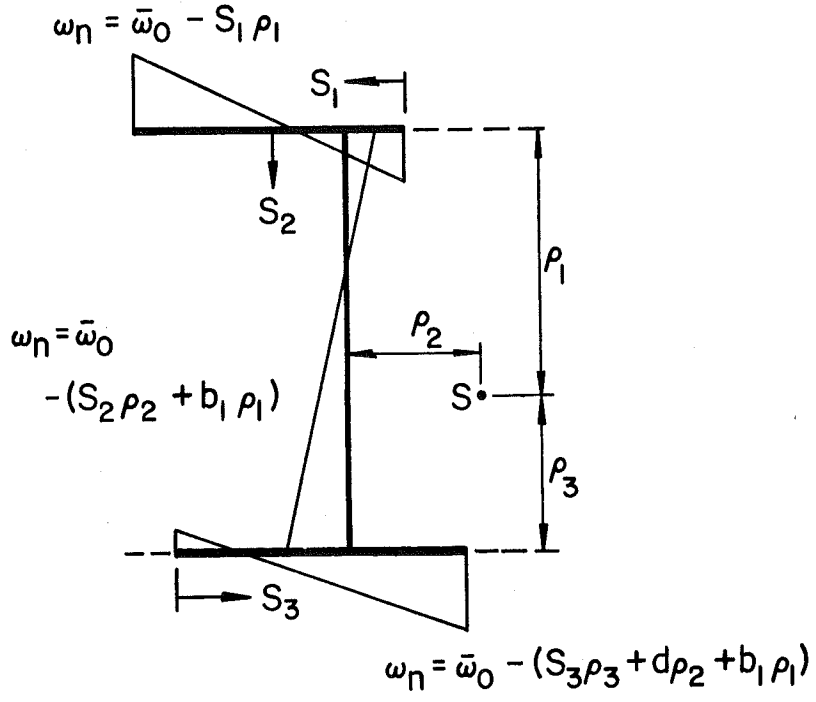

b) Normalized Warping About Point S

Fig. 9.3 Warping Distribution on Elastic Portion of Section

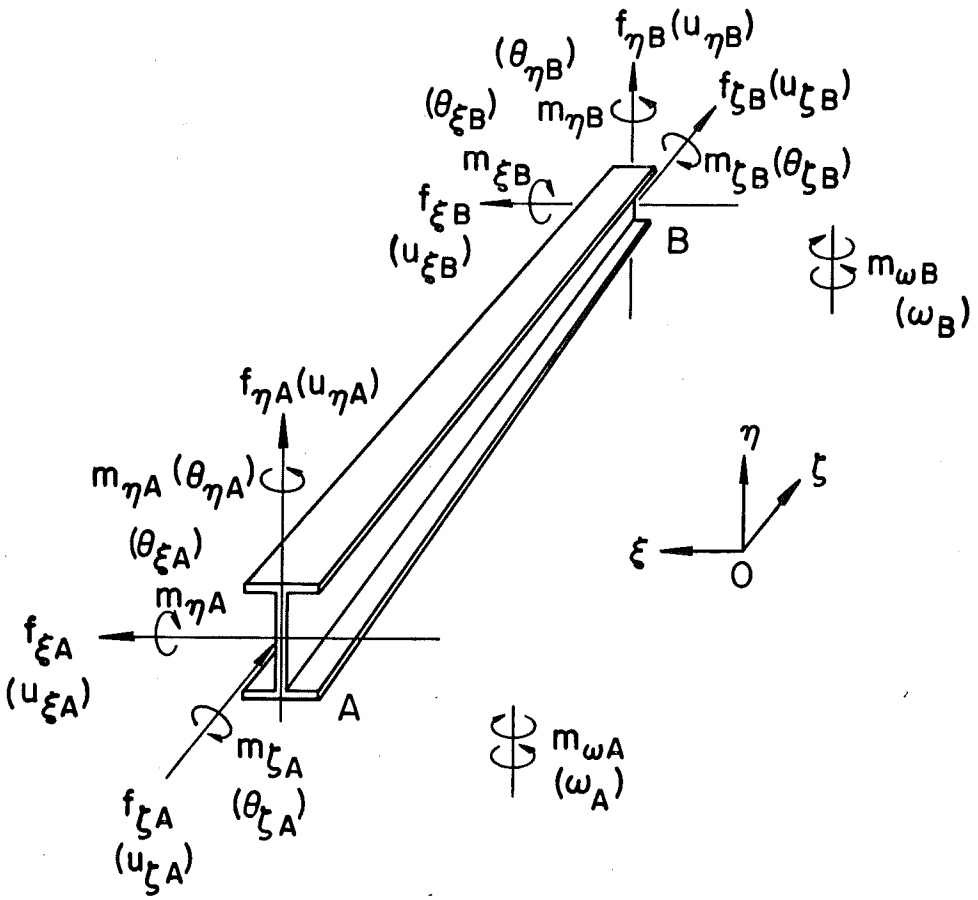

Fig. 9.4 Forces and Displacements of a Segment

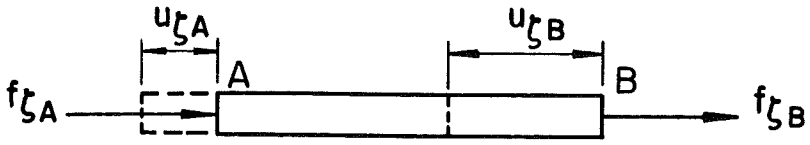

a) Axial Deformation

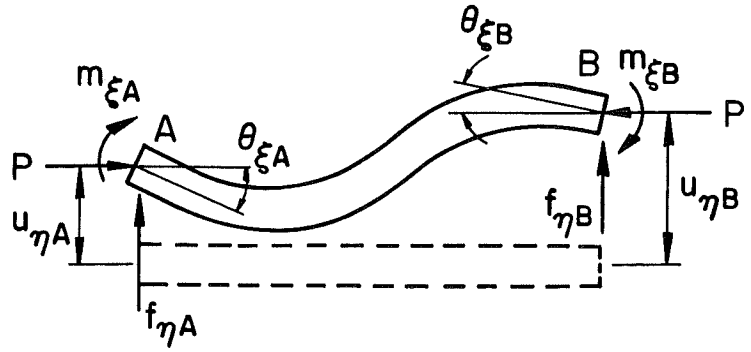

b) Bending and Shear Deformation

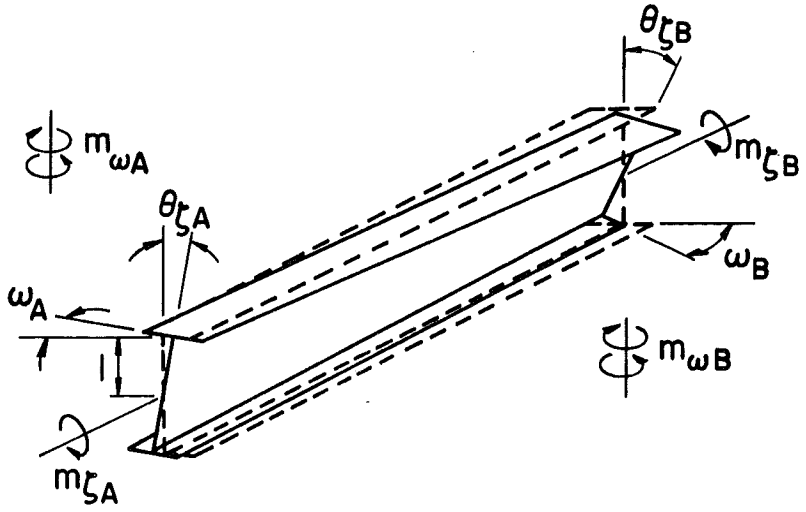

c) Torsion and Warping Deformation

Fig. 9.5 Independent Deformation of a Segment

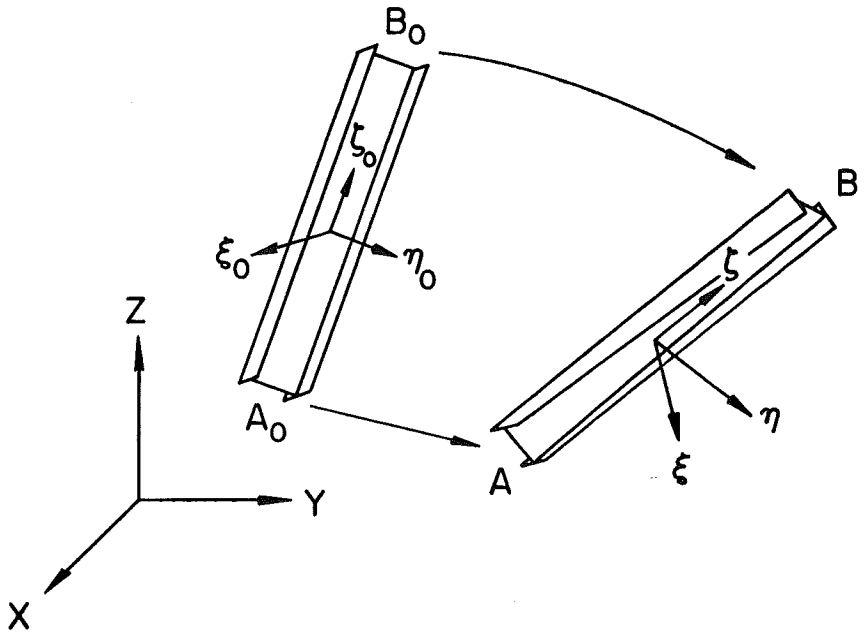

Fig. 9.6 Displacements of a Segment

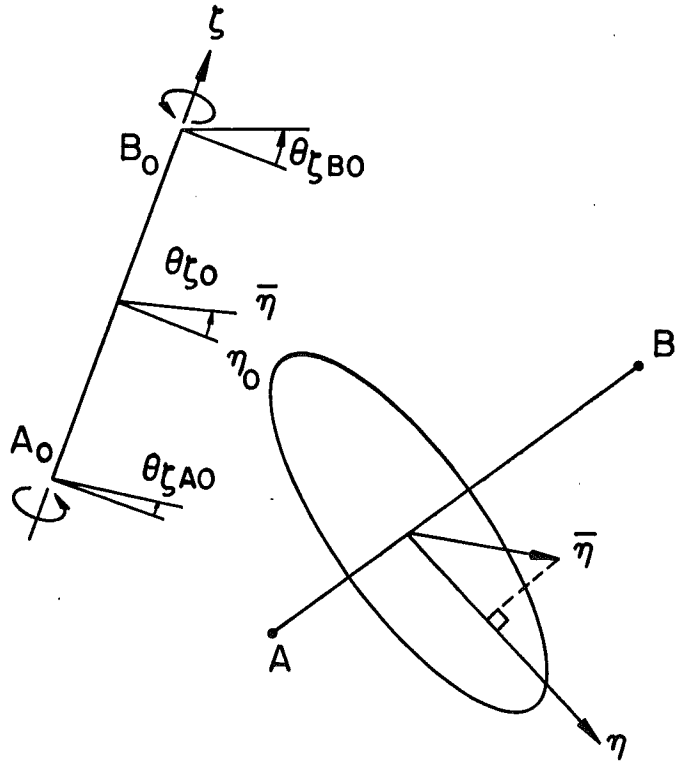

Fig. 9.7 Transformation of η-axis

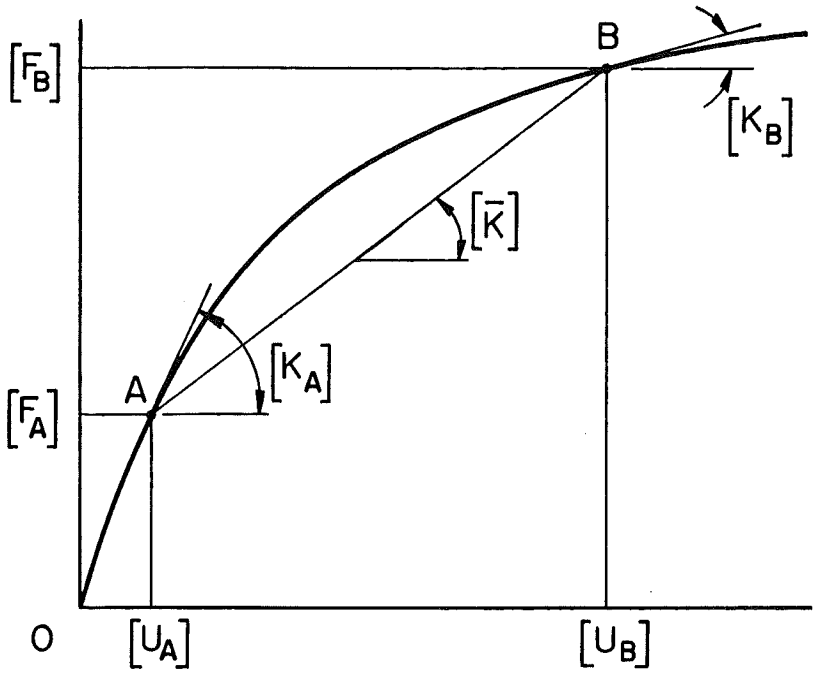

a) Stiffness Change and Second Stiffness

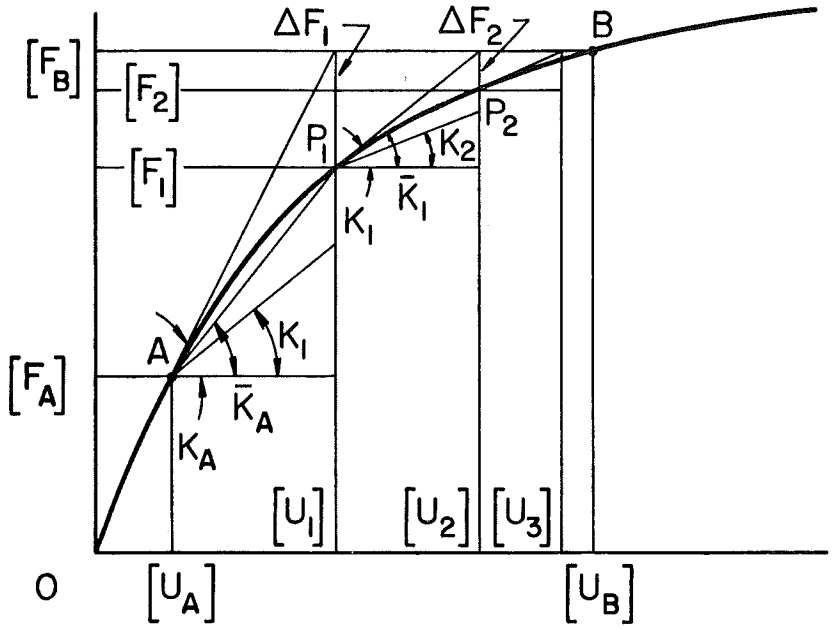

b) Iterative Procedure for Displacements $[U_B]$

Fig. 9.8 Modified Tangent Stiffness Approach

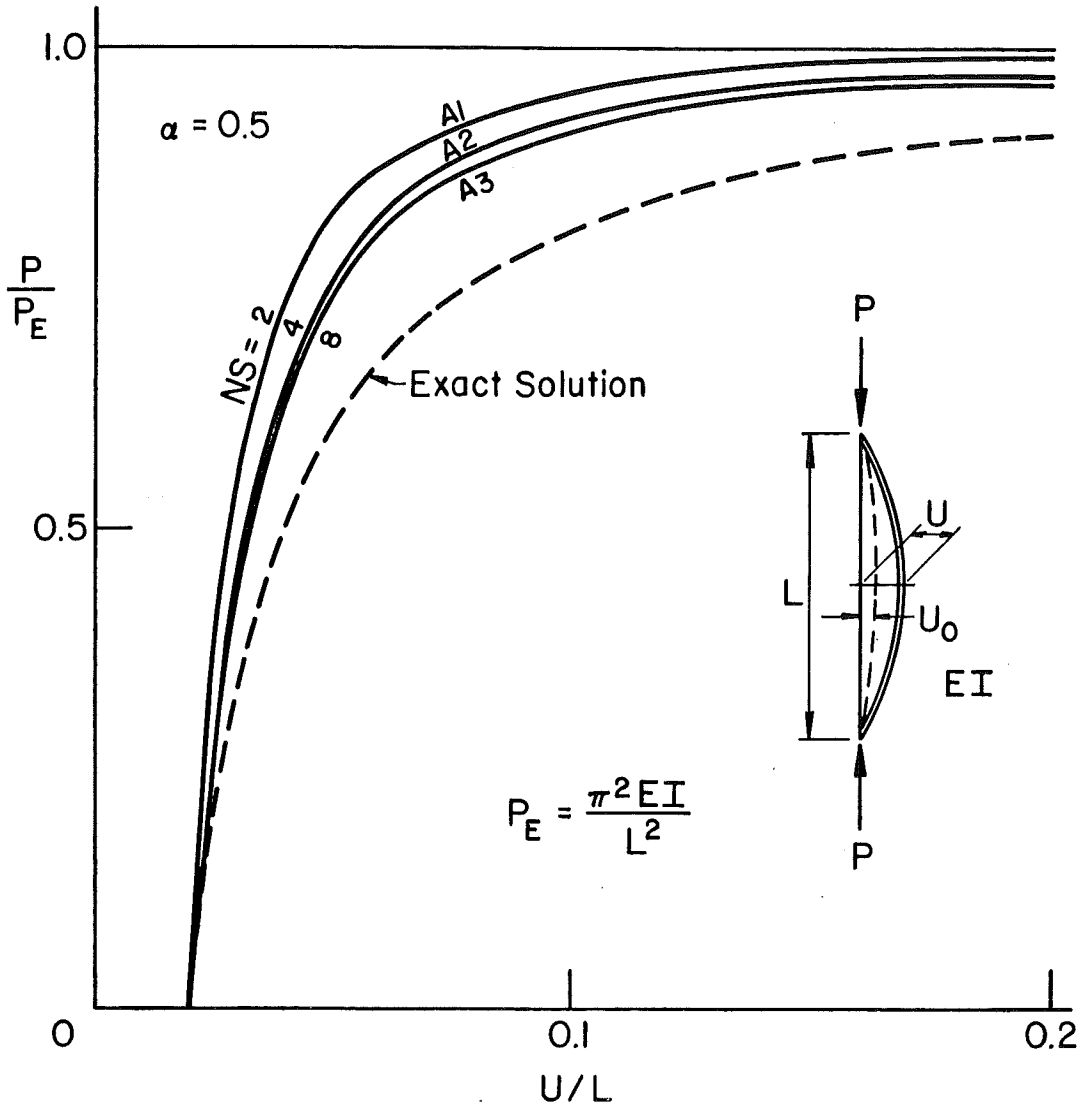

Fig. 9.9 Averaged Solution and Number of Segments

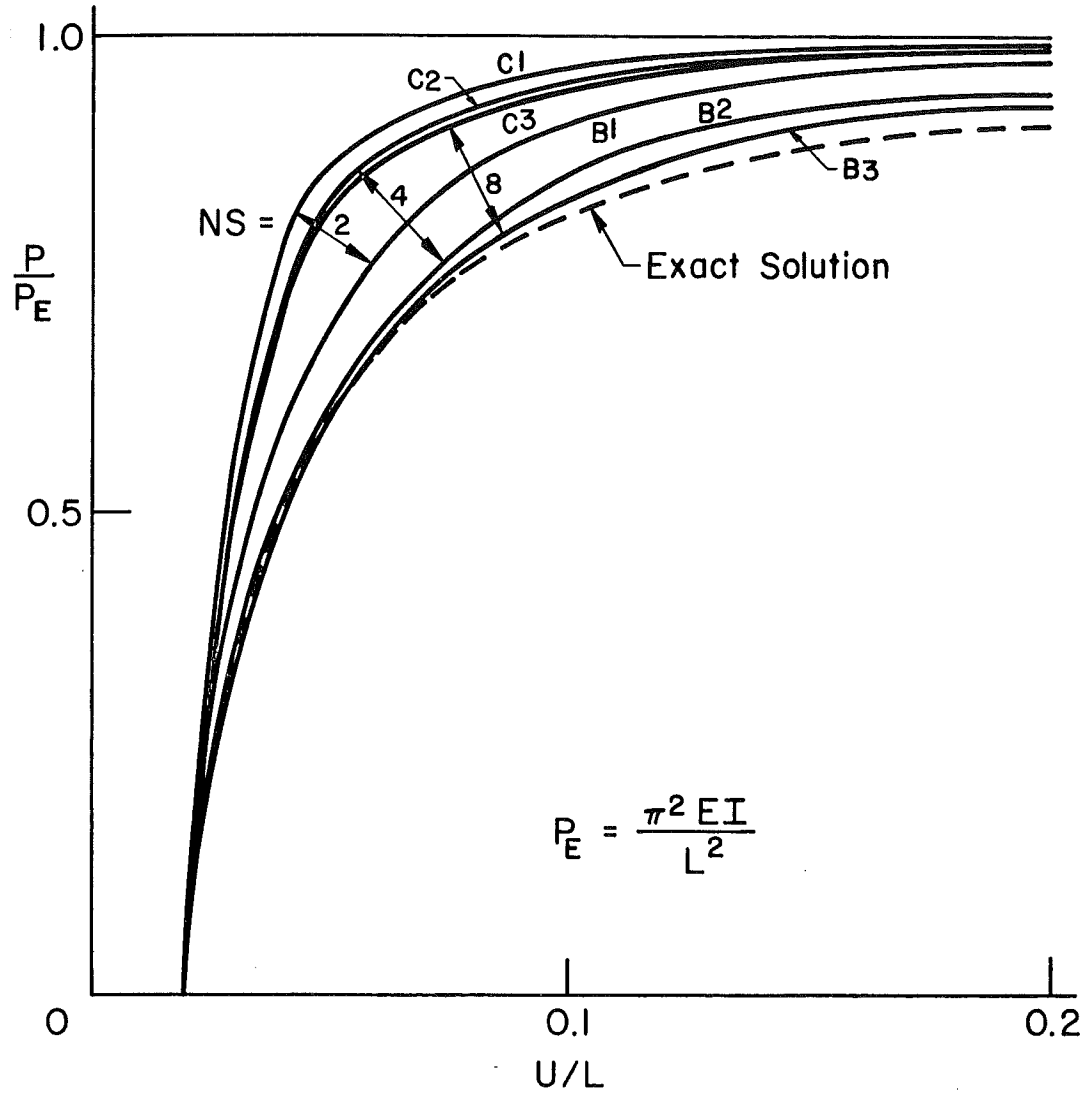

Fig. 9.10 Number of Segments and Boundaries of Solutions

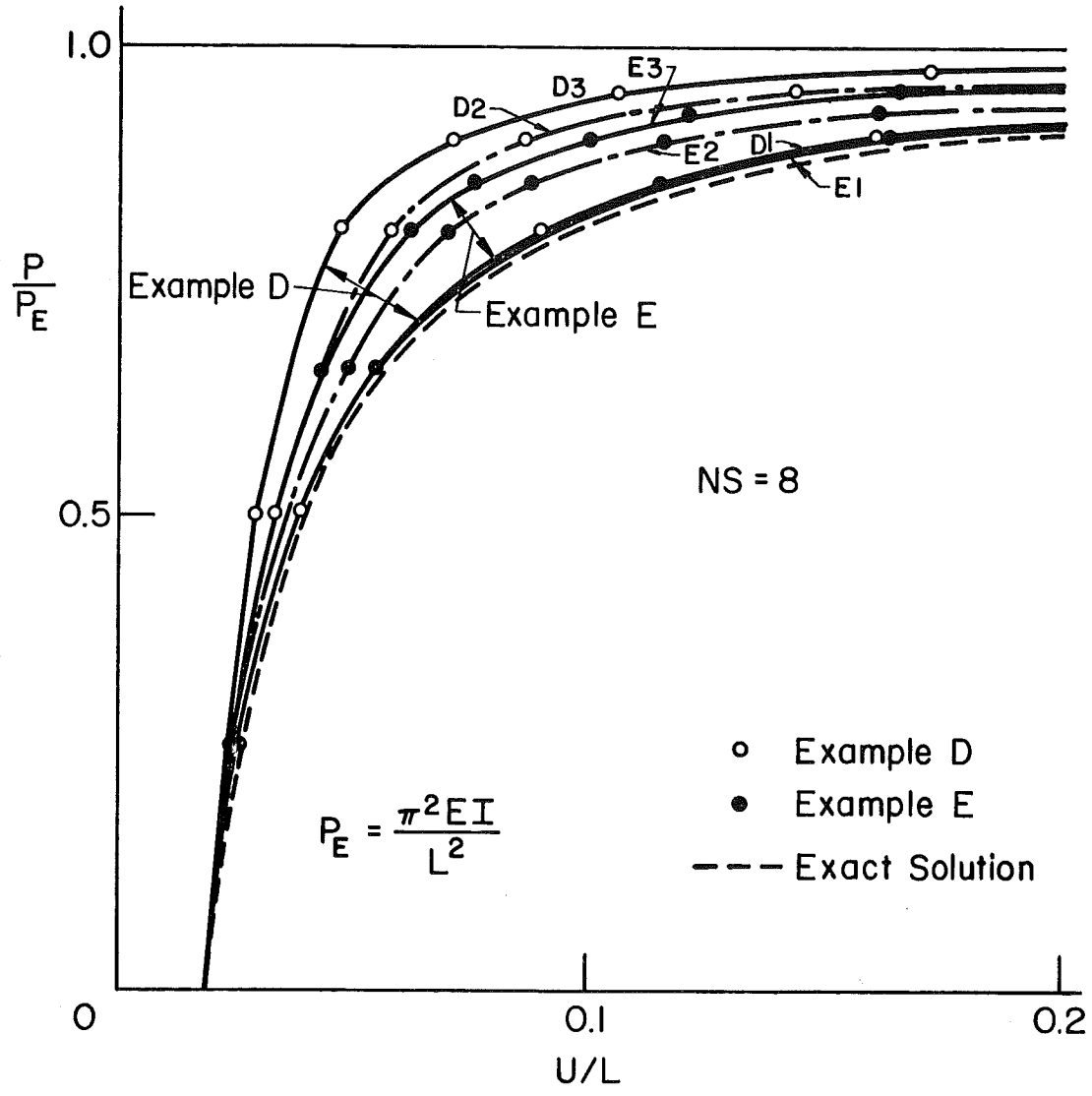

Fig. 9.11 Effect of Load Steps

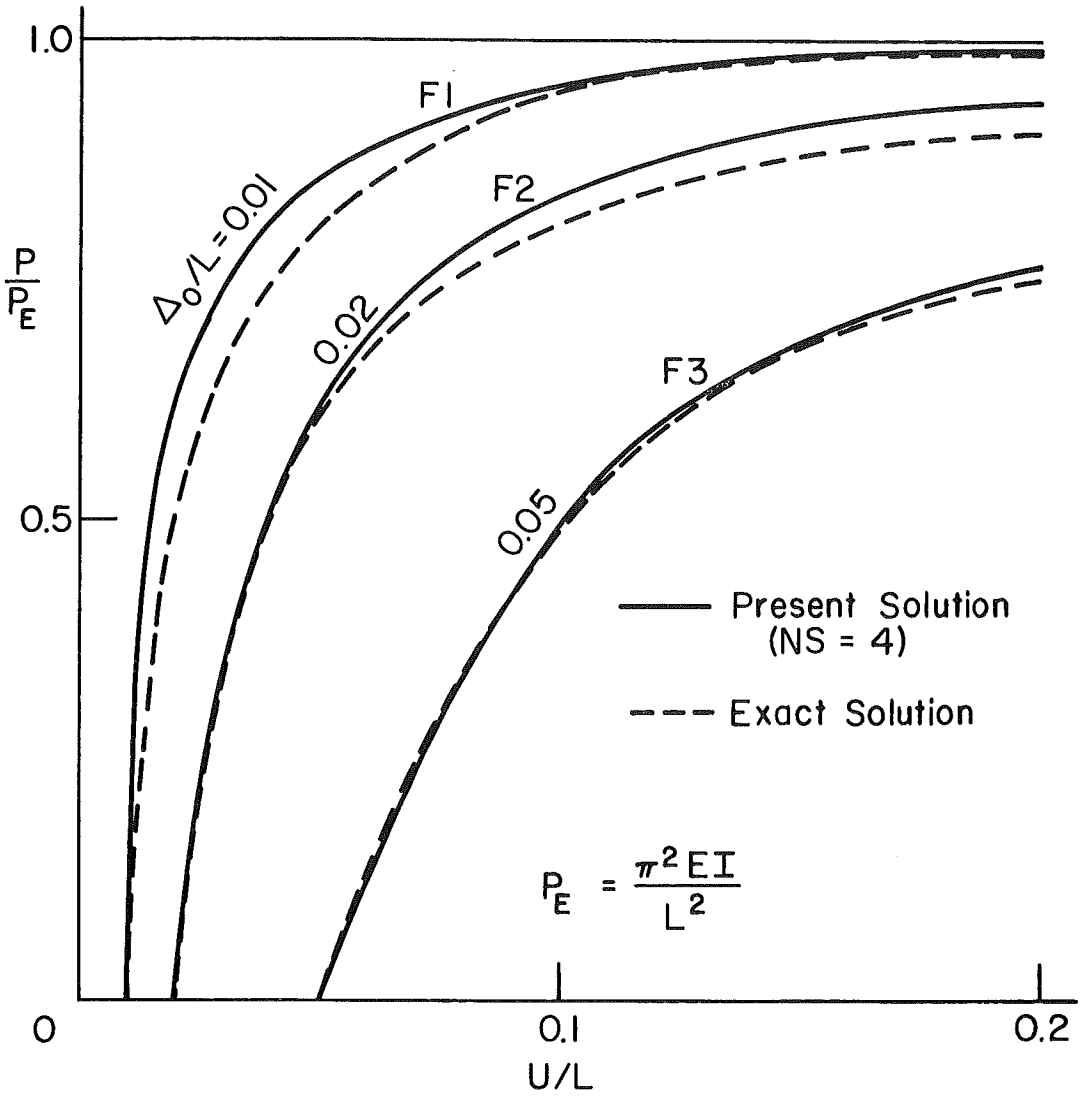

Fig. 9.12 Lower Bound Solution with Initial Deflection

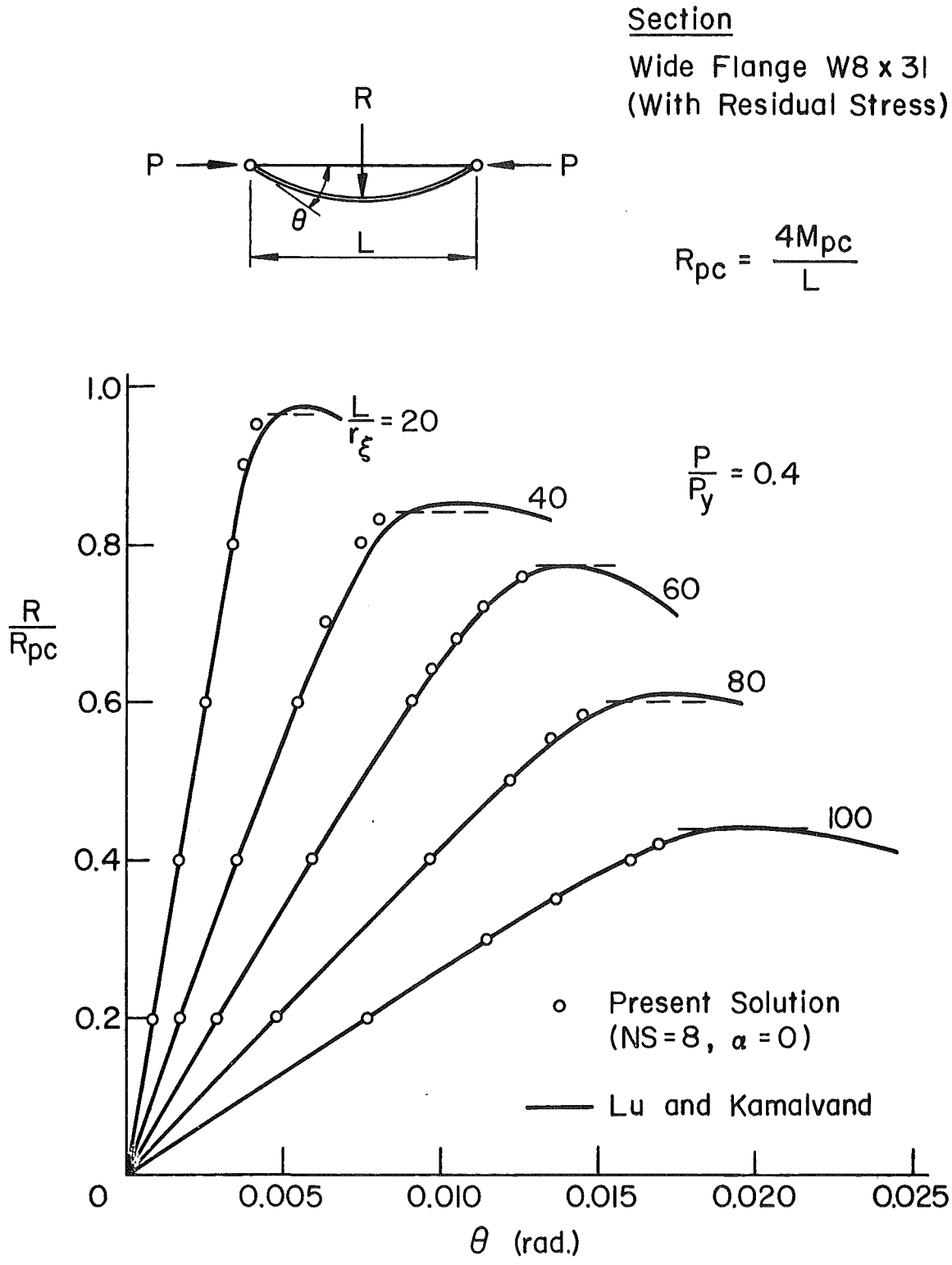

Fig. 9.13 Example of an In-Plane Beam-Columns

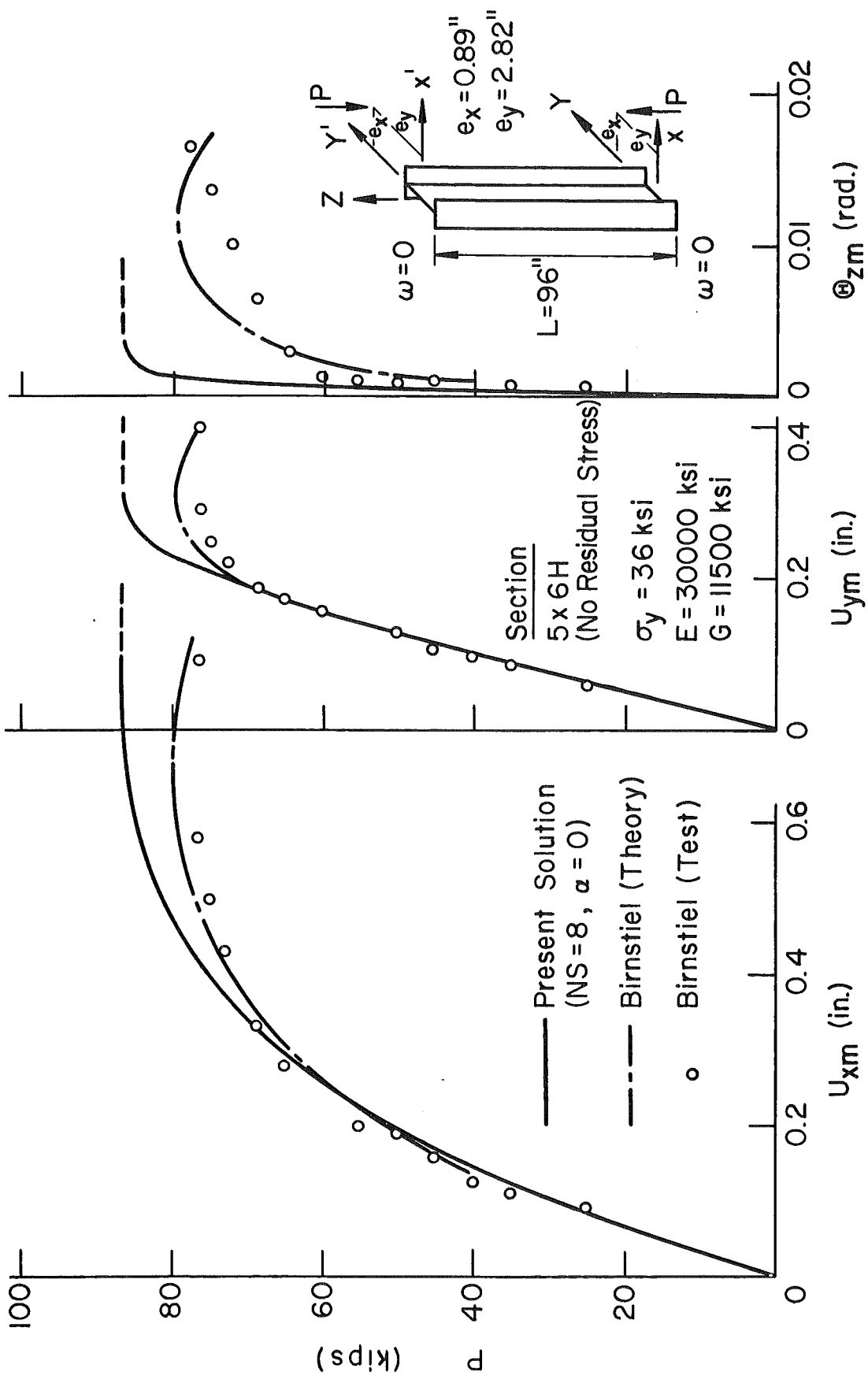

Fig. 9.14 Example of a Biaxially Loaded Column

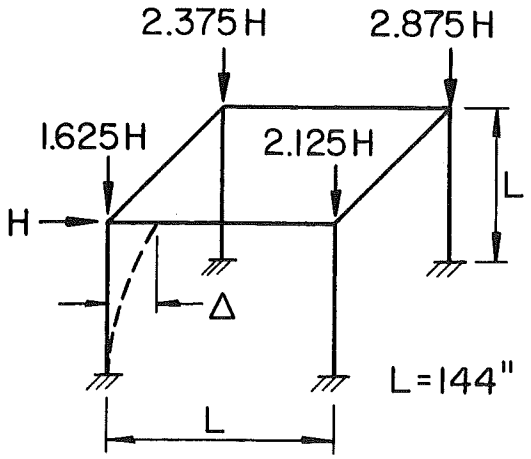

Sections

Beams W18 x 60
Columns W10 x 60

Material

σ_y = 34 ksi
E = 30000 ksi
G = 11500 ksi

a) Space Frame and Load

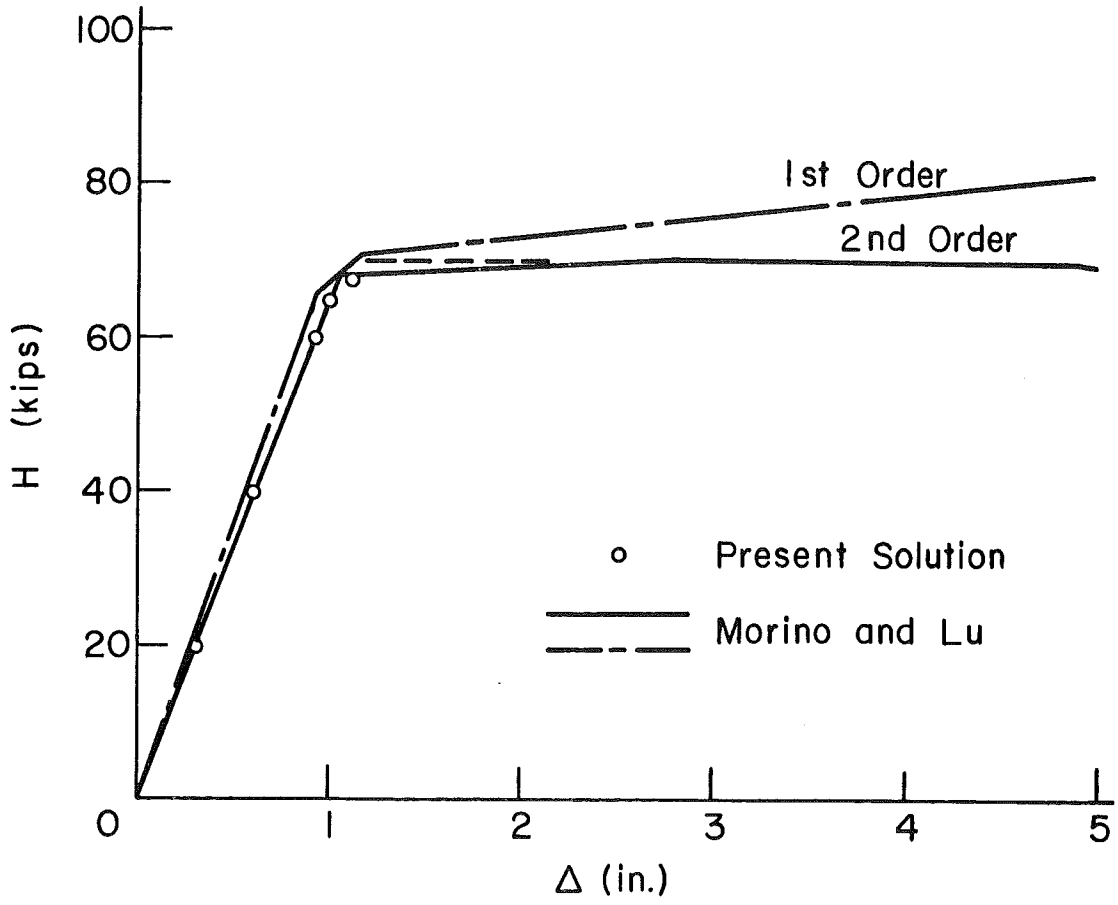

b) Numerical Results for Horizontal Deflection

Fig. 9.15 Example of a Space Frame

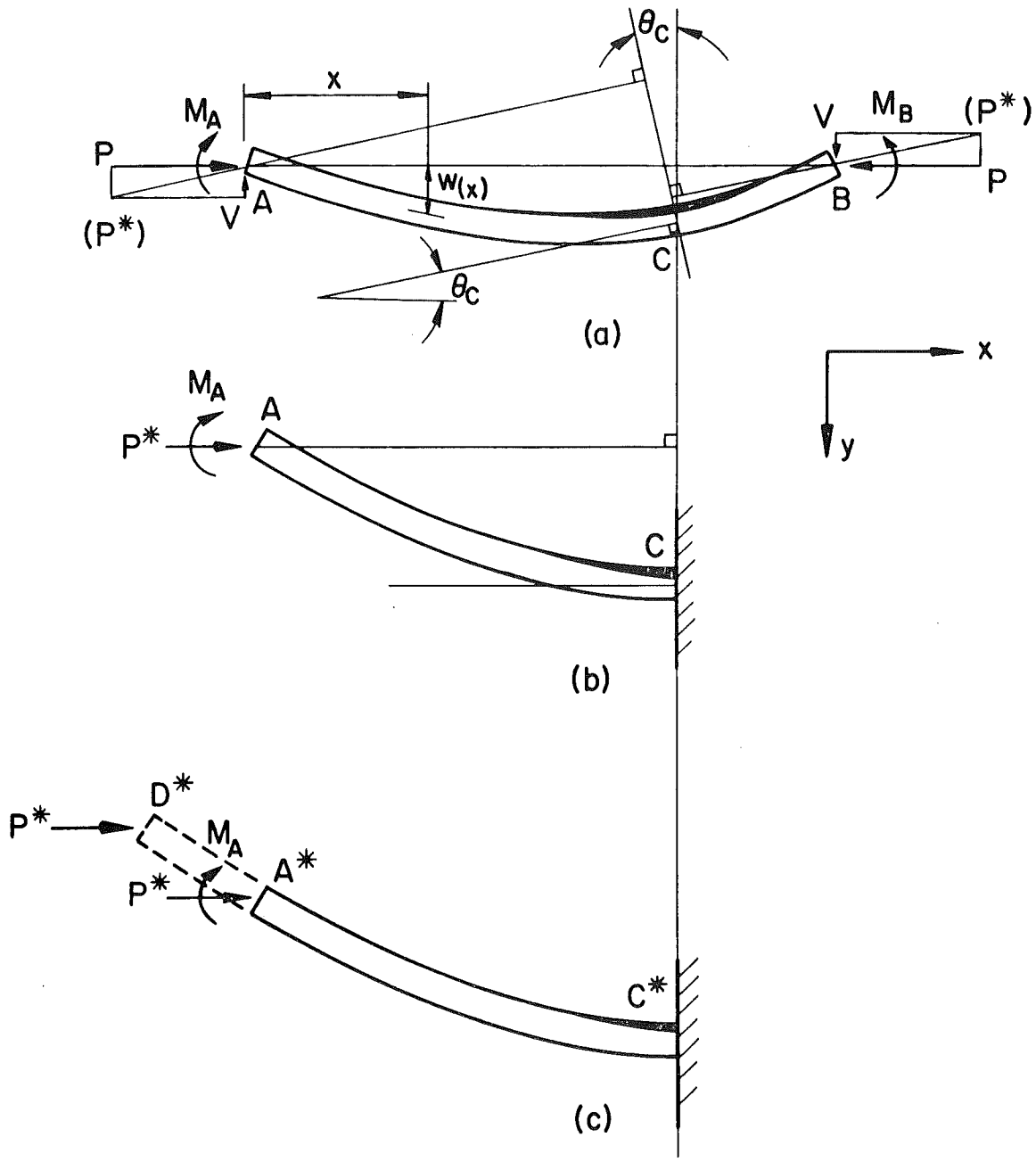

Fig. 11.1 Proof of the Equivalent Column

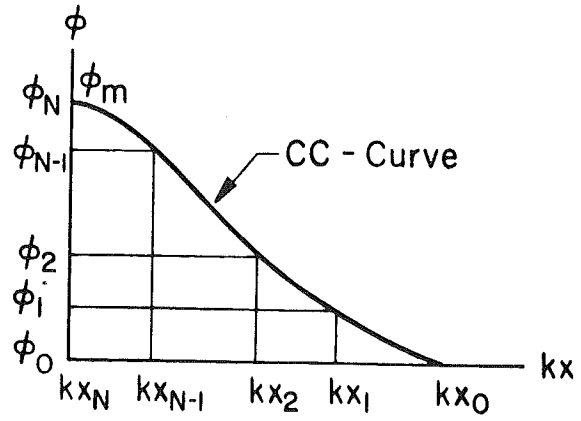

Fig. 11.2 Integration of Curvature Curve

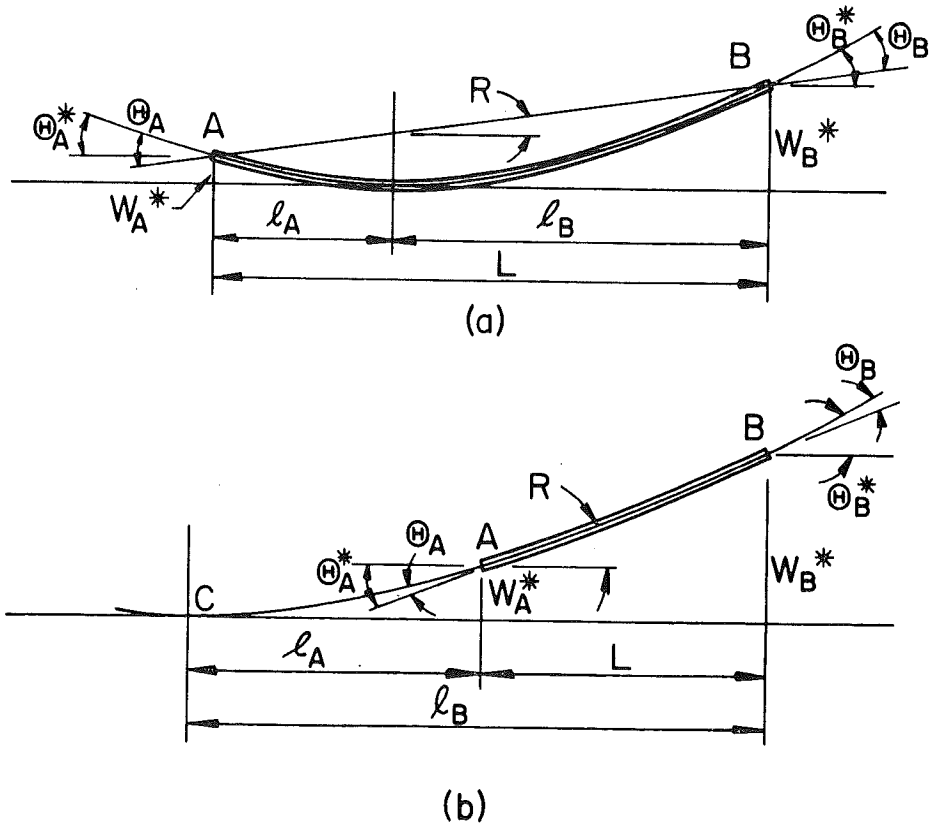

Fig. 11.3 End Rotation of Beam-Columns

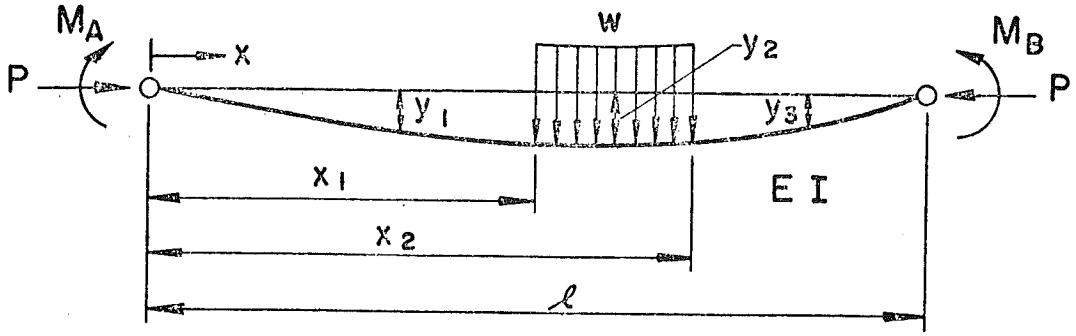

Fig. 11.4 Laterally Loaded Beam-Columns

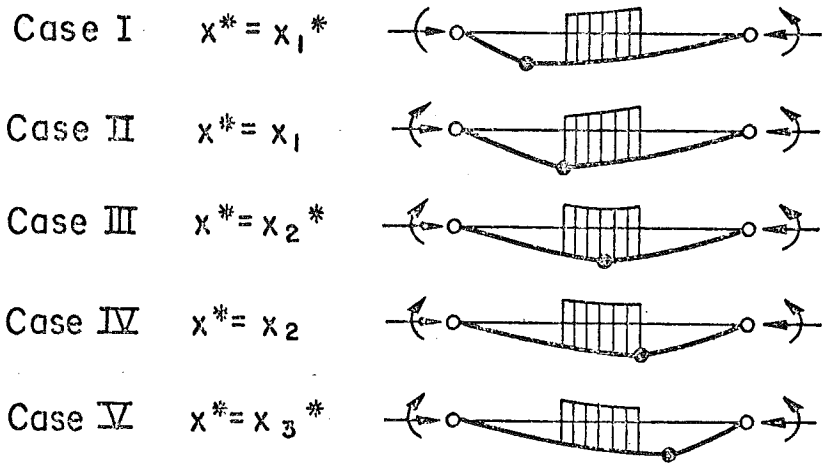

Fig. 11.5 Ultimate States

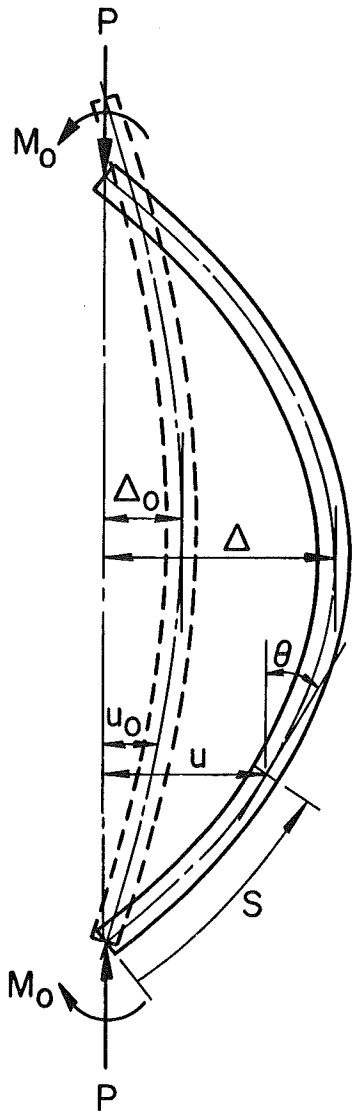

Fig. 11.6 Column with Initial Deflection

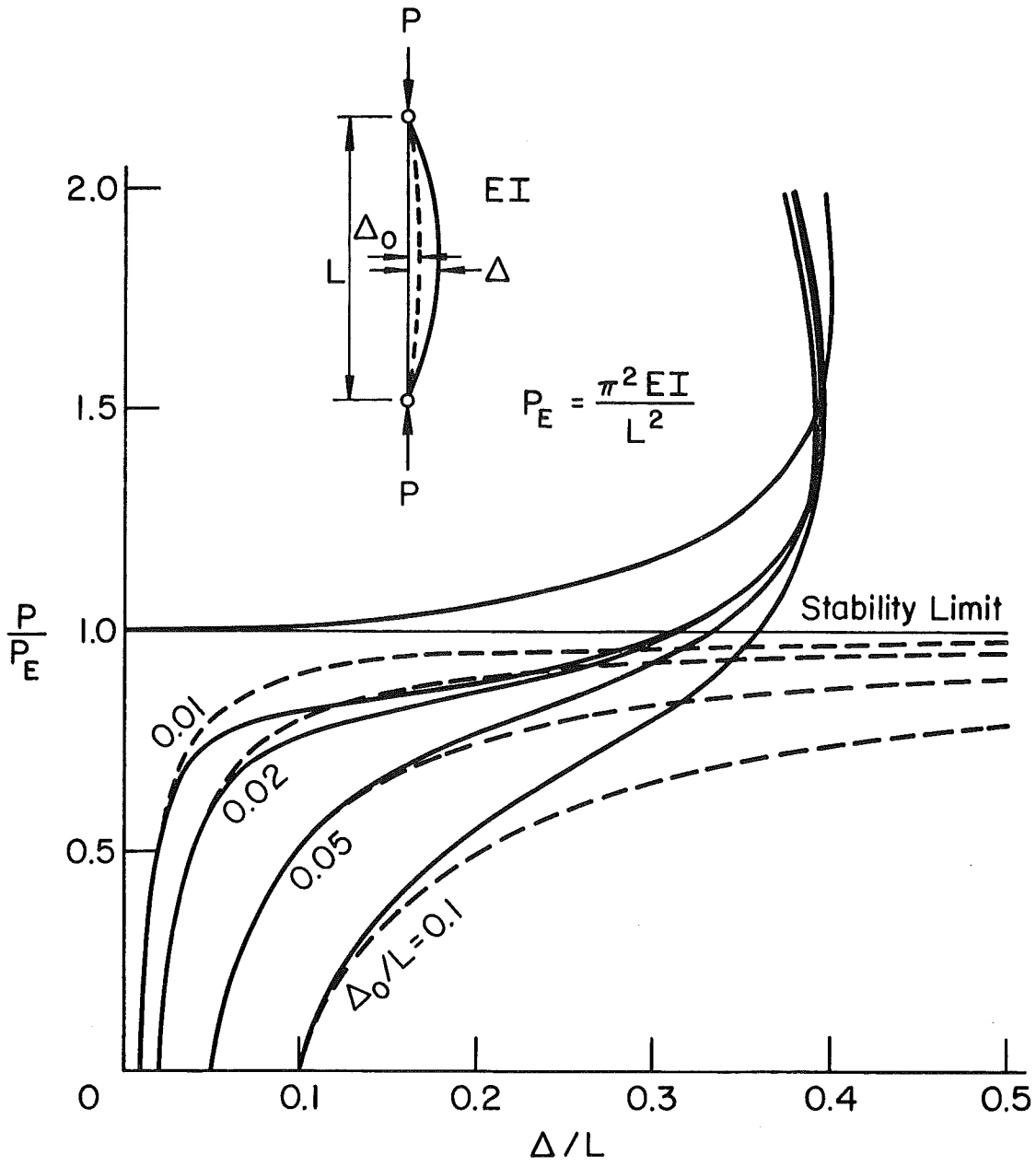

Fig. 11.7 Large Deflection of an Elastic Column

15. REFERENCES

1. Bleich, F.
   BUCKLING STRENGTH OF METAL STRUCTURES, McGraw-Hill, New York, 1952.

2. Timoshenko, S. P. and Gere, J. M
   THEORY OF ELASTIC STABILITY, 2nd Edition, McGraw-Hill, New York, 1961.

3. Chwalla, E.
   THEORIE DES AUSSERMITTIG GEDRUCKTEN STABBS AUS BAUSTAHL, Der Stahlbau, Vol. 7, October and November 1934.

4. Chen, W. F. and Snatathadaporn, S.
   REVIEW OF COLUMN BEHAVIOR UNDER BIAXIAL LOADING, Journal of the Structural Division, ASCE, Vol. 94, No. ST12, Proc. Paper 6316, December 1968, pp. 2999-3021.

5. Chen, W. F.
   FURTHER STUDIES OF INELASTIC BEAM-COLUMN PROBLEMS, Journal of the Structural Division, ASCE, Vol. 97, No. ST2, February 1971.

6. Chen, W. F.
   GENERAL SOLUTION OF INELASTIC BEAM-COLUMN PROBLEM, Journal of the Engineering Mechanics Division, ASCE, Vol. 96, No. EM4, August, 1970.

7. Chen, W. F. and Santathadaporn, S.
   CURVATURE AND THE SOLUTION OF ECCENTRICALLY LOADED COLUMNS, Journal of the Engineering Mechanics Division, Vol. 95, No. EM1, February 1969.

8. Chen, W. F.
   APPROXIMATE SOLUTION OF BEAM-COLUMNS, Journal of the Structural Division, ASCE, Vol. 97, No. ST2, February 1971.

9. Lu, L. W. and Kamalvand, H.
   ULTIMATE STRENGTH OF LATERALLY LOADED COLUMNS, Journal of the Structural Division, ASCE, Vol. 94, No. ST4, June 1968.

10. Yokel, F. Y.
    STABILITY AND LOAD CAPACITY OF MEMBERS WITH NO TENSILE STRENGTH, Journal of the Structural Division, ASCE, Vol. 97, No. ST7, July 1971.

11. Chen, A. C. T. and Chen, W. F.
SOLUTIONS TO VARIOUS REINFORCED CONCRETE BEAM-COLUMN PROBLEMS, Fritz Engineering Laboratory Report No. 370.2, Lehigh University, Bethlehem, Pa., September 1970.

12. Chen, W. F. and Chen, C. H.
ANALYSIS OF CONCRETE-FILLED STEEL TUBULAR BEAM-COLUMNS, Fritz Engineering Laboratory Report No. 370.10, Lehigh University, Bethlehem, Pa., October 1971.

13. Santathadaporn, S. and Chen, W. F.
INTERACTION CURVES FOR SECTIONS UNDER COMBINED BIAXIAL BENDING AND AXIAL FORCE, WRC Bulletin No. 148, February 1970.

14. Morris, G. A. and Fenves, S. J.
APPROXIMATE YIELD SURFACE EQUATIONS, Journal of the Engineering Mechanics Division, ASCE, Vol. 95, No. EM4, Proc. Paper 6741, August 1969, pp. 937-954.

15. Birnstiel, C.
EXPERIMENTS ON H-COLUMNS UNDER BIAXIAL BENDING, Journal of the Structural Division, ASCE, Vol. 94, No. ST10, Proc. Paper 6186, October 1968, pp. 2429-2449. (Research Division Report, School of Engineering and Science, New York University, The Bronx, N. Y., January 1967).

16. Birnstiel, C. and Michalos, J.
ULTIMATE LOAD OF H-COLUMNS UNDER BIAXIAL BENDING, Journal of the Structural Division, ASCE, Vol. 89, No. ST2, Proc. Paper 3503, April 1963.

17. Syal, I. C. and Sharma, S. S.
ELASTIC BEHAVIOR OF BIAXIALLY LOADED STEEL COLUMNS, Journal of the Structural Division, ASCE, Vol. 96, No. ST3, Proc. Paper 7143, March 1970, pp. 469-486.

18. Vogel, U.
TRAGLASTVERSUCHE AN EINGESPANNTEN GESCHOSSSTÜTZEN MIT KASTEN-QUERSCHNITT BIEGUNG UM BEIDE HANPTACHSEN, Die Bautechnik, August 1970.

19. Vogel, U. and Zimmermann, W.
TRAGLASTVERSUCHE AN EINGESPANNTEM GESCHOSSSTÜTZEN MIT I-QUERSCHNITT BEI BIEGUNG UM BEIDE HANPTACHSEN, International Association for Bridge and Structural Engineering, Vo. 28-I, 1968.

20. Santathadaporn, S. and Chen, W. F.
ANALYSES OF BIAXIALLY LOADED COLUMNS, Fritz Engineering Laboratory Report No. 331.12, Lehigh University, Bethlehem, Pa., September 1970.

21. Tezcan, S. and Mahaptra, B. C.
TANGENT STIFFNESS MATRIX FOR SPACE FRAME MEMBERS, Journal of the Structural Division, ASCE, Vol. 95, No. ST6, Proc. Paper 6627, June 1969, pp. 1257-1270.

22. Gurfinkel, German
ANALYSIS OF FOOTINGS SUBJECTED TO BIAXIAL BENDING, Journal of the Structural Division, ASCE, Vol. 96, No. ST6, Proc. Paper 7329, June 1970, pp. 1049-1059.

23. Santathadaporn, S. and Chen, W. F.
TANGENT STIFFNESS METHOD FOR BIAXIAL BENDING, Journal of the Structural Division, ASCE, Vol. 98, No. ST1, January 1972.

24. Pillai, U. S.
BEAM-COLUMNS, Preparatory Paper for the Third Edition of the Column Research Council Guide, Civil Engineering Research Report No. CE71-1, Royal Military College of Canada, Kingston, Ontario, January 1971.

25. Pillai, U. S.
REVIEW OF RECENT RESEARCH ON THE BEHAVIOUR OF BEAM-COLUMNS UNDER BIAXIAL BENDING, Civil Engineering Research Report No. CE70-1, Royal Military College of Canada, Kingston, Ontario, January 1970.

26. Morino, S. and Lu, L. W.
ANALYSIS OF SPACE FRAMES, Fritz Engineering Laboratory Report No. 311.16, Lehigh University, Bethlehem, Pa., September 1970.

27. Von Karman, T.
UNTERSUCHUGEN UBER KNICKFESTIGKEIT, Mitteilungen Uber Forschungsarbeiten auf dem Gebiete des Ingenieurwesens, No. 81, Berlin, 1910.

28. Bleich, H.
REFINEMENT OF THE THEORY OF TORSIONAL BUCKLING OF THIN-WALLED COLUMNS, Reprint from Proceeding of the First Mid-Western Conference on Solid Mechanics, April 1953.

29. Timoshenko, S. P.
THOERY OF BENDING, TORSION AND BUCKLING OF THIN WALLED MEMBERS OF OPEN CROSS SECTION, Journal, Franklin Inst., Philadelphia, Pa., Vol. 239, No. 3, March 1945, pp. 201; No. 4, April 1945, pp. 249; No. 5, May 1945, pp. 343.

30. Chen, W. F.
Discussion of STABILITY AND LOAD CAPACITY OF MEMBERS WITH NO TENSILE STRENGTH, by F. Y. Yokel, Journal of the Structural Division, ASCE, Vol. 98, No. ST5, May 1972. (in press)

31. Culver, C.
EXACT SOLUTION OF THE BIAXIAL BENDING EQUATIONS, Journal of the Structural Division, ASCE, Vol. 92, No. ST2, April 1966.

32. Baron, F. and Venkatesan, M. S.
INELASTIC RESPONSE FOR ARBITRARY HISTORIES OF LOADS, Journal of the Engineering Mechanics Division, ASCE, Vol. 95, No. EM3, June 1969.

33. Popov, E. P. and Pinkney, R. B.
CYCLIC YIELD REVERSAL IN STEEL BUILDING CONNECTIONS, Journal of the Structural Division, Vol. 95, No. ST3, March 1969.

34. Galambos, T. V.
STRUCTURAL MEMBERS AND FRAMES, Prentice-Hall, Inc., New Jersey, 1968.

35. Przemlen, J. S.
THEORY OF MATRIX STRUCTURAL ANALYSIS, McGraw-Hill Book Company, 1968.

36. Krajcinovic, D.
A CONSISTENT DISCRETE ELEMENTS TECHNIQUE FOR THIN WALLED ASSEMBLAGES, International Journal of Solids Structures, Vol. 5, pp. 639-662, Pergamon Press, 1969.

37. Harstead, G. A., Birnstiel, C. and Leu, K. C.
INELASTIC BEHAVIOR OF H-COLUMNS UNDER BIAXIAL BENDING, Journal of the Structural Division, ASCE, Vol. 94, No. ST10, Proc. Paper 6173, October 1968, pp. 2371-2398, (Research Division Report, School of Engineering and Science, New York University, the Bronx, N. Y., November 1967).

VITA

The author was born in Kure, Japan, January 3, 1940, the son of Sataro and Matsuko (Tanaka) Atsuta.

He was graduated from Ogikubo High School in Tokyo in March 1958. From April 1959 to March 1964 he studied at the University of Tokyo and was awarded the Bachelor of Science Degree in Naval Architecture. From April 1964 to May 1966 he was a research associate at Department of Civil Engineering of the University of Tokyo. From June 1966 to July 1969 he was a research engineer at Kawasaki Heavy Industries, Ltd., doing researches on steel structural connections. In September 1969, he started his graduate studies in Civil Engineering at Lehigh University and received the Master of Science Degree in October 1970.

He is married to the former Chika Imai and has a son: Toll.

Beginning May 1972 he will be a research engineer of Steel Structural Division at Kawasaki Heavy Industries, Ltd., Japan.